NASA TECHNICAL
MEMORANDUM

REPORT NO. 53859

N70-13418

drf-08462

LUNAR EXCURSION MODULE RCS ENGINE VACUUM CHAMBER CONTAMINATION STUDY

Gary M. Arnett
Technical Coordinator
Space Sciences Laboratory

July 8, 1969

CASE FILE
COPY
NASA

George C. Marshall Space Flight Center
Marshall Space Flight Center, Alabama

PP-Y 59179

1. Report No. TM X-53859	2. Government Accession No.	3. Recipient's Catalog No.
4. Title and Subtitle Lunar Excursion Module RCS Engine Vacuum Chamber Contamination Study		5. Report Date July 8, 1969
		6. Performing Organization Code
7. Author(s) Gary M. Arnett, Technical Coordinator		8. Performing Organization Report No.
9. Performing Organization Name and Address George C. Marshall Space Flight Center Marshall Space Flight Center, Alabama 35812		10. Work Unit No.
		11. Contract or Grant No.
		13. Type of Report and Period Covered Technical Memorandum
12. Sponsoring Agency Name and Address		
		14. Sponsoring Agency Code

15. Supplementary Notes Prepared by:
Space Sciences Laboratory
Science and Engineering Directorate

16. Abstract The objective of this study was the definition of future contamination studies and procedures, and the investigation extended to the effects of the Reaction Control System (RCS) plume on optical flight experiments. This report is concerned with the effects of the RCS plume deposits on the test beds along with the characteristic changes that occur once these deposits are exposed to the laboratory atmosphere. Test beds consisting of various optical surfaces were exposed to an LM-RCS rocket engine plume in the Manned Spacecraft Center's (MSC) vacuum chamber A. Analysis of the contaminated test beds included optical measurements ranging from the near-ultraviolet through the far-infrared region together with mass spectrometer identification of the deposits. This study demonstrates that the instrumental procedures and sample handling are insufficient in many ways; however, the experience gained has led to an improvement of laboratory techniques and has greatly facilitated the interpretation of the results. In some cases, more suitable apparatus has been utilized that will enhance data analysis from planned orbital flight contamination experiments.

17. Key Words	18. Distribution Statement

19. Security Classif. (of this report) Unclassified	20. Security Classif. (of this page) Unclassified	21. No. of Pages	22. Price $3.00

ACKNOWLEDGMENTS

TABLE OF CONTENTS

LIST OF ILLUSTRATIONS

LIST OF ILLUSTRATIONS (Continued)

LIST OF ILLUSTRATIONS (Continued)

LIST OF ILLUSTRATIONS (Continued)

LIST OF ILLUSTRATIONS (Continued)

LIST OF ILLUSTRATIONS (Continued)

LIST OF ILLUSTRATIONS (Concluded)

LIST OF TABLES

LIST OF TABLES (Concluded)

LUNAR EXCURSION MODULE RCS ENGINE VACUUM CHAMBER CONTAMINATION STUDY

SUMMARY

The objective of this study was the definition of future contamination studies and procedures, and the investigation extended to the effects of the Reaction Control System (RCS) plume on optical flight experiments. This report is concerned with the effects of the RCS plume deposits on the test beds along with the characteristic changes that occur once these deposits are exposed to the laboratory atmosphere. Test beds consisting of various optical surfaces were exposed to an LM-RCS rocket engine plume in the Manned Spacecraft Center's (MSC) vacuum chamber A. Analysis of the contaminated test beds included optical measurements ranging from the near-ultraviolet through the far-infrared region together with mass spectrometer identification of the deposits.

This study demonstrates that the instrumental procedures and sample handling are insufficient in many ways; however, the experience gained has led to an improvement of laboratory techniques and has greatly facilitated the interpretation of the results. In some cases, more suitable apparatus has been utilized that will enhance data analysis from planned orbital flight contamination experiments.

INTRODUCTION

By G. M. Arnett and J. M. Zwiener

During the first week of May 1969, MSC fired a Lunar Module (LM) RCS Engine in their large thermal vacuum chamber (chamber A) to study exhaust plume kinetics. As a separate study, a set of four optical test beds was exposed in the vacuum chamber to the LM-RCS engine plume to study optical contamination. This report is concerned with the optical contamination

analysis as performed by the Space Sciences Laboratory (SSL) contamination team in cooperation with the Astronautics Laboratory (ASTN), both of the George C. Marshall Space Flight Center (MSFC). MSC's prime objective was to determine the LM-RCS "plume characteristics and the effect of exhaust gases on representative LM surfaces" [1]. MSFC's primary objectives were twofold. The first objective was to exercise and evaluate the capabilities of the optical/compositional contamination evaluation team at MSFC (as mentioned above). SSL has been assigned the overall responsibility of evaluating both in-flight and ground-based contamination and its effects on mainstream projects such as the Apollo Telescope Mount (ATM). The problem has been approached by both laboratory studies and by flight experiment TO27 (planned for the NASA AAP Workshop to evaluate in-orbit optical contamination). This exercise has provided vital information as to the usefulness of various measurement techniques, time required for measurement and evaluation, and as a dry run rehearsal for TO27 sample evaluation. Results obtained under this first objective include a need for better sample storage devices, faster data reduction techniques, better composition analysis approaches, and the need for a time-line event contamination monitor. The second objective was to expose a series of optical surfaces (at different locations and orientations) to a typical RCS plume and to then measure the resulting damage. At a minimum, it is difficult to correlate data of this type to actual space flight conditions, especially in quantitative terms, but it reveals the type of damage that can be encountered on critical optical surfaces. Surface studies revealed an inhomogeneous contaminant layer several hundred angstroms thick. Compositional analysis detected engine fuel residues, as expected, plus some residues of uncertain origin. In general, the results show that protective measures must be utilized to prevent RCS plume impingement or condensation on critical optical surfaces, or serious optical degradation can occur. A summary of previous studies of rocket engine exhaust plume contamination can be found in Reference 2. Results under this second objective include considerable decrease in reflectivity and an increase in scattering of the optical surface.

TEST DESCRIPTION

By J. M. Zwiener and P. W. Tashbar

The overall test plan was to expose a series of test beds, each made up of an assortment of optical surfaces, to the exhaust plume of an LM-RCS engine. "Before" and "after" measurements of the optical properties were

2

made to determine damage incurred during the test sequence; a set of controls were established to help identify and eliminate any nontest damage. Test bed positions, relative to the exhaust plume, were dictated mainly by MSC regulations, which resulted in the test beds being located out of the plume, but within the plane of the engine exit nozzle. The overall test chamber configuration is shown in Figure 1 (note that the test bed units were located in the test plane indicated by a dashed line). The vacuum chamber's dimensions are 65 feet in diameter and 120 feet high. The solar simulators were not used during the test. Figure 2 shows the test bed locations relative to the engine (not to scale). Test bed Nos. 1 and 8 faced the engine at a distance of about 80 inches, while at 45 inches away were test bed Nos. 5 and 6, with No. 6 facing toward the engine and No. 5 facing away.

The LM-RCS [3,4] engine is a pressure fed, bipropellant, hypergolic, radiation cooled engine with a thrust of 100 pounds. The RCS engine can be operated in either the pulse modulated or the steady-state mode. The pulse mode is defined as engine operation lasting less than 1 second in duration. The steady-state mode is defined as engine operation in excess of 1 second.

The engine (Fig. 3) consists of a fuel and oxidizer control valve which controls the flow of propellants, an injector head assembly which directs the flow of each propellant from the propellant control valves to the combustion chamber, and the combustion chamber where the propellants atomize and ignite (hypergolic) to produce thrust.

The combustion chamber is a machined molybdenum forging and is coated on all surfaces with silicon. Since the chamber must withstand high temperatures in the presence of oxidizing and embrittling combustion species, i.e., CO_2, H_2O, O_2, and N_2, a protective coating is required to prevent oxidation and interstitial embrittlement of the substrate.

Silicides are used as the oxidation resistant coatings. The coating reacts with, and diffuses into, the metal substrate to form a thin silicide coating which is resistant to penetration of the oxidizing medium. At operating temperature, the silicides form a viscous phase which is self-healing.

The nozzle extension, which extends to the gas outlet, is fabricated of stainless steel.

When the engine propellant valve opens (7 msec to reach full opening), the propellant flows through the valves into the injector and reaches the chamber about 12 msec after the valve opens. Ignition of the propellant

3
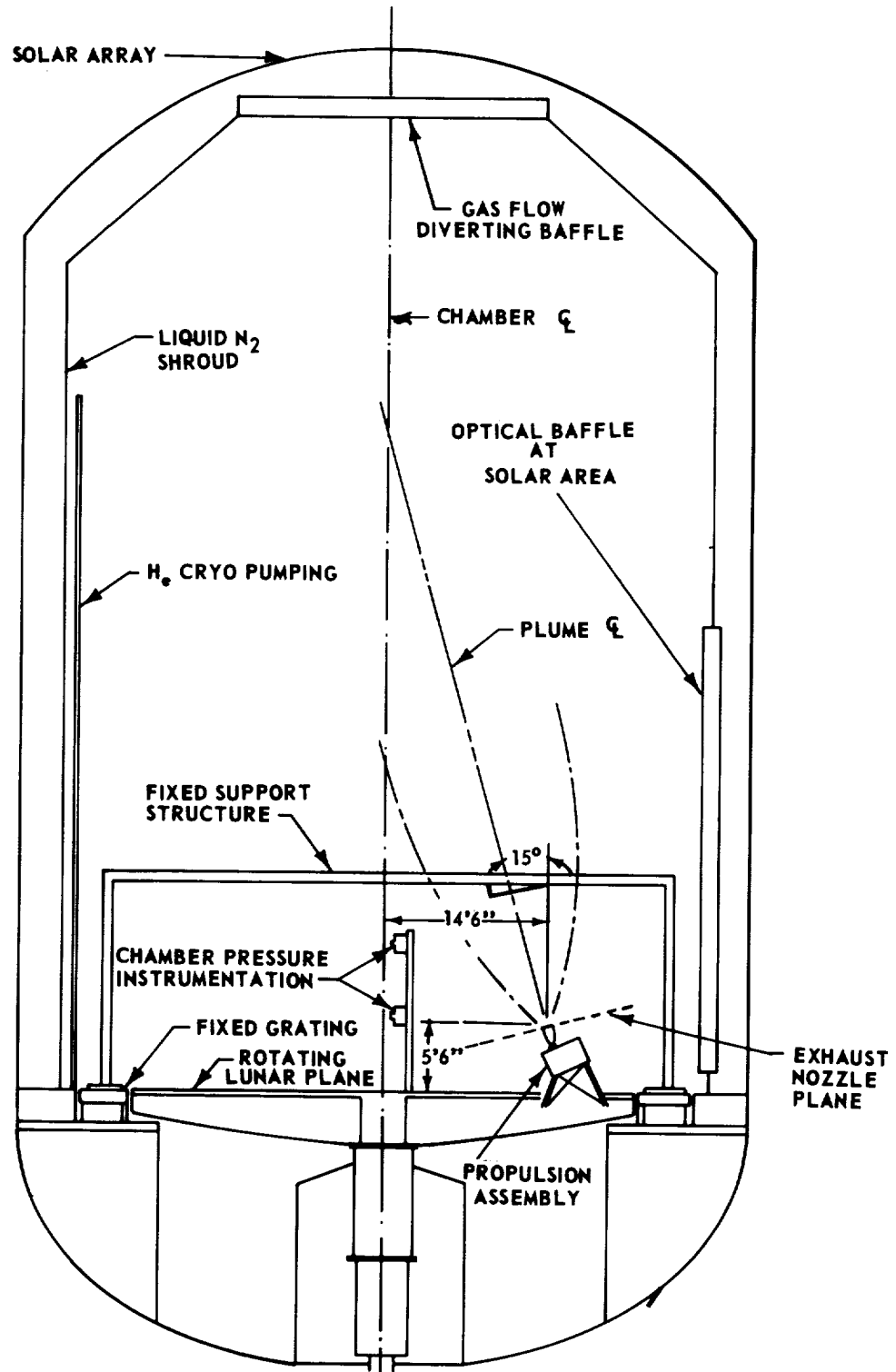
Figure 1. Cross section chamber A — MSC RCS plume
contamination test.
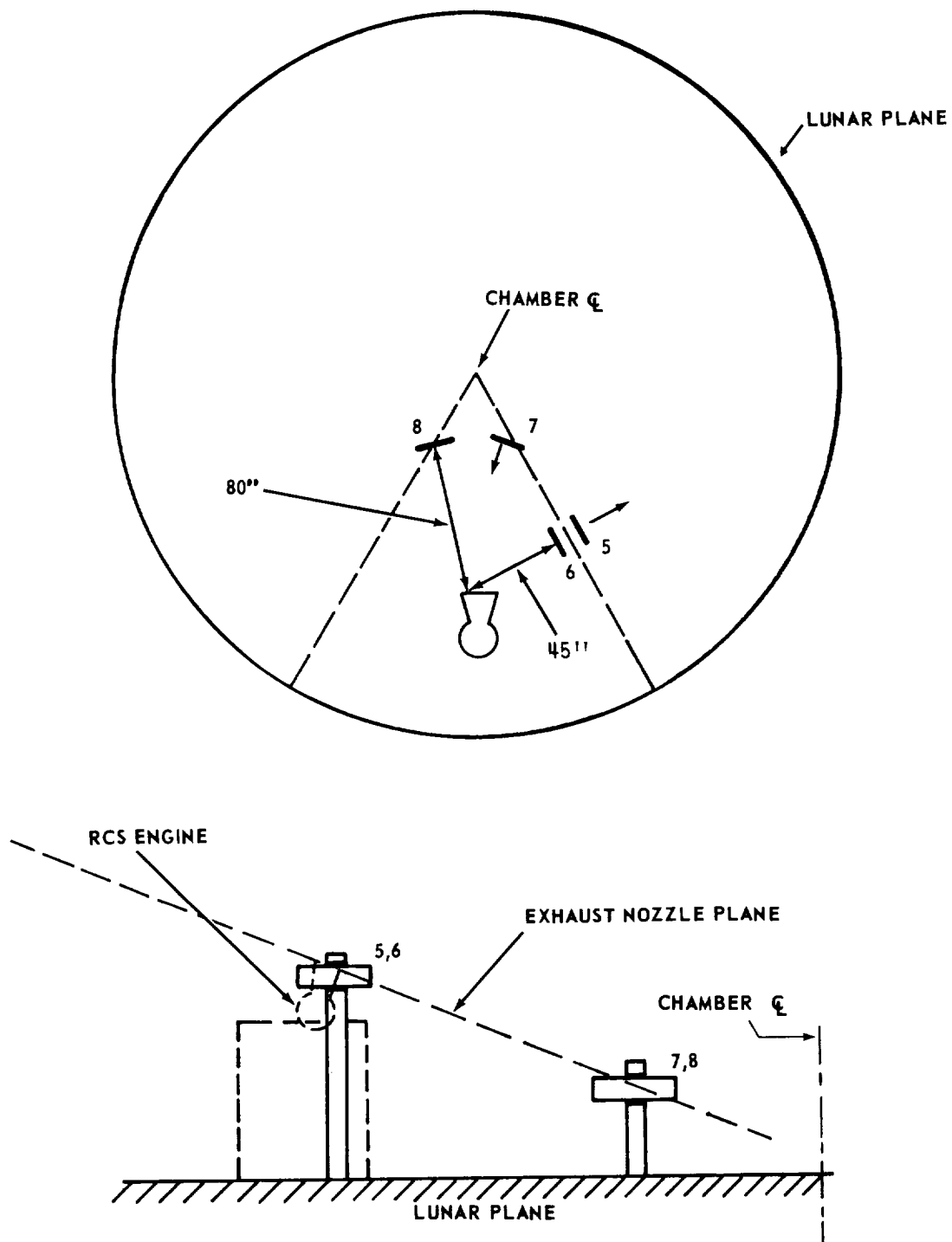
Figure 2. Test bed locations.

NOZZLE EXTENSION

ASSEMBLY

FUEL SOLENOID
VALVE ASSEMBLY

COMBUSTION
CHAMBER

ENGINE
MOUNTING
FLANGE

INJECTOR ASSEMBLY

PROPELLANT
INLETS

OXIDIZER
SOLENOID
VALVE ASSEMBLY

RCS ENGINE CROSS-SECTION
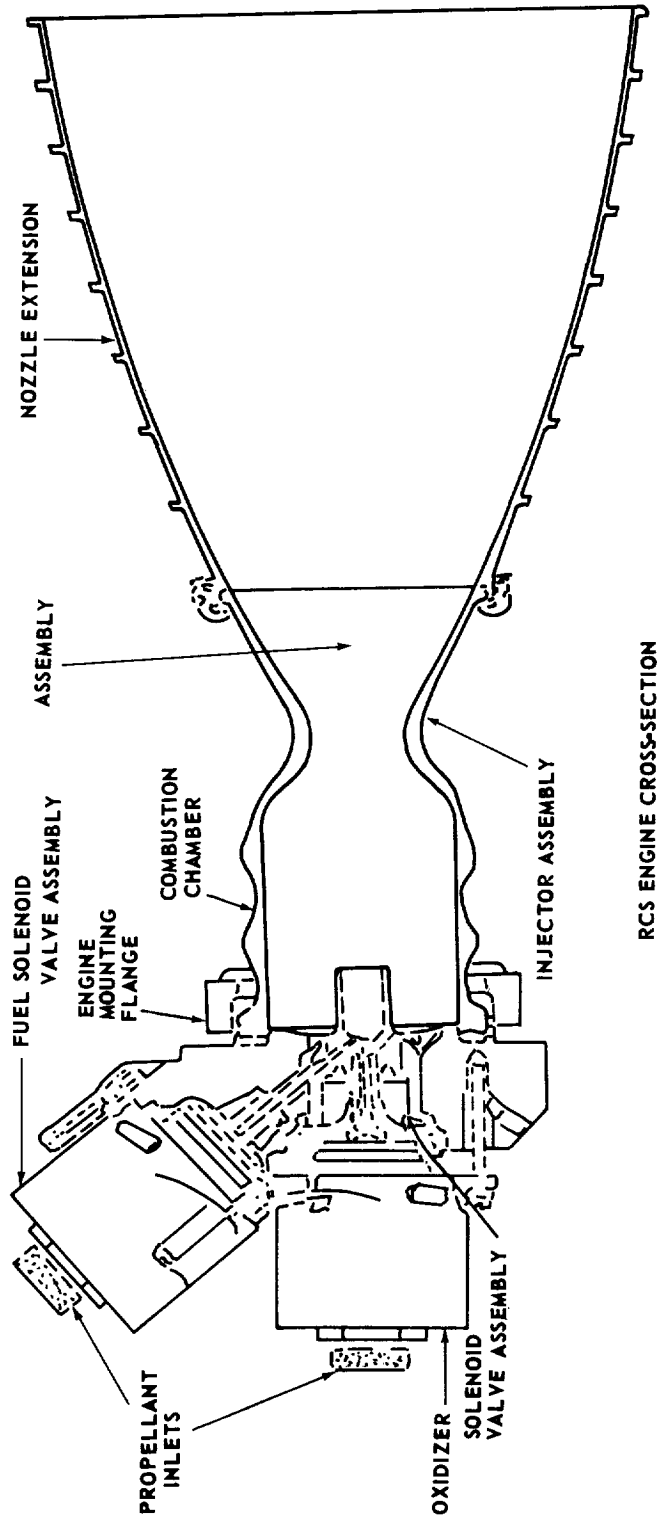
DESIGN AND PERFORMANCE CHARACTERISTICS

Thrust	˜100
Propellants	Nitrogen tetroxide (oxidizer) and 50% hydrazine/50% UDMH (fuel)
Oxidizer/fuel ratio	2.0 :1
Chamber Pressure	95 psi.
Flow rate - oxidizer	0.24 pounds/sec.
Flow rate - fuel	0.12 pounds/sec
Expansion area ratio	40 :1
Overall length	13.5 inches
Nozzle diameter	5.75 inches
Weight	6 lbs.

Engine life (steady state)	500 seconds
Engine life (pulse mode)	500 seconds
Engine life (total)	1000 seconds
Restart capacity	10000 times
Specific impulse	275 seconds (approx.)

Figure 3. LM–RCS engine.

6

occurs soon after the two liquids contact each other. It takes about 40 msec to achieve stable burning. From this point on, engine steady-state operation at the full 100 pounds of thrust continues until the shutdown operation.

It takes about 5 msec for the propellant valves to close completely for the engine shutdown. Propellant flow rate starts decreasing about 4 msec following the shutdown command and is zero about 9 msec later. Propellant flow continues to be injected for a short time. This is caused by the trapped propellant volume within the head. Thrust drops from 100 to 20 pounds in the first 10 msec after the shutdown. The remaining decay from 20 to 0 pounds takes 40 msec.

The fuel aerozine 50 [3, 5, 6] used with all the LM engines is a blend of hydrazine (N_2H_4) and unsymmetrical dimethylhydrazine (UDMH), $(CH_2)_2 NNH_2$. This blend is obtained commercially by the name of aerozine 50 (Table 1). The proportions of the blend are approximately hydrazine 51.5 percent, UDMH 47.5 percent, water 1 percent maximum.

Aerozine 50 is hypergolic with nitrogen tetroxide and will ignite spontaneously if contaminated with metallic oxides. Aerozine 50 is extremely hygroscopic and if exposed to air will deteriorate rapidly. Exposing aerozine 50 to air will produce white vapors.
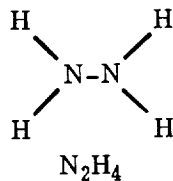
Anhydrous hydrazine [3, 5, 6] (Table 2) is an oily, hygroscopic liquid which fumes in air with a penetrating odor. Anhydrous hydrazine is a powerful reducing agent, particularly with acids, oxidizers, and organic substances. Hydrazine mixes with water and lower alcohols in all proportions, but it is only slightly soluble in other organic solvents. Hydrazine readily undergoes catalytic decomposition on many metal surfaces. Metallic oxides, such as iron, copper, lead, manganese, and molybdenum, will start spontaneous combustion. In contact with organic materials, such as wool and rags, hydrazine may burn spontaneously. Anhydrous hydrazine attacks natural rubber, cork, mild steel, and many other common metals, but polyvinyl chloride, polysiobutylene, and asbestos are resistant at ambient and high temperatures.

UDMH [3, 5, 6] (Table 3) is hygroscopic and miscible in all proportions with most common liquids including water, ethanol, gasoline, and other petroleum products. UDMH, chemically, is an organic base, and its reactions are related to those of the alkalines and substituted hydrazines. UDMH is resistant to air oxidation, although its vapor at ambient temperatures reacts slowly with air to form traces of other compounds. Carbon dioxide reacts

7

TABLE 1. PROPERTIES OF AEROZINE 50 (50/50 UDMH AND HYDRAZINE)

Composition	Wt. Percent
Anhydrous Hydrazine (N_2H_4)	51.0
Unsymmetrical Dimenthyhydrazine ($(CH_3)_2NNH_2$)	48.2
Water H_2O	0.5 to 0.1 max.
Other soluble impurities	0.3
Total N_2H_4 and UDMH, min.	98.2

Structural Formula

$$
\begin{array}{cc}
H \diagdown \diagup H & CH_3 \diagdown \diagup H \\
N\text{-}N & N\text{-}N \\
H \diagup \diagdown H & CH_3 \diagup \diagdown H \\
N_2H_4 & UDMH
\end{array}
$$

Molecular weight N_2H_4 . . . . 32.05
Molecular weight UDMH 60.078
Molecular weight aerozine 50 . . . . 45.39

Physical Properties

Appearance	clear, colorless liquid
Odor	fish-like with a tinge of ammonia
Toxicity	very high
Freezing Point	18.8° F
Boiling Point	158.2° F
Specific Gravity	0.894 to 0.903 (0.9 @ std. atm)
Vapor Pressure	2.75 psia @ 77° F (vapor 90% UDMH)
Liquid Density	56.1 lb/cu. ft. @ 77° F
Critical Temperature	643° F calc.
Critical Pressure	1696 psia calc.
Solubility	infinitely soluble in H_2O (heat evolved when mixed)
Viscosity of liquid	54.9×10^5 lb/ft-sec @ 77° F
Heat of vaporization	425.8 Btu/lb calc.
Heat of formation	527.6 Btu/lb-° F @ 77° F calc.
Specific Heat	0.694 Btu/lb-° F @ 77° F calc.
Thermal Conductivity	0.151 Btu/ft-hr-° F @ 77° F calc.

TABLE 2. PROPERTIES OF ANHYDROUS HYDRAZINE

Structural formula

$$\begin{array}{ccc} H & & H \\ \diagdown & & \diagup \\ & N\text{-}N & \\ \diagup & & \diagdown \\ H & & H \end{array}$$

N_2H_4

Molecular weight	32.05
Color	colorless
Freezing (melting) point	34.5° F (1.4°C)
Critical temperature	716.0° F (380.0°C)
Critical pressure	2135.0 psi (145.0 atm)
Heat of fusion at 77.0° F (25.0°C)	170.1 Btu/lb (94.5 cal/g)
Heat of vaporization at 77.0° F (25.0°C)	601.88 Btu/lb (10 700.0 cal/g mole)
Surface tension at 68.0° F (20.0°C)	0.00512 lb/ft (74.76 dynes/cm)
Boiling point at 1.0 atm	235.4° F (113.0°C)

with UDMH to form a carbonic acid salt. Extended exposure to air or other carbon dioxide containing gases can lead to eventual precipitation of the material.

The oxidizer used with all the LM engines is nitrogen tetroxide (N_2O_4) [3-7] (Table 4). It has a minimum purity of 99.5 percent and a maximum water content of 0.1 percent. Nitrogen tetroxide is a heavy brown liquid at ordinary temperatures containing about 30 percent nitrogen and 70 percent oxygen by weight. In this form, it consists principally of the tetroxide, N_2O_4, in equilibrium with a small amount of nitrogen dioxide, NO_2. Nitrogen tetroxide is a colorless gas and a powerful oxidizing agent, but on heating dissociates to the nitrogen dioxide which is a reddish-brown gas. It is hypergolic with a number of fuels. Pure N_2O_4 (water content under 0.1 percent) is not corrosive; however, water reacts with the N_2O_4 to form nitric acid, and whenever the water content exceeds 0.4 percent, it becomes very corrosive.

Nitrogen tetroxide reacts with water as follows:

$$N_2O_4 + H_2O = HNO_3 + HNO_2.$$
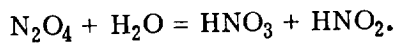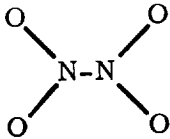
TABLE 3. PROPERTIES OF UNSYMMETRICAL DIMETHYLHYDRAZINE (UDMH)

Structural Formula	$\begin{array}{ccc} CH_3 & & H \\ & N\text{-}N & \\ CH_3 & & H \end{array}$ UDMH

Molecular weight 60.078

Color. . . . . colorless

Odor . . . . ammonical

Freezing (melting) point. . . . . -61.6° F (-52.0°C)

Boiling point . . . . 145.4°F (63.0°C)

Density at 71.6 F (22.0°C) . . . . 49.6 lb/ft (0.7914 g/cm)

Critical temperature . . . . 480.2°F (249.0°C)

Critical pressure . . . . 880.0 psi (60.0 atm)

Triple point temperature. . . . . -70.95°F (-57.2°C)

Coefficient of thermal expansion
at 60.0° F (15.6°C) . . . . 0.00074/°F (0.00133/°C)

Surface tension at 25.0° F (77.0°C). . . . . . 0.0019 lb/ft (28.0 dynes/cm)

Heat of fusion (F.P.) at
-72.0° F (-52.0°C). . . . . 72.0 Btu/lb (40.0 cal/g)

Heat of vaporization at 77.0° F
(25.0°C) . . . . 250.7 Btu/lb (139.3 cal/g)

Viscosity at 60.0°F (15.6°C). . . . . 0.394 × 10⁻³ lb/ft sec
(0.586 centipoise)

Thermal conductivity, liquid . . . . 0.12 Btu/ft hr °F
(0.00049 cal/cm sec °C)

TABLE 4. PROPERTIES OF NITROGEN TETROXIDE

Structural Formula

$$
\begin{array}{ccc}
O & & O \\
\diagdown & & \diagup \\
& N\text{-}N & \\
\diagup & & \diagdown \\
O & & O
\end{array}
$$

Composition	Wt. Percent
Nitrogen tetroxide (N_2O_4)	99.5 min
Water equivalent	0.1 max.
Chloride (Cl) as nitrosylchloride (NOCl)	0.08 max.
Nitric oxide (NO)	0.45 to 0.85
Non-volatile ash	0.01 ma

Physical Properties

Molecular weight	92.016
Specific gravity at 68° F	1.45
Physical description (ambient temperatures)	red-brown liquid
Boiling point	70.0° F
Heat of formation at 77° F (liquid)	-87.62 Btu-lb
Vapor pressure at 77° F	17.7 psia
Viscosity at 77 °F	27.96×10^{-5} lb/ft-sec (0.410 centipoise)
Density at 77° F	11.9 lb/gal
Critical temperature	316.8° F
Critical pressure	1469 psia
Thermal conductivity at 40° F and 200 psia	0.0812 Btu/ft-hr-° F
Heat of vaporization	178 Btu/lb
Heat of fusion	68.4 Btu/lb

The nitrous acid undergoes decomposition:

$$3HNO_2 = HNO_3 + 2NO + H_2O$$
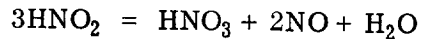
Overall, two thirds of the N_2O_4 goes to form nitric acid; the other third may be oxidized with air or oxygen to reform NO_2 or N_2O_4. Therefore, anyhdrous N_2O_4 will not attack steel (moisture content of 0.1 percent or lower). Contact with water in any form, such as moisture in the air, produces nitrous or nitric acid which is extremely corrosive.

A test flow chart of the chamber pumpdown and engine firing sequence is shown in Figure 4 [1]. According to the flow chart, the engine fired in 10 different positions in the chamber with a total firing time of 100 seconds. The firing sequence consisted of twelve 1-second pulses, two 6-second duty cycles, one 6-second continuous, and one 10-second intermittent. Prefiring chamber pressure was to be at least 1×10^{-5} torr, obtained by using three pumping systems; 20° K gaseous helium cooled surfaces, 100° K liquid nitrogen cooled liner, and the diffusion/mechanical pumping system.

There was a total of eight optical test bed units, each having 12 individually mounted samples. Test bed units were numbered 1 through 8, with Nos. 1 through 4 being controls, while Nos. 5 through 8 were exposed to the test environment. Of the four control test beds, No. 1 was stored in an inert gas environment (dry nitrogen), No. 2 stored in a "clean room," No. 3 stored in the laboratory on a shelf, and No. 4 stored with the other test bed units during shipment to and from MSC. Unit Nos. 1, 2, and 3 served to evaluate different storage techniques. Unit No. 4 helped determine if in-route contamination occurred, since it was stored with the actual test units before and after the test and during transportation. Test unit Nos. 5 through 8 were all exposed to the LM-RCS engine plume in various positions as previously described. Test unit No. 5 faced away from the engine to collect only the scattered particles, while No. 6 faced the engine to obtain a more direct impingement of contaminating particles and serve as a comparison to No. 5. Test unit Nos. 7 and 8 were further away from the engine than No. 6 and served to monitor contamination effects at different distances from the engine. Results of No. 8 are not included in this report, since it was left with MSC for their own analysis.

The individual test bed units are broken down into three separate subunits coded "A," "B," and "C." In turn, each of these are broken down into four sample positions coded 1 through 4 as shown in Figure 5. Descriptions of the individual samples are given in Appendix A, along with a detailed

12

Figure 4. Test flow chart.

13
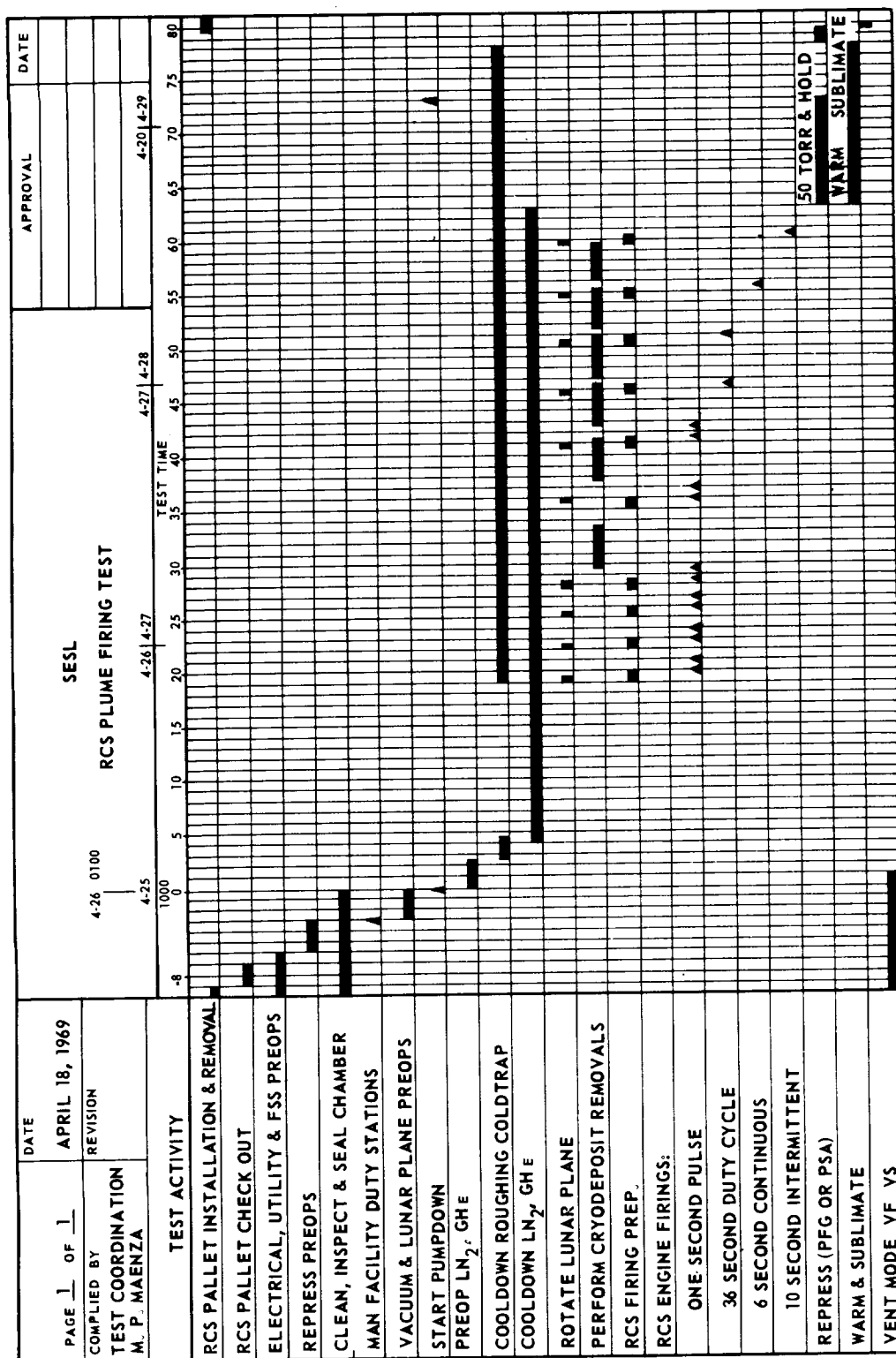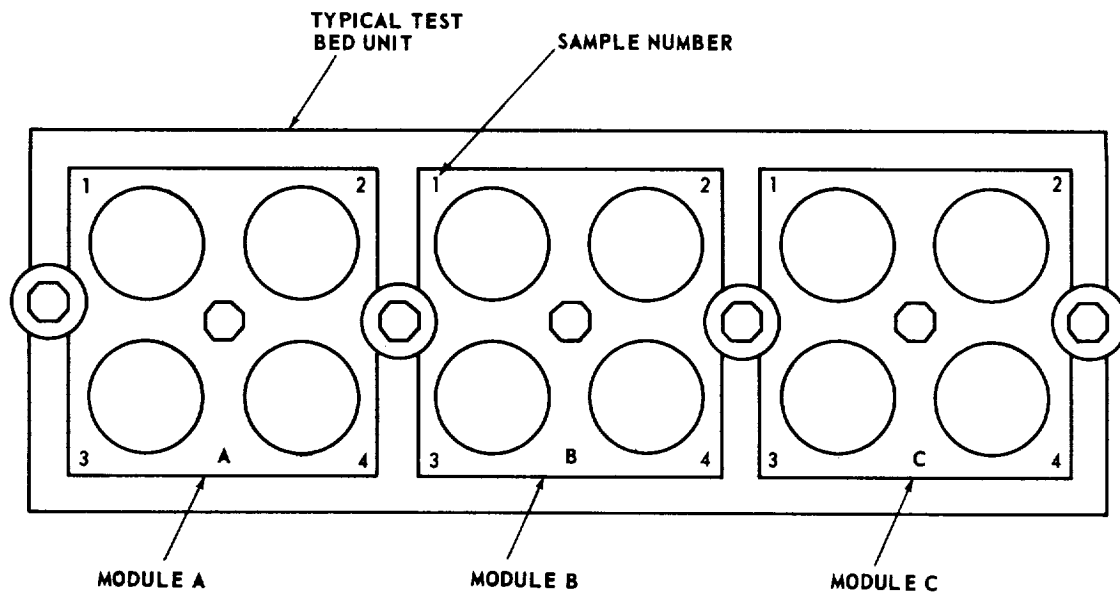
Figure 5. Sample code system.

measurement breakdown for each sample. A typical test bed with protective covers attached is shown in Figure 6. For storage and transportation, each test bed unit was wrapped in a thin sheet of aluminum foil and sealed with a heavy sheet of aluminum foil (Fig. 7).

TEST ANALYSIS

Photographic Evaluation

TEST BEDS — J. M. Zwiener

Upon the return of the optical samples and test bed units to MSFC from MSC, photographs of all test bed units were taken before disassembly and distribution of samples for evaluation. Figures 8 and 9 show photographic comparisons of the control test beds and the exposed (contaminated) test beds. The protective covers of the test beds are removed and shown. Optical damage on the exposed test beds is readily apparent from the scattered light. Damage appears as a smooth haze on the mirror surface. The mirror surfaces on the control test beds appear dark, because the light is specularly reflected away from the camera by the mirror surfaces. Of special interest
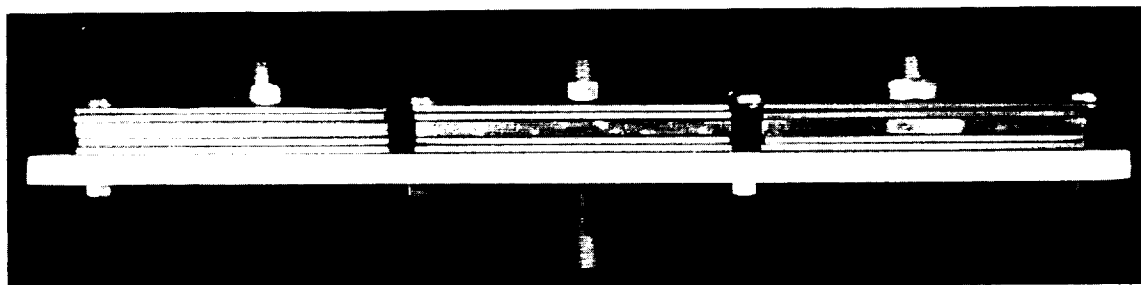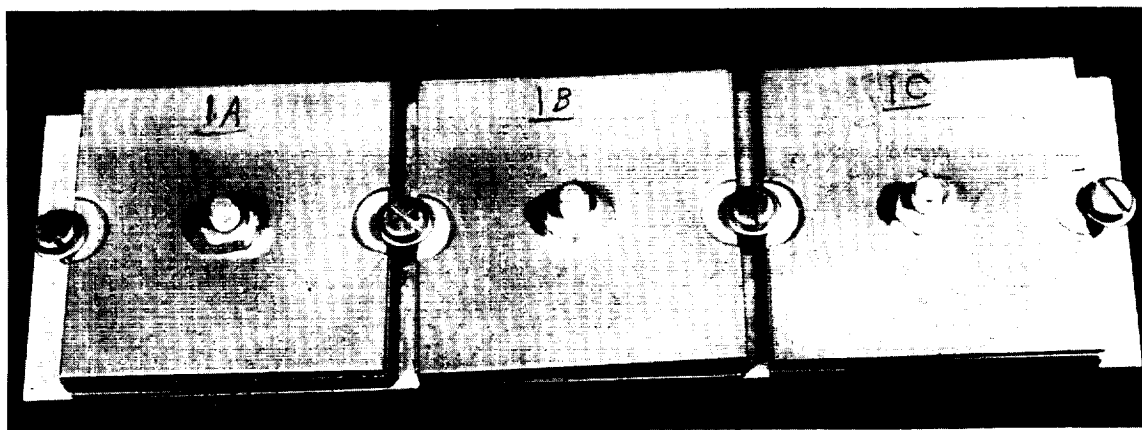
Side View

Figure 6. Typical test bed.

is the stain appearing on the control test bed No. 4. As described in a previous section, this test bed unit was transported with test bed unit Nos. 5, 6, 7, and 8 to and from MSC, but was not exposed in chamber A. The stain appears on all units exposed within the chamber, but does not appear on any of the controls except No. 4. Subsequent optical measurements did not reveal any damage to the mirrors of unit No. 4. This stain, or corrosion, apparently occurred on shipment back to MSFC as relatively low volatile contaminants evaporated and managed to penetrate the aluminum protective wrapping and react with the test bed material.
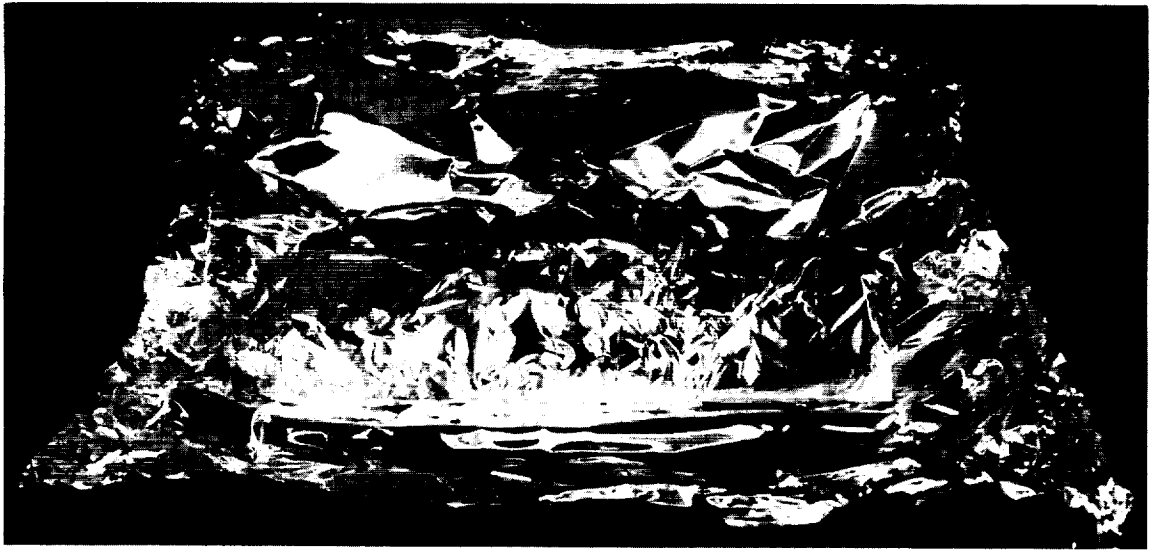
Inner Layer

Outer Layer

Figure 7. Test bed covering.

FACING ENGINE (45" AWAY)
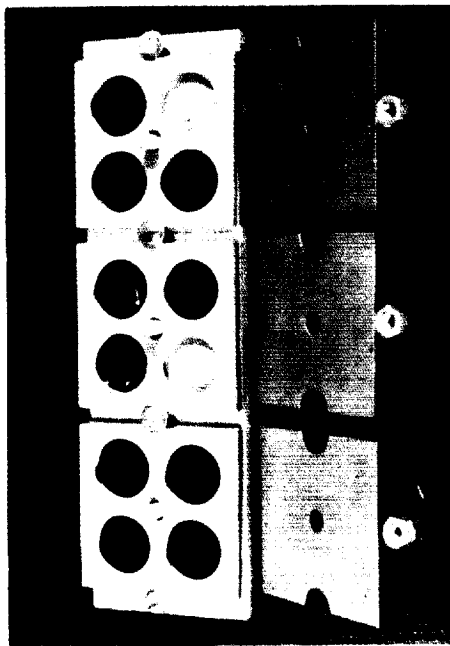
EXPOSED FACING AWAY FROM ENGINE (45")

CONTROL (INERT GAS STORAGE)

CONTROL LABORATORY STORAGE

Figure 8. Sample test beds 1, 3, 5, and 6.
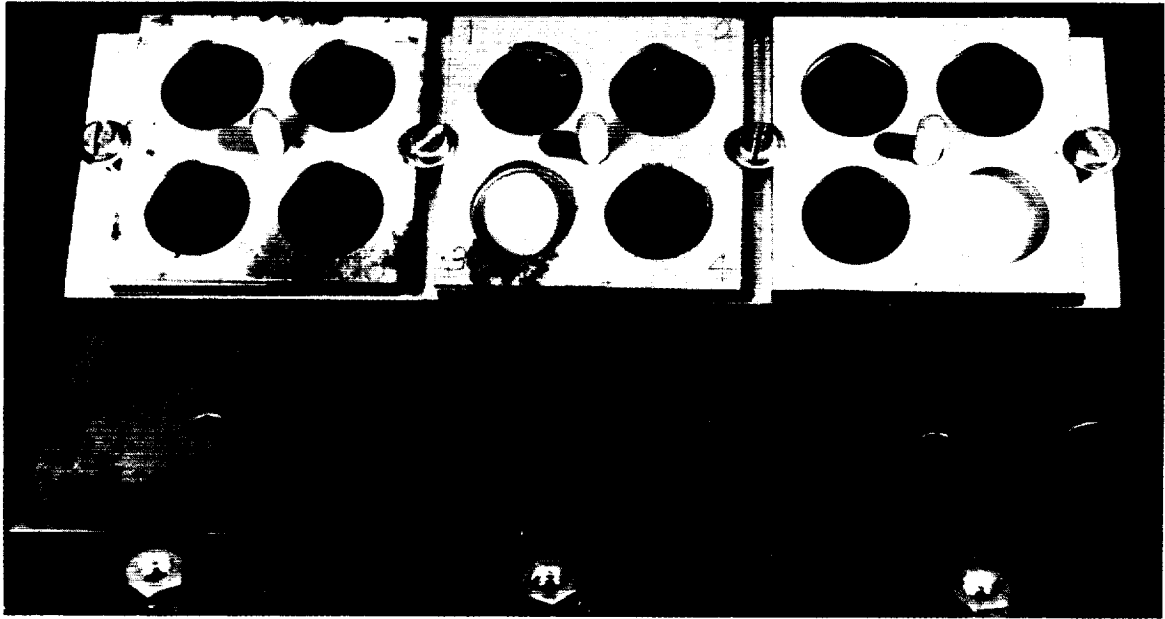
Control-Handling
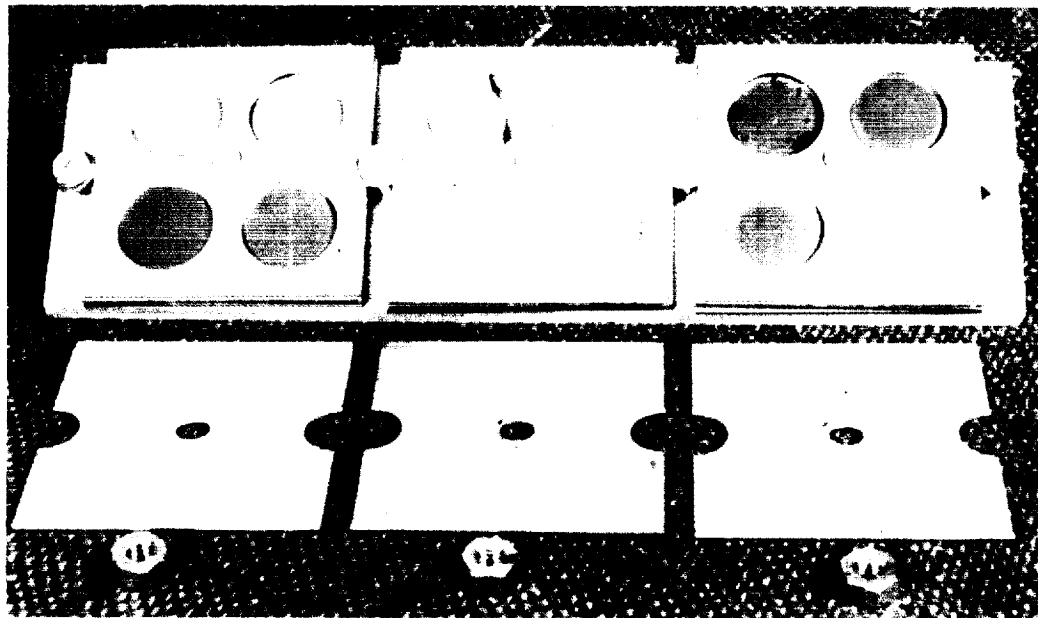
Exposed Facing Engine (80" away)

Figure 9. Sample test beds 4 and 7.

PHOTOMICROGRAPHS — J. M. Zwiener

A series of photomicrographs were taken of selected gold and aluminum coated mirrors from each test bed unit before and after test exposure. As herein described, all photomicrographs were taken using a microscope at powers of 70X and 560X. Both black and white and color polaroid film were used. In the following series of figures, typical pictures are presented to demonstrate the physical appearance of the surface damage. A scale is included on each picture for reference. Figures 10 and 11 are for the gold coatings, where Figure 10 shows before and after pictures at both powers for the control mirror (1A4). Dark spots are visible that are a combination of dust particles and imperfections (such as pin holes) in the coating, but basically the coating is undamaged. Figure 11 shows sample 6A4 which faces the engine about 40 inches away. The contaminant deposition is now most obvious with "particle" size on the order of 2.5 microns. Figures 12, 13, and 14 show, before and after, one of the aluminum coatings from each of the exposed test bed unit Nos. 5, 6, and 7. Some difference in color and contrast is apparent between the pictures. This is not a contamination effect, but is caused by different lighting and exposure techniques. As on the gold coatings, most of the contaminant "particles" are on the order of 2.5 microns in diameter. Figure 12 depicts one of the larger particle concentrations, with particle diameters ranging up to 15 microns. Figure 15 is a photomicrograph of one of the aluminum samples taken 20 days after the pictures shown in Figures 12 through 14. This figure shows the decrease in size of the particles after 20 days of evaporation or sublimation of the particles off of the surface. Figure 15 (samples 6A1 and 6A2) also compares pictures of samples that were ultraviolet irradiated in a vacuum system to a sample which was stored in a "clean room" over the same time span. Notice that the particles on sample 6A2 are smaller than the particles on sample 6A1, indicating that more material was lost under ultraviolet and vacuum, which was anticipated. Optical measurements presented later in this report also show this effect of losing contamination material especially in scatter and absorption.

NORMAL PHOTOGRAPHY, DARK FIELD PHOTOGRAPHY, AND HOLOGRAPHY — J. R. Williams

The objective of the following study was to specifically investigate the usefulness of normal photography, dark field photography, and holography in studying the effect of an RCS thruster plume on optical samples.
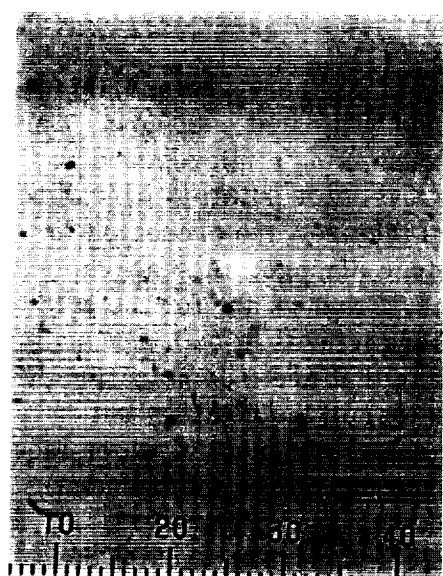
Each Major Division Equals 200 μ
(0.2 mm), Before Exposure
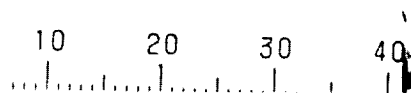
Each Major Division Equals 200 μ
(0.2 mm), After Exposure

Each Major Division Equals 25 μ
(0.025 mm), Before Exposure

Each Major Division Equals 25 μ
(0.025 mm), After Exposure

Figure 10.   Photomicrographs, gold coating, sample 1A4,
(control, inert gas storage).
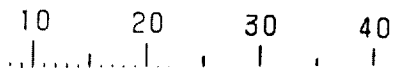
Each Major Division Equals 200 μ
(0.2 mm), Before Exposure
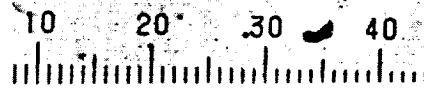
Each Major Division Equals 200 μ
(0.2 mm), After Exposure
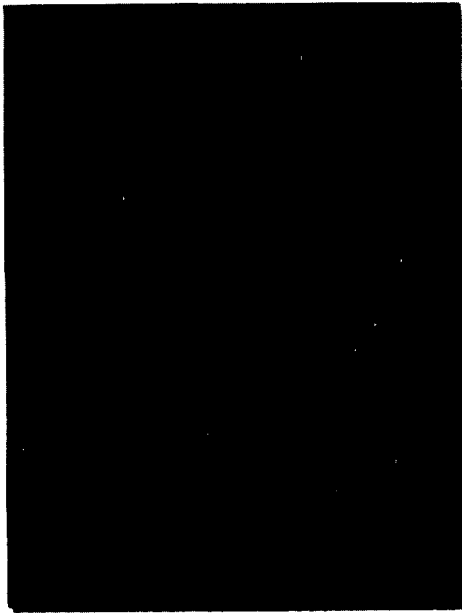
Each Major Division Equals 25 μ
(0.025 mm), Before Exposure

Each Major Division Equals 25 μ
(0.025 mm), After Exposure

Figure 11.   Photomicrographs, gold coating, sample 6A4,
(facing engine, 45 inches).
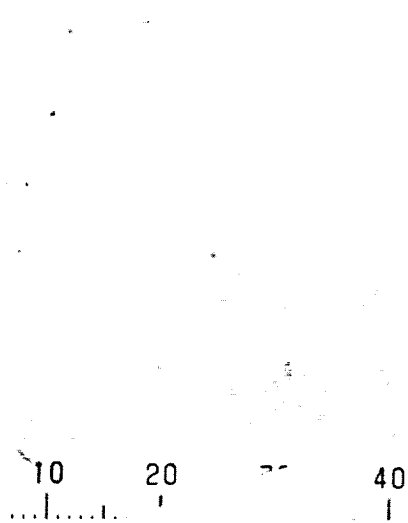
21

10   20   40

10   20   30   40

Each Major Division Equals 200 μ Each Major Division Equals 200 μ
(0. 2 mm), Before Exposure   (0. 2 mm), After Exposure

Each Major Division Equals 25 μ Each Major Division Equals 25 μ
(0. 025 mm), Before Exposure   (0. 025 mm), After Exposure

Figure 12. Photomicrographs, aluminum coating, sample 5A2,
(facing away from engine, 45 inches).
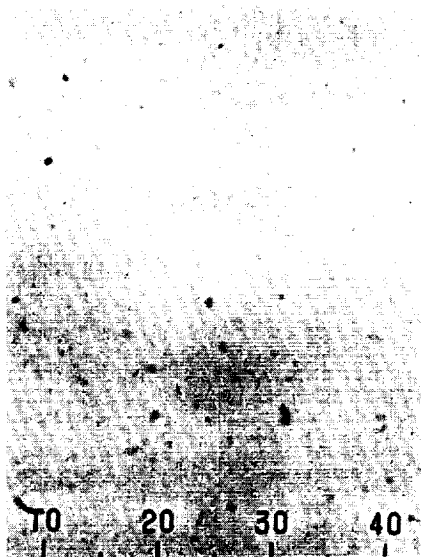
22

Each Major Division Equals 200 μ
(0.2 mm), Before Exposure

Each Major Division Equals 200 μ
(0.2 mm), After Exposure

Each Major Division Equals 25 μ
(0.025 mm), Before Exposure

Each Major Division Equals 25 μ
(0.025 mm), After Exposure

Figure 13. Photomicrographs, aluminum coating, sample 6A2,
(facing engine, 45 inches).
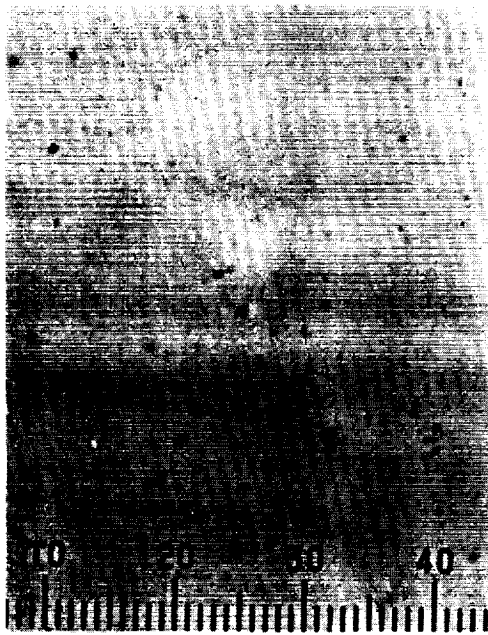
Each Major Division Equals 200 μ (0.2 mm), Before Exposure
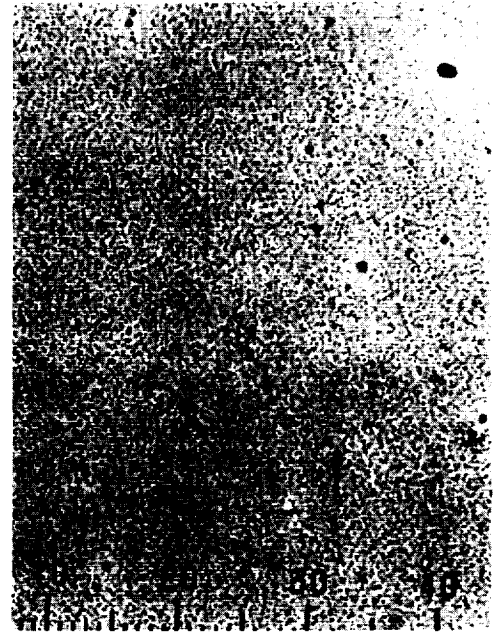
Each Major Division Equals 200 μ (0.2 mm), After Exposure
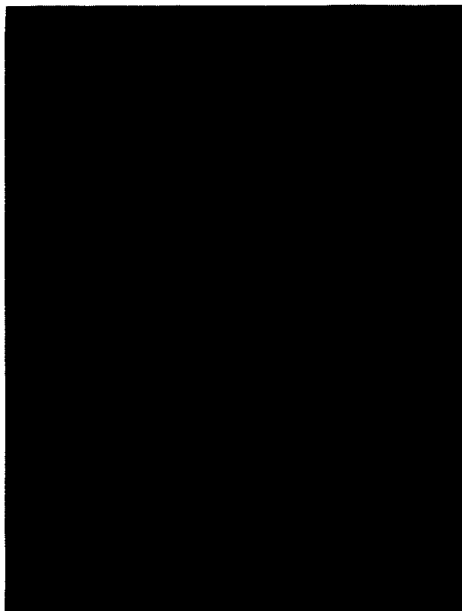
Each Major Division Equals 25 μ (0.025 mm), Before Exposure
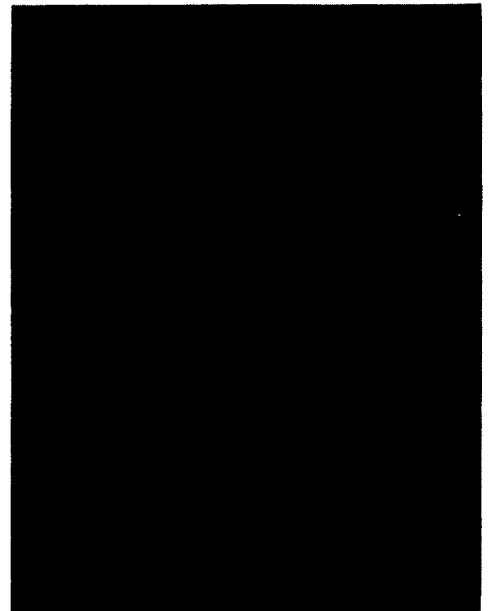
Each Major Division Equals 25 μ (0.025 mm), After Exposure

Figure 14. Photomicrographs, aluminum coating, sample 7A2, (direct lighting).
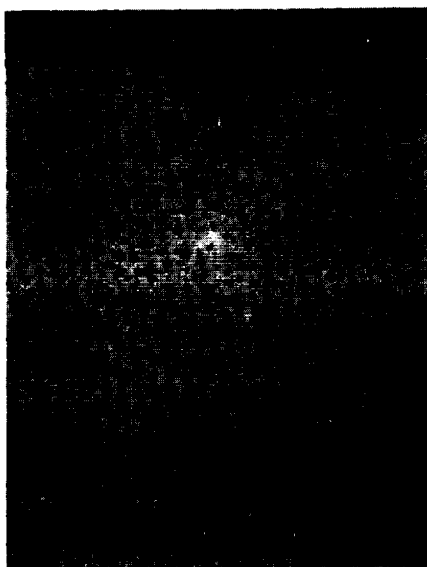
24

6A1   6A2

Each Major Division Equals 25 μ
(0.025 mm), After Plume
Exposure Plus 20 Days

Each Major Division Equals 25 μ
(0.025 mm), After Ultraviolet
Vacuum
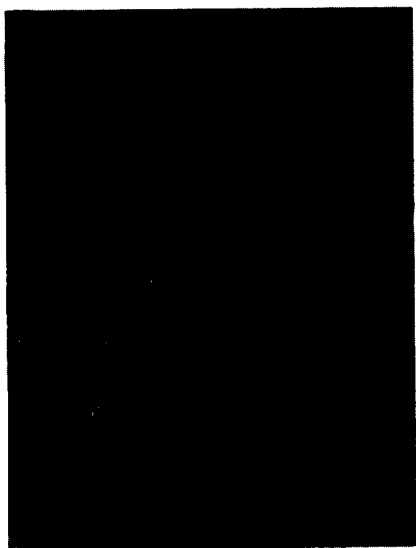
Each Major Division Equals 25 μ
(0.025 mm), After Plume
Exposure Plus 20 Days

Each Major Division Equals 25 μ
(0.025 mm), After Ultraviolet
Vacuum

Figure 15. Photomicrographs, aluminum coating, samples 6A1/6A2
(facing engine, 45 inches).

Figures 16 and 17 show the experimental system used to produce the normal photographs, dark field photographs, and holograms, and Figure 18 is a drawing of the experimental system. Each of the areas, normal photography, dark field photography, and holography, constitutes a different test, but to minimize sample handling they were combined into one test system. This meant that after the sample was placed in the holder all three pieces of information could be obtained simply by rotating the sample holder.

The light source used in this system was a Spectra-Physics Model 125 HeNe laser. This laser has a rated output of 50 mW, but at the time these tests were made, it was producing an output of only 20 to 30 mW. This output fluctuation caused some of the differences in the exposures listed in Tables 5 and 6. As shown in Figure 18, the exposure time was controlled by a camera shutter. This shutter, along with most of the components, was mounted on a 4 × 6 foot granite table supported with Barry air mounts. This eliminated any possible problems as a result of room vibration. After passing through the shutter, the amplitude of the beam was divided by a beam splitter. The beam passing through the beam splitter was then spatially filtered by a microscopic objective and focused onto the film by mirrors. This beam served as the reference beam for the hologram. The beam reflected from the beam splitter was also spatially filtered and directed through the optical sample by mirrors, and it served as the sample illuminating beam for all three tests. As shown in Figure 18, all three tests were run simply by rotating the sample. The diffracted light provided the dark field photographs while the reflected light provided the normal photographs and the holograms.

As indicated by Tables 5 and 6, the order of testing for each sample was normal photography, dark field photography, and holography. Upon receiving the samples, they were placed in the sample holder using "clean room" gloves and stainless steel tongs. Each sample was then tested in the order shown in Tables 5 and 6. For the normal photography, the sample was rotated so that the laser beam illuminating the sample was reflected into the camera. The camera used was a Speed Graphic with a Polaroid back. The results of this test are shown in the figures labeled Normal Photo.

The sample was then rotated so that it was perpendicular to the illuminating beam. In this position, the light passed through the sample striking the DC stop. This meant that all light which passed through the sample undisturbed was blocked out by the stop. Therefore if a sample was completely clean then the large collecting lens would have nothing to image so the resulting dark field photograph would show a smooth black image. However, if the sample contains scattering and diffracting centers such as
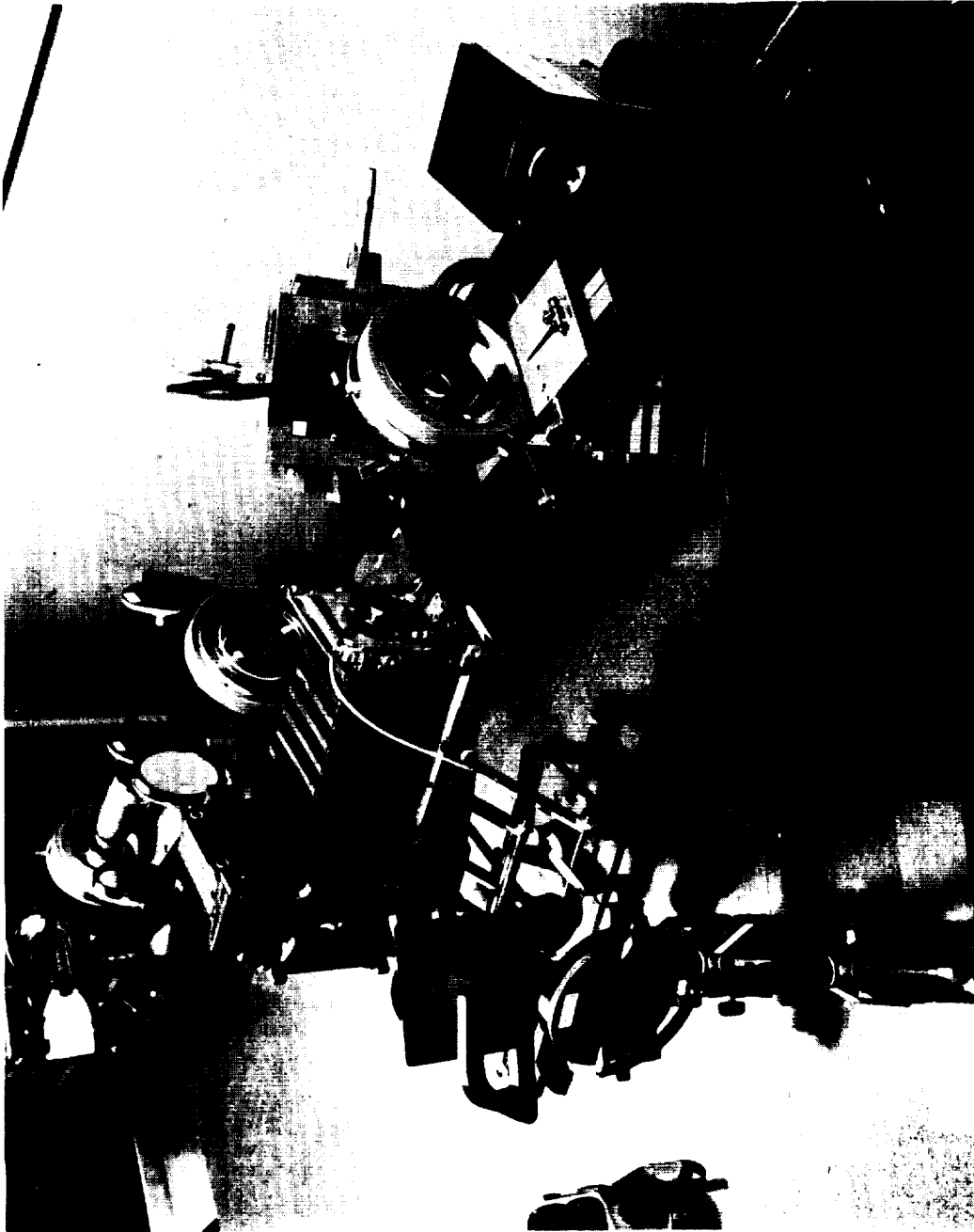
Figure 16. Experimental system photography and holography.
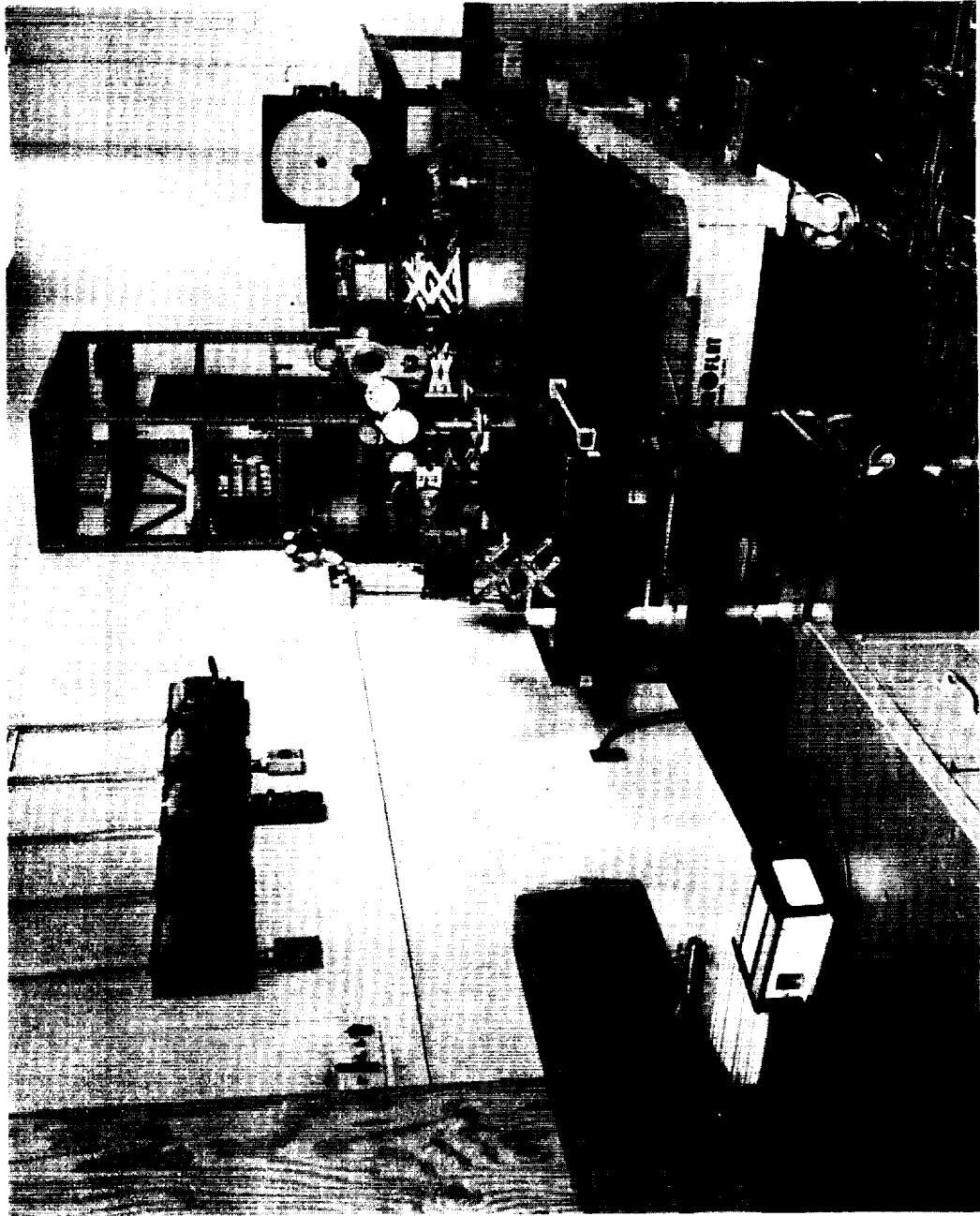
Figure 17. Experimental system photography — overall view.
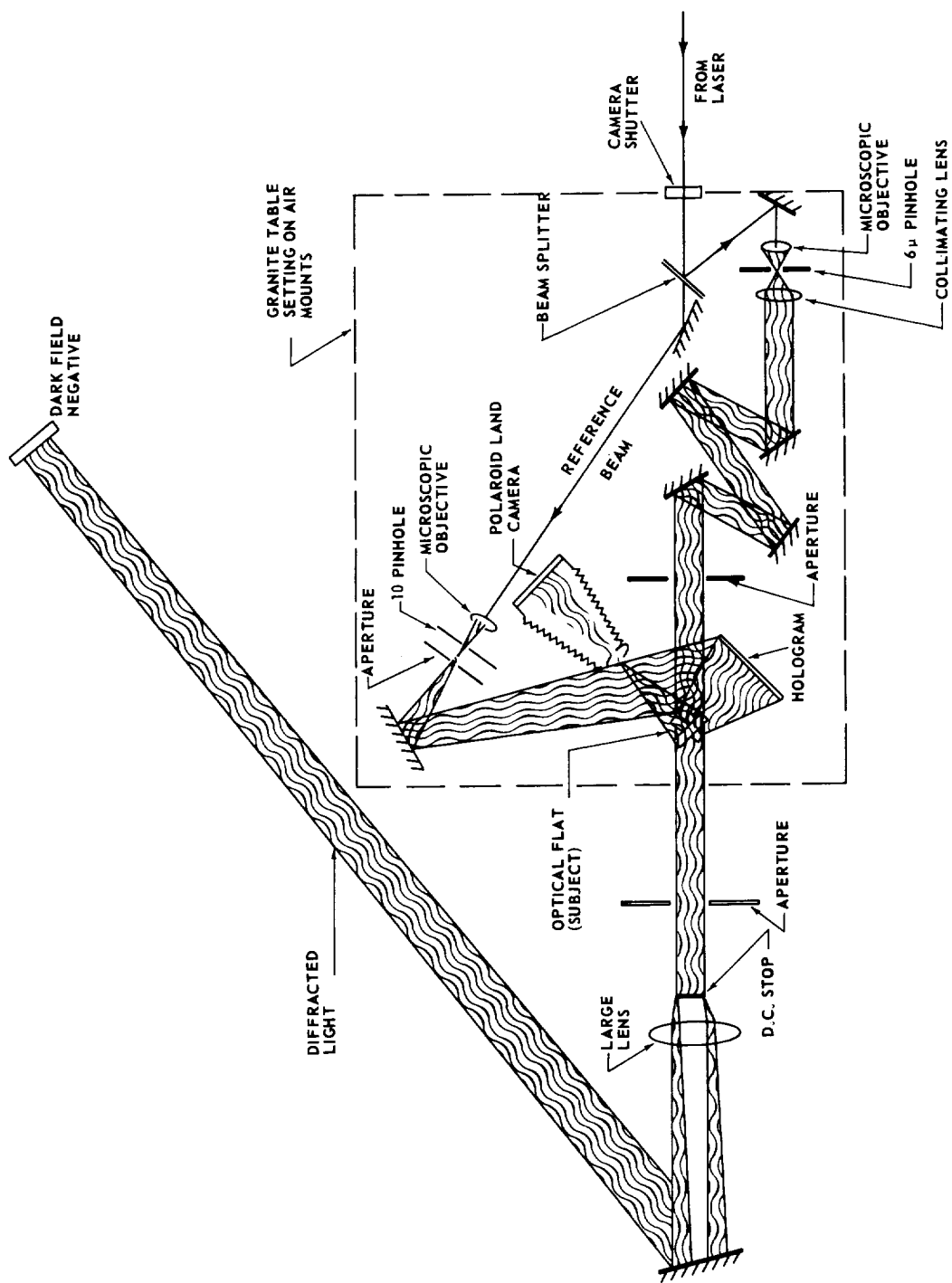
Figure 18. Configuration for holography, regular, and dark field photography of an optical flat.

29

TABLE 5. PRE-TEST DATA, PHOTOGRAPHIC EVALUATION

Sample No.	Test Type*	Film	Exposure
3B3	P	P/N 55	11 sec
3B3	DFP	52	1/60 sec
3B3	H	649F	4.75 sec
4B3	P	P/N 55	14 sec
4B3	DFP	52	1/60 sec
4B3	H	649F	4.75 sec
5B3	P	P/N 55	15 sec
5B3	DFP	52	1/60 sec
5B3	H	649F	4.75 sec
6B3	P	P/N 55	15 sec
6B3	DFP	52	1/60 sec
6B3	H	649F	4.75 sec
7B3	P	P/N 55	15 sec
7B3	DFP	52	1/30 sec
7B3	H	649F	4.75 sec
3B1	P	P/N 55	10 sec
3B1	DFP	P/N 55	0.5 sec
3B1	H	649F	4.5 sec
4B1	P	P/N 55	10 sec
4B1	DFP	52	1/15 sec
4B1	H	649F	4.75 sec
5B1	P	P/N 55	10 sec
5B1	DFP	52	1/3 sec
5B1	H	649F	4.75 sec
6B1	P	P/N 55	10 sec
6B1	DFP	52	1/60 sec
6B1	H	649F	4.75 sec
7B1	P	P/N 55	10 sec
7B1	DFP	52	1/60 sec
7B1	H	649F	4.75 sec

* Test Type: P — Normal Photograph
              DFP — Dark Field Photograph
              H — Hologram

TABLE 6. POST-TEST DATA, PHOTOGRAPHIC EVALUATION

Sample No.	Test Type	Film	Exposure
1B3	P	P/N 55	10 sec
1B3	DFP	P/N 55	1/2 sec
1B3	H	649F	5 min.
2B3	P	P/N 55	1 min.
2B3	DFP	P/N 55	5/8 sec
2B3	H	649F	5 min.
3B3	P	P/N 55	35 sec
3B3	DFP	P/N 55	5/8 sec
3B3	H	649F	5 min.
4B3	P	P/N 55	33 sec
4B3	DFP	P/N 55	4/8 sec
4B3	H	649F	5 min.
5B3	P	P/N 55	13 sec
5B3	DFP	P/N 55	5/8 sec
5B3	H	649F	5 min.
6B3	P	P/N 55	13 sec
6B3	DFP	P/N 55	5/8 sec
6B3	H	649F	5 min.
7B3	P	P/N 55	10 sec
7B3	DFP	P/N 55	5/8 sec
7B3	H	649F	5 min.
1B1	P	P/N 55	20 sec
1B1	DFP	P/N 55	3/4 sec
1B1	H	649F	5 min.
2B1	P	P/N 55	70 sec
2B1	DFP	P/N 55	1 sec
2B1	H	649F	5 min.
3B1	P	P/N 55	80 sec
3B1	DFP	P/N 55	2 sec
3B1	H	649F	5 min.
4B1	P	P/N 55	90 sec
4B1	DFP	P/N 55	2 sec
4B1	H	649F	4.5 min.
5B1	P	P/N 55	115 sec
5B1	DFP	P/N 55	2.25 sec
5B1	H	649F	4.5 min.
6B1	P	P/N 55	2 min.
6B1	DFP	P/N 55	2 sec
6B1	H	649F	5 min.
7B1	P	P/N 55	2 min.
7B1	DFP	P/N 55	2 sec
7B1	H	649F	5 min.

particles, lint, films, etc., then light will be scattered off-axis and will not be blocked by the DC stop. This light is then collected by the large lens and imaged on the film to produce the dark field photographs. This method is sometimes called the "central dark ground method" of observation and is a special case of Zernike's phase contrast method. For a theoretical description, see "Principles of Optics" by Born and Wolf, pages 424-428. The results of this test are shown in the figures labeled Dark Field Photo.

To obtain the third piece of information, the sample was again rotated so that the illuminating beam reflected onto the hologram plane. The reference beam was then directed to the hologram plane and the interference pattern between these two beams recorded on film. This recorded interference pattern is the hologram. It is then possible to reconstruct, from this hologram, a three-dimensional image of the sample and study this image in much the same way as the original object (Fig. 19).

The results of the normal photography are shown in Figures 20 through 29. These figures show samples 3B3, 4B3, 5B3, 6B3, 7B3, 3B1, 4B1, 5B1, 6B1 and 7B1. Each figure shows the photo taken before and after the test. Since samples 3B3, 4B3, 3B1, and 4B1 were controls there is essentially no change in the surface. What change is apparent was due to the sample cleaning between photos. There is, however, very noticeable contamination on the test samples 5B3, 6B3, 7B3, 5B1, 6B1, and 7B1. The interference patterns demonstrated in the post test photos of samples 5B3, 6B3, 7B3, 5B1, 6B1, and 7B1 were noticeable under laser light but vanished when illuminated with incoherent white light.

The results of the Dark Field Tests are shown in Figures 30 through 39 labeled Dark Field Photo. This test also covered the samples 3B3, 4B3, 5B3, 6B3, 7B3, 3B1, 4B1, 5B1, 6B1, and 7B1. In these photos, there is noticeable aberration which was caused by the poor quality of the large collecting lens. This does not, however, detract from the magnitude of particles and aggregates on the sample. The large bright ring apparent in sample 4B3 was caused by a bubble inside the sample. Since the photograph was made in the plane at which the surface of the sample was in best focus, anything within the sample or on its other surface was out of focus. The cleanliness of the after test photo, as compared with the before test photo, is caused by the sample cleaning between photos. Since this technique is most sensitive to particles, it shows very little of the "thin film" type contamination.

A sample of the holographic results is shown in Figure 19. The top photos are normal photographs of the actual sample, while the bottom photos are photographs of the images produced by the holograms. It is apparent that there is as much information obtainable from the holographically produced photo as from the actual sample photograph.

32
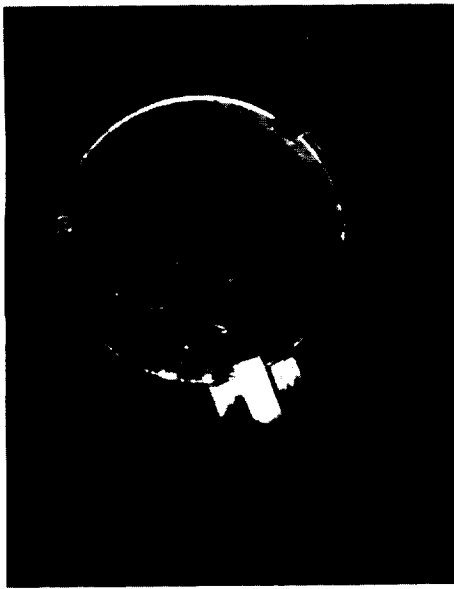
Normal Photos

1B3   2B3
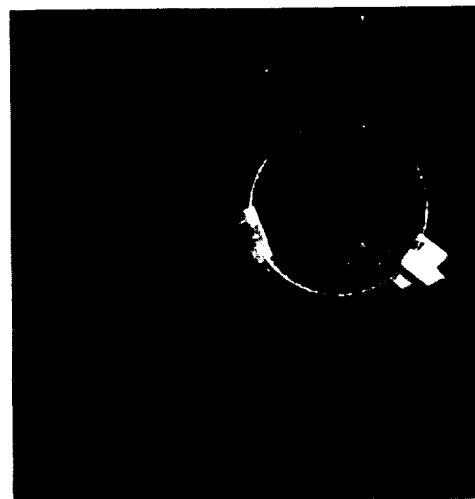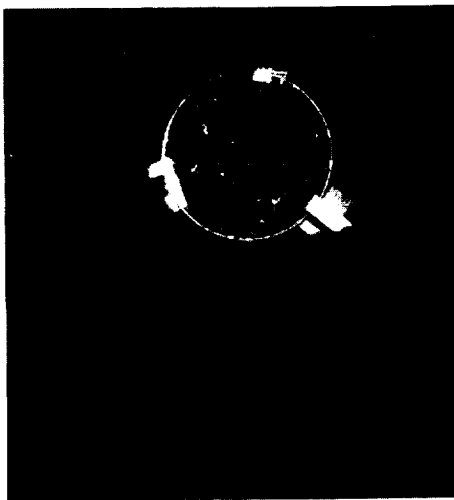
Holographically Produced Photos

Figure 19. Normal and holographically produced photos.
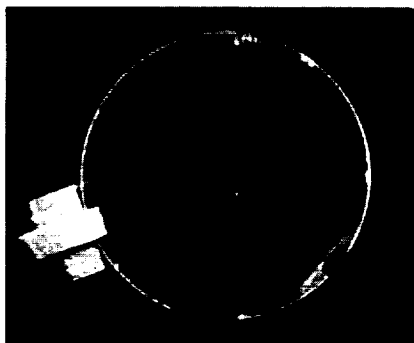
Before Test   After Test

Figure 20. Normal photo, before and after, sample 3B3.
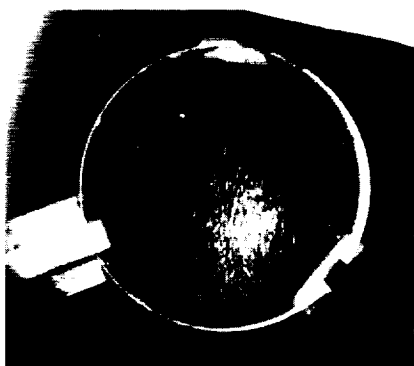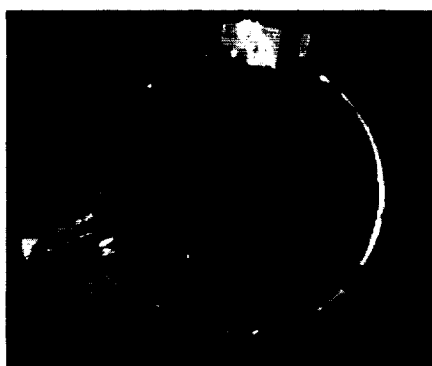
Before Test   After Test

Figure 21. Normal photo, before and after, sample 4B3.
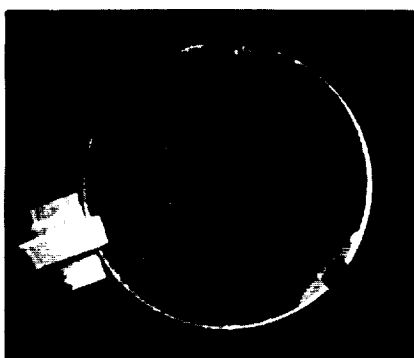
Before Test   After Test

Figure 22. Normal photo, before and after, sample 5B3.
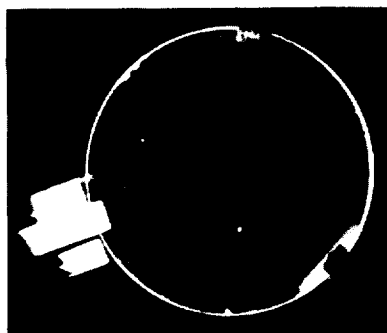
Before Test   After Test

Figure 23. Normal photo, before and after, sample 6B3.
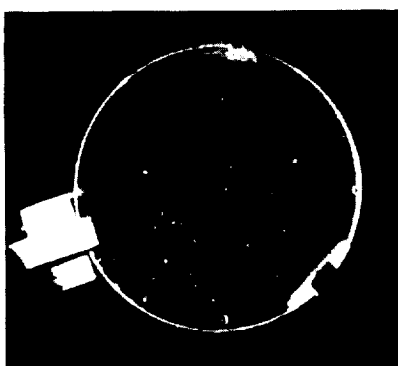
Before Test   After Test

Figure 24. Normal photo, before and after, sample 7B3.
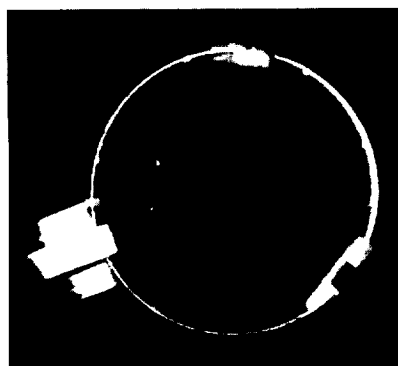
Before Test   After Test

Figure 25. Normal photo, before and after, sample 3B1.

Before Test   After Test

Figure 26. Normal photo, before and after, sample 4B1.
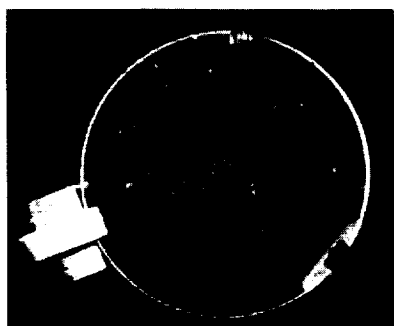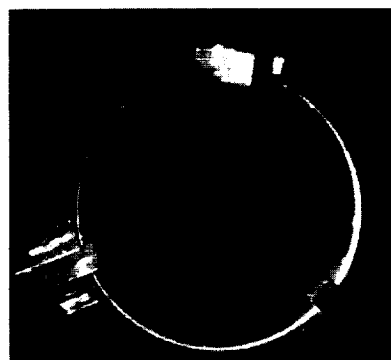
Before Test   After Test

Figure 27. Normal photo, before and after, sample 5B1.
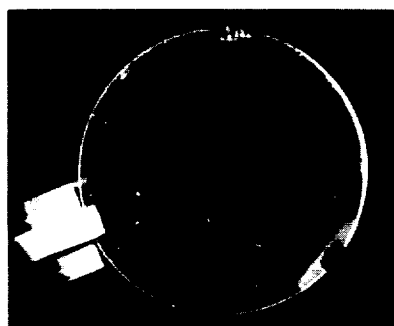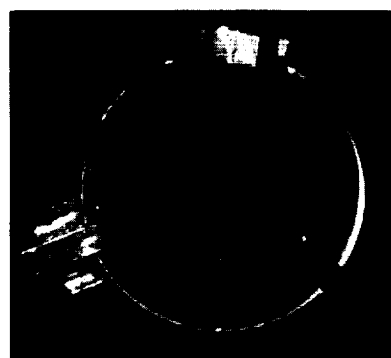
Before Test   After Test

Figure 28. Normal photo, before and after, sample 6B1.
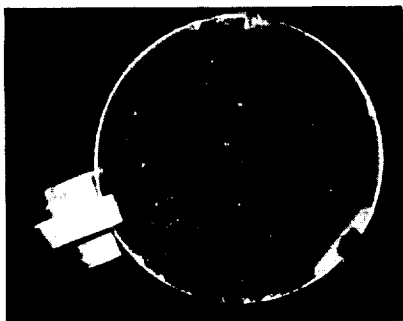
Before Test   After Test

Figure 29. Normal photo, before and after, sample 7B1.

Before Test   After Test

Figure 30. Dark field photo, before and after, sample 3B3.
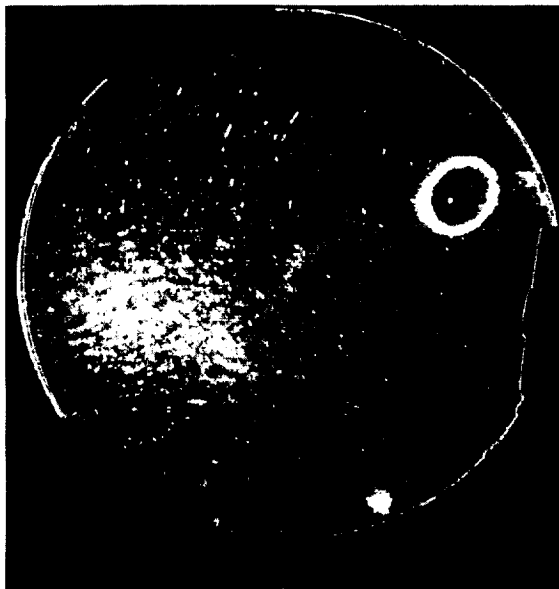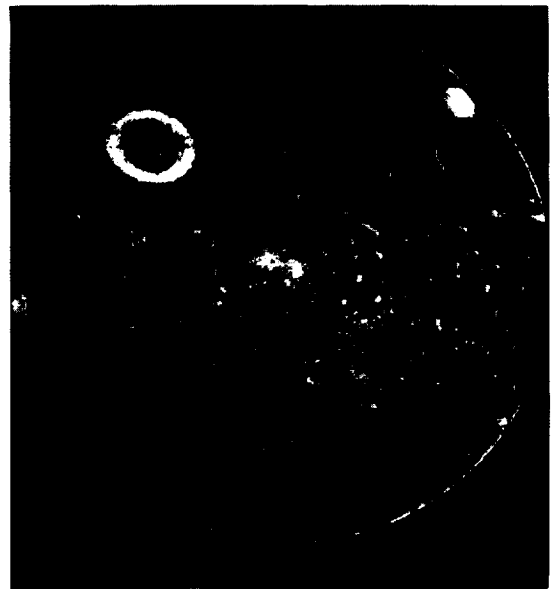
Before Test   After Test

Figure 31. Dark field photo, before and after, sample 4B3.
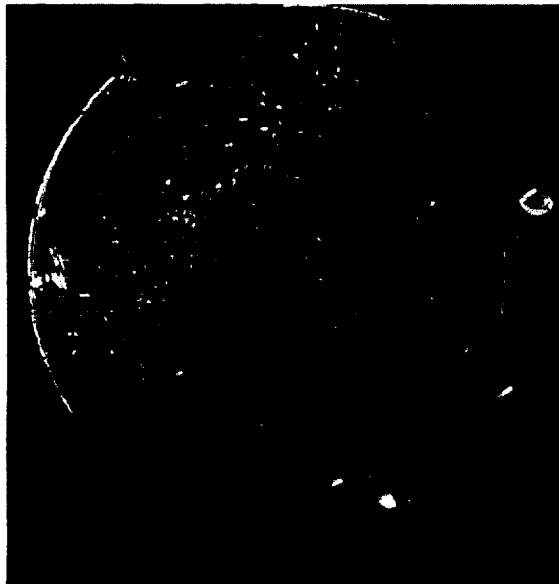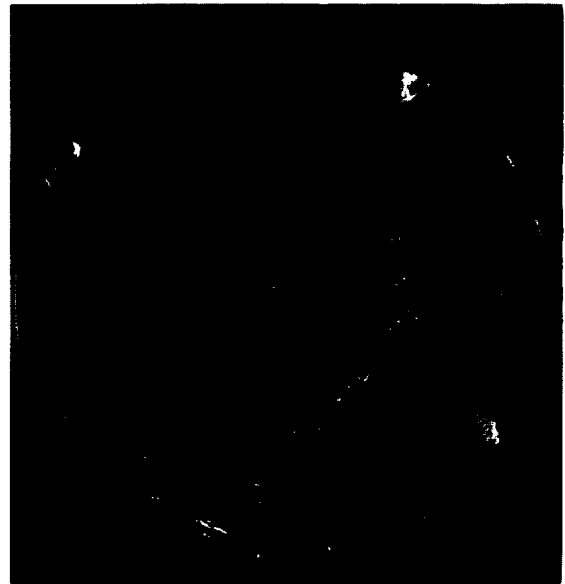
Before Test   After Test

Figure 32. Dark field photo, before and after, sample 5B3.

38

Before Test   After Test

Figure 33. Dark field photo, before and after, sample 6B3.
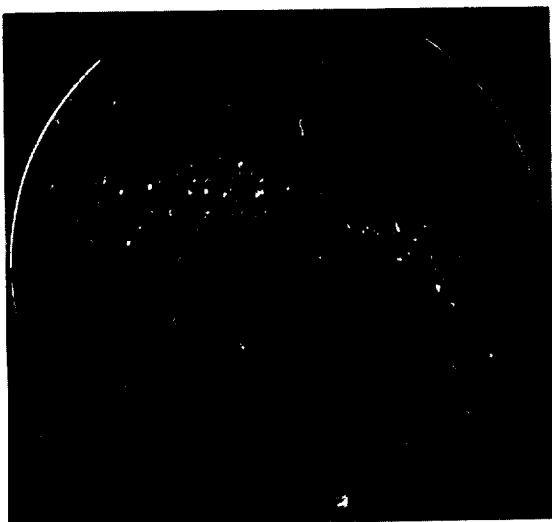
Before Test   After Test

Figure 34. Dark field photo, before and after, sample 7B3.
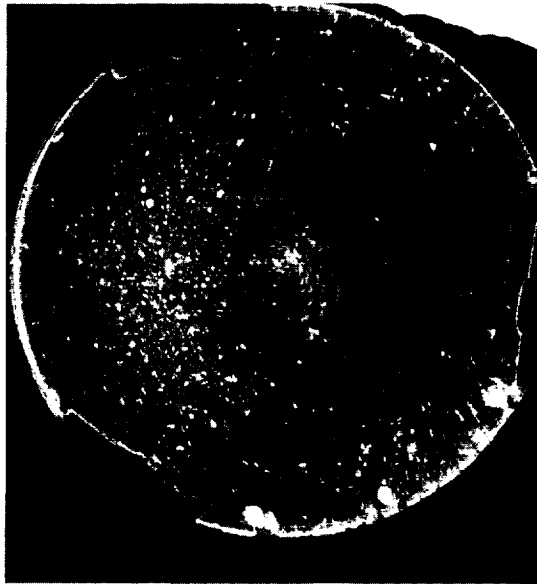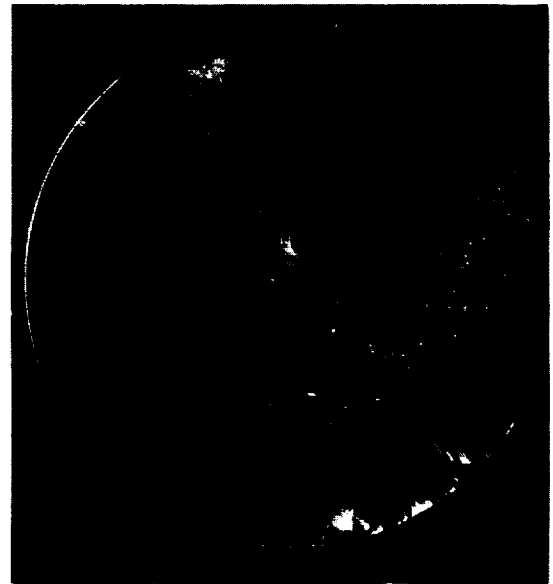
Before Test   After Test

Figure 35. Dark field photo, before and after, sample 3B1
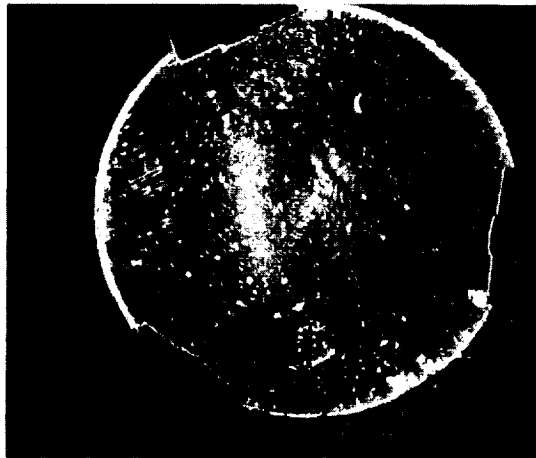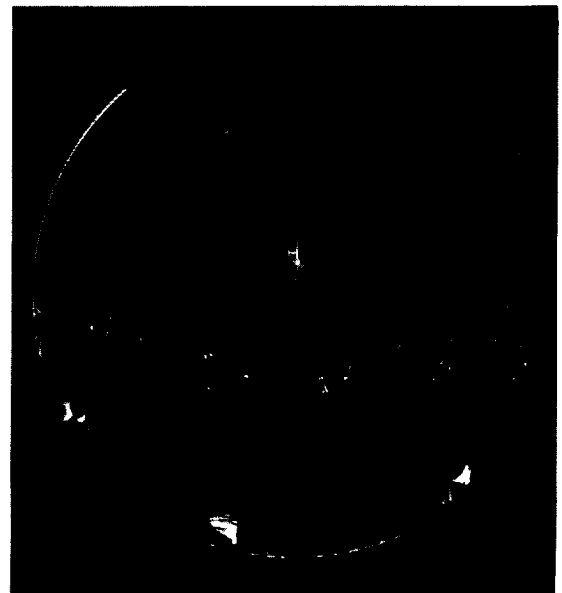
Before Test   After Test

Figure 36. Dark field photo, before and after, sample 4B1
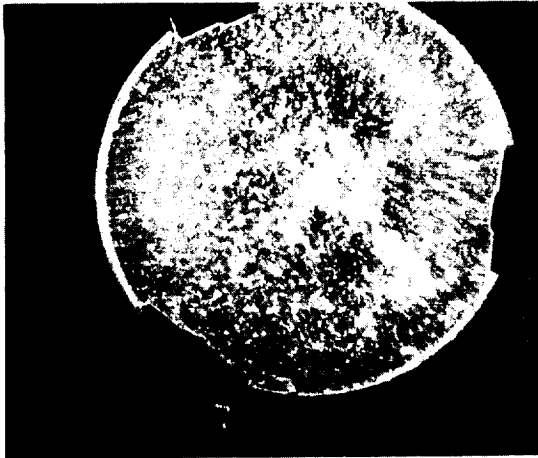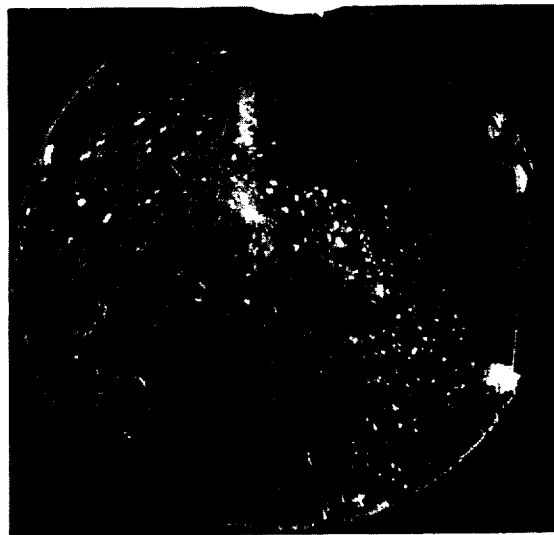
Before Test   After Test

Figure 37. Dark field photo, before and after, sample 5B1.
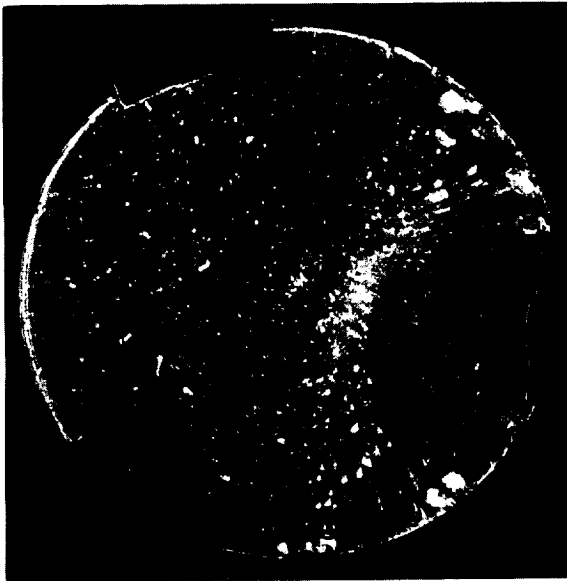
Before Test   After Test

Figure 38. Dark field photo, before and after, sample 6B1.
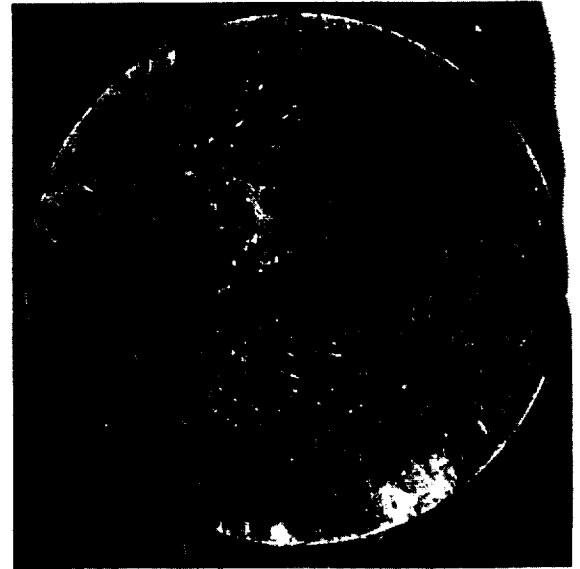
Before Test   After Test

Figure 39. Dark field photo, before and after, sample 7B1.

The results obtained from these three tests indicate that they are worthwhile tests for studying contaminates. The normal photography is an obvious asset in most testing techniques, but the dark field photography and holography have shown that they too can be extremely useful. As indicated previously, the dark field method is primarily used for particles and when properly designed has a sensitivity to particles down to submicron size. This was not demonstrated in these test results because of the poor quality of some of the optical components, a problem which can be eliminated.

The holography has demonstrated that it can be used as a storage technique. The information on the optical sample can be "stored" in a hologram and studied at a later date by reconstructing the sample image. Other techniques for obtaining information from the holograms are still under investigation.

INTERFEROGRAMS — W. W. Moore

In support of the objective of measuring the optical properties changes due to contaminant deposition, measurements of the surface deposit thickness were made by a multiple beam interferometer.

42

The A-Scope Multiple Beam Interferometer provides an absolute measure of microscopic vertical surface variations in the range from 30 to 20 000 Angstrom units. Accuracy is normally ± 30 Å. This can be improved to ± 10 Å for measurement of thin films on smooth specimens.

This instrument employs a sodium vapor lamp and optics to direct light through a specially coated Fizeau plate, which makes contact with the specimen at a slight angle and forms an air wedge. An interference fringe pattern is produced in the air wedge and viewed through a filar eyepiece. The spacing and shape of the fringe lines are interpreted to determine an extremely accurate contour map of the specimen surface. For record keeping, photo interferograms were taken with a Polaroid camera attachment.

Because the specimen must have a high reflectivity (over 90 percent) if one is to achieve maximum quality (sharp, dark, narrow) fringe lines, the specimen area of interest was overcoated as shown with an opaque, vacuum-deposited layer of aluminum about 1300 Å thick. (1000 Å is recommended.)

Careful experiments have shown that a reflective overcoat deposited at normal incidence will follow the contours of the specimen so faithfully that it will not invalidate the measurements.

The actual steps to the experimental method execution on the Angstrometer-Scope are as follow:

1. Establish an interference fringe pattern (described later).

2. Align fringe pattern parallel to field-of-view reticle lines and hairline.

3. Record position readings, while moving hairline always in the same direction, of two adjacent lines plus the associated offset line — A, B, and C of Figure 40.

4. Calculate fringe SPACING and OFFSET in "filar units" as shown in these formulas:

$$\text{SPACING (filar units)} = B + (100 \times \text{number of reticle lines crossed by the hairline}) - A$$

$$\text{OFFSET (filar units)} = C + (100 \times \text{number of reticle lines crossed by the airline}) - A$$

43

Example (Fig. 40):

$$\text{SPACING} = 75 + (100 \times 3) - 30$$

$$= 345 \text{ filar units}$$

$$\text{OFFSET} = 45 + (100 \times 5) - 30$$

$$= 515 \text{ filar units}$$
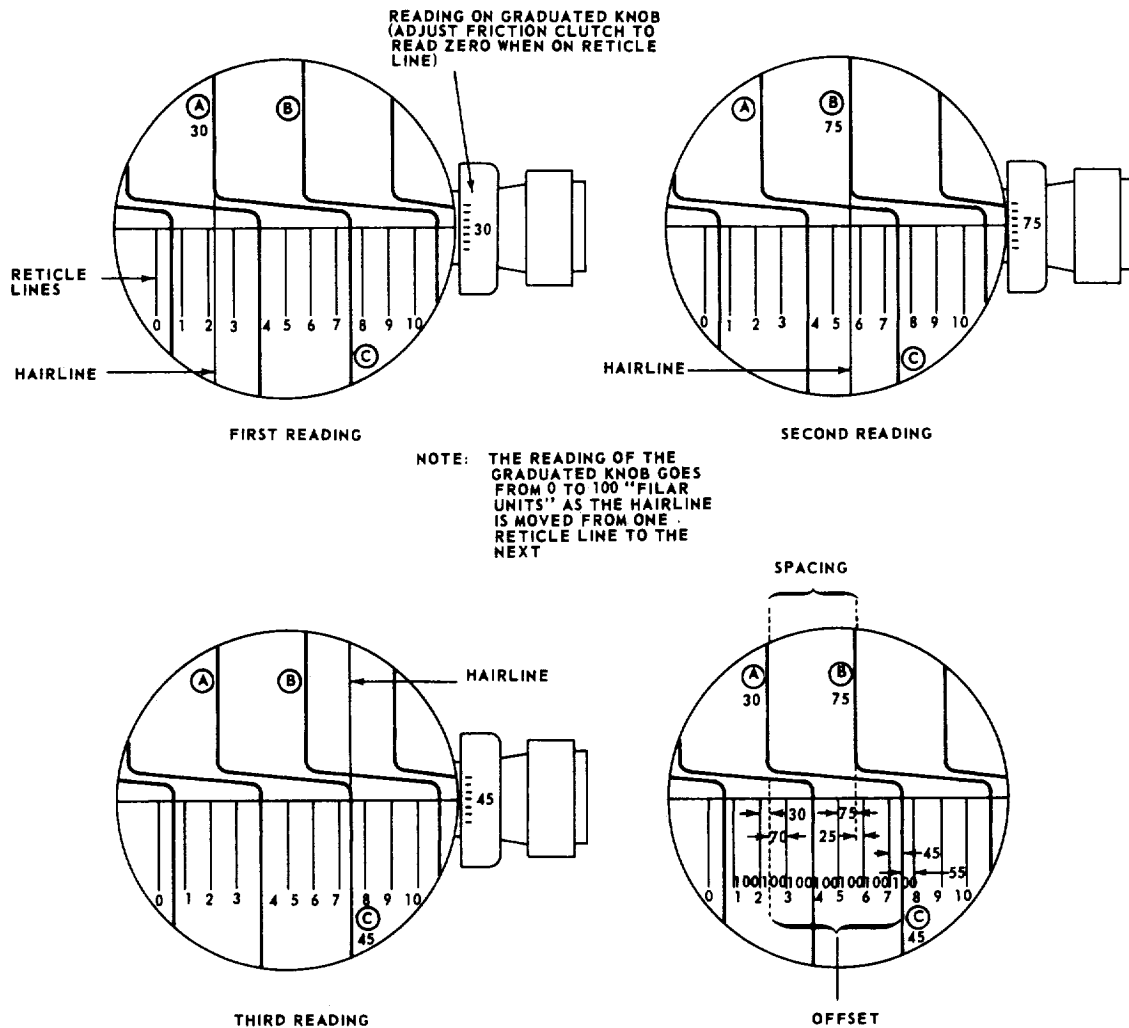
Figure 40. Measuring fringe line offset (Reference 8).

5. Calculate the thin film thickness in Angstrom units. The under-
lying principle of measurement is the fact that the fringe line SPACING is
always equivalent to 2946 Å (one-half of the wavelength of the sodium vapor
light source), even though the actual spacing in inches will change as the
Fizeau plate tilt angle is varied. The amount of fringe line OFFSET created
by a surface variation is directly related to the height of the surface variation.
The actual height is determined by measuring OFFSET in relation to the
2946 Å SPACING of the fringe lines as shown below.

GENERAL FORMULA

$$\frac{\text{Fringe OFFSET (filar units)}}{\text{Fringe SPACING (filar units)}} \times 2946 \text{ Å} = \text{Height of Surface Variation (A)}$$

The instrument employs a sodium vapor lamp with an effective wave-
length of 5892 Angstrom units (5892 Å is a weighted average, based on the
relative intensities of the 5890 Å and 5896 Å sodium vapor "D" lines). The
light is directed to a Fizeau plate as shown in Figure 41.

The Fizeau plate contacts the specimen and is tilted at a slight angle to
form an air wedge. The interference fringe pattern produced in the air wedge
is transmitted through the Fizeau plate to a filar eyepiece. The pattern is
measured by alignment with the eyepiece hairline, whose movement is
indicated in arbitrary units on a graduated knob.

Spatial relationships between the specimen, the Fizeau plate, and the
fringe line pattern are shown in Figures 42 and 43. A three-dimensional view
is shown in Figure 42. Figure 43 shows how the air wedge thickness and angle
determine location of the fringe lines. Notice how the vertical distance between
fringe lines is one-half wavelength (2946 Å). Thus, fringe line SPACING is
equivalent to 2946 Å.

An interference fringe pattern is formed between the Fizeau plate and
specimen when a series of reflected light beams (up to 60) all meet at once
at point "A" as indicated on Figure 44. As the light beams converge, phase
interference produces a fringe line.

It is desirable to minimize the air wedge thickness (t) (Fig. 44)
to improve fringe line resolution. To achieve this, the A-Scope Fizeau plate
is a small diameter (0.150 inch, 3.8 mm) and the field of view, as seen
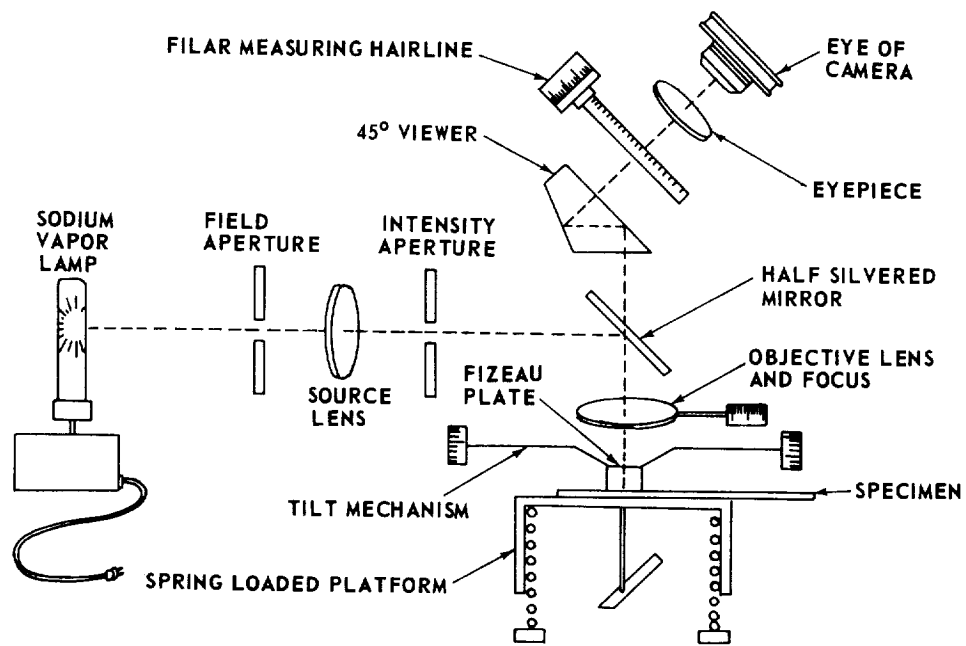
Figure 41. Schematic of optical elements (Reference 8).
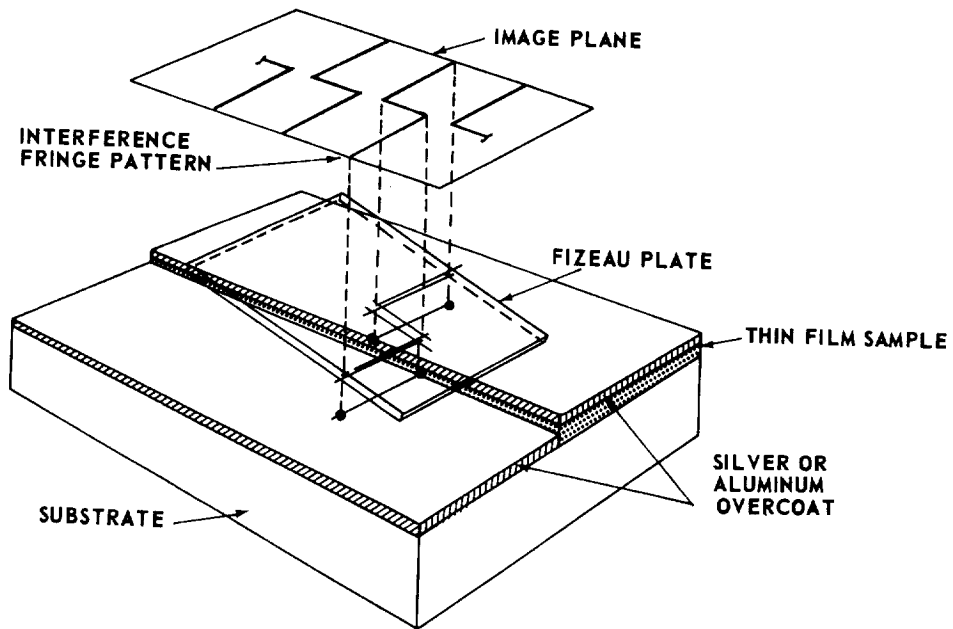
Figure 42. Three-dimensional view of specimen, Fizeau plate and fringe line pattern (Reference 8).

46
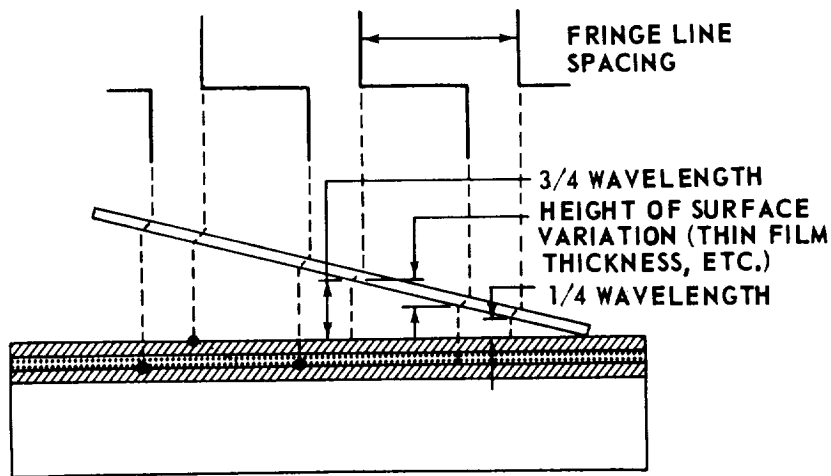
Figure 43. Air wedge thickness and angle determine location
of fringe lines (Reference 8).
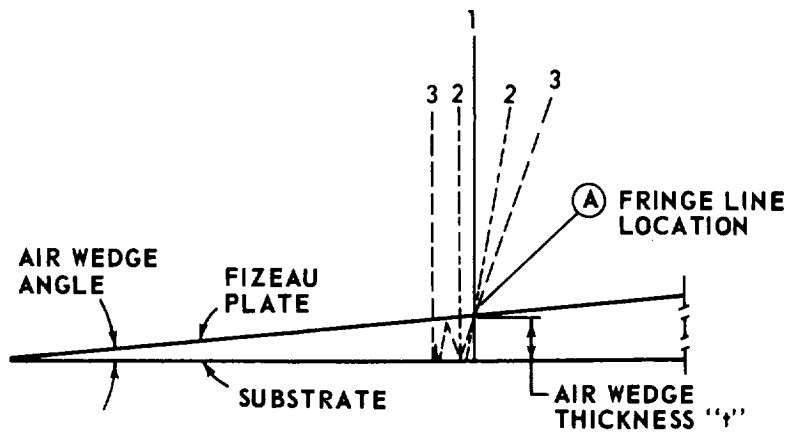
Figure 44. Forming interference fringe pattern (Reference 8).

through the eyepiece, extends to the outer edge of the plate. Thus, one edge
of the field of view is the contact point on the specimen and t is minimized.

Figure 44 also shows why a highly reflective specimen and Fizeau
plate are required (the A-Scope Fizeau plate has 94 percent reflectivity).
Since the light beams must reflect many times before meeting at point "A,"
low reflectivity would reduce the total number of beams forming a fringe and

would result in broader fringe lines and less accurate measurements. It follows also that absorption must be low to conserve the intensity of the light beams. The A-Scope Fizeau plate has an extremely low absorption factor of less than 0.2 percent.

As stated previously, the underlying principle of measurement is the fact that the fringe line SPACING in every surface pattern is equivalent to one-half wavelength (2946 Å). The actual height of the surface variations is determined by the ratio of the fringe line OFFSET and SPACING, where it is known that the SPACING is a constant 2946 Å, no matter what the actual distance between fringe lines.

Because it was empirically determined to be necessary to reflectively overcoat the contaminated optics, only sample 7B2 was measured. In addition, as was indicated by the transmission measurements, there was little difference between the deposit which accumulated under the covering aluminum foil and that accumulated on the exposed portion of the optic. Thus, it was found the deposit thickness could only be measured by establishing an interference fringe pattern on the edge between the deposit and the circumference band of the mirror which had been covered by the optic test mount. Thus, in Figure 45 the edge offsets will be noted to have a distinct curvature. In addition to this feature, another set of fringe offsets is noted which was produced by masking during overcoating for reference purposes.

Since it was known from photomicrograms and other analyses that the deposits have a granular, crystalline structure, a uniform thickness was not expected. In fact, as given in Table 7, the measurements made on sample 7B2 ranged from 589 to 796 Å, with an approximate accuracy of ± 50 Å.

TABLE 7. MEASUREMENTS OF DEPOSIT THICKNESS

Overcoat Measurement	A	B	C	Value	Deposit Measurement	A	B	C	Value
One	4/05	4/48	4/23	1233A	One	4/38	4/91	4/52	778A
Two	4/47	4/94	4/68	1316A	Two	6/02	5/92	5/55	796A
Three	5/82	6/33	6/01	1133A	Three	6/95	7/50	7/06	589A
Four	7/23	7/69	7/39	1571A	Four	7/50	8/07	7/61	596A
·Average				1313A	Average				690A
Estimated Accuracy				±50A	Estimated Accuracy				±50A

48
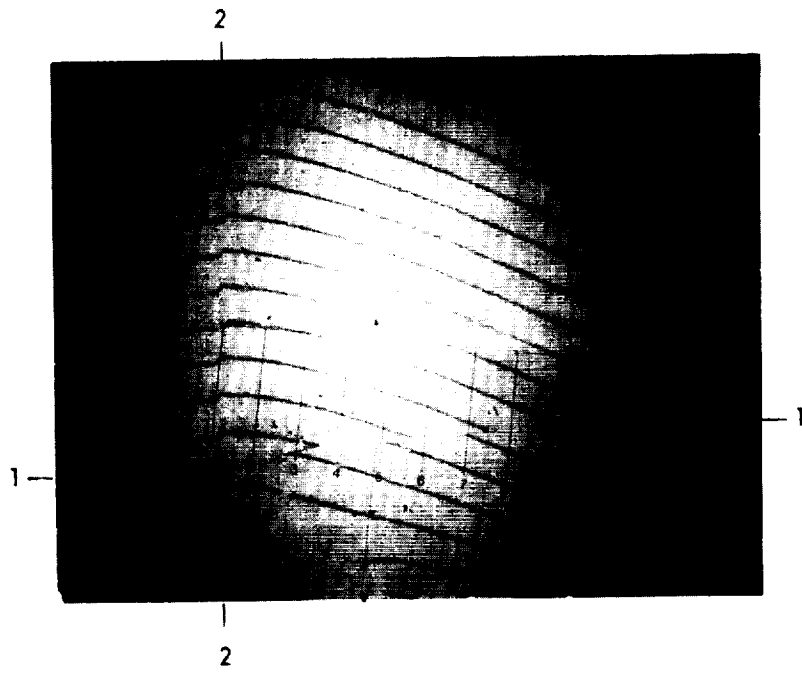
(a)
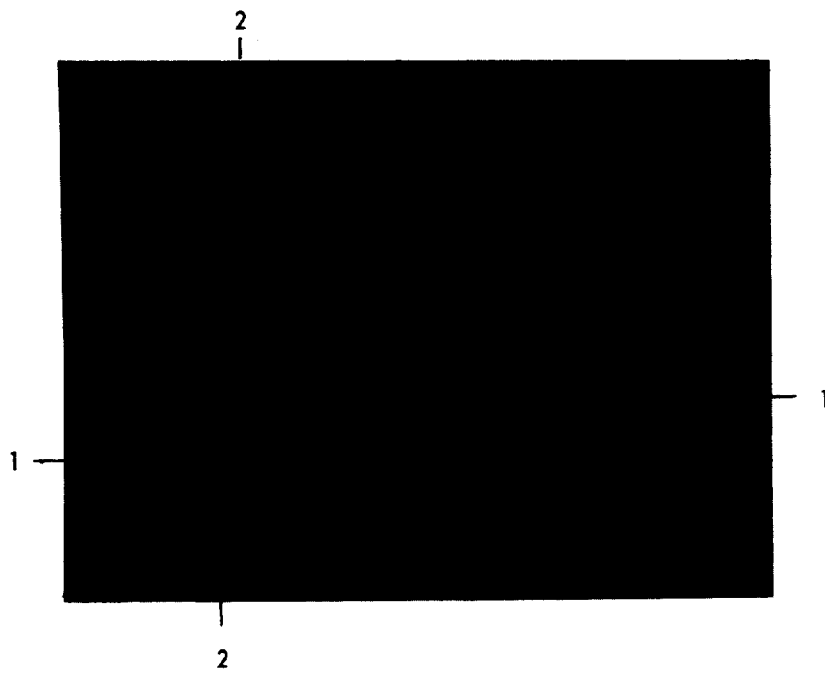
(b)

Figure 45. Interferograms of sample 7B2.

Optical/Compositional Evaluation

NEAR ULTRAVIOLET/VISIBLE/NEAR INFRARED
REFLECTION — J. M. Zwiener

Measurements of the change of reflectance were performed on several of the aluminum coated and one of the gold coated fused quartz disks. Wavelength region covered was roughly from 2000 Å (200 nm) to 2.5 microns (2500 nm) with measurements of changes in total hemispherical reflectance and decrease in specularity. These two measurements were combined and used to demonstrate how a typical reflectance curve of a corresponding aluminum or gold surface is effected by exposure to RCS engine contamination under the defined test parameters.

The optical coating selected for use in this (200 to 2500 nm) wavelength region was aluminum because of its high reflectance, extensive usage as an optical surface, ease of coating, and the considerable experience which has been obtained with it as a contaminant monitoring coating. Selection of the substrate was for similar reasons and consisted of fused quartz disks approximately 1 inch (254 cm) in diameter, 0.125 inch (0.32 cm) thick, with a surface figure of a quarter wave. The coating consisted of a high purity aluminum wire (99.99 percent) deposited onto the substrate with a hot tungsten filament. Surface cleaning of the quartz substrate before coating consisted of an ultrasonic cleaner with distilled water and a detergent solution, then rinsed in distilled water and heated trichloroethylene, with a final cleaning in hot ethyl alcohol vapor as described by Holland [9]. In the vacuum coater glow discharge cleaning was used before coating deposition. Glow discharge was maintained for about five minutes at a pressure of 50 microns. Actual coating was carried out at a pressure below 10^{-7} torr. After coating, the reflectances of all the mirrors were compared to a reference mirror as a means of ensuring initially that all samples were identical. The instrument used to perform these measurements and all reflectance-type measurements as described in this section was a Beckman DK2A Ratio-Recording spectrophotometer with a spectroreflectometer attachment. A schematic of the instrument is shown in Figure 46 [10]. As shown in the figure, the monochrometer is a double-pass prism type instrument. Monochromatic radiation is deviated into two different optical paths by the oscillating mirror and focused on the sample positions on the integrating sphere, thereby providing dual-beam type measurements. The integrating sphere is coated on its inner surface with MgO which provides a highly reflective and diffuse surface.
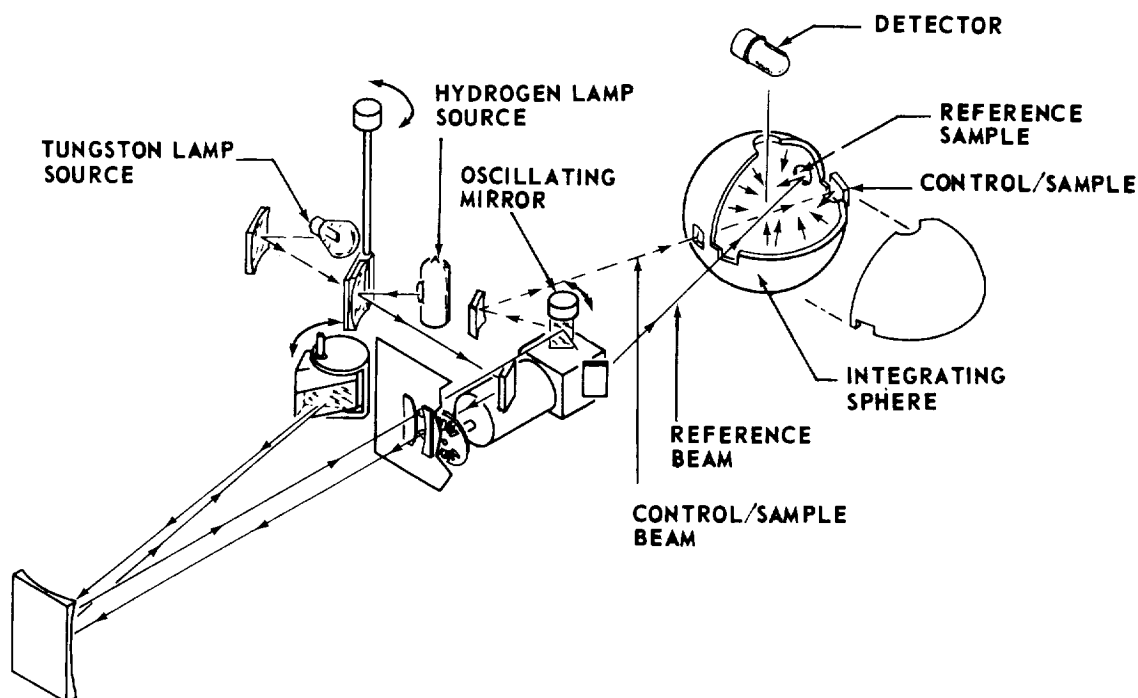
Figure 46. Spectroreflectometer schematic, Beckman DK2A.

This diffused light, or sphere brightness, is detected by the photomultiplier or lead sulfide detector.

A total of 16 mirrors was selected for the test, two per test bed (see previous test bed description). Of these 16, 8 were used as controls and 8 were exposed. Of the 8 mirrors 2 were selected for measurement references and mounted on test bed No. 2 which was stored in a "clean room." Actual measurements are made by comparing the reflected energies from two mirrors in the position as shown in Figure 46. One mirror was coded 2A2 and used in the "reference" position, while the other mirror was coded 2A1 and used in the "control" or "sample" position. The ratios of the reflected energies from these two mirrors were used to establish a reference curve to which the ratios of reflected energies of all other samples to the reference (2A2) mirror were compared. In this manner, the change in reflectance can be measured. Table 8 provides a breakdown of optical measurements performed before and after the test on various samples. Before test measurements are made to ensure that all mirrors are identical to the control (sample 2A1) or establish differences for use in later data analysis. It is interesting to note that if differences of total hemispherical reflectance between samples exist they are

TABLE 8. SAMPLE SERIES A1/A2 MEASUREMENTS

Sample	Total 360-200		Total 2500-360		Diffuse 360-200		Diffuse 2500-360	
	Before	After	Before	After	Before	After	Before	After
1A1	X	X	X	X				
1A2	X							
2A1	CONTROL			-	X	X	X	X
2A2	REFERENCE			-				
3A1	X		X	X				
3A2	X	X						
4A1	X	X	X	X				
4A2	X							
5A1	X	X	X	X		X		X
5A2	X				X	X		X
6A1	X	X	X	X		X		X
6A2	X	X		X	X	X		X
7A1	X	X	X	X	X	X		X
7A2	X							
8A1	X		X		X			
8A2	X							

in the near ultraviolet, below 360 nm; therefore, all samples were measured below 360 nm and at least one from each test bed was measured over the full wavelength region of the instrument. Diffuse measurements were performed before the test on only a few representative samples. This was done to establish that the diffuse component of the reflected light from a "clean" mirror was insignificant (less than 0.1 percent).

The reduced reflectance data are presented in Figures 47 through 50. Figure 47 shows the percent decrease of reflectance $(\Delta R/R)$ caused by the contamination on the surfaces. As anticipated, the absorption increases in the near ultraviolet, but the amount of increase (up to 80 percent) was surprising. Figure 48 represents the percent increase in the diffuse component of the reflected energy or increase in scatter. In the visible and near infrared, scatter is the predominant mode of degradation, but in the ultraviolet, absorption becomes the dominant mechanism. Figure 49 demonstrates the specular reflectance degradation at near normal incidence. These data represent the loss of reflectance of the specular component of the incident energy, caused by both scatter and absorption. The same general trend in
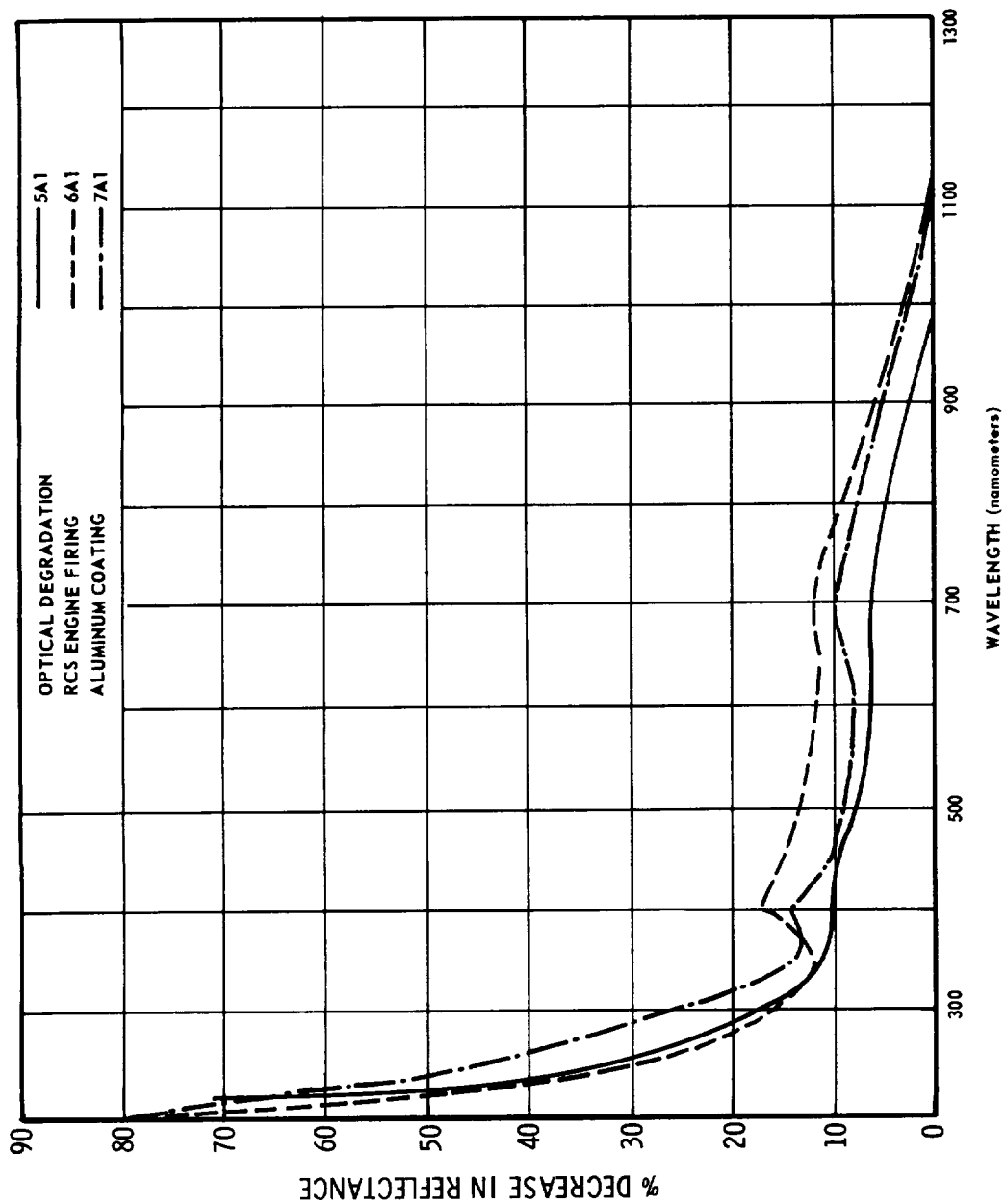
Figure 47. Total hemispherical reflectance degradation, samples 5A1, 6A1, and 7A1.

53
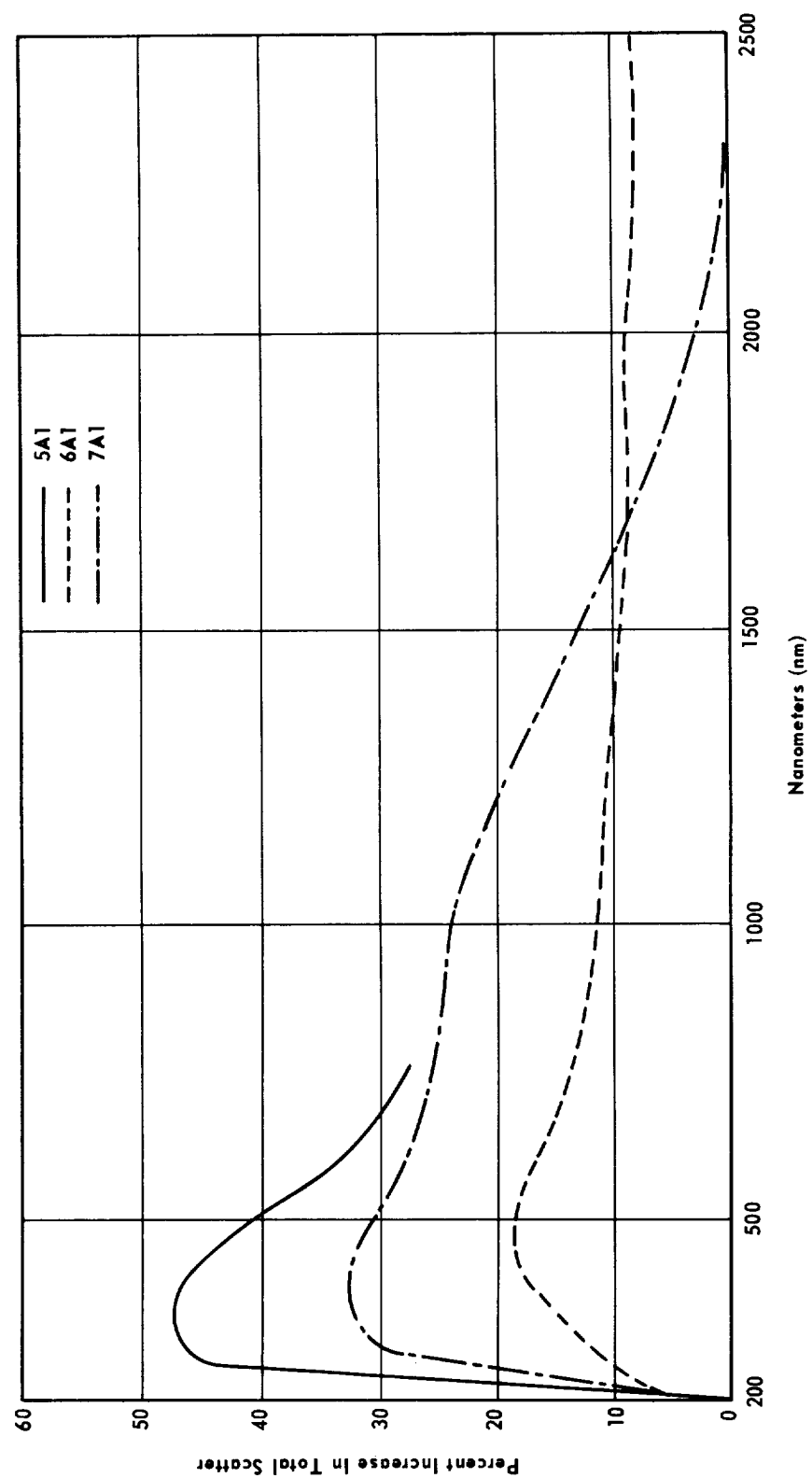
Figure 48. Diffuse reflectance, samples 5A1, 6A1, and 7A1.
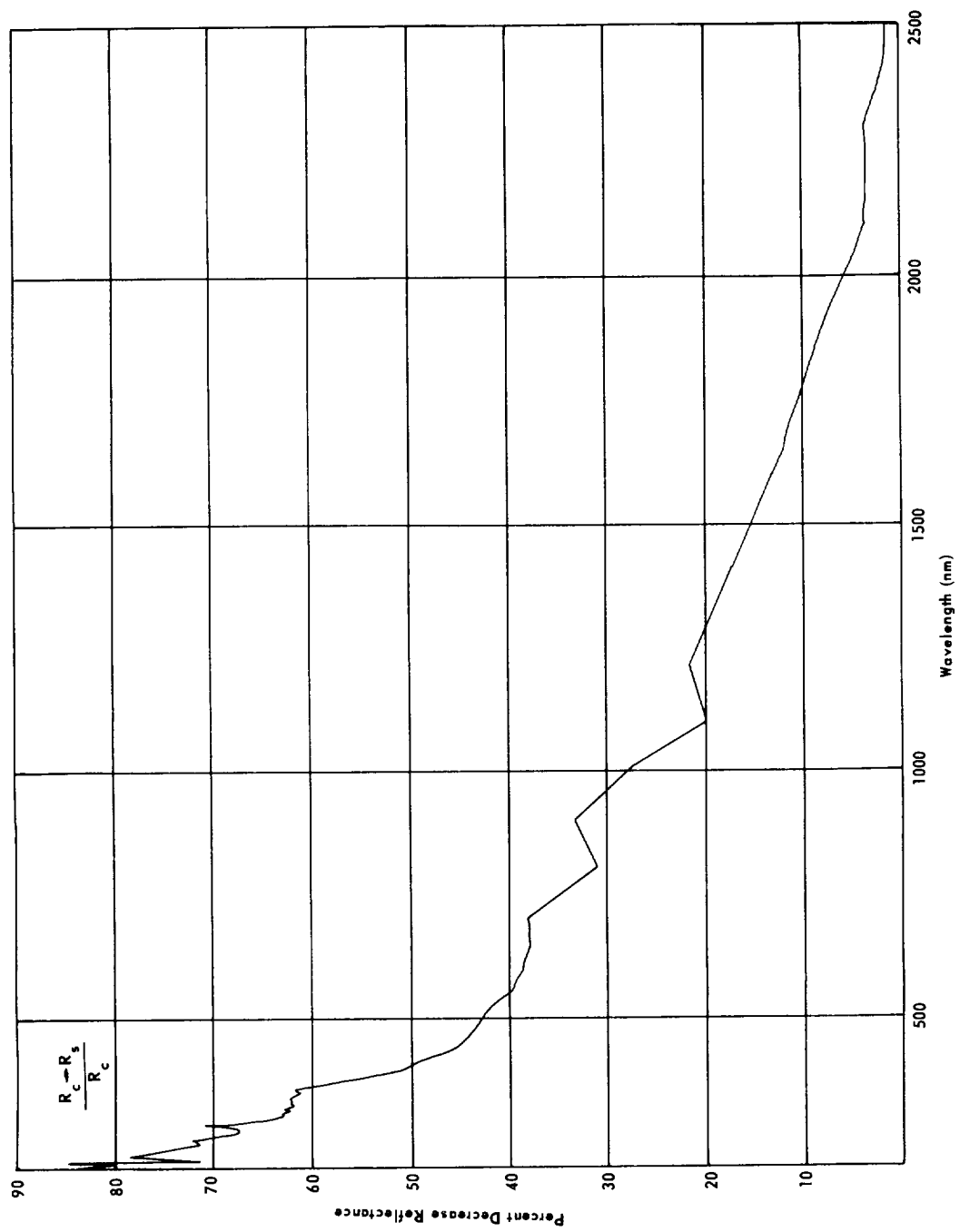
Figure 49. Decrease of specular reflectance, sample 7A1, aluminum (near normal incidence).

55
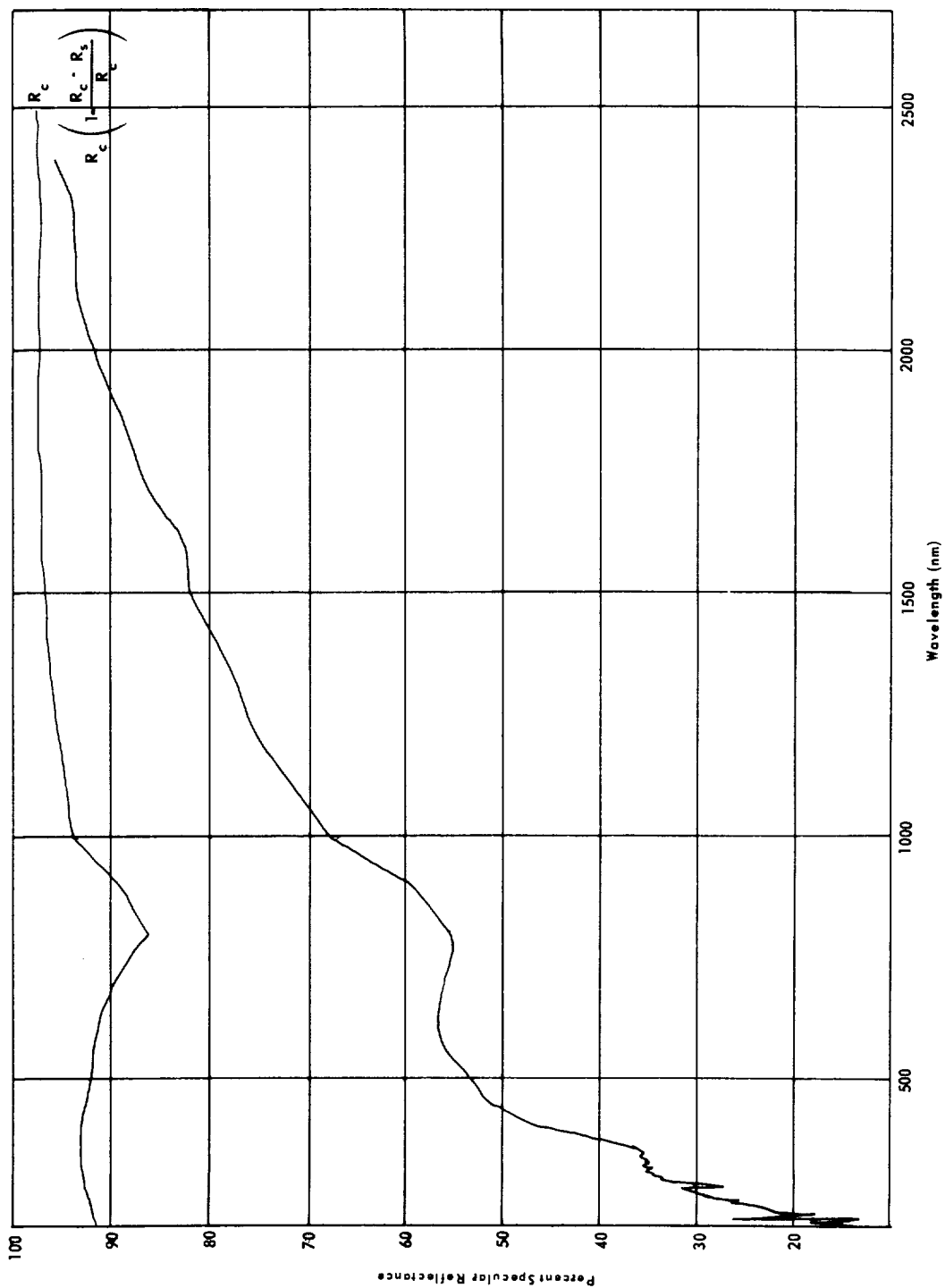
Figure 50. Reflectance degradation of aluminum, sample 7A1 (near normal spectral reflectance).

56

the optical damage with wavelength, toward the ultraviolet, is apparent, but somewhat more severe over the wavelength range covered. Figure 50 is the reflectance of a fresh aluminum coating, as taken from the "American Institute of Physics Handbook," and shows the effects of the specular reflectance loss on this typical reflectance curve. During the time that the measurements were being performed, it was observed that the highly visible contaminant layer was evaporating from the mirror surfaces. Therefore, one of the gold samples (5A3) was selected to study the extent of residual damage remaining after the contaminant sublimed or vaporized. Figures 51 through 54 present the resultant measurements taken 5 weeks after the test, in the same manner as those performed on the aluminum. All measurements on the aluminum were performed within 10 days after the test. Measurements after 3 weeks on sample 5A1 showed a considerable decrease in the visible diffuse damage. It is felt that the reason the aluminum samples display more damage than the gold is only because of the time delay in making measurements on the gold surfaces. By comparing Figures 49 and 53, it can be seen that the damage in the near ultraviolet still exists, while the visible damage has practically vanished and the near infrared damage is no longer detectable. The diffuse reflection curves (Figs. 48 and 52), illustrate a decrease in scatter, caused by the vaporizing of a considerable amount of the contamination from the surface. Measurements of the sample just after the contamination test and over a month later are plotted in Figure 55 for the aluminum sample 6A1. The absorption losses in the ultraviolet still exist but have less structure than before, which is possibly because of the more intense interference effects of the thicker layers. The changes in diffuse damage are plotted (Fig. 56) showing the general trend of time-decreasing visible and near infrared damage.

The final set of curves in this section show the results of putting one of the contaminated aluminum mirrors (sample 6A2) in a "clean" (ion, liquid nitrogen, and sorption pumps) vacuum system and irradiating its surface with ultraviolet irradiation (with a spectral distribution as shown in Figure 57). Reflectance measurements, as presented in Figures 58 through 61 show the damage before irradiating with ultraviolet under vacuum after 100 and 200 hours irradiation. The damage after 200 hours was identical to that after 100 hours. The visible and near infrared damage has all but disappeared while the near ultraviolet damage has persisted and broadened, but decreased in peak magnitude. These effects probably resulted from extensive evaporation (or sublimation) of the contaminant before insertion in chamber and during pump-down to 10^{-8} torr. The loss of some of the contaminants, as shown before in the photomicrographs, results in a decrease of the visible damage. Changes in the near ultraviolet wavelength damage, which the data show, is mainly because of the high energy irradiation effects within the contaminant materials.
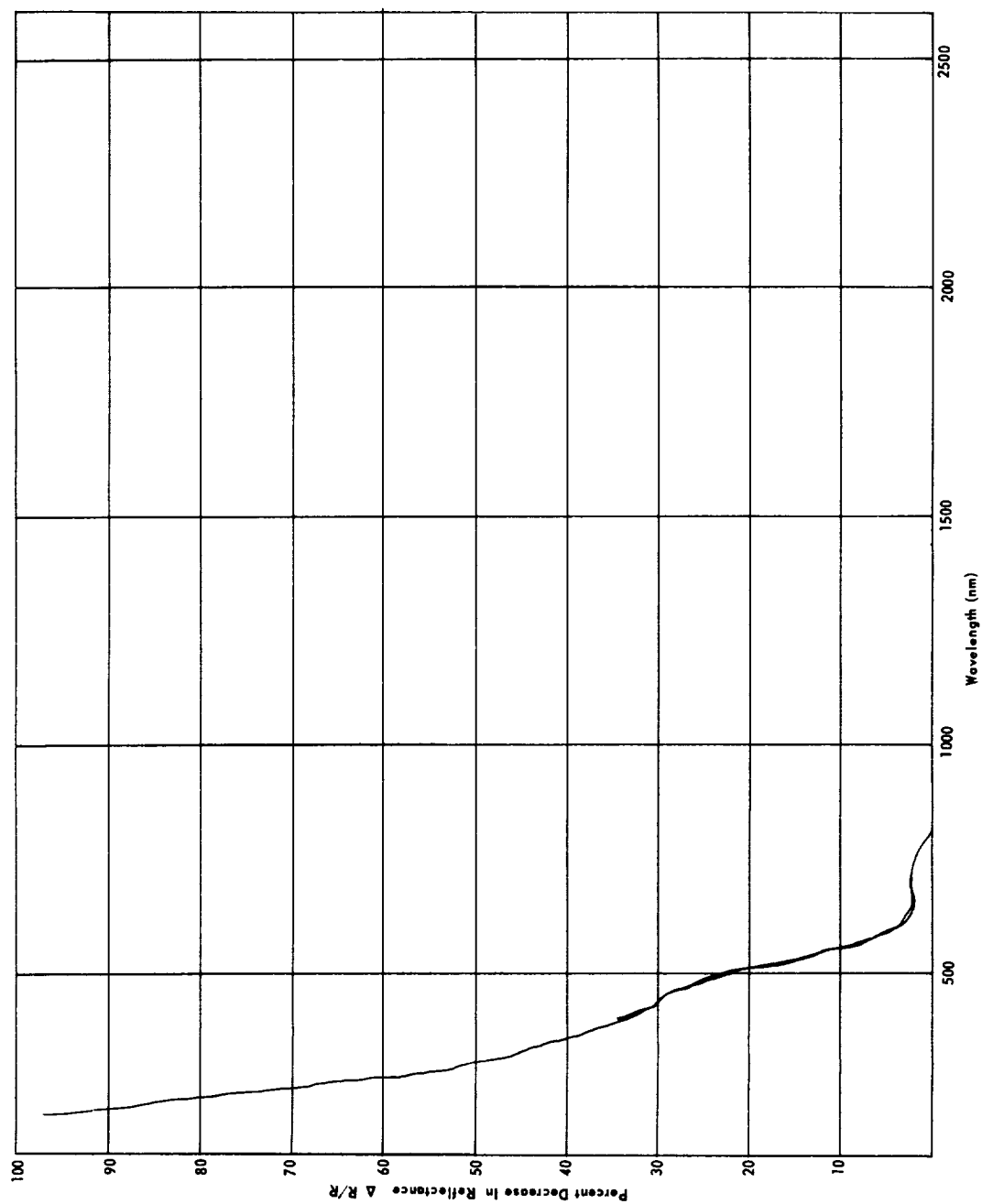
Figure 51. Change of total hemispherical reflectance, sample 5A3, gold (near normal incidence).

58
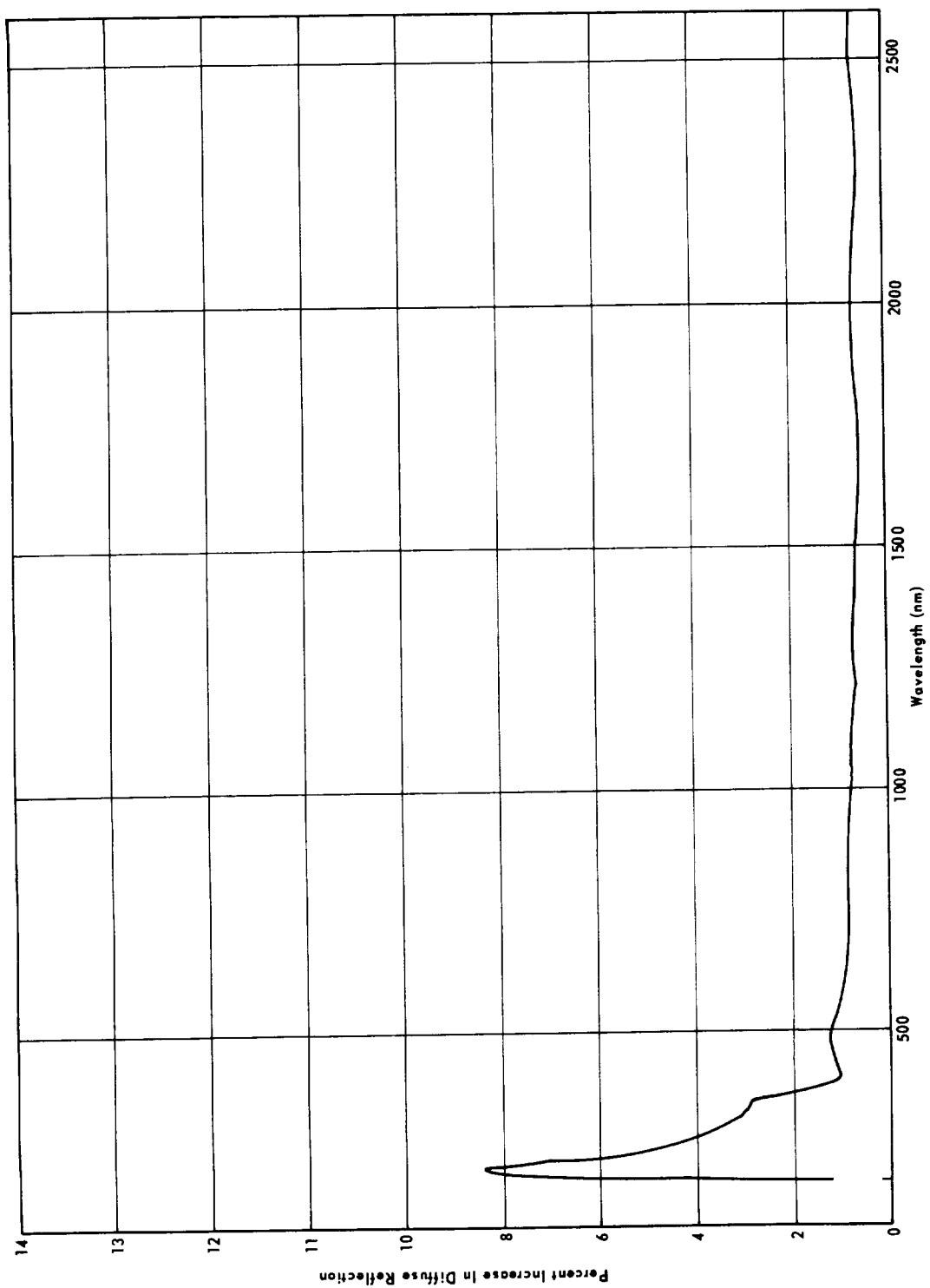
Figure 52. Diffuse reflectance, sample 5A3, gold.

59
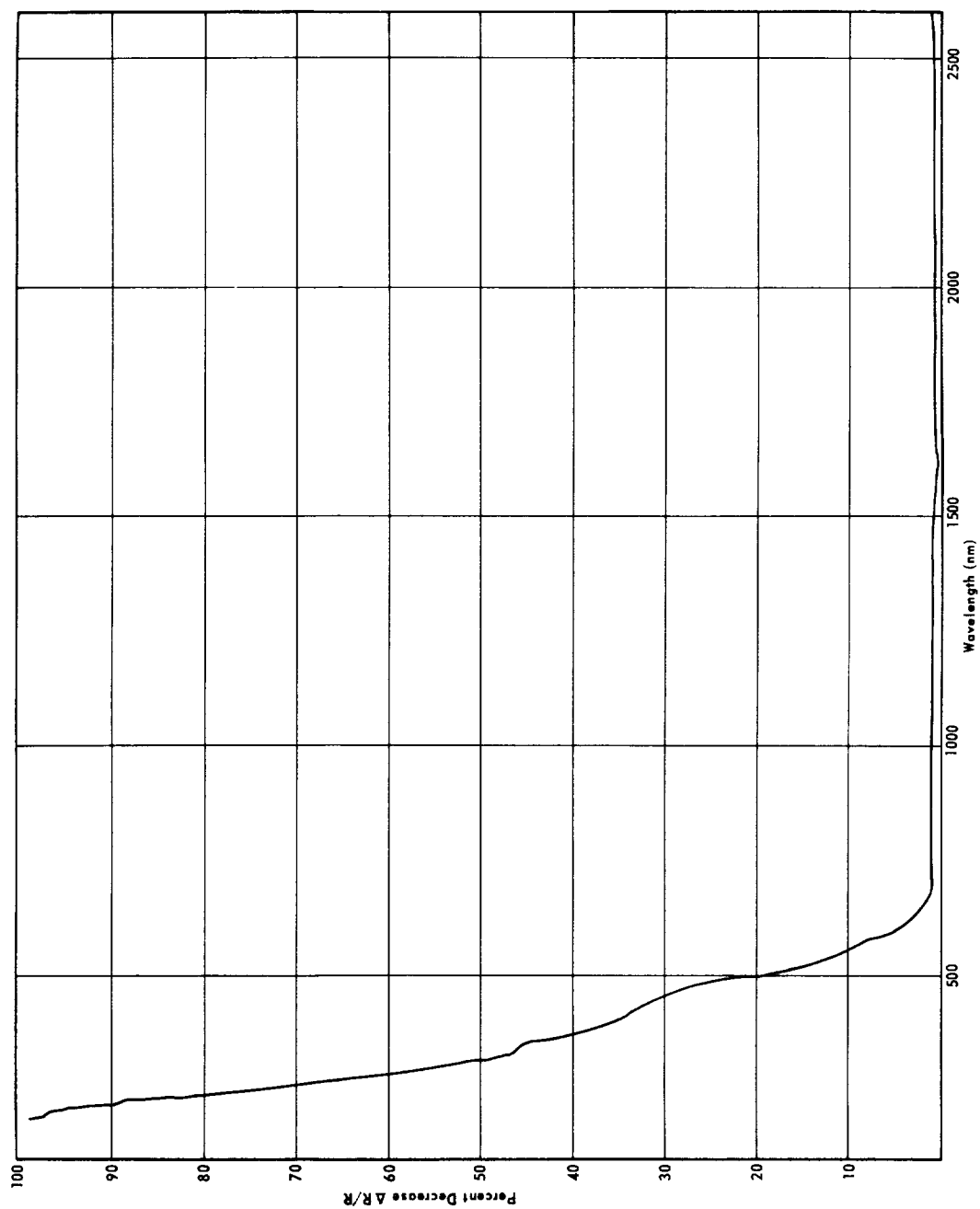
Figure 53. Decrease of specular reflectance, sample 5A3, gold (near normal incidence).

60
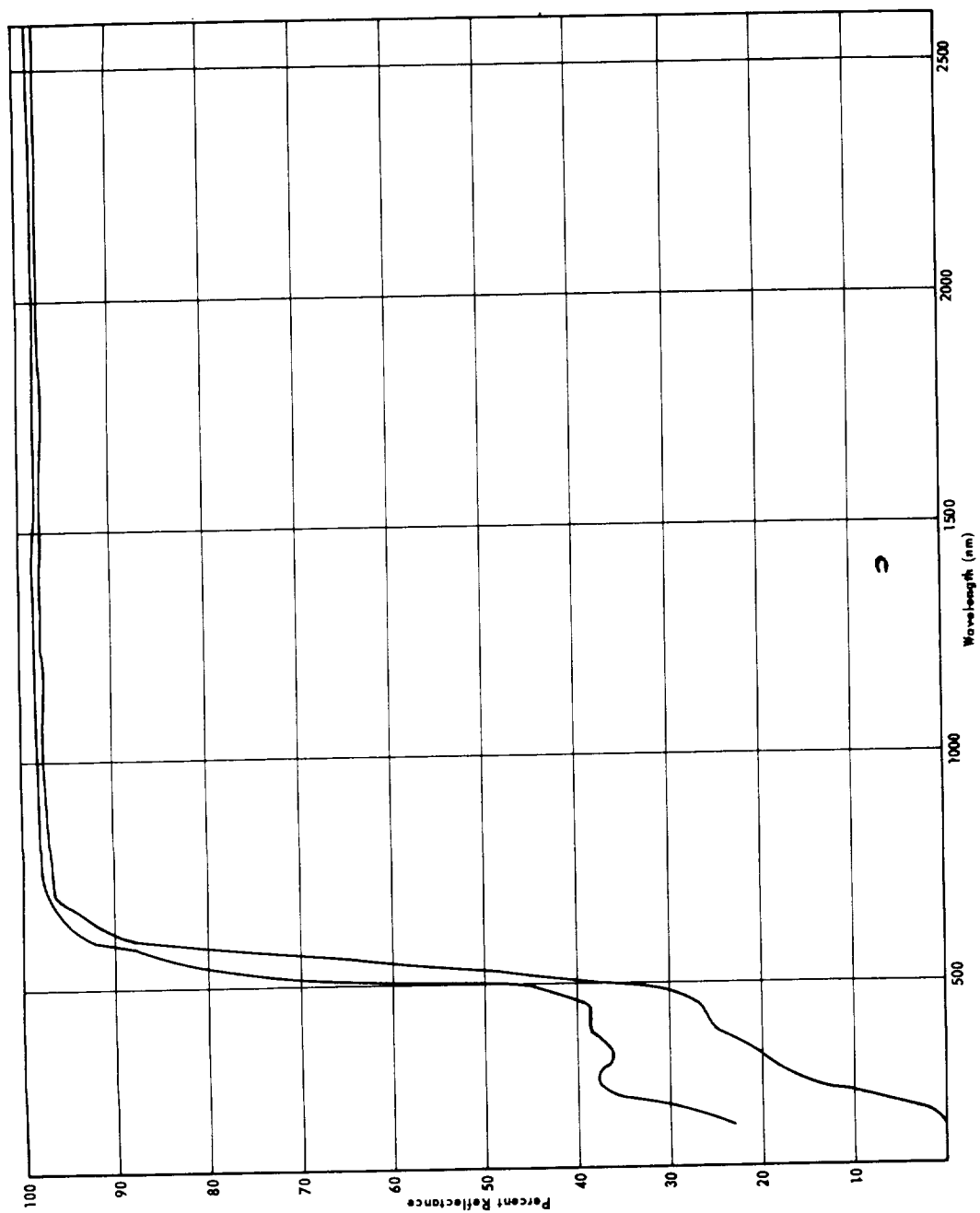
Figure 54. Reflectance, sample 5A3, gold, before and after damage (specular, near normal).

61
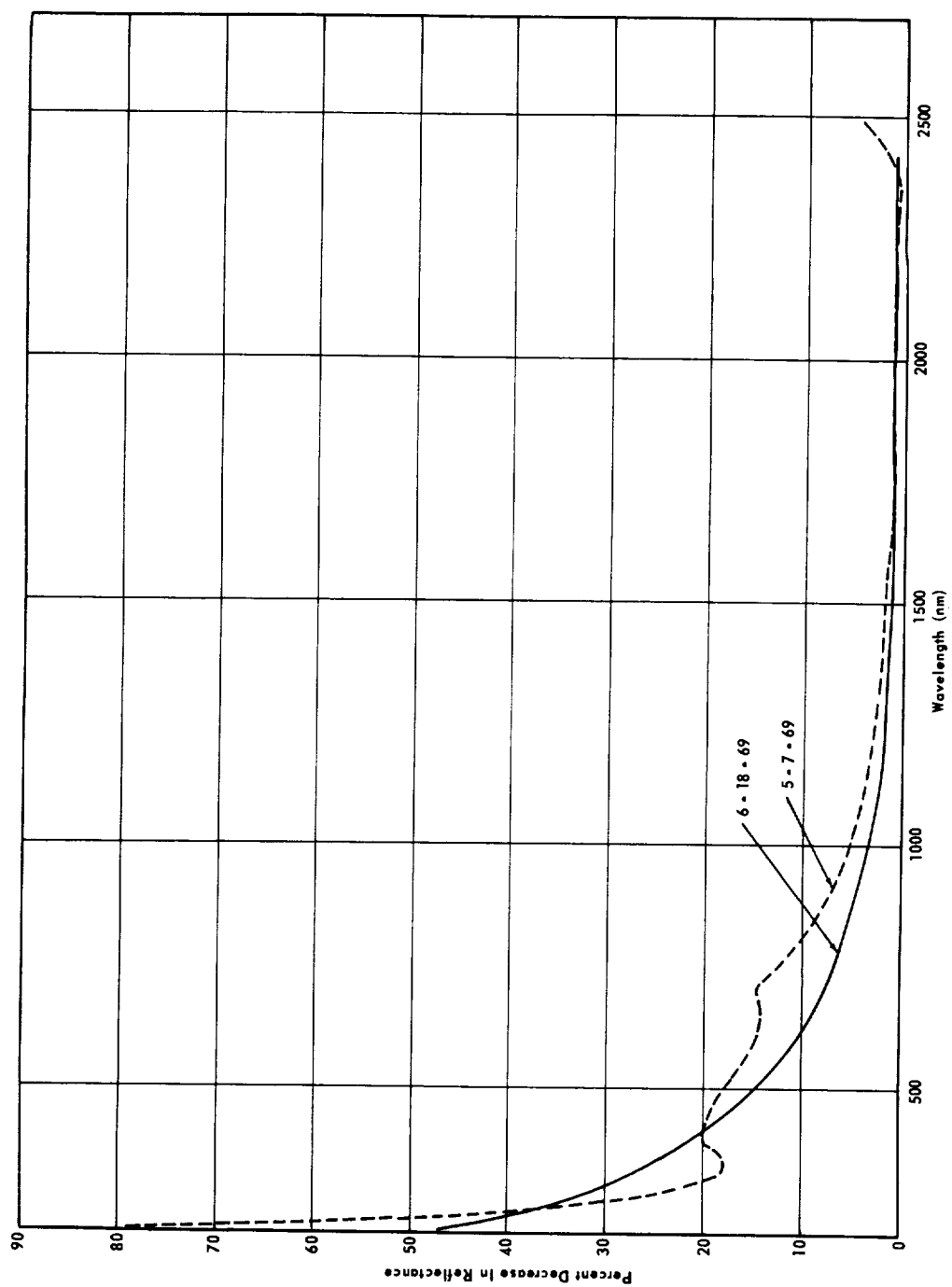
Figure 55. Change of total hemispherical reflectance, sample 6A1, aluminum, effects of aging.

62
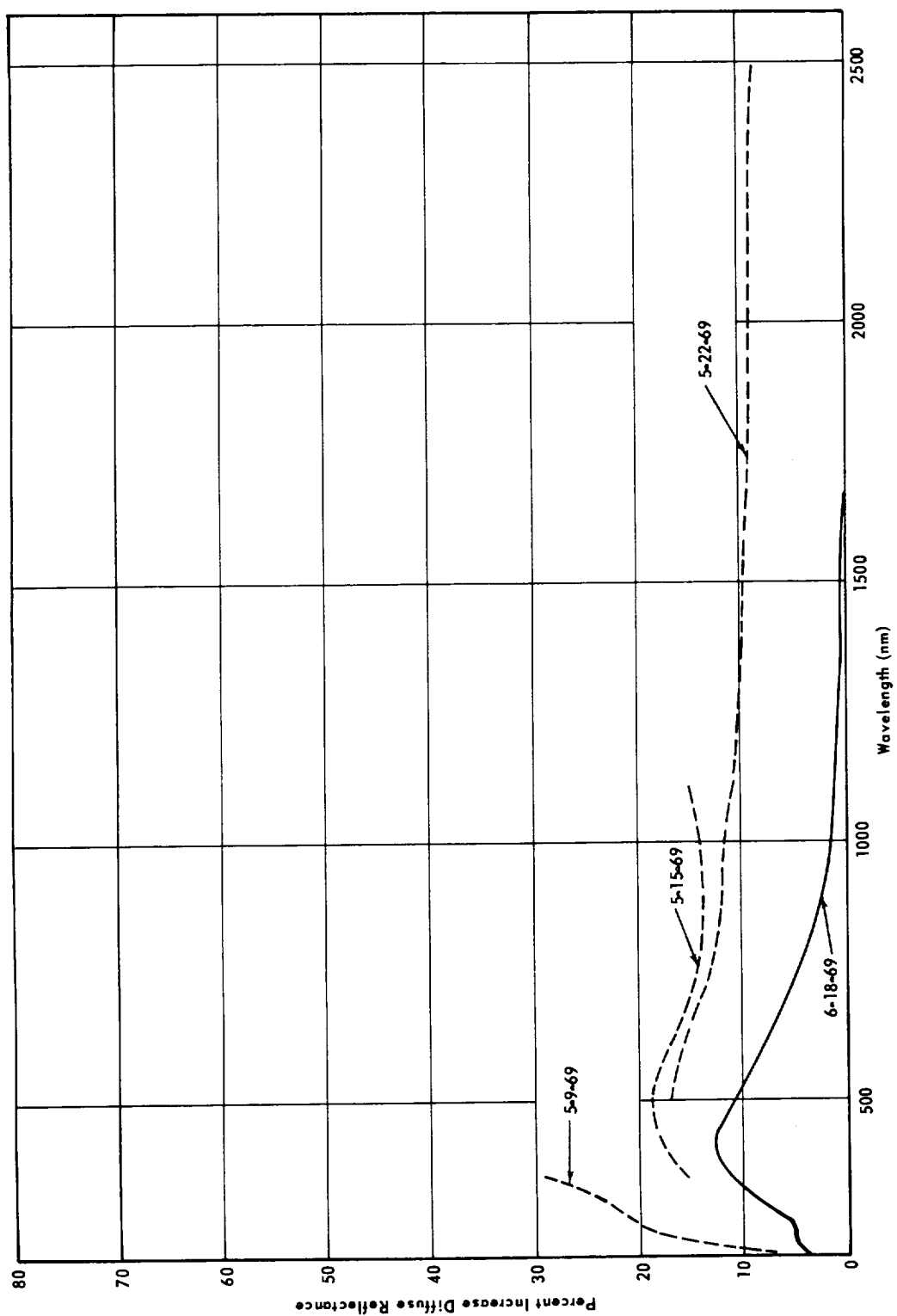
Figure 56. Diffuse reflectance, sample 6A1, effects of aging.

63
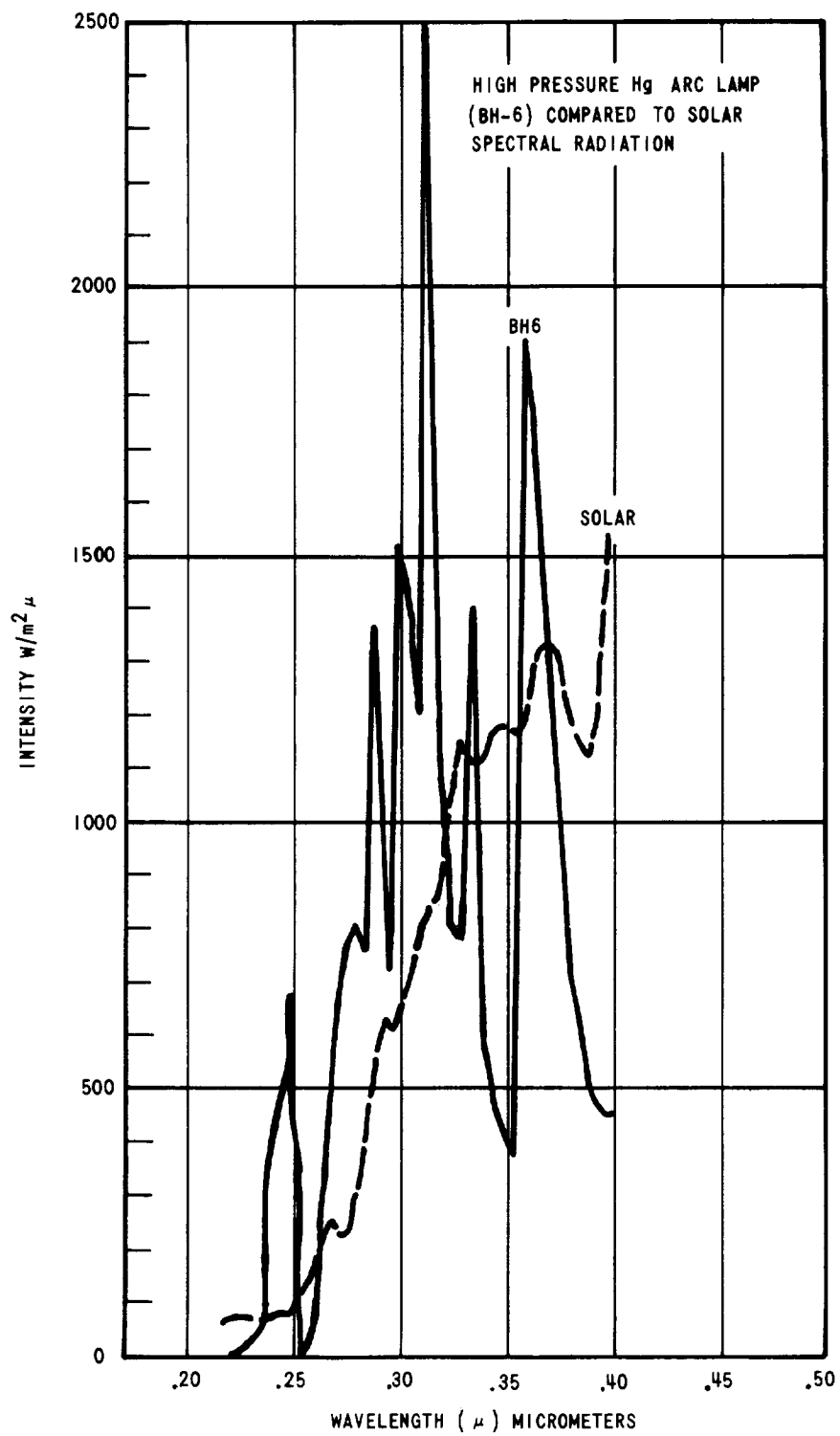
Figure 57. Spectrum of a high pressure mercury arc lamp.
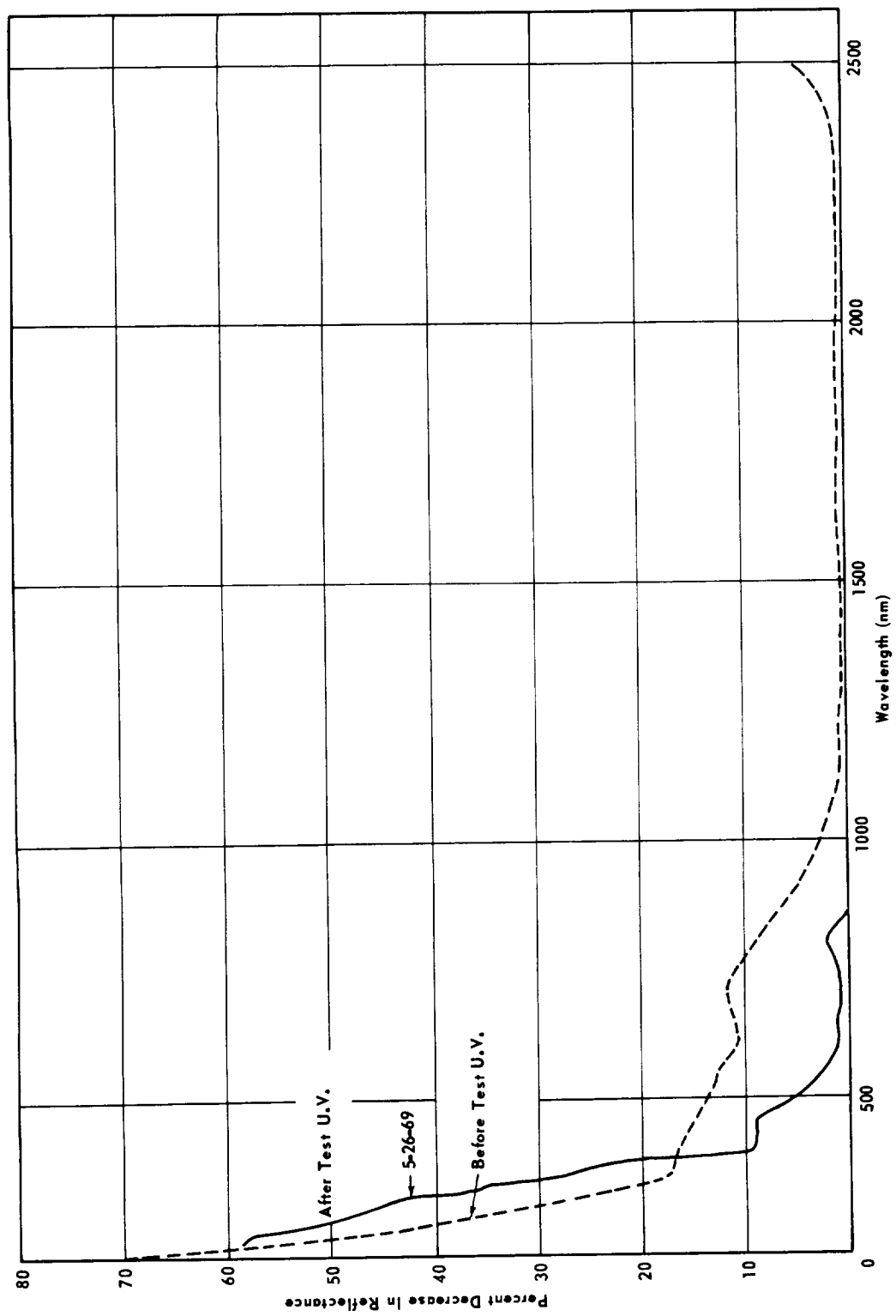
Figure 58. Total hemispherical reflectance degradation, ultraviolet irradiation effects, sample 6A2.

65
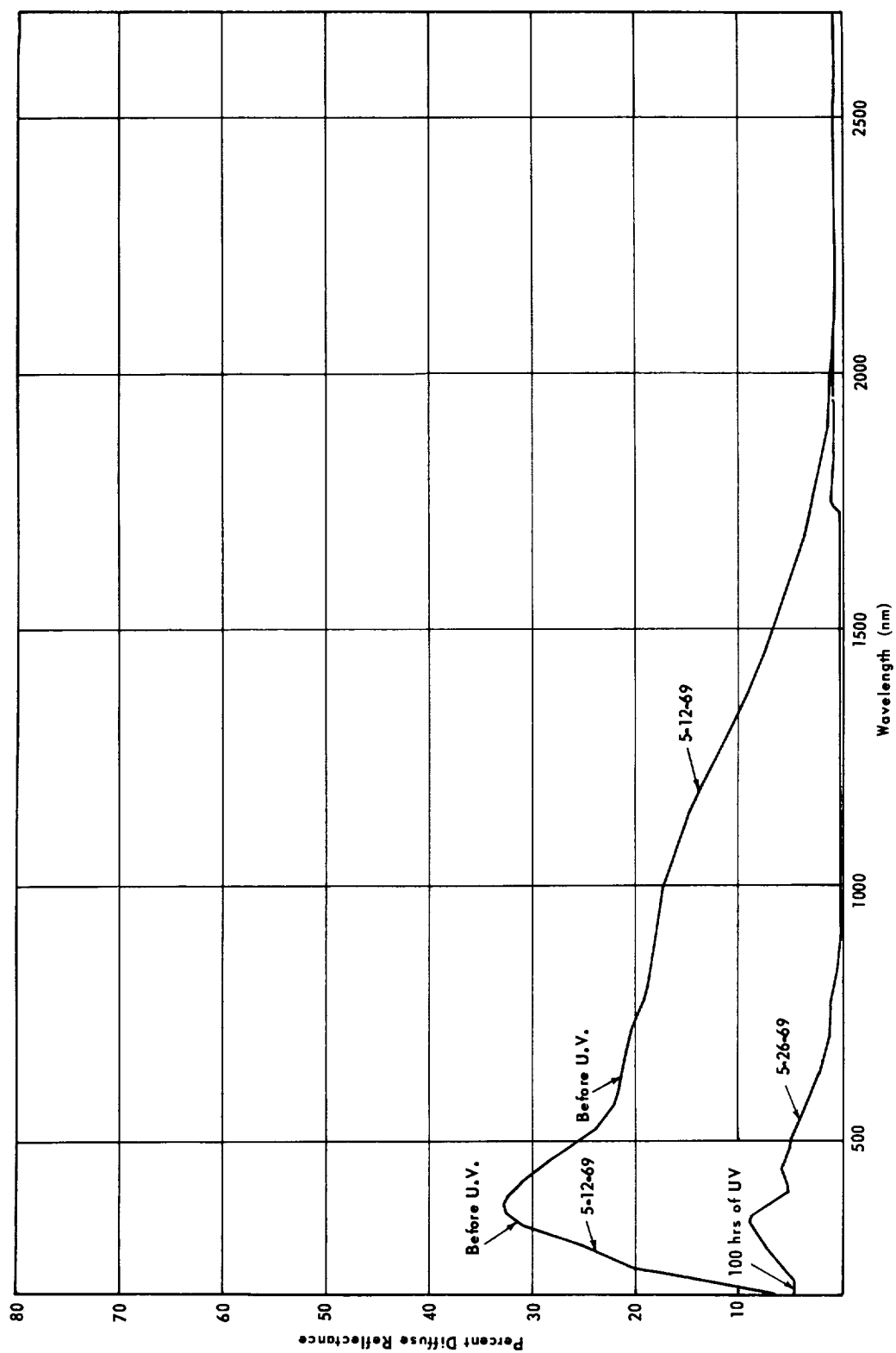
Figure 59. Diffuse reflectance, ultraviolet irradiation effects, sample 6A2.

66
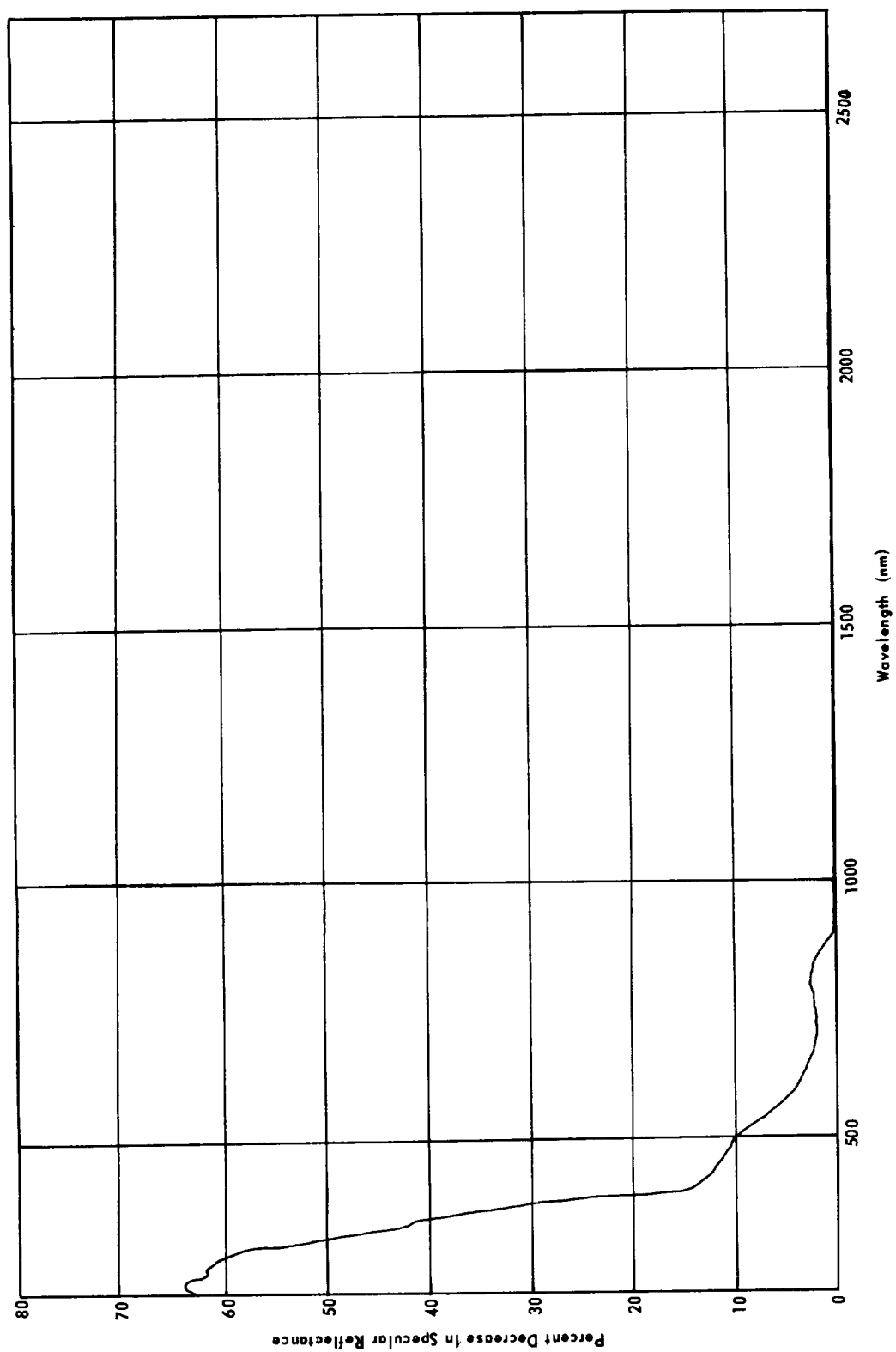
Figure 60. Decrease of specular reflectance, ultraviolet irradiation effects, sample 6A2.

67
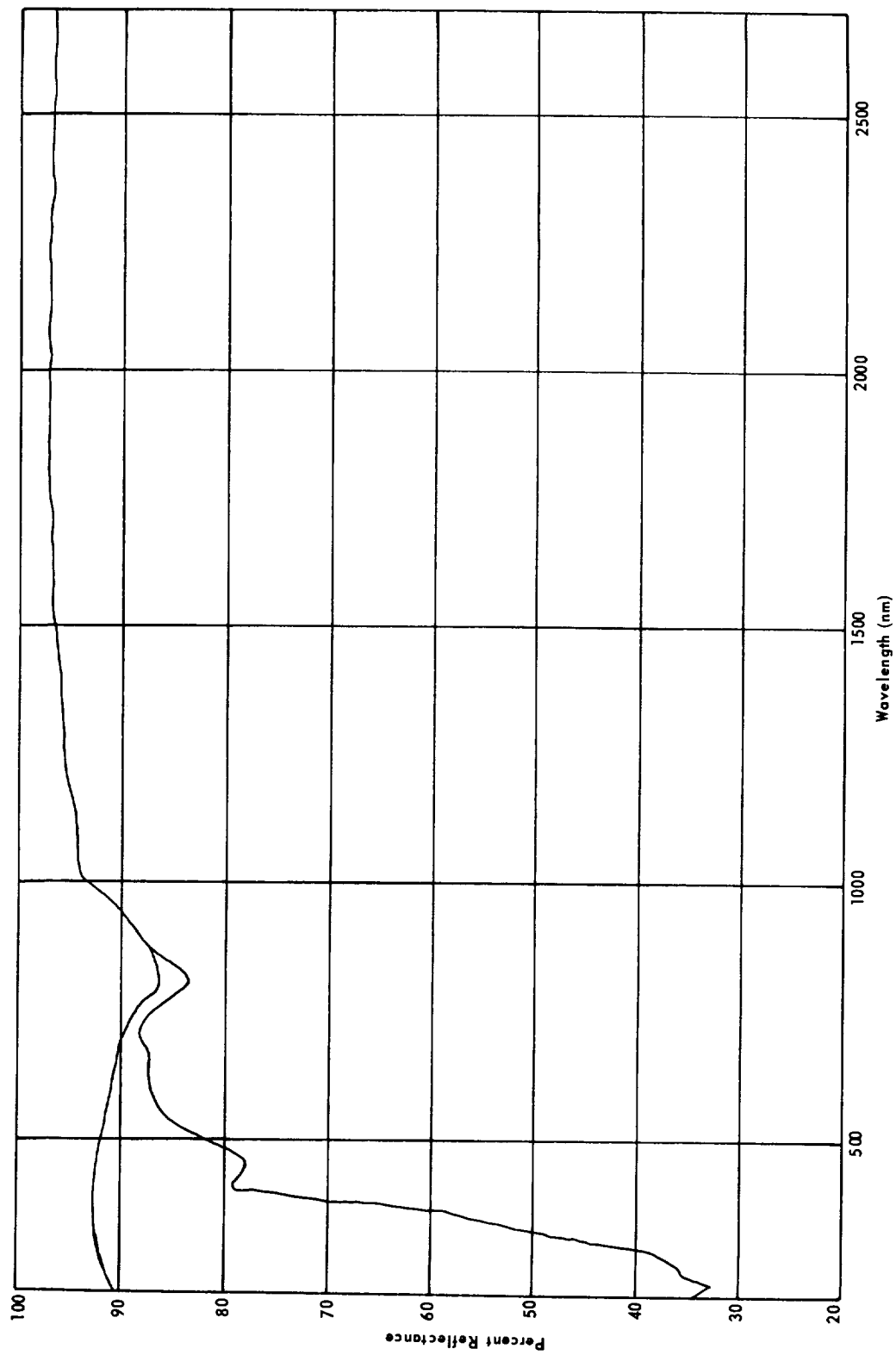
Figure 61. Reflectance degradation, ultraviolet irradiation effects, sample 6A2.

68

The irradiation increased the damage over most of the near ultraviolet range except at the lower end where it decreased in magnitude. Continued irradiation after the first 100 hours had little additional effect indicating that the remaining contaminant had been reduced to a stable semipermanent overcoat.

NEAR ULTRAVIOLET/VISIBLE/NEAR INFRARED
TRANSMISSION — W. W. Moore

As a portion of the Optical Evaluation objective of measuring the optical properties degradation of the sample exposed in this test, spectral and continuum transmittance of elements in the B1 and B3 series was determined for the near ultraviolet/visible/near infrared.

Data on optical element transmittance were obtained by using mercury vapor lamps and a photomultiplier detector in combination with a monochromator to complete a custom, single-beam spectrophotometer system (Figs. 62, 63, and 64). First reproducibility within acceptable confidence limits (Table 9) of the source stability, chart drive and scanning drive accuracy, and detector stability was established. It was then feasible to collect data by "delta amplitude" techniques on successive records of control and test sample transmission. Thus, the experimental method is the standard approach differential spectrophotometry of the deposit transmission effect.

The central unit in this custom system is the monochromator. A Czerny-Turner design optical spectrometer/spectrograph (model 78-466) by Jarrell-Ash was used. It is a 1-meter pathlength, scanning drive, grating instrument. A 1180 groove/mm grating of face dimension 102 by 102 mm and blazed for 500 nm was used. This gave a dispersion of 0.82 nm/mm with an effective aperture of f/8.7 in the first order. The simultaneously driven entrance and exit slits, for light-gathering, were set at 400 microns. Nitrogen flushing was not used; therefore, the effective ultraviolet cutoff was about 200 nm. The scanning drive was set at 25 nm/min and has a total periodic and accumulated error of ± 30 microns. The monochromator at this time was set to an accuracy of about ± 0.2 nm with a resolution (aberration limit) of < 0.01 nm (Figs. 65 and 66) measured at the 313.1 nm mercury doublet in first order. The summed scattered light background of the unit is about 0.20 percent (Fig. 67) at standard settings. These values were degraded by the slit settings.

The dual source system consisted of a 250-watt Beck/Ealing mercury vapor lamp in a glass envelope plus a superimposed Ultraviolet Products, Inc.

69
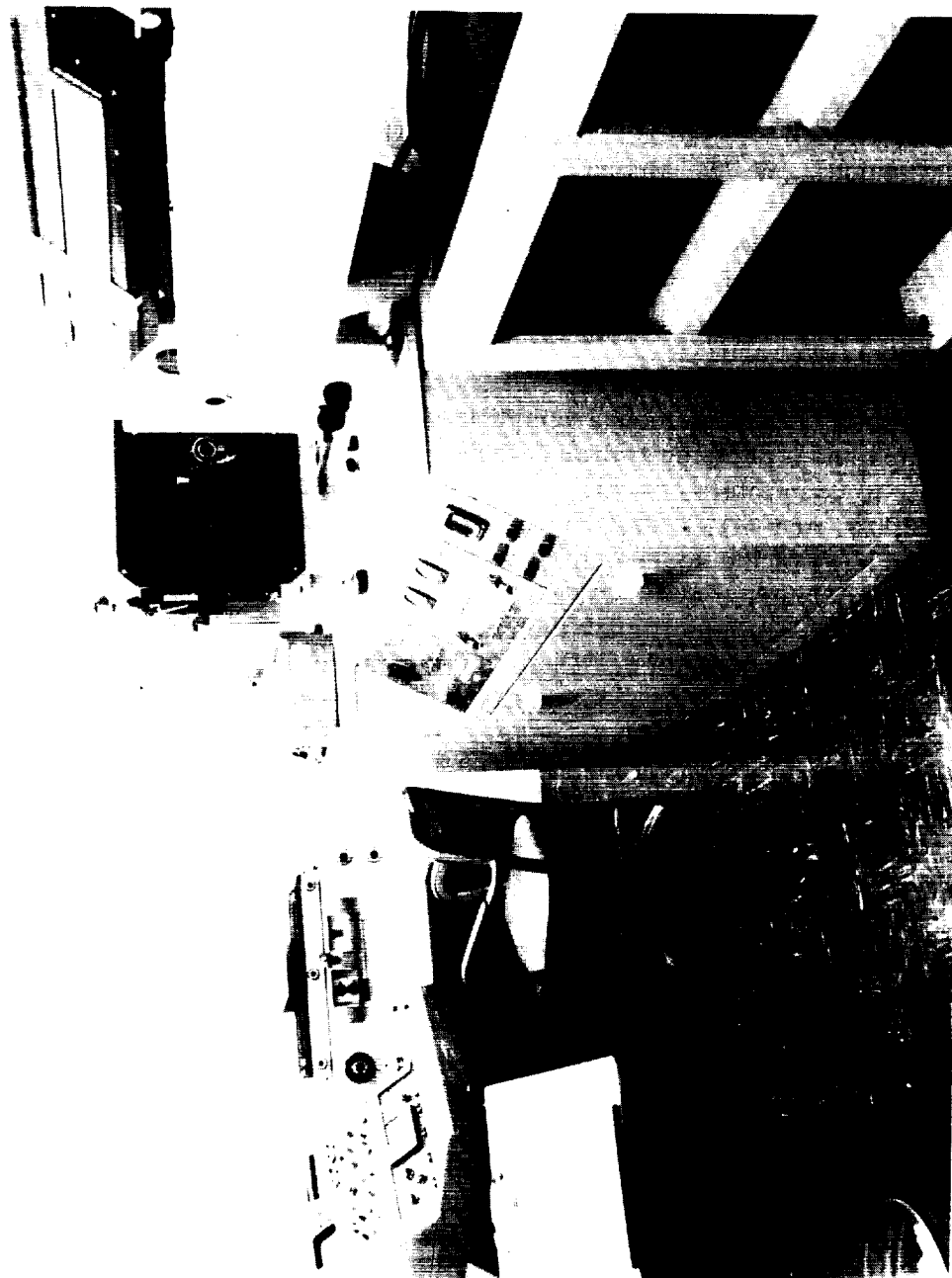
Figure 62. Test system monochrometer.

Figure 63. Source/optic holder.

1 Dual-Lamp Source System; Hg. Vapor
2 Optic in Position Mount
3; 3 Collimating, Czerny-Turner Mirrors
4 Grating In Rotating Mount
5 Photomultiplier Detector Unit
6 Optical Bar
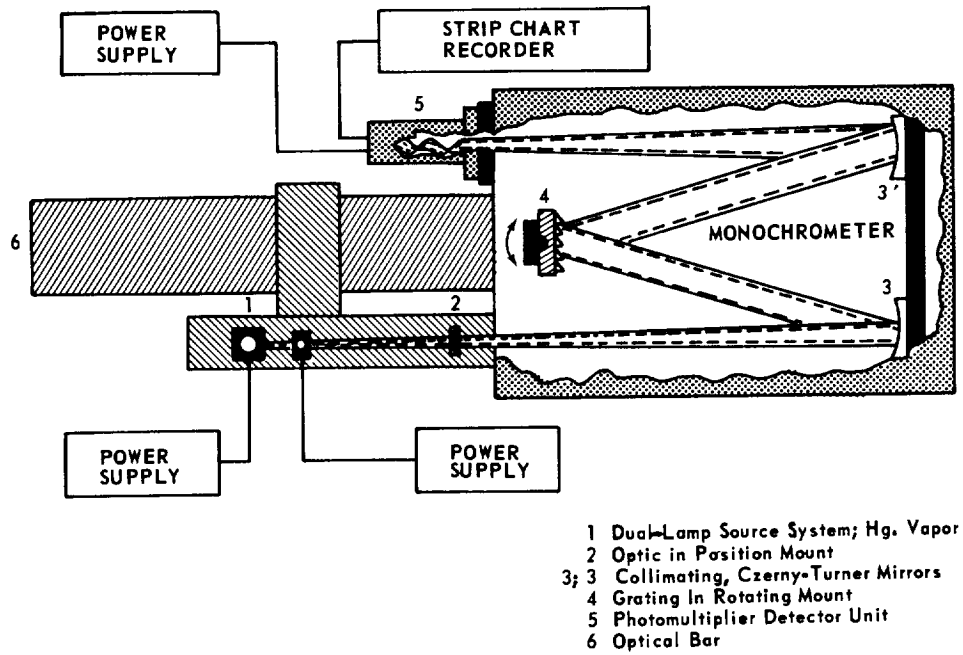
Figure 64. Schematic of monochrometer.

TABLE 9. EVALUATION OF SYSTEM CONFIDENCE LIMITS

Wavelength \ Date	253.6	Dev.	365.0	Dev.	404.8	Dev.	436.0	Dev.	507.5	Dev.	546.5	Dev.	575.4	Dev.	626.0	Dev.	668.5	Dev.	731.0	Dev.
April 7, 1969	68.2	−0.2	91.2	−6.5	97.2	−1.7	102.5	−0.1	69.2	−0.7	69.0	−5.2	66.3	−0.5	55.5	−0.3	57.0	−0.7	68.3	−1.4
April 7	68.8	+0.4	93.0	−4.7	96.8	−2.1	102.5	−0.1	69.8	−0.1	69.7	−4.5	66.6	−0.2	55.7	−0.1	57.5	+0.2	68.7	−1.0
April 8	69.0	+0.6	92.5	−5.2	97.4	−1.5	102.7	+0.1	70.7	+0.8	70.5	−3.7	66.8	0.0	56.0	+0.2	57.7	0.0	70.4	+0.7
April 9	70.4	+2.0	99.4	+1.7	99.5	+0.6	103.0	+0.4	71.8	+1.9	72.7	−1.5	67.7	+0.9	57.0	+1.2	59.0	+1.3	71.8	+2.1
April 9	69.6	+1.2	99.5	+1.8	100.5	+1.6	102.7	+0.1	70.4	+0.5	73.0	−1.2	67.9	+1.1	56.4	+0.6	58.7	+1.0	71.2	+1.5
April 10	70.7	+2.3	99.2	+1.5	99.4	+0.5	102.6	0.0	71.6	+1.7	72.9	−1.3	68.0	+1.2	56.2	+0.4	59.0	+2.7	72.0	+2.3
April 10	68.0	−0.4	97.5	−0.2	97.7	−1.2	102.6	0.0	68.7	−1.2	71.4	−2.8	65.8	−1.0	54.5	−1.3	56.2	−1.5	68.8	−0.9
April 17	69.4	+1.0	99.0	+1.3	98.5	−0.4	102.7	+0.1	71.2	+1.3	76.7	+2.5	66.0	−0.8	55.0	−0.8	58.7	+1.0	72.3	+2.6
April 17	68.0	−0.4	99.8	+2.1	100.0	+1.1	102.7	+0.1	70.0	+0.1	76.8	+2.6	66.0	−0.8	55.0	−0.8	58.0	+0.3	71.6	+1.9
May 9	65.1	−3.3	98.8	+1.1	99.5	+0.6	102.7	+0.1	67.0	−2.9	76.5	+2.3	66.4	−0.4	55.4	−0.4	56.5	−1.2	67.0	−2.7
May 12	70.0	+1.6	100.0	+2.3	100.3	+1.4	102.5	−0.1	71.0	+1.1	79.8	+5.6	67.0	+0.2	56.3	+0.5	57.3	−0.4	69.2	−0.5
May 12	65.0	−3.4	99.7	+2.0	99.5	+0.6	102.5	−0.1	67.6	−2.3	76.8	+2.6	66.7	−0.1	55.5	−0.3	57.0	−0.7	67.7	−2.0
May 13	67.2	−1.2	100.4	+2.7	100.0	+1.1	102.5	−0.1	69.8	−0.1	78.5	+4.3	67.0	+0.2	56.2	+0.4	57.5	−0.2	68.5	−1.2
Averages/Extremes	68.4	−3.4 +2.3	97.7	−6.5 +2.7	98.9	−2.1 +1.6	102.6	−0.1 +0.4	69.9	−2.9 +1.9	74.2	−5.2 +5.6	66.8	−1.0 +1.2	55.8	−1.3 +1.2	57.7	−1.5 +2.7	69.7	−2.7 +2.6
Summed Totals	761.7	−26.7 +22.2																		
Average Deviation	761.7	±24.4																		
% Deviation (Confidence Limits)	±3.2																			

72
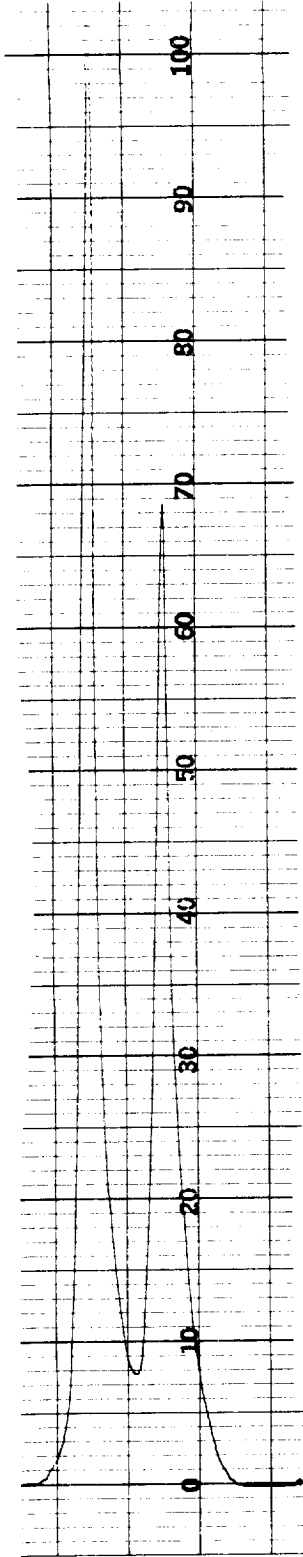
Figure 65. System resolution evaluation I.
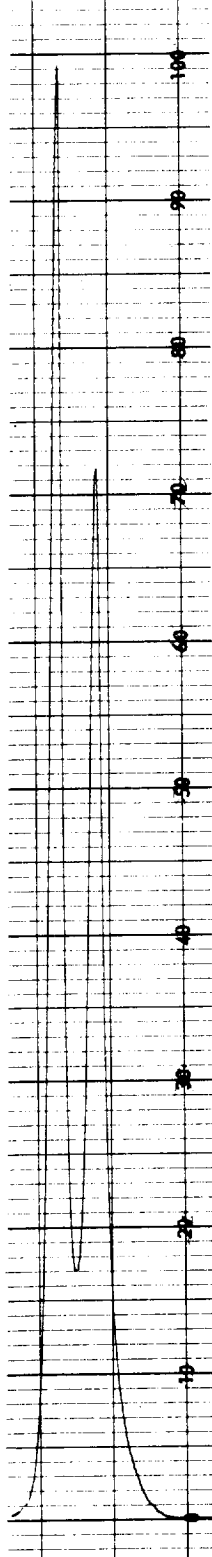
Figure 66. System resolution evaluation II.
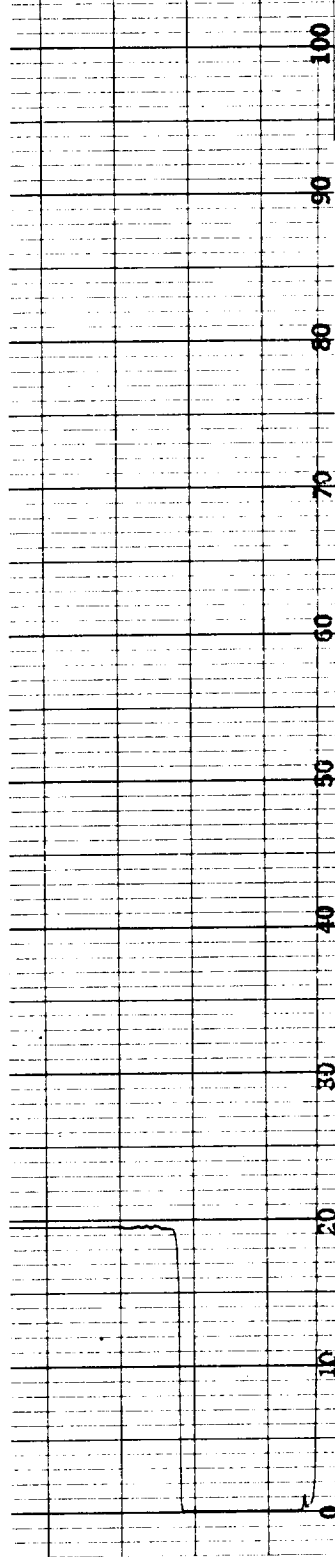
Figure 67. System scattering evaluation.

73

25-watt mercury pen-light calibration unit in a quartz envelope. This gave a combination of continuum and spectral output with enhanced characteristic peaks as shown in Figure 68. The peak heights are indicated on a 0 to 100 percent relative amplitude scale. The following is a definition of the code numbers shown at the peak heights on Figure 68.

Code No.	Definition
a	992.5 nm
b	983.5 nm (Hg I 983.808 nm @ 10 RI)
c	939.5 nm
d	872.0 nm
e	862.5 nm
f	Transient Instability in Mercury Vapor Source; Did Not Affect Test Results
g	Approximate Cutoff of Continuum Source
h	816.0 nm
i	810.0 nm
j	797.0 nm
k	761.0 nm
l	758.0 nm
m	750.5 nm
n	732.5 nm
o	731.0 nm
p	729.5 nm
q	712.5 nm
r	709.0 nm
s	691.5 nm
t	678.5 nm
u	668.5 nm
v	629.0 nm (Hg II 629.126 nm @ 50 RI)
w	626.0 nm
x	585.6 nm (Hg I 579.0654 nm @ 1000 RI)
y	578.0 nm (Hg I 578.966 nm @ 500 RI)
z	575.4 nm (Hg I 576.959 nm @ 200 RI)
aa	549.5 nm
ab	546.5 nm (Hg I 546.0740 nm @ 2000 RI)
ac	545.5 nm
ad	507.5 nm
ae	440.5 nm
af	436.0 nm (Hg I 435.835 nm @ 500 RI)
ag	433.5 nm

ah	431.0 nm
ai	408.5 nm
aj	407.0 nm
ak	404.8 nm (Hg I 404.6561 nm @ 300 RI)
al	403.5 nm
am	398.5 nm
an	391.0 nm
ao	386.0 nm
ap	382.0 nm
aq	379.5 nm
ar	377.4 nm (Hg II 377.452 nm @ 30 RI)
as	375.5 nm
at	372.5 nm
au	366.5 nm (Hg I 366.3276 nm @ 400 RI)
av	365.6 nm (Hg I 365.483 nm @ 200 RI)
aw	365.0 nm (Hg I 365.0146 nm @ 500 RI)
ax	362.0 nm
ay	356.0 nm
az	354.5 nm
ba	339.2 nm (Hg I 339.006 nm @ 50 RI)
bb	334.2 nm (Double Peak?) (Hg I 334.1478 nm @ 100 RI)
bc	312.0 nm, 313.0 nm, 313.5 nm (Hg I 312.5663 nm @ 150 RI, Hg I 313.1546 nm @ 300 RI, Hg I 313.1833 nm @ 100 RI)
bd	302.4 nm (Hg I 302.1499 nm @ 40 RI)
be	Approximate Cutoff of Continuum Source
bf	297.0 nm (Hg II 296.7278 nm @ 100 RI)
bg	289.5 nm (Hg I 289.3595 nm @ 50 RI)
bh	275.5 nm (Hg I 275.2775 nm @ 50 RI)
bi	265.5 nm (Hg I 265.2042 nm @ 60 RI)
bj	253.6 nm (Hg I 253.6519 nm @ 1000 RI)
bk	248.2 nm (Hg II 248.062 nm @ 40 RI)

The overall source spectrum used to obtain data was 200 to 1000 nm (2000 Å to 1 micron). The usable continuum was considered to extend from about 300 to 800 nm (3000 to 8000 Å). The source system and the optical elements were mounted in front of the monochromator entrance slit by a custom mount unit (Figs. 63 and 64) designed by the laboratory personnel and fabricated by the Manufacturing Engineering Laboratory shop.
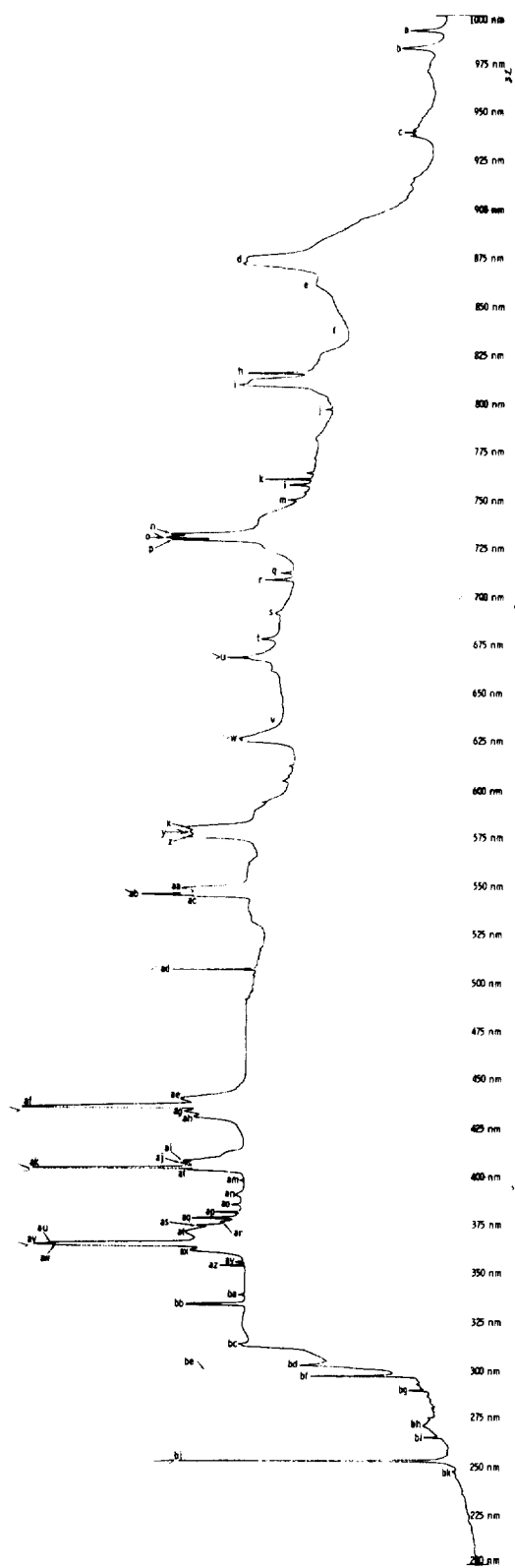
Figure 68. Recorded source spectrum.

76

The detection and recording subsystem consisted of an EM I photomultiplier tube (model 9558) with a quartz envelope and a type 20Q response curve (Fig. 69) which spans the spectral band 165 to 850 nm with peak responses at 260 and 420 nm. The high voltage supply used was the Jarrell-Ash (model 26-780) universal power supply/amplifier with a full-scale sensitivity of 10^{-10} amperes. The unit was set on fixed sensitivity and fast frequency response. No dark current zeroing was necessary for these measurements, as with the shutter closed, the background level was always set and returned to strip chart zero. The output of the photomultiplier was recorded on a Sargent Model SR variable range millivolt unit. The range setting used was 0.1 mv full scale and the chart drive was set at 1 in./min. This resulted in a spectrum distribution on each strip chart of 25 nm/in.

Transmittances at normal source incidence were measured on the testing system described by introducing the optical elements into the beam geometry just before the monochromator entrance slit. Two series of seven samples each (B1 and B3 series; Table 10) were measured (Fig. 70). Each series was composed of four control and three test elements. In addition, because the optics were kept in the laboratory during a test delay period, an additional control run was made on samples 1B3, 5B3, 6B3, and 7B3 to determine any initial period age effects. Also, the elements in the B1 set were only partially exposed to the test system. This was because the covering of aluminum foil fitted to each so that approximately two-thirds of the optic was protected. Because of this, two sets of test measurements were made on each of samples 5B1, 6B1, and 7B1. One transmission check was made on the exposed portion and one check on the unexposed portion. All of these values were taken from strip charts (Figs. 71 through 78)[1] and are expressed in the columns of Tables 11, 12, 13, and 14 with the exposed after (A) reading always the first value and percent listed.

The data points recorded in Tables 11 and 12 are the numerical amplitude values of spectral peak and/or continuum level for the respective wavelengths. They may be converted by using the equality 100 units = 0.1 mv. The data points have been averaged in the case of multiple measurements and the selected sets recharted in Tables 13 and 14. In addition, these tables include the relative percents of change which occurred in the control samples whether it represents enhanced or degraded transmission, as well as overall averages of the latter values. The percentages for the test samples represent

_____

1. Abscissa and ordinate scales are identical to that of Figure 68.

77
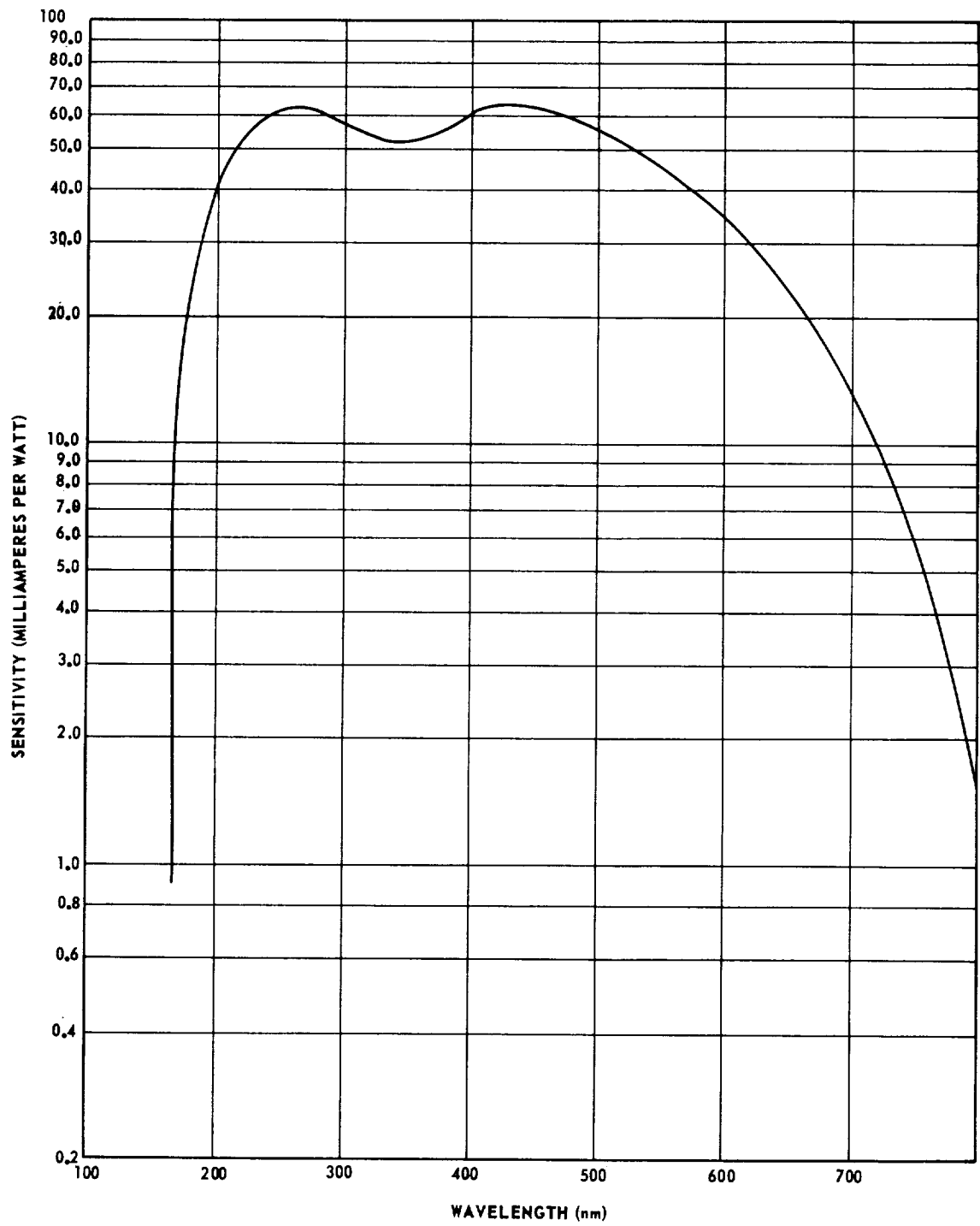
Figure 69. S-20Q response curve.

TABLE 10. CHRONOLOGICAL TABLE OF TESTING EVENTS

Chronological Record Number	Test Description	Date	Comments
1	Source Spectrum	4-7-69	
2	Transmission Check — Sample 1B1	4-7-69	Preliminary Work
3	Transmission Check — Sample 2B1	4-7-69	Preliminary Work
4	Source Spectrum	4-7-69	
5	Control — Sample 1B1	4-7-69	
6	Control — Sample 1B3	4-7-69	
7	Control — Sample 2B1	4-7-69	
8	Source Spectrum	4-8-69	
9	Control — Sample 2B3	4-8-69	
10	Control — Sample 3B1	4-8-69	
11	Control — Sample 4B1	4-8-69	
12	Control — Sample 5B1	4-8-69	
13	Source Spectrum	4-9-69	
14	Control — Sample 6B1	4-9-69	
15	Control — Sample 7B1	4-9-69	
16	Control — Sample 8B1	4-9-69	
17	Control — Sample 3B3	4-9-69	
18	Control — Sample 4B3	4-9-69	
19	Control — Sample 5B3	4-9-69	
20	Control — Sample 6B3	4-9-69	
21	Source Spectrum	4-9-69	
22	Source Spectrum	4-10-69	
23	Control — Sample 7B3	4-10-69	
24	Control — Sample 8B3	4-10-69	
25	Source Spectrum	4-10-69	
26	Source Spectrum	4-17-69	
27	Control — Sample 1B3	4-17-69	
28	Control — Sample 5B3	4-17-69	
29	Control — Sample 6B3	4-17-69	
30	Control — Sample 7B3	4-17-69	
31	Source Spectrum	4-17-69	
32	Source Spectrum	5-9-69	
33	Contaminated — Sample 1B3	5-9-69	Control Optic
34	Contaminated — Sample 2B3	5-9-69	Control Optic
35	Contaminated — Sample 3B3	5-9-69	Control Optic
36	Contaminated — Sample 4B3	5-9-69	Control Optic
37	Source Spectrum	5-9-69	
38	Source Spectrum	5-12-69	
39	Contaminated — Sample 5B3	5-12-69	Test Optic
40	Contaminated — Sample 6B3	5-12-69	Test Optic
41	Contaminated — Sample 7B3	5-12-69	Test Optic
42	Source Spectrum	5-12-69	Sample Beds 8B3 and 8B1 to MSC
43	Source Spectrum	5-13-69	
44	Contaminated — Sample 1B1	5-13-69	Control Optic
45	Contaminated — Sample 2B1	5-13-69	Control Optic
46	Contaminated — Sample 3B1	5-13-69	Control Optic
47	Contaminated — Sample 4B1	5-13-69	Control Optic
48	Contaminated — Sample 5B1	5-13-69	Test Optic; Exposed Portion
49	Contaminated — Sample 5B1	5-13-69	Test Optic; Unexposed Portion
50	Source Spectrum	5-13-69	
51	Source Spectrum	5-14-69	
52	Contaminated — Sample 6B1	5-14-69	Test Optic; Exposed Portion
53	Contaminated — Sample 6B1	5-14-69	Test Optic; Unexposed Portion
54	Contaminated — Sample 7B1	5-14-69	Test Optic; Exposed Portion
55	Contaminated — Sample 7B1	5-14-69	Test Optic; Unexposed Portion
56	Source Spectrum	5-14-69	
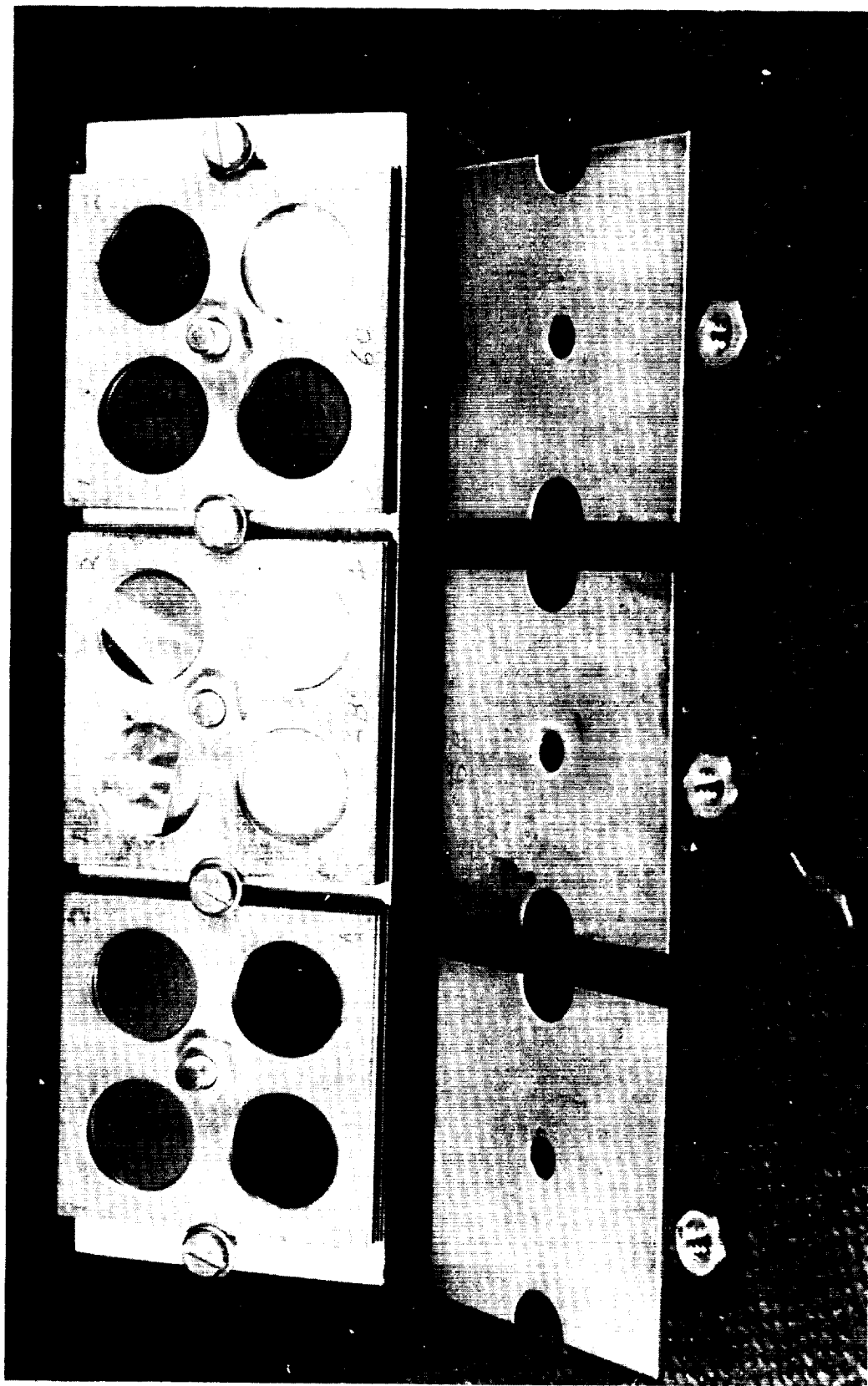
Figure 70. B1 and B3 series samples.
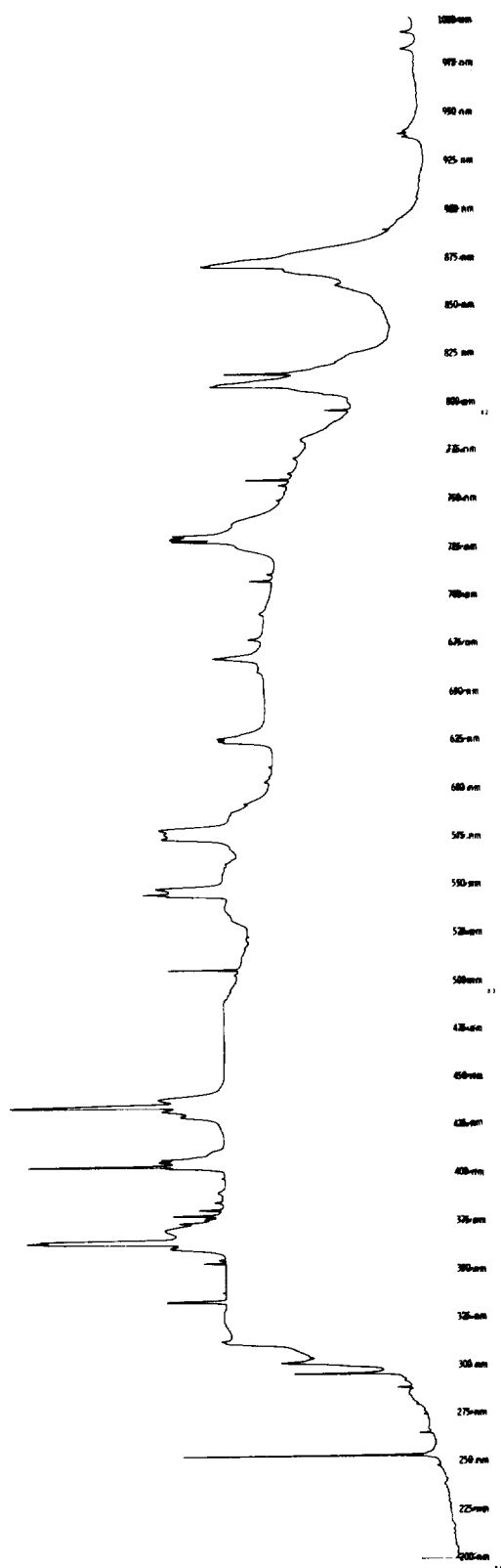
Figure 71.   Transmission data, sample 1B1.
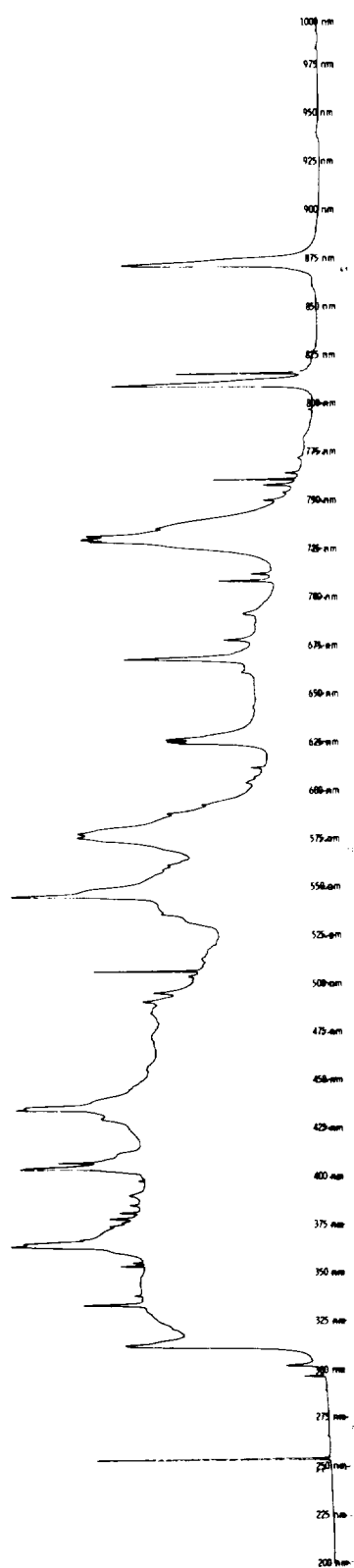
Figure 72.   Transmission data, sample 5B1, exposed section.

81
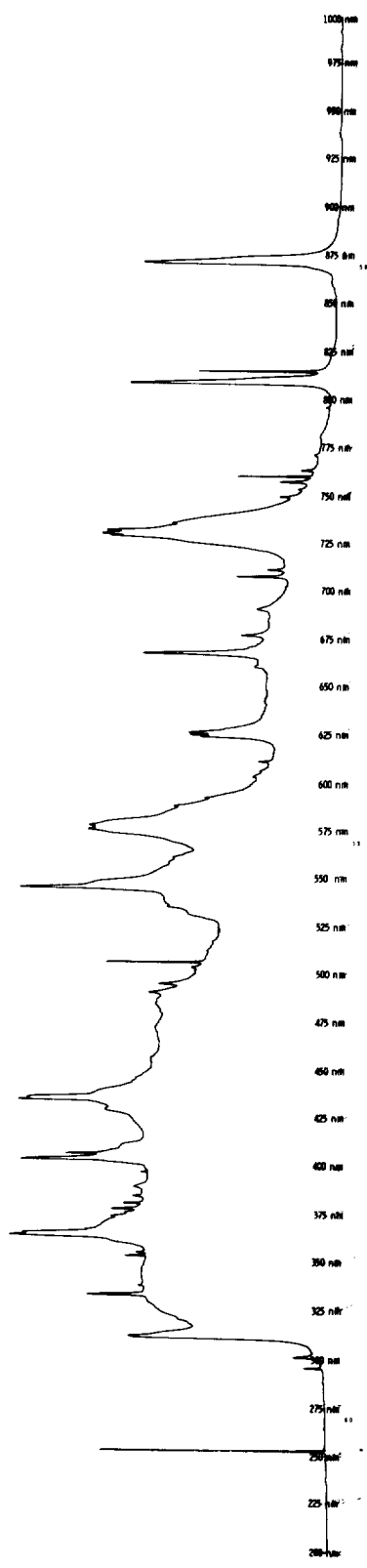
Figure 73. Transmission data, sample 6B1, exposed section.
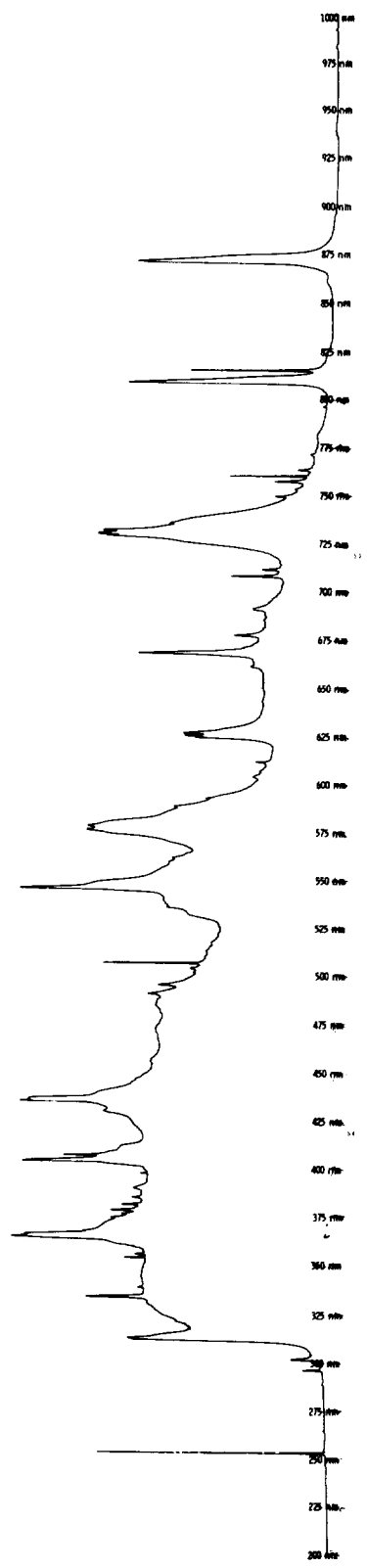
Figure 74. Transmission data, sample 7B1, exposed section.

82
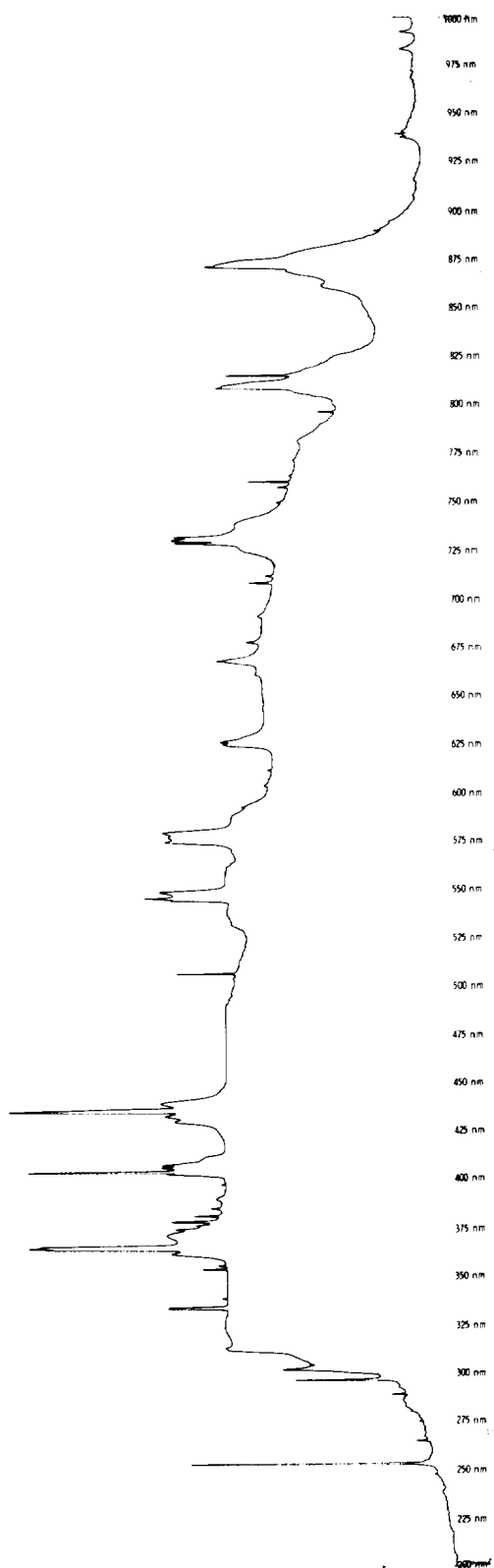
Figure 75. Transmission data, sample 1B3.
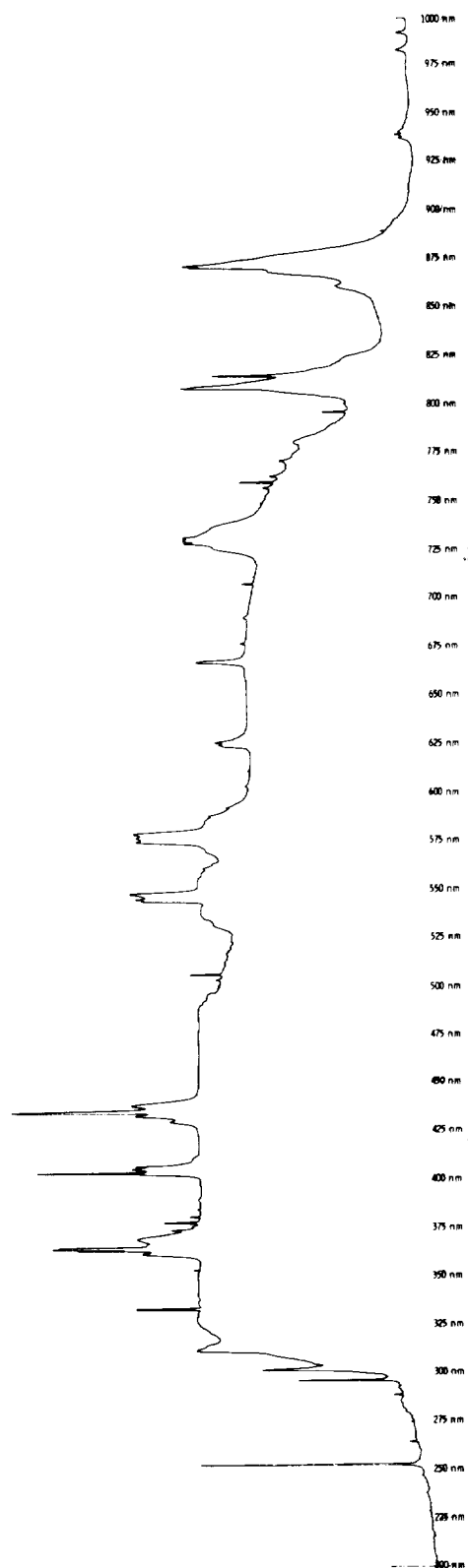
Figure 76. Transmission data, sample 5B3.
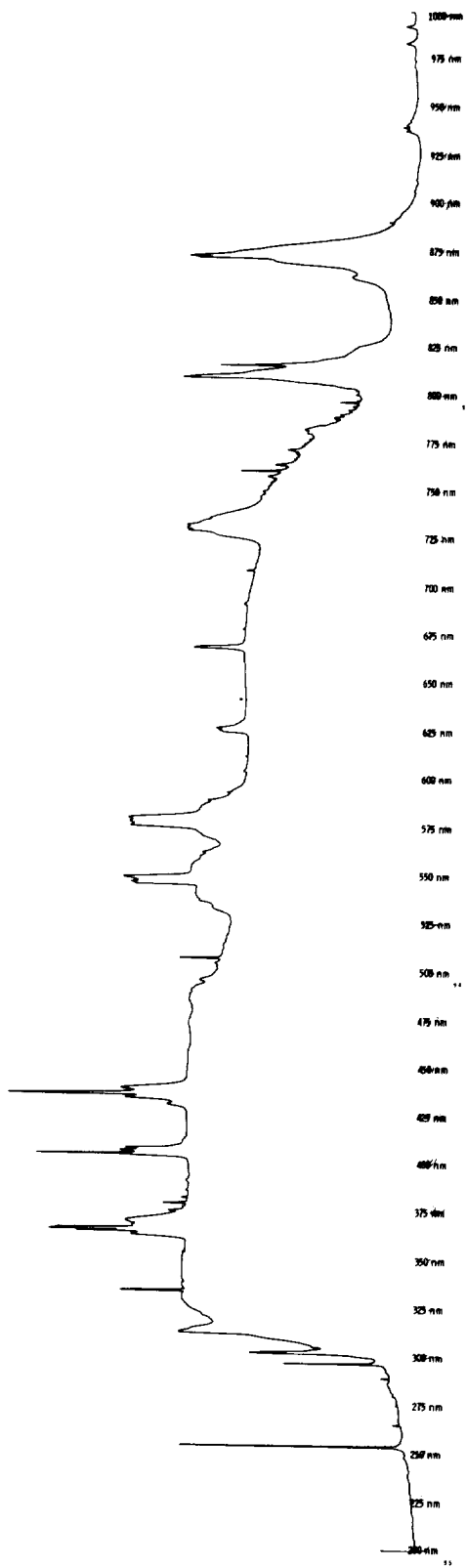
Figure 77. Transmission data, sample 6B3.
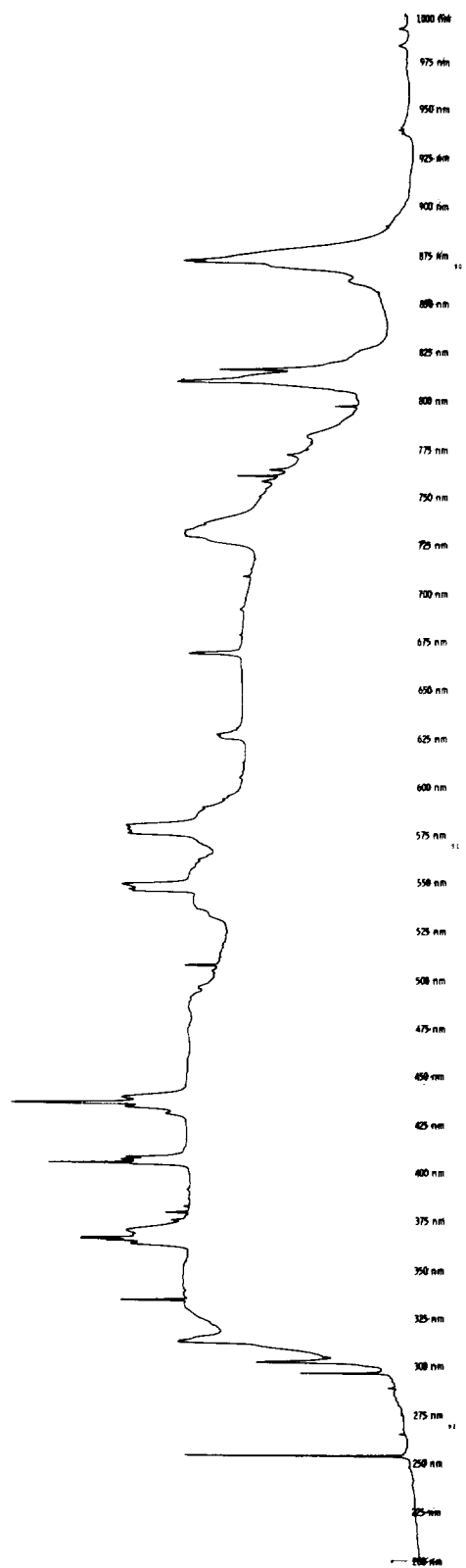
Figure 78. Transmission data, sample 7B3.

TABLE 11. TRANSMISSIVE DATA FOR THE B1 GROUP

Spectral:

Wavelength (nm)	1B1		2B1		3B1		4B1		5B1			6B1			7B1		
	B	A	B	A	B	A	B	A	B	A	A	B	A	A	B	A	A
248.2	8.3	9.1	8.7	9.0	8.8	8.7	8.7	8.7	8.7	2.3	1.7	9.4	N/R*	N/R	8.8	1.8	1.0
253.6	68.1	64.9	66.4	65.2	67.7	64.2	67.8	64.0	66.7	52.2	53.1	69.5	50.5	53.2	68.6	50.9	52.9
265.5	13.0	12.8	14.2	12.6	13.9	12.4	13.4	12.4	13.7	1.7	1.8	14.8	1.5	2.4	14.4	1.4	1.7
289.5	15.5	17.6	16.5	17.3	16.7	16.8	16.2	16.6	16.5	2.3	2.4	17.6	1.9	3.3	16.8	1.8	2.3
297.0	40.0	40.3	39.6	43.0	40.2	39.6	40.0	39.4	39.8	6.9	7.4	41.2	6.0	7.7	40.8	6.0	7.5
302.4	43.0	43.2	42.8	43.0	43.2	42.9	43.4	42.9	43.2	10.6	11.3	43.8	8.4	12.3	43.8	8.7	10.9
313.5	55.6	56.2	55.5	55.9	55.9	56.0	56.0	56.0	56.0	45.7	46.0	56.7	44.7	46.7	56.7	44.6	45.6
334.2	66.9	68.0	67.0	68.0	67.4	67.8	67.5	67.8	67.7	54.7	55.2	68.0	53.7	55.5	68.0	53.7	55.0
354.5	57.0	59.9	57.7	60.0	58.7	59.7	58.0	59.8	58.6	46.5	47.4	58.7	45.6	47.8	58.4	45.5	48.0
356.0	55.4	56.5	55.7	56.5	56.3	56.4	56.3	56.5	56.4	44.0	44.8	58.0	43.2	45.3	56.5	43.1	45.5
362.0	65.7	67.3	66.0	67.3	66.5	67.2	66.6	67.0	66.5	N/R	N/R	67.3	N/R	N/R	67.2	N/R	N/R
365.0	89.2	94.8	89.3	94.5	91.9	94.3	91.8	94.6	91.5	70.5	77.4	92.3	70.8	68.8	91.8	70.4	69.2
365.6	94.5	98.6	94.3	98.4	97.2	97.9	97.0	98.5	96.5	67.7	67.4	97.4	68.0	66.7	97.2	67.5	61.7
366.5	91.0	95.7	91.9	95.7	94.3	95.5	93.8	95.7	93.8	55.3	56.5	97.3	54.3	57.1	93.4	54.6	57.1
372.5	66.6	68.4	66.9	68.3	67.5	68.2	67.5	68.2	67.5	N/R	N/R	68.0	N/R	N/R	68.0	N/R	N/R
375.5	60.3	65.3	62.2	65.6	63.3	65.2	62.6	65.1	63.0	48.9	49.5	62.5	48.7	49.5	61.7	48.5	49.3
379.5	61.9	66.6	63.5	66.7	64.6	66.5	64.2	66.3	64.4	48.9	49.3	64.4	48.6	49.3	63.6	48.5	49.1
382.0	57.2	60.8	58.2	61.0	59.3	60.9	58.8	60.6	59.2	46.7	47.4	58.6	46.1	48.0	58.0	46.2	47.9
386.0	55.5	57.4	56.2	57.5	56.7	57.2	56.5	56.5	56.8	44.5	45.5	56.5	44.0	46.2	56.0	44.0	46.0
403.5	66.3	68.0	66.6	68.0	67.0	67.7	67.0	67.7	67.0	N/R	N/R	67.6	N/R	N/R	67.5	N/R	N/R
404.8	94.7	98.0	95.2	97.8	97.6	98.3	97.3	97.5	97.1	68.4	68.0	97.2	68.5	67.4	96.6	68.1	67.4
407.0	67.7	69.5	67.9	69.3	68.4	69.3	68.5	69.2	68.5	67.3	67.0	69.2	67.5	66.6	69.1	57.0	66.4
408.5	67.0	68.8	67.3	68.9	67.3	68.7	67.7	68.6	68.0	60.0	61.1	68.2	58.7	61.9	68.2	59.0	61.3
431.0	60.8	64.7	62.0	65.3	63.4	64.8	62.6	64.3	63.6	50.6	51.3	61.7	50.4	51.2	61.3	50.4	51.0
433.5	67.2	68.7	67.3	68.5	67.7	68.5	67.8	68.5	67.9	69.1	68.4	68.5	69.2	57.7	68.4	68.7	57.8
436.0	100.7	102.0	102.2	102.2	103.0	101.7	102.8	101.5	102.6	67.3	62.3	102.8	67.4	66.9	102.5	66.8	66.7
440.5	67.7	69.5	68.0	69.3	68.4	69.3	68.5	69.3	68.5	N/R	N/R	69.3	N/R	N/R	69.1	N/R	N/R
507.5	68.5	67.0	68.4	66.7	68.8	66.1	68.7	65.6	68.7	56.9	57.7	69.5	50.5	53.0	69.8	50.8	52.8
545.5	65.8	67.0	66.0	67.0	66.3	67.0	66.4	66.8	66.5	N/R	N/R	67.0	N/R	N/R	66.9	N/R	N/R
546.5	69.2	72.3	69.3	73.6	70.2	71.9	70.5	71.8	70.5	69.8	70.7	70.6	69.6	70.7	70.3	69.2	70.2
549.5	67.9	69.5	68.1	69.4	68.5	69.3	68.6	69.3	68.7	N/R	N/R	69.3	N/R	N/R	69.2	69.3	N/R
575.4	66.7	68.3	66.9	68.0	67.3	67.9	67.5	67.9	67.5	N/R	N/R	68.1	N/R	N/R	68.0	N/R	N/R
578.0	67.0	67.6	67.1	67.4	67.4	67.4	67.5	67.6	67.5	55.3	55.7	68.2	54.8	55.7	68.2	54.7	55.3
585.6	67.2	68.7	67.4	68.5	67.7	68.5	67.8	68.5	68.0	55.0	55.4	68.5	54.6	55.2	68.5	54.5	55.0
626.0	54.8	55.3	54.9	55.5	55.5	55.2	55.7	54.8	55.5	35.5	37.5	56.6	32.6	38.6	56.4	33.5	37.3

TABLE 11. (Concluded)

Sample Wavelength (nm)	1B1 B	1B1 A	2B1 B	2B1 A	3B1 B	3B1 A	4B1 B	4B1 A	5B1 B	5B1 A	5B1 A	6B1 B	6B1 A	6B1 A	7B1 B	7B1 A	7B1 A
668.5	56.8	56.5	57.0	56.7	57.3	56.3	57.6	56.3	57.6	44.7	46.1	58.2	43.3	46.8	57.8	43.7	45.8
678.5	48.5	48.7	48.8	54.1	48.5	48.3	49.9	48.3	50.0	23.0	25.6	49.7	21.9	27.4	49.4	22.7	26.7
709.0	48.2	48.2	48.6	48.3	49.2	47.8	49.6	47.4	49.7	23.8	26.2	49.4	23.0	27.3	49.2	23.7	27.3
712.5	44.4	44.3	44.8	44.5	45.4	44.4	45.8	43.7	46.7	16.7	18.7	45.6	16.3	20.0	45.3	16.8	20.2
729.5	66.1	65.0	66.4	65.0	67.7	64.4	67.6	64.2	67.5	52.0	53.0	68.2	50.5	53.5	68.2	51.0	55.3
731.0	67.3	65.7	67.3	65.9	69.0	66.1	69.0	64.7	68.3	53.9	54.7	70.2	52.5	54.7	69.5	52.8	54.7
732.5	66.5	65.0	66.7	65.1	67.9	64.7	68.0	64.0	67.7	52.7	53.3	68.3	51.4	53.7	68.3	51.8	53.5
758.0	42.8	41.5	43.5	41.8	43.7	41.5	44.2	41.0	44.5	14.1	16.0	43.6	13.7	16.8	43.6	14.6	16.7
761.0	49.9	48.8	51.2	48.7	51.0	48.4	51.0	47.9	50.9	24.9	27.9	51.5	22.9	29.9	51.0	24.2	30.2
797.0	35.6	31.3	36.3	31.6	36.5	31.0	36.7	29.9	37.1	4.0	4.5	36.3	3.8	4.5	36.2	3.8	4.5
810.0	55.8	56.5	56.0	56.4	56.2	56.6	56.2	56.5	56.3	46.9	47.0	56.6	46.7	46.5	56.5	46.6	46.5
816.0	54.5	53.3	54.7	53.3	55.0	53.0	55.0	53.0	55.2	32.7	34.6	55.3	31.7	35.7	55.3	32.8	35.1
862.5	38.8	28.7	39.1	29.3	39.0	27.4	39.0	25.9	39.5	N/R	N/R	38.8	N/R	N/R	38.5	N/R	N/R
872.0	56.6	58.2	56.7	58.3	56.7	57.6	56.9	57.6	57.0	44.5	46.1	57.1	44.0	46.6	57.1	44.6	45.9
939.5	17.5	14.8	18.0	15.2	18.2	14.1	19.0	13.6	18.4	1.9	2.2	18.0	1.7	2.0	17.5	1.7	1.9
983.5	17.0	13.9	17.7	14.2	17.7	13.0	17.6	12.5	18.5	1.7	1.9	18.0	1.5	1.7	17.7	1.5	1.7
992.5	15.5	13.9	16.4	14.1	16.0	13.5	16.3	12.5	16.8	1.7	1.8	16.6	1.5	1.7	16.4	1.5	1.7
Continuum:																	
300.0	25.5	27.0	27.0	26.5	28.0	26.0	24.0	26.5	26.5	2.7	3.5	23.0	3.0	3.4	30.2	2.5	3.3
325.0	55.4	55.5	55.5	55.5	55.7	55.7	55.8	55.3	55.9	37.8	39.3	56.7	37.6	39.4	56.2	37.0	39.2
350.0	55.0	55.0	55.2	55.0	55.3	55.0	55.5	55.0	55.5	41.8	42.3	55.8	41.4	42.2	55.8	41.3	42.0
375.0	58.0	62.5	58.0	60.5	59.0	62.0	55.5	60.0	60.0	48.0	48.8	62.5	46.0	49.3	57.0	47.0	48.5
400.0	54.6	55.2	55.1	55.3	55.4	55.2	55.4	55.0	55.5	41.7	42.7	55.5	41.5	43.0	55.4	41.3	42.8
425.0	55.3	56.0	55.7	56.3	56.2	56.0	55.9	56.0	56.2	44.4	45.7	56.0	44.5	46.0	55.9	44.3	45.8
450.0	54.9	55.1	55.0	55.1	55.3	55.0	55.4	55.0	55.5	42.0	42.0	55.8	41.0	42.5	55.5	41.0	42.0
475.0	54.5	54.9	54.7	54.9	55.0	54.8	55.2	54.8	55.2	39.3	39.8	55.6	38.4	39.5	55.0	38.8	39.3
500.0	56.5	52.4	50.8	52.6	51.7	52.9	51.7	51.6	52.2	31.5	32.8	51.5	31.4	33.5	50.6	31.4	33.5
525.0	47.5	49.5	47.8	50.9	49.0	49.0	48.6	48.3	49.3	24.7	27.0	48.7	26.0	27.7	47.5	25.3	27.8
550.0	56.5	60.0	56.5	60.0	57.0	60.0	59.0	57.5	60.0	52.0	50.0	63.0	46.5	50.5	57.0	49.5	50.0
575.0	66.7	68.2	67.0	68.0	67.0	67.9	66.0	67.5	67.5	49.5	57.5	62.0	53.0	51.0	62.5	51.0	51.0
600.0	43.7	44.7	44.2	45.4	44.7	45.0	44.8	44.4	45.0	18.4	19.8	44.5	19.0	20.8	44.0	18.5	20.4
625.0	54.8	55.3	54.8	55.5	55.4	55.0	54.8	54.5	55.5	33.0	37.0	55.8	32.5	38.0	50.6	30.5	26.0
650.0	45.0	45.3	45.3	45.7	45.7	45.0	46.0	44.7	46.3	16.3	18.5	45.8	16.3	19.5	45.5	16.3	19.2
675.0	46.0	45.8	46.3	46.3	46.7	45.7	47.2	45.2	47.4	17.5	19.8	46.8	17.0	21.3	46.5	17.5	20.7
700.0	43.8	43.8	44.0	44.0	44.4	43.6	44.7	43.3	45.0	13.0	14.5	44.7	12.5	15.0	44.2	12.8	15.0
725.0	50.7	50.4	51.2	50.7	51.3	49.3	51.3	50.0	51.3	26.0	31.5	50.5	31.0	31.5	51.6	29.5	32.3
750.0	41.5	41.3	42.0	41.5	42.5	41.0	44.3	40.7	43.0	11.7	13.0	42.6	11.5	14.0	42.0	14.0	16.0
775.0	38.2	36.4	38.5	36.7	38.6	35.9	39.0	30.0	39.3	5.3	6.0	38.5	5.0	6.0	38.2	5.0	6.0
800.0	33.0	26.0	34.2	26.7	34.2	25.9	34.4	24.7	35.0	3.3	3.5	33.0	3.0	3.5	33.3	3.0	3.5

* N/R — Not Readable

TABLE 12. TRANSMISSIVE DATA FOR THE B3 GROUP

Spectral:

Wavelength (nm)	B	1B3 B	1B3 A	2B3 B	2B3 A	3B3 B	3B3 A	4B3 B	4B3 A	B	5B3 B	5B3 A	B	6B3 B	6B3 A	B	7B3 B	7B3 A
248.2	8.5	7.4	9.3	8.8	9.4	8.5	9.0	8.4	8.8	8.8	8.6	7.0	8.7	7.5	6.2	6.9	7.2	5.5
253.6	67.0	66.7	62.5	67.8	62.8	68.8	62.8	68.6	62.6	69.3	67.0	54.8	68.8	67.2	55.2	66.2	66.6	54.5
265.5	13.0	13.0	13.2	14.1	13.2	13.6	12.7	13.3	12.4	14.3	13.5	9.6	13.9	13.3	8.6	12.2	13.5	7.5
289.5	16.0	16.0	18.5	16.7	18.2	16.2	17.6	16.0	17.2	16.6	16.5	12.9	16.2	16.2	11.4	14.6	16.0	10.0
297.0	39.7	39.2	39.4	40.3	39.4	40.6	39.2	40.5	38.8	40.6	39.3	33.7	40.5	39.2	32.7	38.4	39.0	29.3
302.4	42.9	41.7	42.2	43.2	42.3	43.8	42.2	43.7	42.2	43.6	41.8	41.4	43.7	41.8	40.2	41.4	41.7	38.9
313.5	55.5	54.5	54.8	56.0	55.0	56.7	55.0	56.7	55.0	56.6	54.6	50.6	56.6	54.6	55.6	54.2	54.6	56.2
334.2	67.0	66.5	67.0	67.2	67.0	68.0	67.0	68.0	67.2	68.2	66.6	68.6	68.2	66.6	68.5	66.0	66.6	68.7
354.5	57.0	57.5	59.6	58.0	60.0	58.4	59.8	58.3	60.0	58.5	57.5	56.0	58.7	57.4	55.2	56.3	57.3	54.7
356.0	55.5	54.7	56.1	56.0	56.3	56.4	56.3	56.4	56.5	56.5	54.8	54.9	56.6	54.9	54.6	54.3	54.8	54.5
362.0	65.6	65.7	66.4	66.5	66.4	67.2	66.5	67.3	66.6	67.2	65.8	67.2	67.5	65.9	66.5	65.4	65.8	66.6
365.0	89.0	92.2	93.5	91.2	93.8	91.5	93.0	91.3	93.5	92.5	92.4	81.3	82.0	82.6	78.3	89.9	92.6	72.0
365.6	94.2	96.7	97.4	96.2	97.8	96.8	96.9	96.6	97.3	97.5	97.0	86.8	97.0	97.2	84.5	95.0	97.0	77.6
366.5	91.4	93.4	95.0	93.0	95.2	93.0	94.7	91.6	95.2	94.4	93.7	85.2	93.8	93.8	83.0	91.4	94.0	77.4
372.5	66.6	66.6	67.4	67.4	67.4	68.0	67.4	68.2	67.5	68.2	66.7	68.3	68.4	67.0	67.8	66.3	67.0	67.6
375.5	61.2	62.0	65.5	62.0	65.4	61.8	65.2	61.8	65.7	63.0	62.2	60.9	62.7	62.5	58.4	60.2	62.2	57.7
379.5	62.6	63.5	66.5	63.7	66.2	63.5	66.3	63.6	66.5	64.5	63.7	62.5	64.4	64.0	59.6	62.0	63.7	59.0
382.0	57.6	57.7	61.4	58.2	61.2	58.2	61.2	58.2	61.5	59.0	57.9	56.9	58.8	58.2	55.6	56.3	58.0	50.0
386.0	55.8	55.0	57.7	56.2	57.5	56.2	57.6	56.2	58.0	57.0	55.2	55.2	56.6	55.4	54.6	54.2	55.5	54.2
403.5	66.3	66.2	67.2	66.2	67.2	67.5	67.2	67.5	67.4	67.7	66.4	67.6	67.7	66.5	67.0	65.6	66.5	66.7
404.8	94.9	96.5	97.5	96.3	97.9	96.0	97.7	96.4	97.5	97.5	96.7	93.0	97.5	96.9	87.4	94.8	97.0	84.7
407.0	67.8	67.7	68.5	68.3	68.5	69.0	68.5	69.2	68.5	69.2	67.8	69.4	69.2	68.0	69.0	67.2	68.0	68.8
408.5	66.6	67.0	68.2	67.5	68.2	68.2	68.2	68.4	68.2	68.5	67.0	68.5	68.5	67.3	68.0	66.5	67.4	67.7
431.0	61.2	62.2	65.5	62.2	65.5	61.2	65.6	61.4	65.7	63.9	62.2	61.0	62.5	63.0	59.0	59.2	63.0	59.2
433.5	67.0	67.0	67.6	67.6	67.6	68.4	67.6	68.5	67.8	68.5	67.0	68.6	68.6	67.2	68.3	66.5	67.2	68.0
436.0	100.8	102.0	101.5	102.2	101.6	102.0	101.3	102.2	102.2	102.3	102.2	95.5	103.0	102.4	93.7	100.5	102.2	93.0
440.5	67.9	67.7	68.5	68.4	68.5	69.0	68.5	69.2	68.5	69.3	67.9	69.5	69.3	68.0	69.2	67.2	68.0	68.8
507.5	68.6	69.0	64.9	69.2	65.5	70.0	64.9	70.5	64.6	70.7	70.0	56.6	70.0	69.4	56.7	68.0	69.0	55.2
545.5	65.7	65.5	66.0	66.3	66.2	66.9	66.2	67.0	66.3	67.0	65.5	66.7	67.2	65.7	66.6	65.0	65.6	66.5
546.5	69.2	70.5	71.7	70.0	72.0	70.5	70.6	70.2	71.4	70.5	70.8	68.2	70.5	70.6	67.8	68.3	70.0	67.5
549.5	68.0	67.9	68.5	68.5	68.5	69.2	68.5	69.3	68.6	69.4	68.0	69.5	69.5	68.0	69.4	67.3	68.0	69.0
575.4	66.9	66.5	67.2	67.3	67.2	68.0	67.2	68.2	67.4	68.2	66.6	68.0	68.2	66.8	68.0	66.2	66.7	67.7
578.0	67.0	66.2	66.5	67.5	66.5	68.2	66.6	68.4	66.7	68.2	66.4	68.0	68.2	66.5	68.2	66.2	66.4	67.7
585.6	67.2	67.0	67.6	67.7	67.6	68.5	67.6	68.6	67.9	68.6	67.2	68.6	68.6	67.2	68.5	66.5	67.2	68.2
626.0	55.5	55.0	54.5	55.5	54.6	56.2	54.2	56.0	54.2	56.0	55.0	50.0	56.0	55.0	48.8	54.5	54.5	47.8

TABLE 12. (Concluded)

Wavelength (nm)	B	1B3 B	1B3 A	2B3 B	2B3 A	3B3 B	3B3 A	4B3 B	4B3 A	5B3 B	5B3 B	5B3 A	6B3 B	6B3 B	6B3 A	7B3 B	7B3 B	7B3 A
668.5	57.2	56.8	55.7	57.4	55.9	57.9	55.7	58.0	55.8	57.9	56.7	54.9	57.9	56.7	54.7	56.0	56.5	54.6
678.5	49.4	49.2	49.2	49.2	49.0	49.2	48.6	49.3	48.6	49.5	49.0	45.2	49.6	49.4	44.0	47.6	48.9	43.5
709.0	48.8	48.7	48.6	48.8	48.5	49.0	48.2	49.0	48.2	49.2	48.8	44.6	49.2	48.6	43.5	47.5	48.5	42.8
712.5	45.2	44.8	44.9	45.0	44.7	45.2	44.5	45.3	44.5	45.4	44.8	42.2	45.5	45.2	41.5	43.5	44.6	41.2
729.5	67.0	68.9	64.8	67.5	63.6	68.2	64.0	68.2	63.7	68.5	69.2	57.2	68.5	68.7	56.2	67.5	68.6	55.5
731.0	68.2	70.4	65.4	68.6	64.2	69.5	64.5	69.5	64.2	69.8	70.7	57.5	69.9	70.0	56.5	69.0	70.0	55.6
732.5	67.0	69.0	64.9	67.6	63.8	68.3	64.2	68.4	63.8	68.8	69.4	57.4	68.8	68.9	56.5	67.6	68.8	55.6
758.0	43.6	43.0	42.2	43.5	41.7	43.5	41.6	43.5	41.6	43.8	42.8	40.0	43.7	43.0	39.0	42.0	43.0	38.8
761.0	50.9	50.3	48.6	50.9	48.4	51.3	48.4	51.2	48.4	51.6	48.8	45.0	50.6	49.0	45.0	48.8	48.5	44.2
797.0	36.4	35.9	33.4	36.2	33.0	36.0	32.7	36.0	32.2	36.4	35.7	27.0	36.4	35.8	23.5	34.4	35.8	22.9
810.0	55.9	54.8	55.6	56.0	55.6	56.6	55.7	56.6	56.0	56.8	55.0	57.6	56.8	55.0	57.7	54.5	55.0	57.4
816.0	54.5	53.6	53.3	54.8	53.2	55.3	53.0	55.4	53.0	55.4	53.2	53.8	55.4	53.6	53.8	53.2	53.6	48.2
862.5	38.9	38.0	32.4	38.8	31.5	38.6	31.5	38.9	30.0	39.0	38.0	24.2	39.0	38.0	21.0	37.0	38.2	20.0
872.0	56.4	56.4	57.8	56.6	57.7	57.2	57.7	57.3	57.4	57.2	54.7	57.2	57.2	55.0	56.6	54.8	55.0	56.2
939.5	18.2	17.9	16.2	17.9	15.5	17.3	15.2	17.3	15.0	17.4	17.2	11.0	17.9	16.8	10.4	15.4	17.0	9.0
983.5	17.9	18.1	14.9	17.6	15.0	17.2	14.5	17.2	14.4	17.6	17.5	10.7	18.3	17.4	9.9	15.4	17.6	9.0
992.5	16.4	16.4	14.9	16.5	15.0	15.8	14.2	16.0	14.5	16.2	15.6	10.6	17.2	15.6	9.9	13.9	15.6	9.0
Continuum:																		
300.0	24.0	24.5	23.5	27.0	26.5	24.5	28.0	27.0	25.0	23.0	24.4	20.0	23.0	22.2	22.0	25.0	25.0	13.5
325.0	55.4	54.2	54.7	55.6	54.7	56.2	54.7	56.2	54.8	56.2	54.4	54.7	56.2	54.4	53.5	54.0	54.5	51.4
350.0	55.0	53.5	54.2	55.2	54.2	55.8	54.2	55.9	54.4	55.9	53.7	55.2	55.8	53.8	55.2	53.6	53.8	55.0
375.0	58.0	62.0	64.5	59.5	63.5	61.0	61.0	58.6	64.0	61.5	61.0	56.6	62.0	61.5	56.5	56.5	61.0	57.7
400.0	54.9	55.5	54.7	55.0	54.8	55.4	54.9	55.5	55.0	55.8	53.2	54.6	55.5	53.8	54.4	55.3	53.9	54.0
425.0	55.4	54.2	55.9	55.6	56.0	55.9	56.2	56.0	56.3	56.5	54.3	55.2	56.2	54.6	54.7	53.8	54.6	54.6
450.0	54.9	53.6	54.5	55.0	54.4	55.6	54.4	55.7	54.6	55.8	53.3	54.8	55.8	53.8	54.7	53.4	53.8	54.5
475.0	54.5	53.5	54.2	54.8	54.2	55.2	54.3	55.3	54.4	55.5	53.2	54.8	55.4	53.6	54.4	53.2	53.6	54.3
500.0	50.0	50.7	52.5	51.0	52.3	50.8	52.2	50.5	52.3	51.9	51.4	50.2	51.5	51.0	50.2	48.5	51.7	44.2
525.0	47.2	47.6	49.5	48.0	49.4	47.6	49.7	46.4	49.5	48.0	47.6	47.4	48.5	47.9	47.4	45.5	47.9	41.0
550.0	59.0	61.5	66.5	59.0	62.0	60.0	59.0	57.5	61.5	61.0	59.5	56.0	63.0	63.5	56.2	55.2	63.5	60.5
575.0	64.5	64.0	65.0	66.5	67.2	65.0	66.8	67.5	67.0	66.0	64.5	67.8	63.5	62.5	67.2	65.5	66.7	65.5
600.0	43.5	43.5	45.0	44.0	45.0	44.2	44.2	43.9	45.0	44.4	43.2	43.8	44.5	43.5	43.0	41.8	43.6	43.0
625.0	55.4	54.2	52.5	55.5	54.0	55.2	54.9	55.5	53.5	55.0	54.3	50.0	55.0	54.0	48.8	54.3	54.2	47.3
650.0	45.0	44.7	45.5	45.5	45.3	45.6	45.2	45.6	45.3	45.2	44.6	43.8	45.6	44.9	43.3	43.6	44.6	42.8
675.0	46.0	46.2	46.7	46.5	46.2	46.5	46.0	46.5	45.9	46.7	45.8	44.0	46.8	46.8	43.4	44.6	45.8	43.0
700.0	44.2	43.4	44.2	44.2	43.7	44.4	43.7	44.4	43.6	44.6	43.3	42.7	44.6	43.6	42.4	42.4	43.2	41.8
725.0	51.0	50.0	49.5	50.8	49.8	51.0	49.8	51.4	49.7	51.2	49.7	49.5	50.7	49.8	45.0	49.4	50.2	44.5
750.0	42.5	42.5	41.7	42.8	42.2	42.8	41.2	42.3	42.0	43.0	42.0	40.0	42.7	42.0	39.3	41.5	42.5	39.2
775.0	38.5	37.3	37.8	38.4	37.4	38.3	37.2	38.3	36.8	39.6	37.7	33.3	38.5	37.8	30.4	36.2	37.7	28.8
800.0	33.0	33.6	29.5	33.7	29.2	32.2	29.0	32.9	27.4	32.8	33.4	22.0	32.8	33.5	20.0	31.3	33.7	17.8

TABLE 13. TRANSMISSIVE REDUCED DATA/PERCENT CHANGES FOR THE B1 GROUP

Sample / Wavelength (nm)	1B1			2B1			3B1			4B1			%*
	B	A	%	B	A	%	B	A	%	B	A	%	
Spectral:													
248.2	8.3	9.1	+ 9.6	8.7	9.0	+ 3.4	8.8	8.7	- 1.1	8.7	8.7	0.0	+ 3.0
253.6	68.1	64.9	- 4.7	66.4	65.2	- 1.8	67.7	64.2	- 5.2	67.8	64.0	- 5.6	- 4.3
265.5	13.0	12.8	- 1.5	14.2	12.6	-11.3	13.9	12.4	-10.8	13.4	12.4	- 7.5	- 7.8
289.5	15.5	17.6	+13.6	16.5	17.3	+ 4.8	16.7	16.8	+ 0.6	16.2	16.6	+ 2.5	+ 5.4
297.0	40.0	40.3	+ 0.8	39.6	39.8	+ 0.5	40.2	39.6	- 1.5	40.0	39.4	- 1.5	- 0.4
302.4	43.0	43.2	+ 0.5	42.8	43.0	+ 0.5	43.2	42.9	- 0.7	43.4	42.9	- 1.2	- 0.2
313.5	55.6	56.2	+ 1.1	55.5	55.9	+ 0.7	55.9	56.0	+ 0.2	56.0	56.0	0.0	+ 0.5
334.2	66.9	68.0	+ 1.6	67.0	68.0	+ 1.5	67.4	67.8	+ 0.6	67.5	67.8	+ 0.4	+ 1.0
354.5	57.1	59.9	+ 5.1	57.7	60.0	+ 4.0	58.7	59.7	+ 1.7	58.0	59.8	+ 3.1	+ 3.5
356.0													
362.0													
365.0	89.2	94.8	+ 6.3	89.3	94.5	+ 5.8	91.9	94.3	+ 2.6	91.8	94.6	+ 3.0	+ 4.4
365.6													
366.5													
372.5	61.9	66.6	+ 7.6	63.5	66.7	+ 5.0	64.6	66.5	+ 2.9	64.2	66.3	+ 3.3	+ 4.7
375.5													
379.5													
382.0	55.5	52.4	- 5.6	56.2	57.5	+ 2.3	56.7	57.2	+ 0.9	56.5	56.5	0.0	- 0.6
386.0													
403.5													
404.8	94.7	98.0	+ 3.5	95.2	97.8	+ 2.7	97.6	98.3	+ 0.7	97.3	97.5	+ 0.2	+ 1.8
407.0	100.7	102.0	+ 1.3	102.2	102.2	0.0	103.0	101.7	- 1.3	102.8	101.5	- 1.3	- 0.3
408.5													
431.0													
433.5													
436.0	68.5	67.0	- 2.2	68.4	66.7	- 2.5	68.8	66.1	- 3.9	68.7	65.6	- 4.5	- 3.3
440.5													
507.5													
545.5													
546.5													
549.5													
575.4	67.0	67.6	+ 0.9	67.1	67.4	+ 0.4	67.4	67.4	0.0	67.5	67.6	+ 0.1	+ 0.4
578.0	54.8	55.3	+ 0.9	54.9	55.5	+ 1.1	55.5	55.2	- 0.5	55.7	54.8	- 1.6	0.0
585.6													
626.0													

TABLE 13. (Continued)

Sample / Wavelength (nm)	1B1			2B1			3B1			4B1			%*
	B	A	%	B	A	%	B	A	%	B	A	%	
668.5													
678.5	48.5	48.7	+ 0.4	48.8	54.1	+10.9	48.5	48.3	- 0.4	49.7	47.7	- 4.4	+ 1.4
709.0	48.2	48.2	0.0	48.6	48.3	- 0.6	49.2	47.8	- 3.8	49.6	47.4	- 4.4	- 2.2
712.5													
729.5	66.1	65.0	- 1.7	66.4	65.0	- 2.1	67.4	64.4	- 4.9	67.6	64.2	- 5.0	- 3.4
731.0													
732.5													
758.0													
761.0	50.9	48.8	- 4.1	51.2	48.7	- 4.9	51.0	48.4	- 5.1	51.0	47.9	- 6.1	- 5.0
797.0	35.6	31.3	-12.1	35.3	31.6	-10.5	36.5	31.0	-15.1	36.7	29.9	-18.5	-14.0
810.0													
816.0	54.5	53.3	- 2.2	54.7	53.3	- 2.6	55.0	53.0	- 3.6	55.0	53.0	- 3.6	- 3.0
862.5													
872.0													
939.5													
983.5													
992.5													
Continuum:													
300.0													
325.0													
350.0	55.0	55.0	0.0	55.2	55.0	- 0.4	55.3	55.0	- 0.5	55.5	55.0	- 0.9	- 0.4
375.0													
400.0													
425.0	55.3	56.1	+ 1.4	55.7	56.3	+ 1.1	56.2	56.0	- 0.4	55.9	56.0	+ 0.2	+ 0.6
450.0	54.9	55.1	+ 0.4	55.0	55.1	+ 0.2	55.3	55.0	- 0.5	55.4	55.0	- 0.7	- 0.2
475.0	54.5	54.9	+ 0.7	54.7	54.9	+ 0.4	55.0	54.8	- 0.4	55.2	54.8	- 0.7	0.0
500.0	56.5	52.4	- 7.3	50.8	52.6	+ 3.5	51.7	52.9	+ 2.3	51.7	51.6	- 0.2	- 0.4
525.0	47.5	49.5	+ 4.2	47.8	50.9	+ 6.5	49.0	49.0	0.0	48.6	48.3	- 0.6	+ 2.5
550.0	56.5	60.0	+ 6.2	56.5	60.0	+ 6.2	57.0	60.0	+ 5.3	59.0	57.5	- 2.5	+ 3.8
575.0													
600.0	43.7	44.7	+ 2.3	44.7	45.4	+ 1.6	44.7	45.0	+ 0.7	44.8	44.4	- 0.9	+ 1.0
625.0													
650.0	45.0	45.3	+ 0.7	45.3	45.7	+ 0.9	45.7	45.0	- 1.5	46.0	44.7	- 2.8	- 0.7
675.0	46.0	45.8	- 0.4	46.3	46.3	0.0	46.7	45.7	- 2.1	47.2	45.2	- 4.2	- 1.7
700.0	43.8	43.8	0.0	44.0	44.0	0.0	44.4	43.6	- 1.8	44.7	43.3	- 3.1	- 1.2
725.0	49.7	49.4	- 0.6	51.2	50.7	- 1.0	51.3	49.3	- 3.9	51.3	50.0	- 2.5	- 2.0
750.0	41.5	41.3	- 0.5	42.0	41.5	- 1.2	42.5	41.0	- 3.5	43.3	40.7	- 6.0	- 2.8
775.0	38.2	36.4	- 4.7	38.5	36.7	- 4.7	38.6	35.9	- 7.0	39.0	35.0	-10.3	- 6.7
800.0													

* Average change in control samples

90

TABLE 13. (Continued)

Sample	5B1					6B1					7B1				
Wavelength (nm)	B	A	%	A	%	B	A	%	A	%	B	A	%	A	%
Spectral:															
248.2	8.7	2.3	-73.6	1.7	-80.5	9.3	1.0	-89.2	1.1	-88.2	8.8	1.8	-79.5	1.0	-88.6
253.6	66.7	52.2	-21.7	53.1	-20.4	69.5	50.5	-27.3	53.2	-23.4	68.6	50.9	-25.8	52.9	-22.9
265.5	13.7	1.7	-87.6	1.8	-86.9	14.8	1.5	-86.9	2.4	-83.8	14.4	1.4	-90.3	1.7	-88.2
289.5	16.5	2.3	-86.1	2.4	-85.5	17.6	1.9	-89.2	3.3	-81.2	16.8	1.8	-89.3	2.3	-86.3
297.0	39.8	6.9	-82.7	7.4	-81.4	41.2	6.0	-85.4	7.7	-81.3	40.8	6.0	-85.3	7.5	-81.6
302.4	43.2	10.6	-75.5	11.3	-73.8	43.8	8.4	-81.8	12.3	-71.9	43.8	8.7	-80.1	10.9	-75.1
313.5	56.0	45.7	-18.4	46.0	-17.9	56.7	44.7	-21.2	46.7	-17.6	56.7	44.6	-21.3	45.6	-19.6
334.2	67.7	54.7	-19.2	55.2	-18.5	68.0	53.7	-21.0	55.5	-18.4	68.0	53.7	-21.0	55.0	-19.1
354.5	58.6	46.5	-20.6	47.4	-19.1	58.7	45.6	-22.3	47.8	-18.6	58.4	45.5	-22.1	48.0	-17.8
356.0															
362.0															
365.0	91.5	70.5	-23.0	77.4	-19.4	92.3	70.8	-23.3	68.8	-25.5	91.8	70.4	-23.3	69.2	-24.6
365.6															
366.5															
372.5															
375.5															
379.5	64.4	48.9	-24.1	49.3	-23.4	64.4	48.9	-24.1	49.3	-23.4	68.6	48.5	-23.7	49.1	-22.8
382.0	56.8	44.5	-21.7	45.5	-19.9	56.5	44.0	-22.1	46.2	-18.2	56.0	44.0	-21.4	46.0	-17.9
386.0															
403.5															
404.8	97.1	68.4	-29.6	68.0	-30.0	97.2	68.5	-29.5	67.4	-30.7	96.6	68.1	-29.5	67.4	-30.2
407.0															
408.5															
431.0															
433.5	102.5	67.3	-34.4	62.3	-39.3	102.8	67.4	-34.4	66.9	-34.9	102.5	66.8	-34.8	66.7	-34.9
436.0															
440.5	68.7	51.9	-24.5	52.7	-23.3	69.5	50.5	-27.3	50.3	-23.7	69.8	50.8	-27.2	52.8	-24.4
507.5															
545.5															
546.5															
549.5															
575.4	67.5	55.3	-18.1	55.7	-17.5	68.2	54.8	-19.6	55.7	-18.3	68.2	54.7	-19.8	55.3	-19.9
578.0															
585.6	55.5	35.5	-36.0	37.5	-32.4	56.6	32.6	-42.4	38.6	-31.8	56.4	33.5	-40.6	37.3	-33.9
626.0															

TABLE 13. (Concluded)

Sample Wavelength (nm)	5B1					6B1					7B1				
	B	A	%	A	%	B	A	%	A	%	B	A	%	A	%
668.5															
678.5	50.0	23.0	-54.0	25.6	-48.8	49.7	21.9	-55.9	27.4	-44.9	49.4	22.7	-54.0	26.7	-46.0
709.0	49.7	23.8	-52.1	26.2	-47.3	49.4	28.0	-43.3	32.3	-34.6	49.2	23.7	-51.8	27.3	-44.5
712.5															
729.5	67.5	52.0	-23.0	53.0	-21.5	68.2	50.5	-26.0	53.5	-21.6	68.2	51.0	-25.2	53.3	-21.8
731.0															
732.5															
758.0	50.9	24.9	-51.1	27.9	-45.2	51.3	22.9	-55.4	29.9	-41.7	51.0	24.2	-52.5	30.2	-40.8
761.0	37.1	4.0	-89.2	4.5	-87.9	36.3	3.8	-89.5	4.5	-87.6	36.2	3.8	-89.5	4.5	-87.6
797.0															
810.0															
816.0	55.2	32.7	-40.8	34.6	-37.3	55.3	31.7	-42.6	35.7	-35.4	55.3	32.8	-40.7	35.1	-36.5
862.5															
872.0															
939.5															
983.5															
992.5															
Continuum:															
300.0															
325.0															
350.0	55.5	41.8	-24.7	42.3	-23.8	55.8	41.4	-25.8	42.2	-24.4	55.8	41.3	-26.0	42.0	-24.7
375.0															
400.0															
425.0	56.2	44.4	-21.0	45.7	-18.7	56.0	44.5	-20.5	46.0	-17.9	55.9	44.3	-20.8	45.8	-18.1
450.0	55.5	42.0	-24.3	42.0	-24.3	55.8	41.0	-26.5	42.5	-23.8	55.5	41.0	-26.1	42.0	-24.3
475.0	55.2	39.3	-28.8	39.8	-27.9	55.6	38.4	-30.9	49.5	-11.0	55.0	38.8	-29.4	39.3	-28.5
500.0	52.2	31.5	-39.7	32.8	-37.2	51.5	31.4	-39.0	33.5	-35.0	50.6	31.4	-38.0	33.5	-33.8
525.0	49.3	24.7	-49.9	27.0	-45.2	48.7	26.6	-46.6	27.7	-43.1	47.5	25.3	-46.7	27.8	-41.5
550.0	60.0	52.0	-13.3	50.0	-16.7	63.0	46.5	-26.2	50.5	-19.8	57.0	49.5	-13.2	50.0	-12.3
575.0															
600.0	45.0	18.4	-59.1	19.8	-55.0	44.5	19.0	-57.3	20.8	-53.3	44.0	18.5	-53.0	20.4	-53.6
625.0															
650.0	46.3	16.3	-64.8	18.5	-60.0	45.8	16.3	-64.4	19.5	-57.4	45.5	16.3	-64.2	19.2	-57.8
675.0	47.4	17.5	-63.1	19.8	-58.2	46.8	17.0	-63.7	21.3	-54.5	46.5	17.5	-62.4	20.7	-55.5
700.0	45.0	13.0	-71.1	14.5	-67.8	44.7	12.5	-72.0	15.0	-66.4	44.2	12.8	-71.0	15.0	-66.1
725.0	51.3	25.0	-49.3	31.5	-38.6	50.5	31.0	-38.2	31.5	-37.6	51.6	29.5	-42.8	32.3	-37.4
750.0	43.0	11.7	-72.8	13.0	-69.8	42.6	11.5	-73.0	14.0	-67.1	42.0	14.0	-66.7	16.0	-61.9
775.0	39.3	5.3	-86.5	6.0	-84.7	38.5	5.0	-87.0	6.0	-84.4	38.2	3.0	-92.7	3.5	-90.8
800.0															

* Average change in control samples

TABLE 14. TRANSMISSIVE REDUCED DATA/PERCENT CHANGES FOR THE B3 GROUP

Wavelength (nm)	1B3			2B3			3B3			4B3			5B3			6B3			7B3			%z
	B	A	%	B	A	%	B	A	%	B	A	%	B	A	%	B	A	%	B	A	%	
248.2	7.95	9.3	+17.0	8.8	9.4	+6.8	8.5	9.0	+5.9	8.4	8.8	+5.2	8.20	7.0	-14.6	8.10	6.2	-23.5	7.05	5.5	-22	- 8.7
253.6	66.85	62.5	- 6.5	67.8	62.8	-7.4	68.8	62.8	-9.7	68.6	62.6	-9.7	68.15	54.8	-19.6	68.00	55.2	-19.6	66.40	54.5	-17.9	- 8.3
265.5	13.00	13.2	+ 1.5	14.1	13.2	-6.4	13.6	12.7	-6.6	13.3	12.4	-6.8	13.90	9.6	-30.9	13.60	8.6	-36.8	12.85	7.5	-41.6	- 4.6
289.5	16.00	18.5	+15.6	16.7	18.2	+9.0	16.2	17.6	+8.6	16.0	17.2	+7.5	16.55	12.9	-22.1	16.20	11.4	-29.6	15.30	10.0	-34.6	+10.2
297.0	39.45	39.4	- 0.9	40.3	39.4	-2.2	40.6	39.2	-3.4	40.5	38.8	-4.2	39.95	33.7	-15.6	39.85	34.7	-12.9	38.70	29.3	-24.3	- 2.7
354.5	57.25	59.6	+ 4.1	58.0	60.0	-3.4	58.4	59.8	+2.4	58.3	60.0	+2.9	58.00	56.0	- 3.4	58.05	55.2	- 4.9	56.80	54.7	- 3.7	+ 3.2
365.0	95.45	97.4	+ 2.0	96.2	97.8	+1.7	96.8	96.9	+0.1	96.6	97.3	+0.7	97.25	86.8	-10.7	97.10	84.5	-13.0	91.00	77.6	-14.7	+ 1.1
379.5	63.65	66.5	+ 5.5	63.7	66.2	+3.9	63.5	66.3	+4.4	63.6	66.5	+4.6	64.10	62.5	- 2.5	64.20	59.6	- 7.2	62.85	59.0	- 6.1	+ 4.6
404.8	95.70	97.5	- 1.9	96.3	97.9	+1.7	96.0	97.7	-1.8	96.4	97.5	+1.1	97.10	90.0	- 7.3	97.20	87.4	-10.1	95.90	84.7	-11.7	- 1.6
436.0	101.40	101.5	+ 0.1	102.2	101.6	-0.6	102.0	101.3	-0.7	102.2	102.2	0.0	102.24	95.5	- 6.6	102.70	93.7	- 8.8	101.35	93.0	- 8.2	+ 0.3
440.5	68.80	64.9	- 5.7	69.2	65.5	-5.3	70.0	64.9	-7.3	70.5	64.6	-8.4	70.35	56.6	-19.5	69.70	56.7	-18.6	68.50	55.2	-19.4	+ 6.7
546.5	69.85	72.7	+ 4.1	70.0	72.0	+2.9	70.5	70.6	+0.1	70.2	71.4	+1.7	70.65	68.2	- 3.5	70.55	67.8	- 3.9	69.15	67.5	- 2.4	+ 2.2
626.0	55.25	54.5	- 1.4	55.5	54.6	-1.6	56.2	54.2	-3.6	56.0	54.2	-3.2	55.50	50.0	- 9.9	55.50	48.8	-12.1	54.50	47.8	-12.3	- 2.4

93

TABLE 14. (Concluded)

Sample / Wavelength (nm)	1B3 B	1B3 A	1B3 %	2B3 B	2B3 A	2B3 %	3B3 B	3B3 A	3B3 %	4B3 B	4B3 A	4B3 %	5B3 B	5B3 A	5B3 %	6B3 B	6B3 A	6B3 %	7B3 B	7B3 A	7B3 %	%*
668.5																						
678.5	49.30	49.2	-0.2	49.2	49.0	-0.4	49.2	48.6	-1.2	49.3	48.6	-1.4	49.25	45.2	-8.2	49.50	44.0	-11.1	48.25	43.5	-9.8	-0.8
709.0	48.75	48.6	-0.3	48.8	48.5	-0.6	49.0	48.2	-1.6	49.0	48.2	-1.6	49.00	44.6	-9.0	49.10	43.5	-11.4	48.00	42.8	-10.8	-1.0
712.5	67.95	64.8	-4.6	67.5	63.6	-5.8	68.2	64.0	-6.2	68.2	63.7	-6.6	68.85	57.2	-16.9	68.60	56.2	-18.1	68.05	55.5	-18.4	-5.8
729.5																						
731.0																						
732.5																						
758.0																						
761.0	50.60	48.6	-4.0	50.9	48.4	-4.9	51.3	48.4	-5.7	51.2	48.4	-5.5	50.70	45.0	-11.2	49.80	45.0	-9.6	48.65	44.2	-9.2	-5.0
797.0																						
810.0																						
816.0	54.05	53.3	-1.4	54.8	53.2	-2.9	55.3	53.0	-4.2	55.4	53.0	-4.3	54.50	50.8	-6.8	54.50	49.5	-9.2	53.40	48.2	-9.7	-3.2
862.5																						
872.0																						
939.5																						
983.5																						
992.5																						
Continuum:																						
300																						
325																						
350																						
375																						
400																						
425																						
450																						
475																						
500																						
525																						
550																						
575																						
600																						
625																						
650																						
675																						
700																						
725																						
750																						
775																						
800																						

* Average change in control samples

the relative degrees of optical degradation of transmittance. The calculation procedure for arriving at the ordinate values was:

$$\text{Percent degradation} = 100 - \frac{\text{after amplitude (A)}}{\text{before amplitude (B)}} \times 100 \quad .$$

These percentages were then plotted in graph form in two ways. First, Figures 79, 80, and 81 plot the percentages versus wavelength without adjusting individual values for control samples changes. Second, Figures 82, 83, and 84 plot percentages versus wavelength with adjustment for control sample changes, represented in each case by the respective average.

It will be immediately noted that not all points for each set of samples have been plotted and that the entire recorded spectrum band has not been plotted. First, the selection of graph points was based on several factors. Some point values were associated with too-closely spaced wavelengths to contribute to the curve definition. Some selected portions of the recorded spectra were not readable. Finally, some selected portions of the recorded spectra gave either apparent anomalous calculated percentages or values which were felt to be unsure within the system confidence limits. In this last area, there did not appear to be any evident simple reason for the occurrences. Then, the entire recorded spectrum was selectively plotted because of low continuum levels, sharp continuum gradients, second order peaks, and the practical response limits of the detector.

The graphical presentation of the test data is in two forms. First, a plot is made of percent relative degradation without adjusting or correcting for the changes which occurred in the control samples. Second, and considered more significant, is a set of plots for each sample group which is normalized by using the average percent change in the four control samples.

In presenting the data, primarily in this latter form, the question that must be answered is whether or not the normalizing of the plots "created" data. In the set of graphs for the B3 group one anomaly of this type does occur around 459 to 525 nm. The twin peaks of samples 6B3 and 7B3 are not true data. Likewise, in the case of the B1 samples groups there is again one anomaly. In this case, a small prominence appears to have been lost at around 350 nm during normalization.
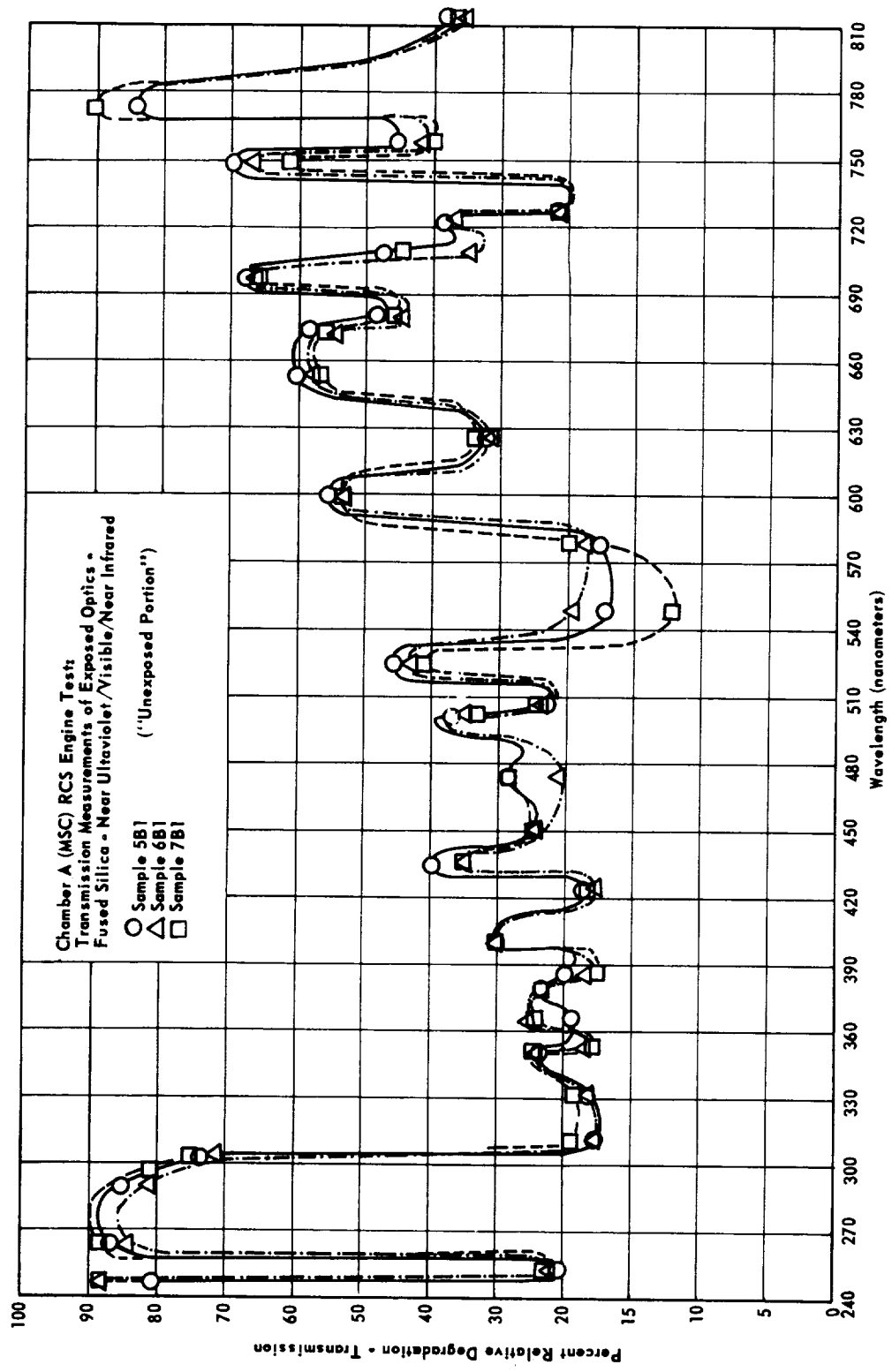
Figure 79. Transmission curves, samples 5B1, 6B1, and 7B1, unexposed portion.

96
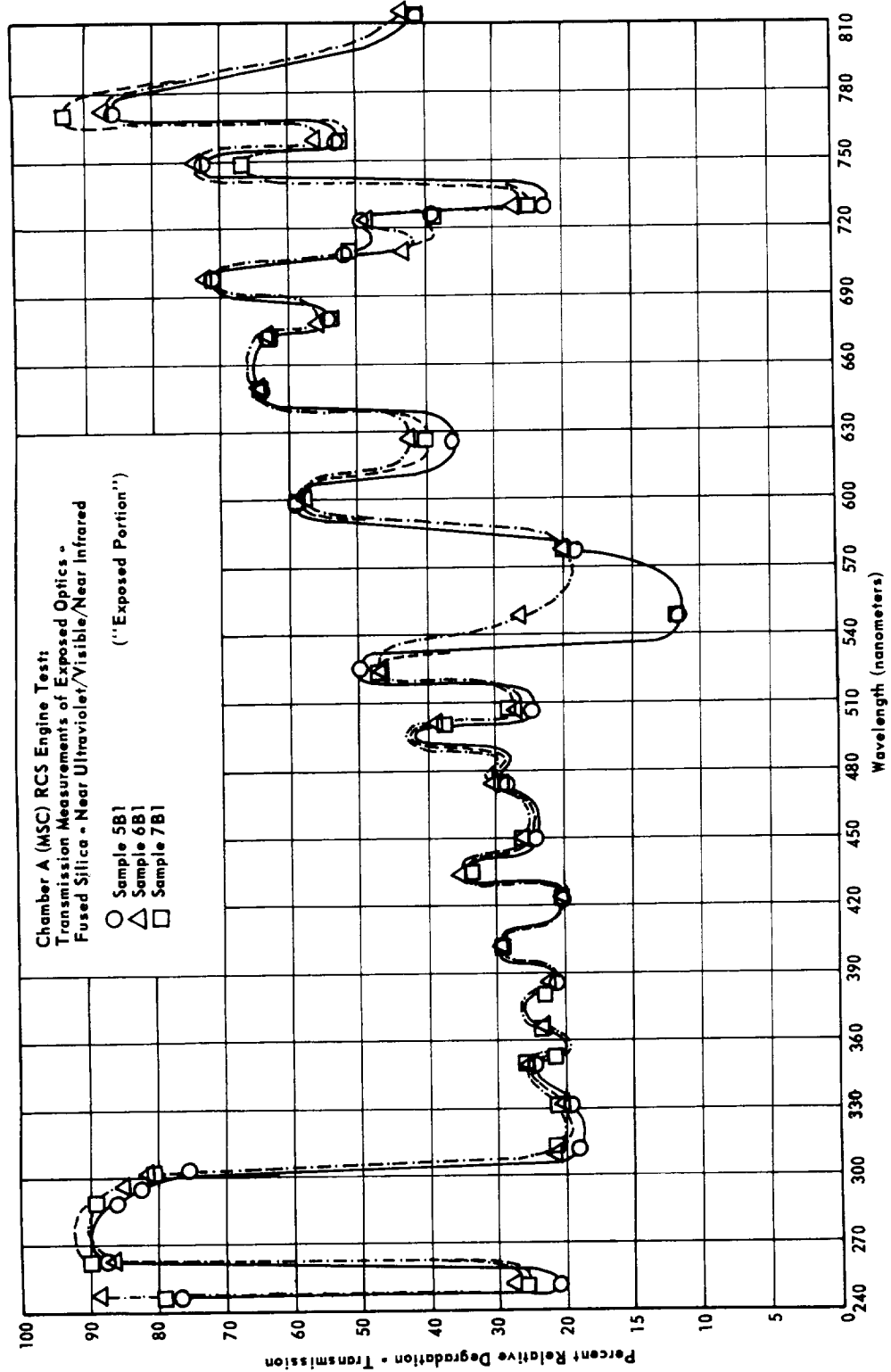
Figure 80. Transmission curves, samples 5B1, 6B1, and 7B1, exposed portion.

97

Figure 81. Transmission curves, samples 5B3, 6B3, and 7B3.

98

Figure 82. Transmission curves, samples 5B1, 6B1, and 7B1, corrected for control changes, unexposed portion.

99

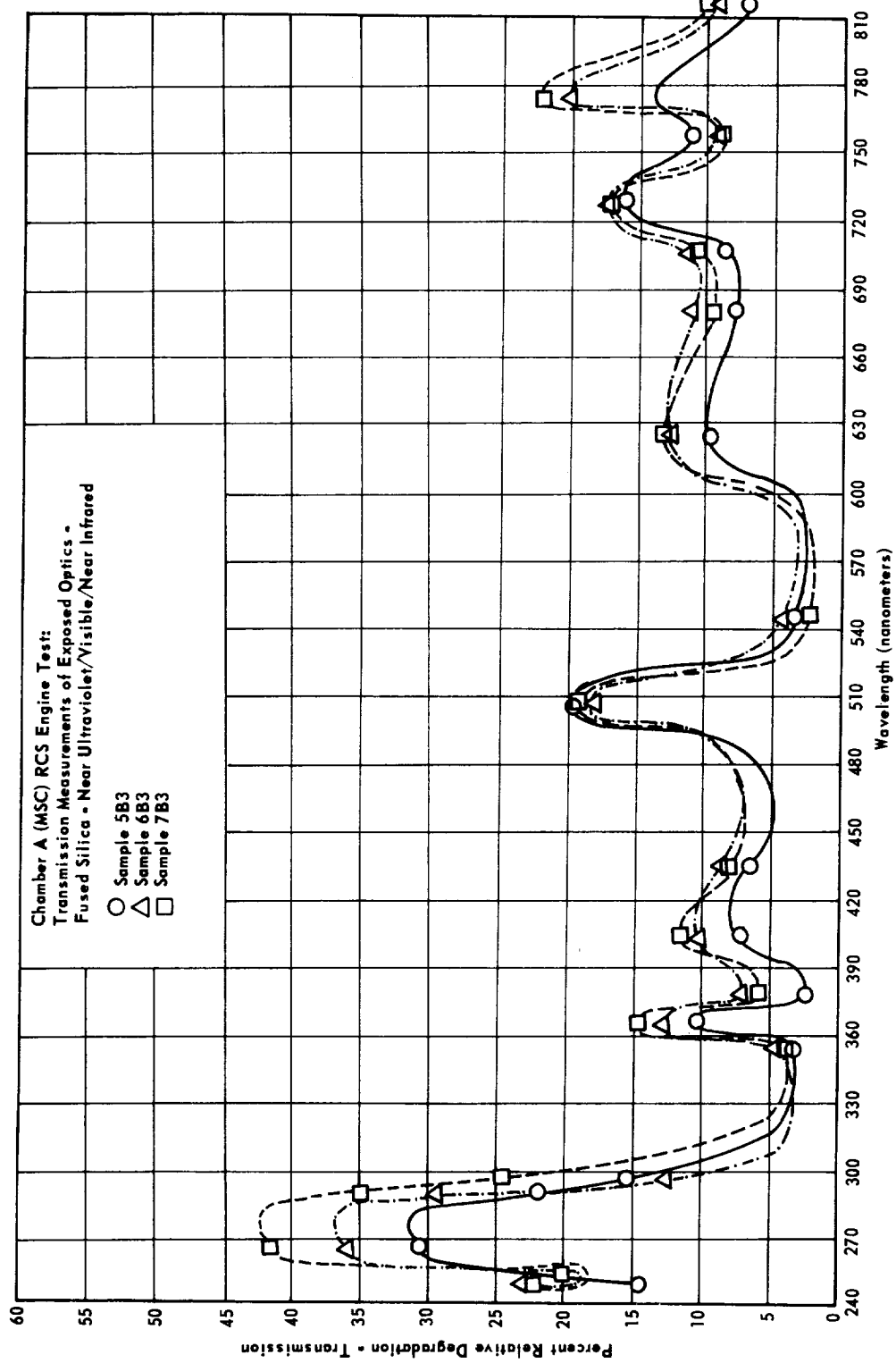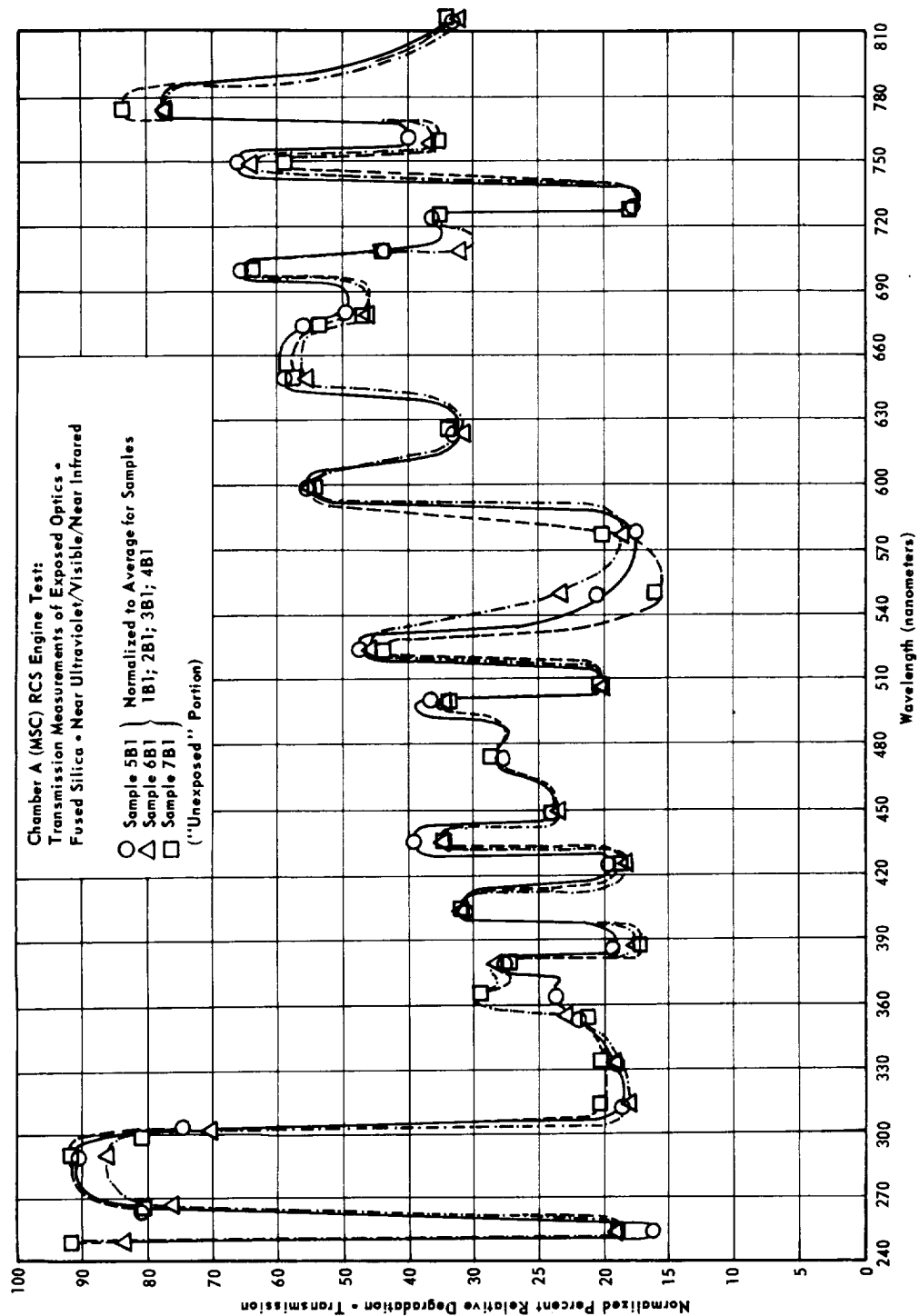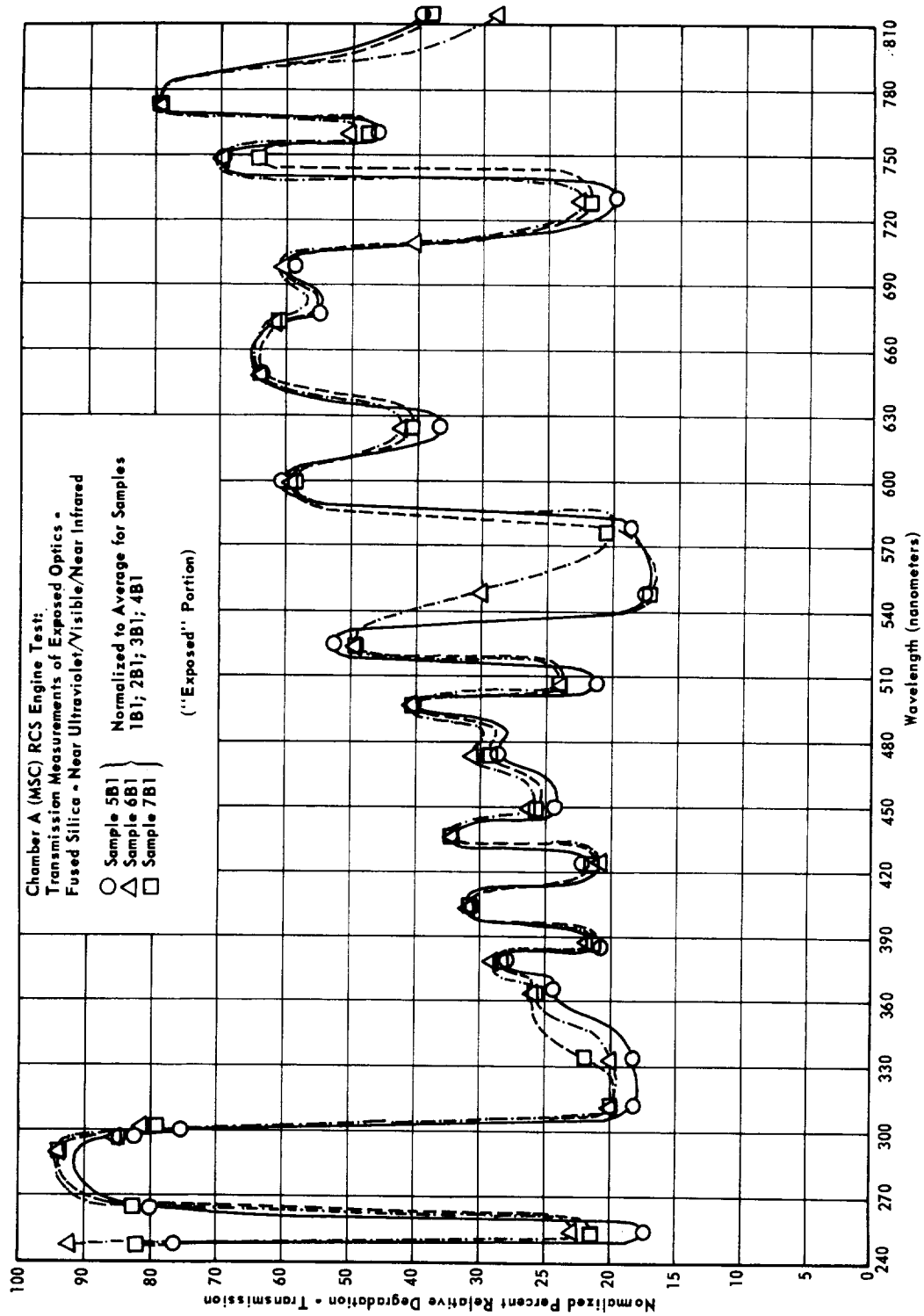Figure 83. Transmission curves, samples 5B1, 6B1, and 7B1, corrected for control changes, exposed portion.
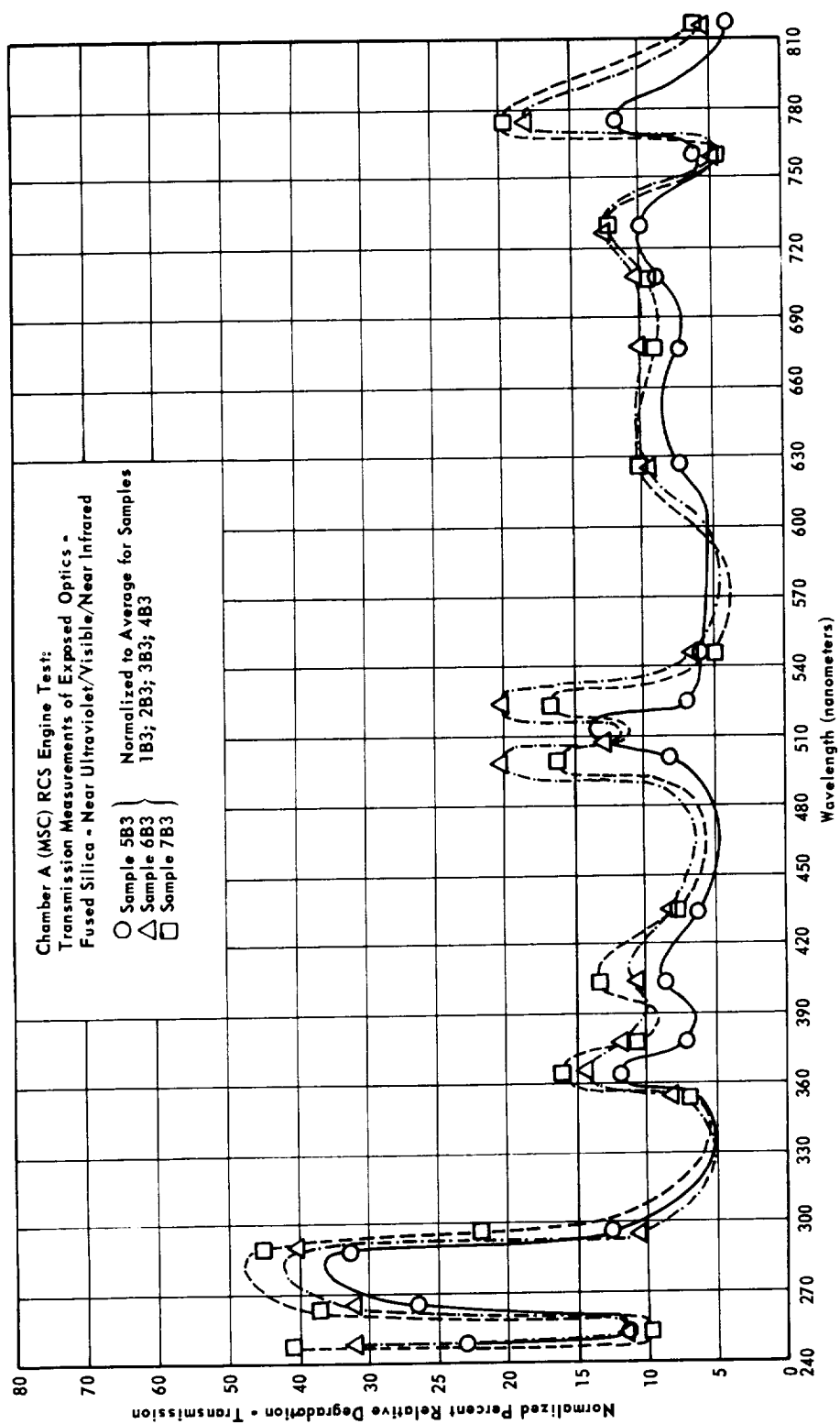
100

Figure 84. Transmission curves, samples 5B3, 6B3, and 7B3, corrected for control changes.

If an attempt is made to estimate the trend of overall degradation of transmission from these data, the following values would perhaps be chosen. For the B3 sample group in the near infrared and visible, the average degradation appears around 7 to 10 percent. The degradation appears to be increasing with frequency below about 250 nm. For the B1 samples group in the near infrared and visible, the averaged degradation appears to occur between 30 and 40 percent. The degradation again appears to increase with frequency below about 250 nm. This is approximately the same for both the exposed and the unexposed test sets.

In an overall view of the graphs of this report, the two items which will probably be noted are: (1) the greater detail of the plots of the B1 sample group and (2) the significant difference in overall degradation at all wavelengths between the B1 and B3 groups.

First, the B1 sample plots show more detail than the B3 sample plots because of the greater number of individual data points which were acceptable for plotting. The second area is not so easily discussed. The sample elements were individually, for example, 5B1 and 5B3, very close to the same sample position and view factor for this chamber test. The B1 samples were covered with aluminum foil so that only about one-third of the surfaces was exposed. A few points can, however, be made from the measurements. The B3 group saw less degradation or deposition, apparently because of a mechanical effect of the aluminum on the B1 samples. This foil covering was not tight-fitting. This is evident from comparing the exposed and unexposed transmission degradation curves. There is little difference. Thus, it is assumed, since little if any real plume flow field existed, that the foil simply served as a "funnel" and collected contaminants for the optic underneath. This hypothesis is proposed rather than any electrostatic mechanism since all the rocket exhaust products would not remain in an ionic condition during their suspended particulate state in the chamber volume. Thus, it is not expected that any electrostatic negative charge, which would have preferentially attracted and physisorbed the contaminants resulting in a deposit, would build up on the optic test beds or, in particular, the aluminum foil.

The general shape of the graphs of percent degradation appear to have the following basic structure. A scattering contribution basically similar to an "exponential" curve increasing toward the ultraviolet because of deposit thickness, particle size distribution, crystal structure, and characteristic absorption bands. Superimposed on this appears to be one other major contribution. This is the absorption peaks and bands characteristic of the deposit composition. Since the primary purpose of this work was to present data on optical properties degradation, no further qualitative work will be reported.

102

Based on the above reported measurements of optical transmission degradation in the near ultraviolet/visible/near infrared, the following conclusions are reached:

1. The optical samples of the B1 and B3 groups were degraded in transmission by matter deposition.

2. The optical degradation of transmission ranged from 7 to 10 percent for the B3 group to 30 to 40 percent for the B1 group with increasing degradation as frequency increased in the ultraviolet.

3. The optical degradation mechanism was composed primarily of scattering and characteristic absorption.

The above results compare favorably with those obtained in the reflectance mode, covering the same wavelength region and reported previously.

The potential instrumental sources of error in this measurement include the following:

1. A difference in optical pathlength between measurements of control and test samples would result in an uncompensated absorption by the constituents of laboratory air in the beam path. This of course would cause spectral absorption bands similar to data peaks to appear in the detector output.

Because the system used for this measurement was single beam, no pathlength inequalities, unequalized transmissions, or unequalized reflections occurred from one measurement to another. In addition, if uniformity of air chemical composition is assumed, then the spectral absorption bands would be removed during data reduction due to the "delta amplitude" differential approach.

2. Any significant light scattered from any area of the beam to the detector would cause erroneous intensity readings.

Because the detector is light-tight mounted against the exit slit area of the monochromator housing, all stray light must come through the slit. In the monochromator this would mean stray light must get past two collimating mirrors and the grating, not to mention the entrance and exit slit. In addition, the monochromator casting is coated inside with optical black and all hardware is likewise coated. As mentioned earlier, this monochromator under standard conditions has a scattered light background of about 0.20 percent.

3. The reproducibility of passage of light through the optical element at the same angle to avoid nonuniform natural effects such as internal scatter or reflection.

This area was covered by the custom source/optic mounting system mentioned in the text.

4. Most critical to single beam spectrophotometric measurements are the source stability and repeatability, the chart drive and scanning drive accuracy and repeatability, and the detector stability. Variations in any of these areas may appear as "data."

As mentioned in the discussion of method, these areas were experimentally evaluated. Table 9 summarizes these measurements and calculations. This points toward this system for these measurements being reproducible to transient extremes to an accuracy of ± 3.2 percent and to average conditions to < 2.0 percent.

It is concluded that the overall accuracy of the measurements reported herein are within confidence limits of ± 5 percent.

VACUUM ULTRAVIOLET/NEAR ULTRAVIOLET REFLECTION — R. C. Linton

Vacuum Ultraviolet Reflectance Measurements. A McPherson Model 225 spectrometer was utilized for obtaining reflectance data in the vacuum ultraviolet spectral region. This facility is presently designed for luminescence studies and does not provide a means of ratioing the incident beam to the reflected beam. The method chosen involved positioning the gold-coated mirrors selected for vacuum ultraviolet measurements (samples NA3 and NA4), where N designates the test bed number (see appendix) so that the monochrometer receiving the source intensity provided a scanning beam from 140 to about 500 nm; the beam was reflected from the positioned sample and entered a second monochromator set at central image. A sodium salicylate coated photomultiplier tube served as the detector.

Measurements were taken before and after the RCS test on both control and chamber exposed samples. The results shown in Figures 85 and 86 show the damage measured by the method described above, assuming no damage on the reference sample 2A4.
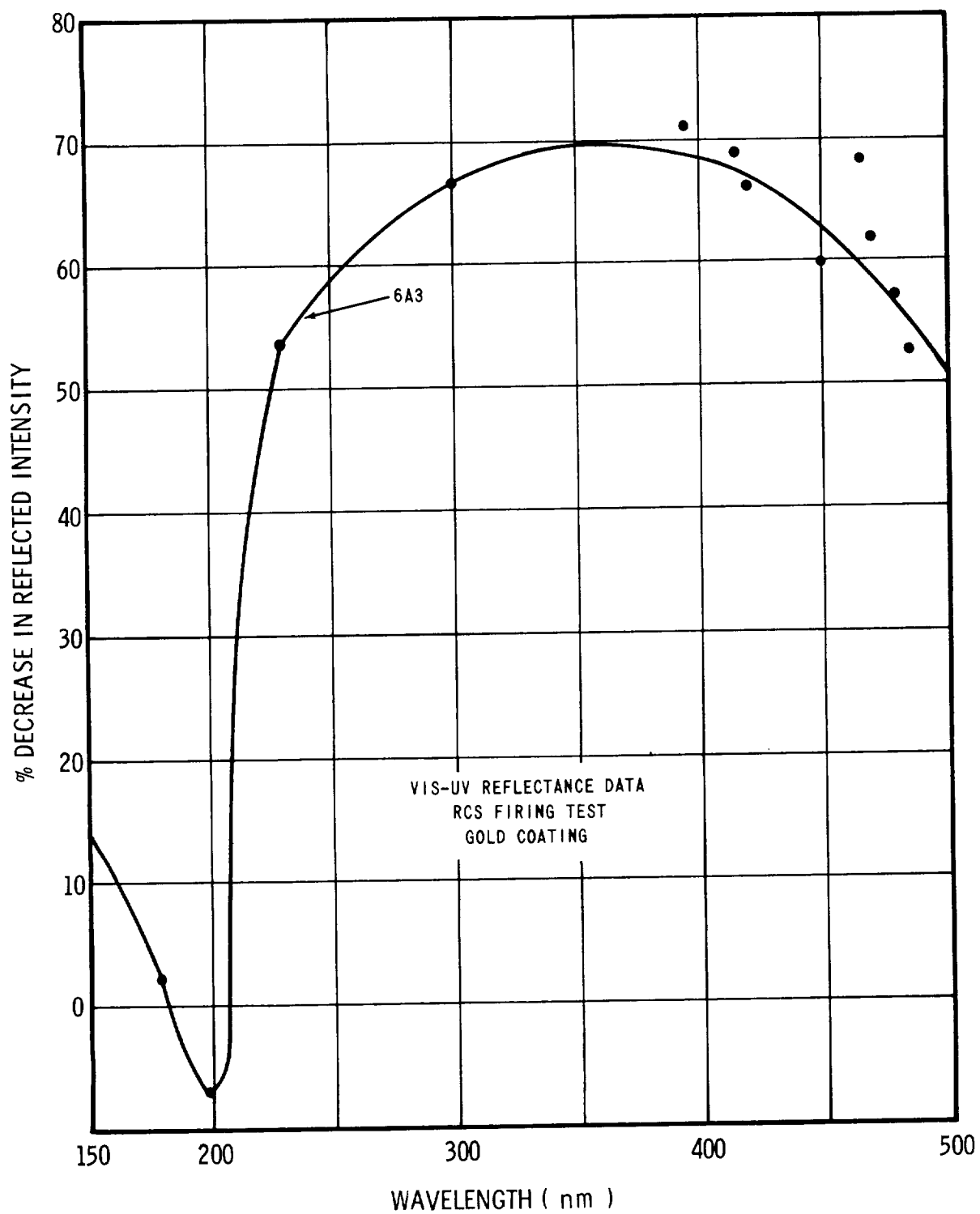
Figure 85. Visible/ultraviolet reflectance data, gold, sample 6A3.
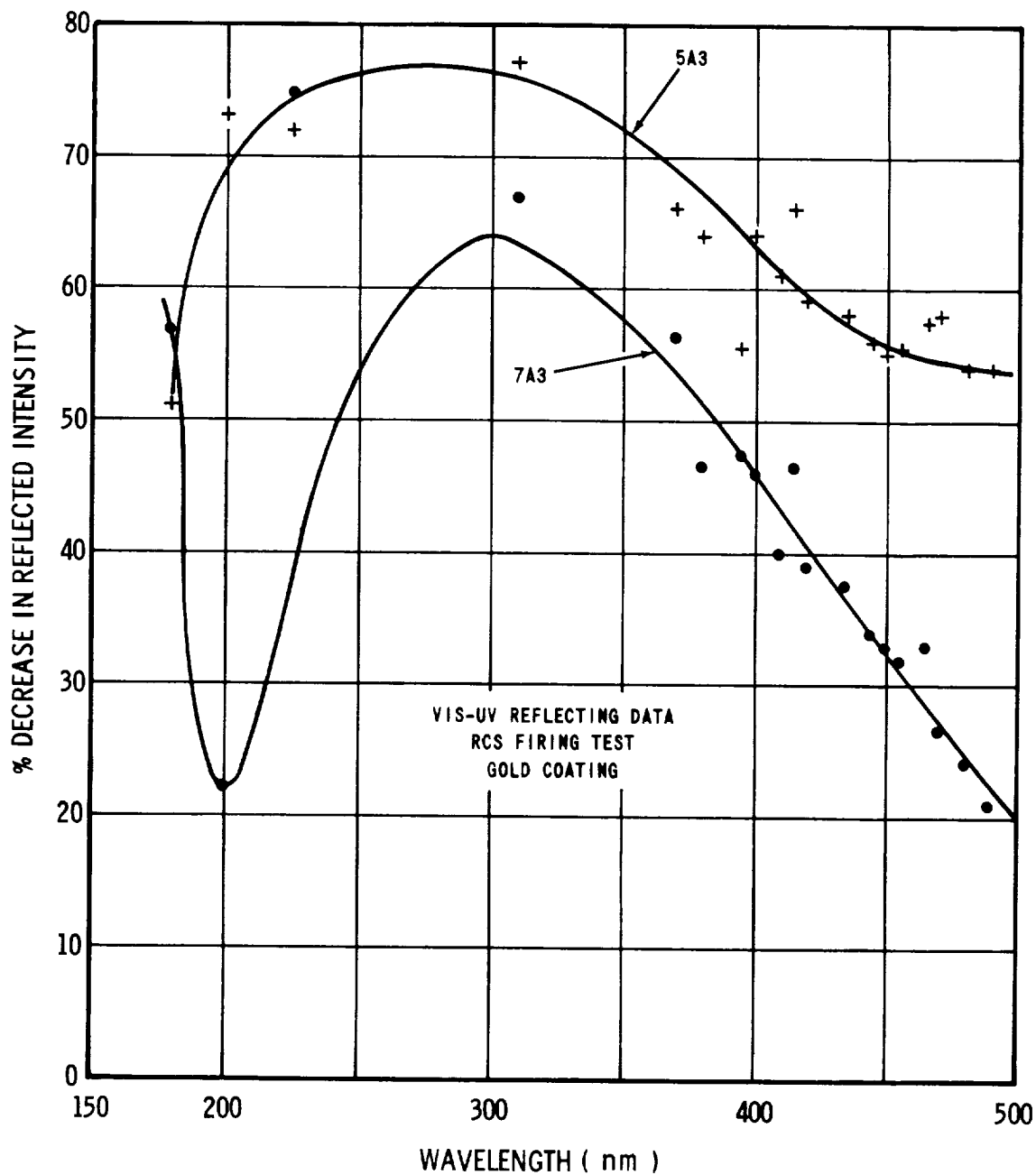
Figure 86. Visible/ultraviolet reflectance data, gold, samples 5A3 and 7A3.

As in the case for the aluminum coating, the damage peaks in the near ultraviolet and starts to decrease below 200 nm. A degree of correlation is between the apparent absorption peaks observed in the samples, although the peak wavelengths are shifted. This may be because of differences in contaminant thicknesses on the different samples.

106

Vacuum ultraviolet reflectance data will be noticeably improved in the near future by the expected addition of a dual-beam reflectometer attachment for the McPherson facility. Also, work is in progress to improve the available sources and extend measurements down to 60 nm.

X-RAY REFLECTION — S. A. Fields and J. M. Reynolds

Quartz optical flats were vacuum coated with 1000 Å nickel and placed in two positions on each of eight test beds. These samples were inserted into the chamber A contamination test program to determine the effect of the deposited contamination on the reflection efficiency of 1.54 Å radiation.

The measurements were made on a modified X-ray diffractometer in an atmospheric environment. At the date of this report, the modification and checkout of the diffractometer has not been completed and, therefore, the optical flats have not been tested.

All of the nickel-coated flats have remained sealed in the clean room since being returned to MSFC except for the two samples on test bed No. 6. These two samples have been removed and are currently undergoing pre-liminary tests.

Current plans are to leave the remainder of the samples in the clean room until the X-ray test apparatus is operational. At that time, they will be removed and tested along with the control samples.

INFRARED TRANSMISSION — E. R. Miller

Cesium Bromide (CsBr) samples numbered 1C4, 2C4, 3C4, 4C4, 5C4, 6C4, 7C4, and 8C4 were measured with a Beckman IR-12 Infrared Spectro-photometer before and after the RCS engine vacuum chamber tests (with the exception of 8C4 which remained at MSC). This measurement determines the near normal specular transmittance from 2.5 to about 50 μm (Figs. 87 through 93).

No degradation is seen on the control samples 1C4, 2C4, 3C4, and 4C4. On the samples that were exposed in the chamber (samples 5C4, 6C4, and 7C4), considerable degradation was noted in the form of scattering (deviation from the specular) and is more pronounced at the shorter wave-lengths; i.e., 2.5 μm, and is apparent to about 20 μm.
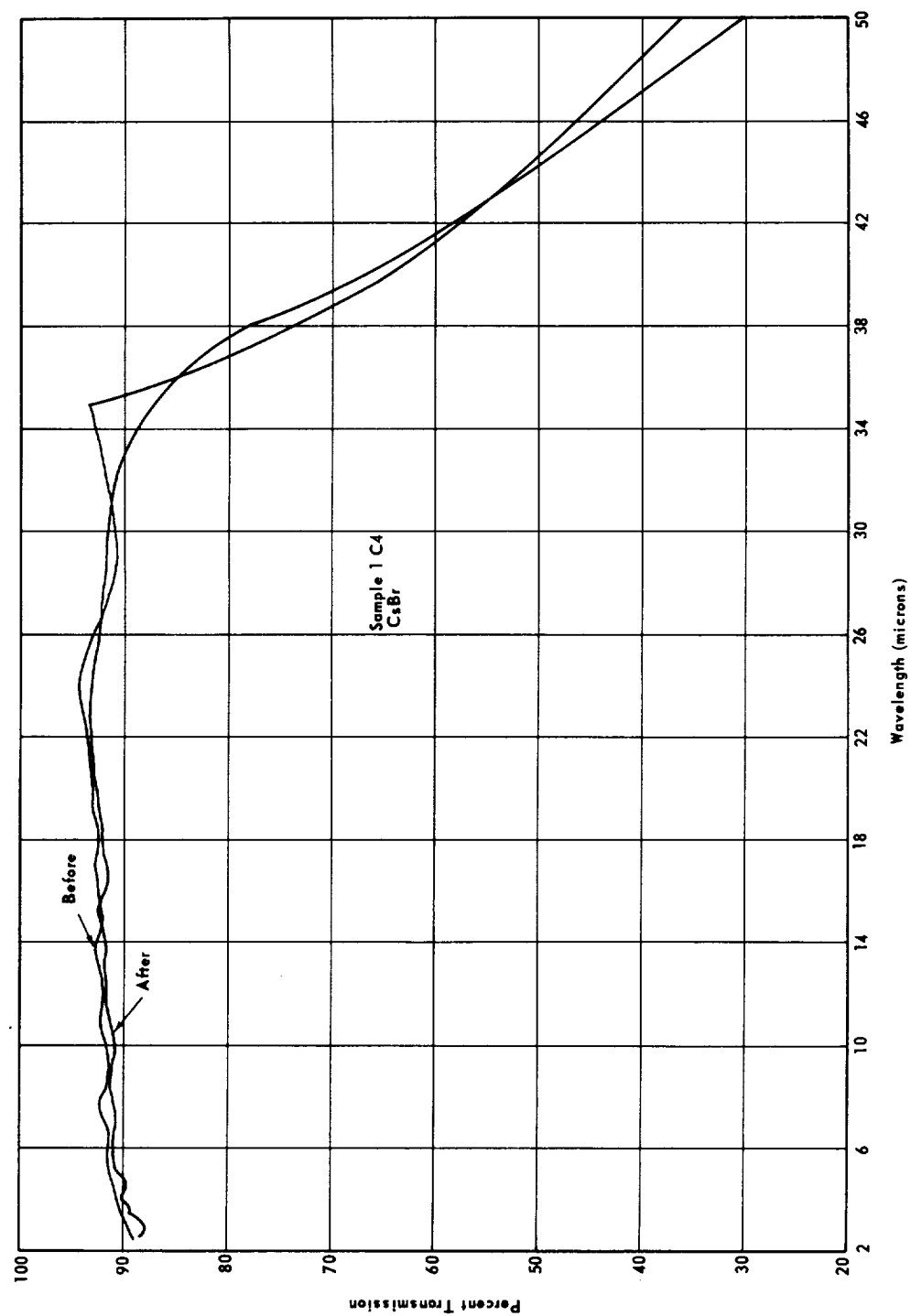
Figure 87. Infrared transmission data, sample 1C4.
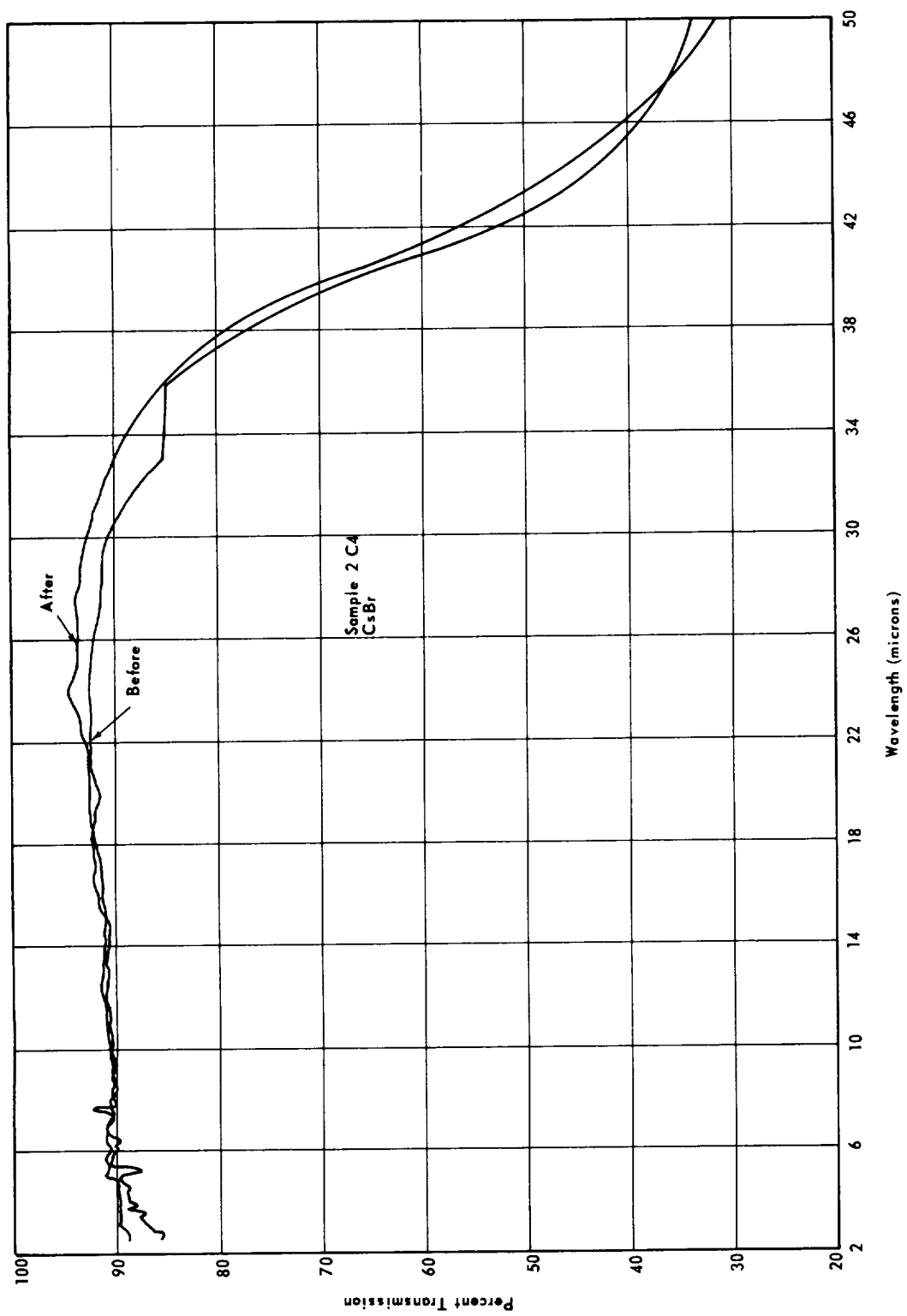
108

Figure 88.   Infrared transmission data, sample 2C4.
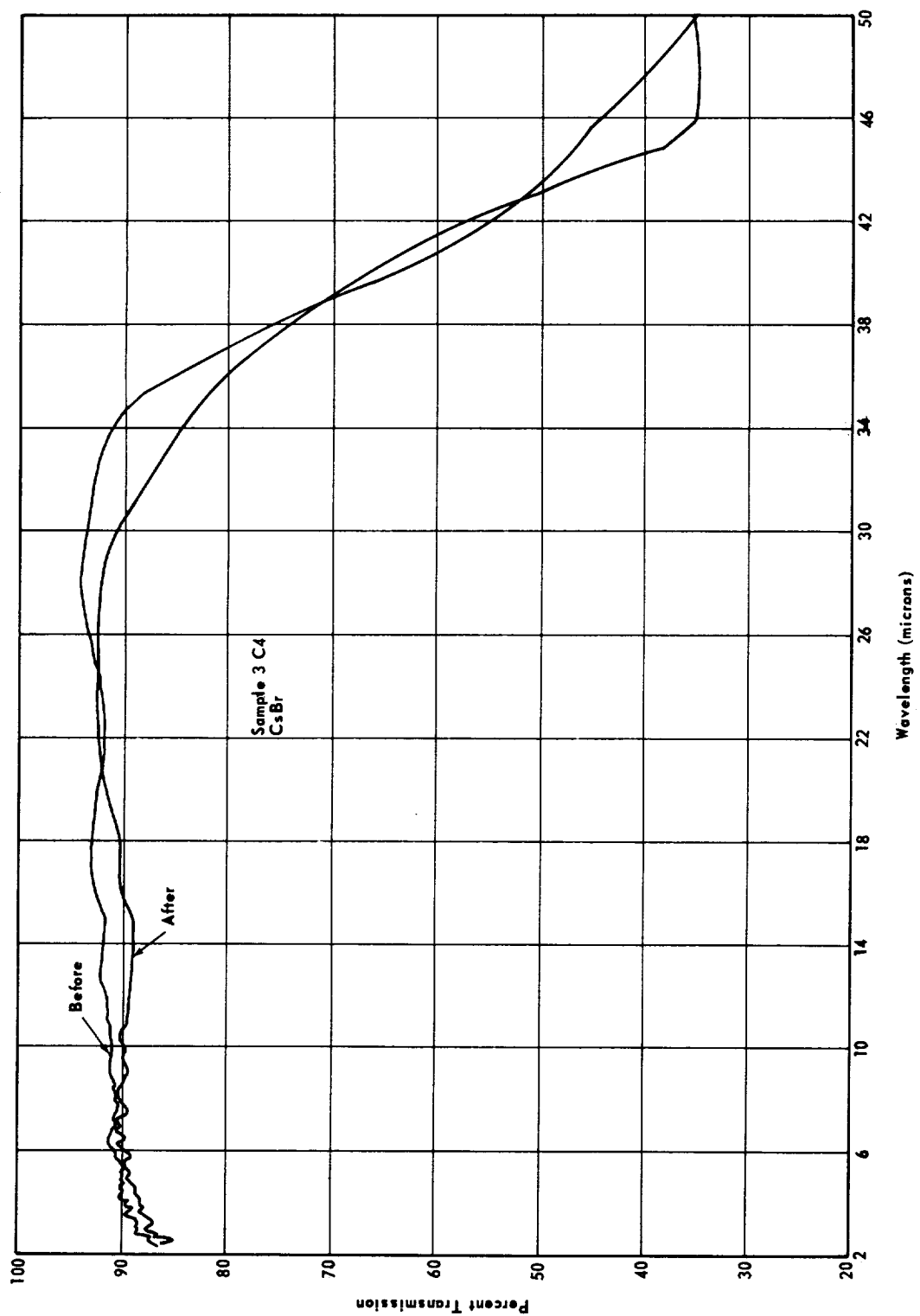
Figure 89. Infrared transmission data, sample 3C4.

110
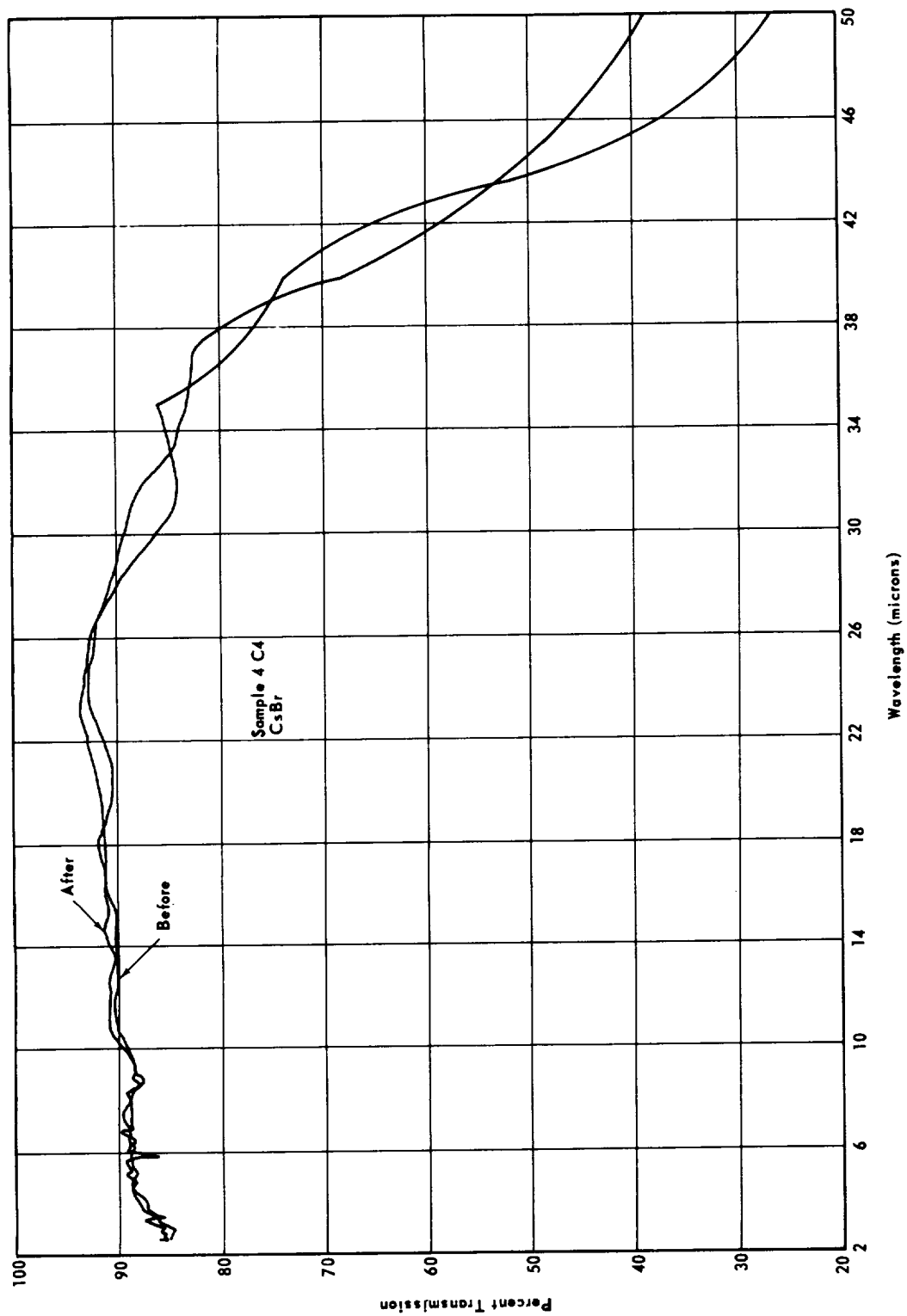
Figure 90. Infrared transmission data, sample 4C4.

111
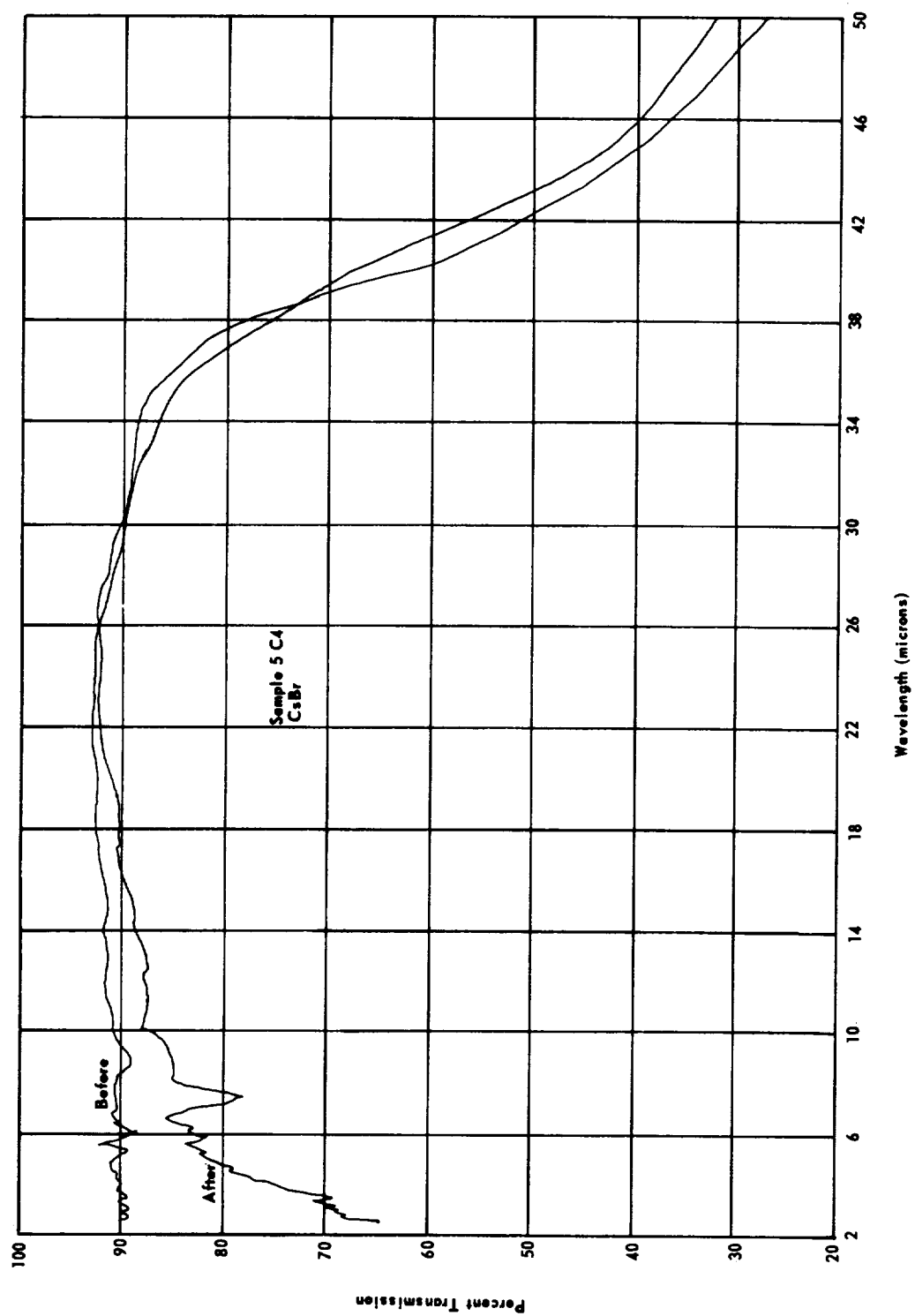
Figure 91. Infrared transmission data, sample 5C4.

112
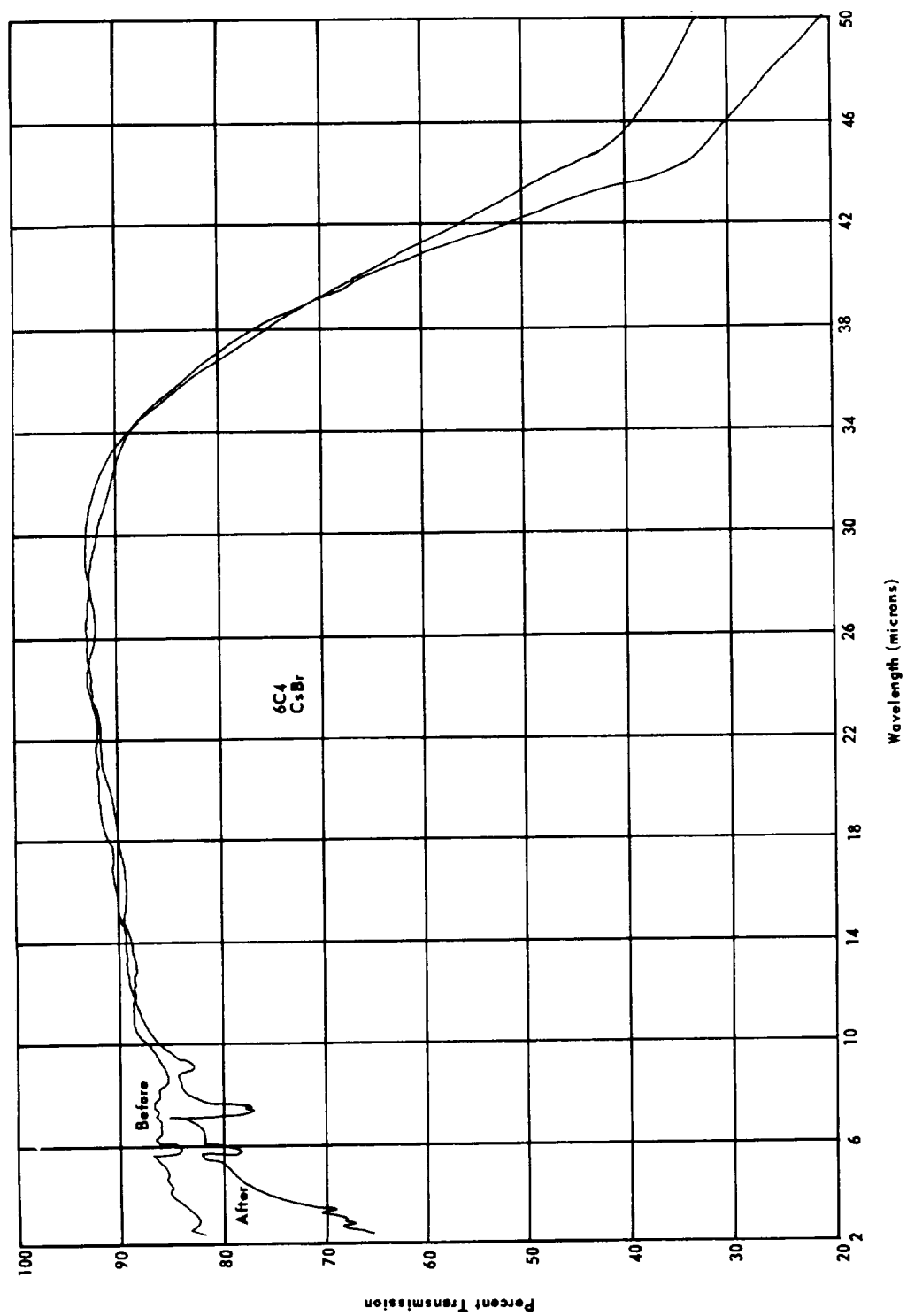
Figure 92. Infrared transmission data, sample 6C4.

113
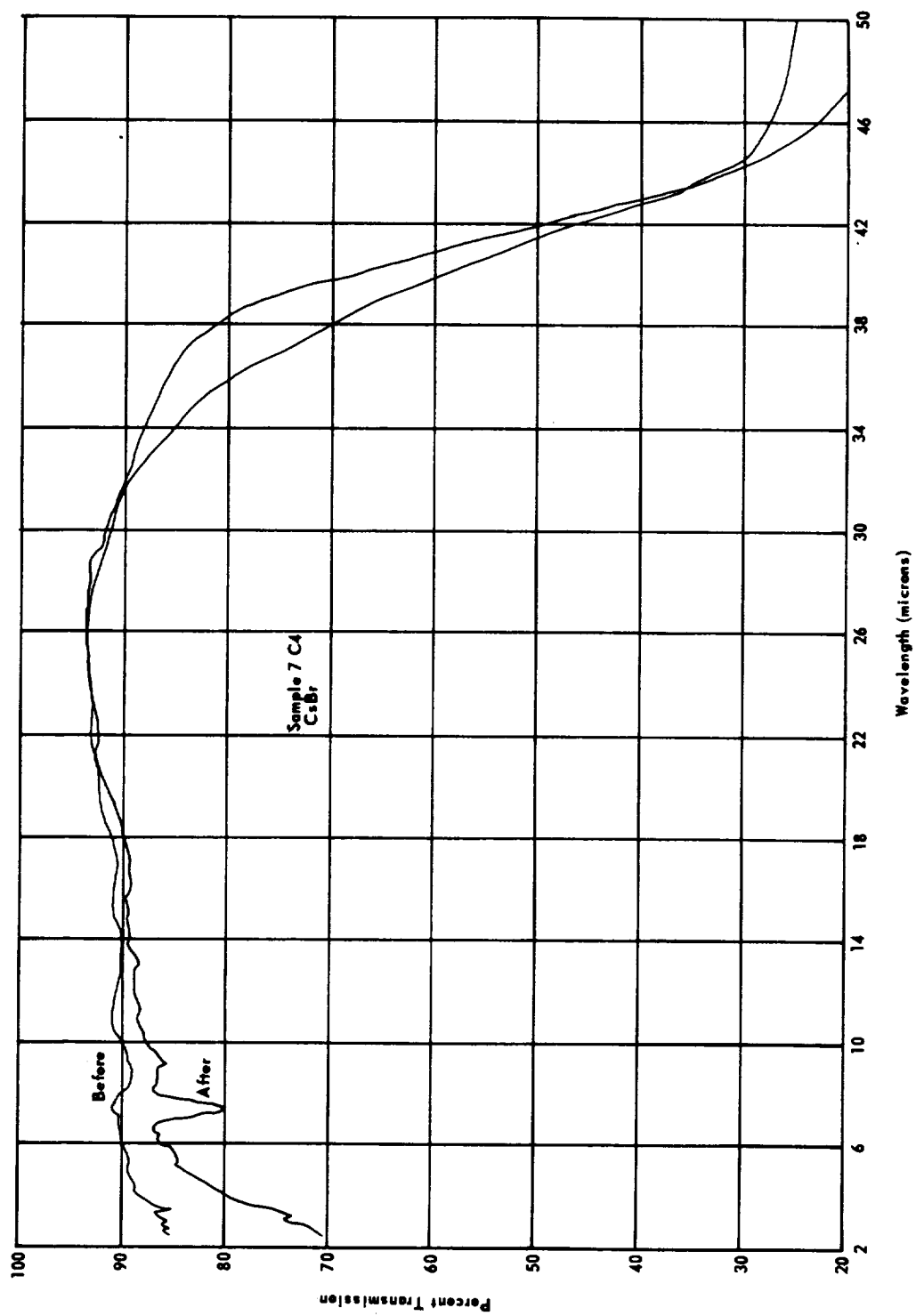
Figure 93. Infrared transmission data, sample 7C4.

114

Less pronounced is the degradation due to absorption, the most promi-
nent occurring at about 7.4 μm (1360 cm^{-1}) and in decreasing strengths 3.4 μm
(2950 cm^{-1}) and 9 μm (1100 cm^{-1}). Although these are weak bands and are
few in number, an attempt is being made to analyze the compounds or components
responsible for the absorption. This is being done with a computer program.
If there is more than one compound present, the chances of successfully
analyzing the samples for chemical composition of the contaminant layer are
very small.

The after vacuum test samples were run on May 7 and 8, 1969. Since
those runs, it was discovered that the contaminant layer is evaporating (or
more likely, decomposing), and the absorption lines are no longer detectable
(~ June 4, 1969).

It appears that the best method for obtaining data from such small
quantities of contaminant is by the use of multiple attenuated total reflectance
(ATR) techniques, and compatible samples should be included in future tests
of this type.

MASS SPECTROMETRIC INVESTIGATIONS — P. Tashbar

Mass spectrometric investigations of the contaminated 7B2 sample were
performed using a medium resolution mass spectrometer. The objectives are
to identify the contaminants present on the 7B2 sample and to identify the 7B2
fragmented ions that are created in the ion source of the mass spectrometer.
In addition, molecules that exist as backround in the mass spectrometer were
determined along with their contribution to the mass spectra of the 7B2 sample.

Mass spectrum was obtained from a Varian M-66 mass spectrometer
[11]. The M-66 is a double-focusing, cycloidal mass spectrometer having a
mass range of 1 to 2000 amu. The cycloidal method uses a crossed electric
and magnetic field. The magnetic field deflects the ions on an essentially
circular path, and the electric field, at right angles to the magnetic field,
applies a transverse force to change this circular path to a cycloidal trajectory.
This cycloidal path makes it possible to have the ion emitter and the target
linearly displaced. Varying the intensity of either field causes a change in
trajectory so that a different part of the ion beam focuses at the detector,
monitoring a different point in the mass spectrum.

The M-66 Inlet System (Figs. 94 and 95) is a dual inlet system con-
sisting of two inlets, two chamber pumpout valves, and two variable leak valves.
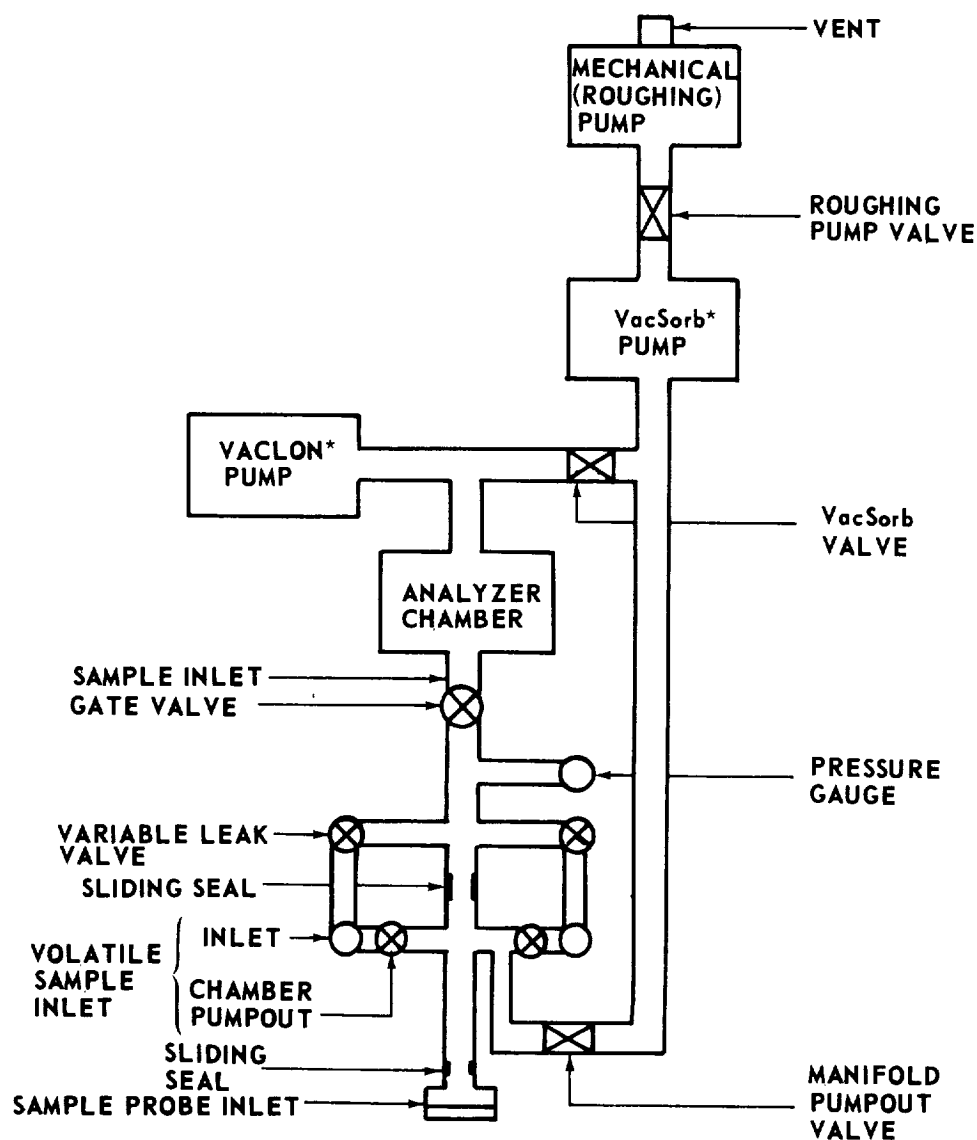
Figure 94. Inlet system schematic.

The sample chambers are symmetrically placed on opposite sides of the tube where the direct sample introduction probe is introduced through sliding seals. The volatile inlet is duplicated so that cleanup between samples can be performed in one inlet while a sample is being introduced into the spectrometer from the other inlet. The inlet may be heated to approximately 200°C by forced air circulating around the inlet components. Air is blown over heated coils as it enters the box that surrounds the entire inlet.
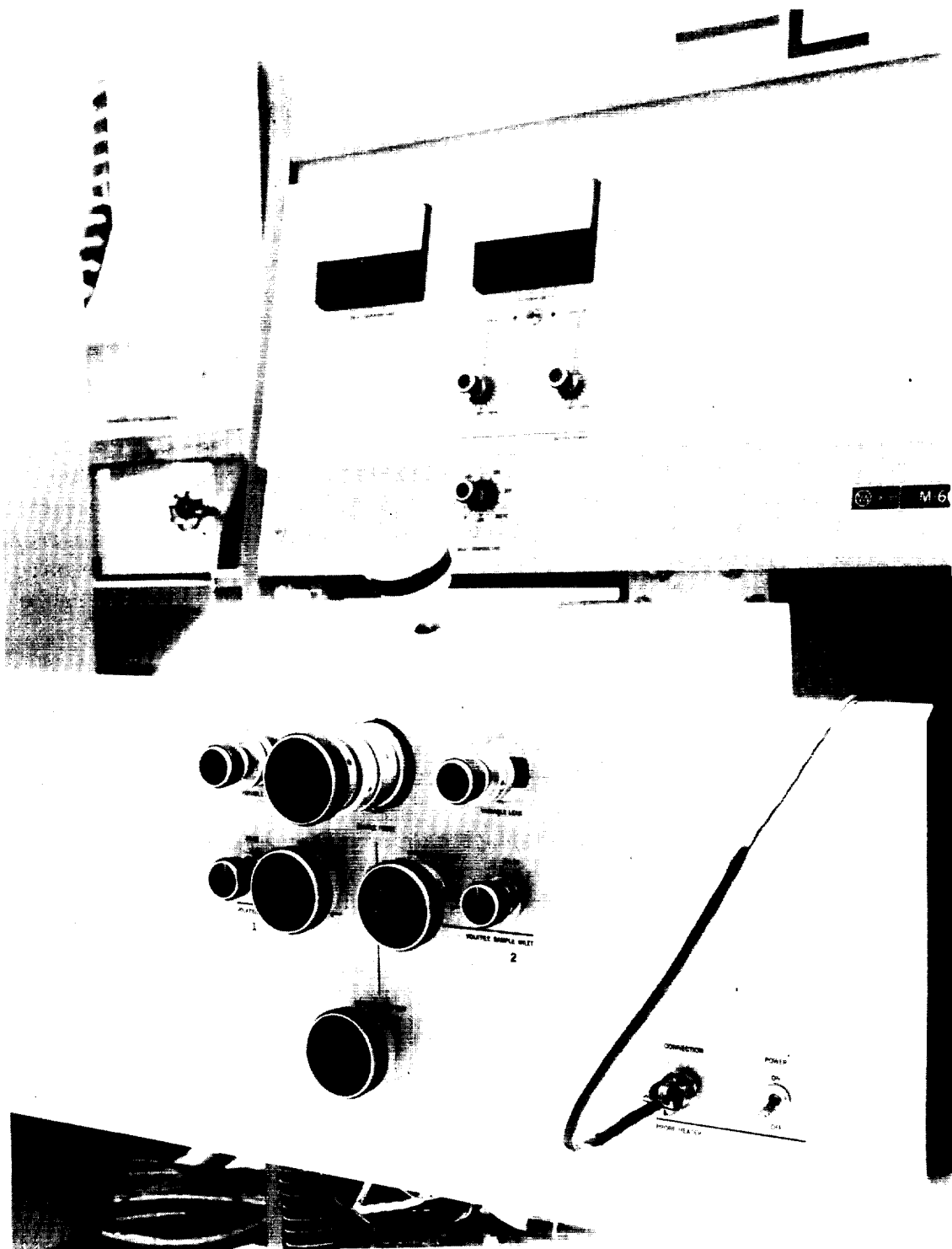
Figure 95. Inlet system and analyzer.

The mass analyzer chamber (Fig. 96) is pumped by a sputter ion pump. The sputter ion pump will pump from 10^{-4} to 10^{-8} torr or lower. A mechanical pump in series with a modified sorbtion pump is used as the pumping system for the inlet system during normal operation. The sorbtion pump stands between the mechanical pump and the inlet system.

Samples are inserted into the volatile sample inlet (Fig. 97) by means of a small pit in the side of the cylindrical piston. Material is placed in the pit in the piston that is then pushed through a sliding seal, so that the pit with the sample moves into the sample chamber that is under vacuum. The sample then enters the source through the leak valve and the gate valve. The gate valve isolates the source from the inlet system.

For solid samples (Figs. 96 and 98), the sample is placed in a melting point capillary that is inserted in the sample well of the direct sample introduction probe. The well is capped with a nozzle and the probe is inserted through the sliding seals in the inlet. The inserted probe seats in a ceramic insulator at the rear of the source so the sample is approximately 5 mm from the ionizing electron beam. Samples introduced with the direct sample introduction probe are heated until a temperature that gives the desired pressure of material in the source is reached.

Vapors to be analyzed are introduced from the inlet into the analyzer chamber. A beam of electrons in the source ionizes the molecules and the ions are propelled through the source slit into the analyzer where they follow a cycloidal path to the collector slit and detector.

The mass spectrometer displays data on either an oscilloscope or an XY recorder. The oscilloscope displays portions of a mass spectrum for adjusting sample conditions and optimizing resolution. The XY recorder presents the data linearly on precalibrated charts and in a permanent form. The XY recorder is used for calibrating the instrument.

Regulation of the source environment is accomplished with the following controls; electron energy, electron current, ion energy, temperature, and the variable leak valve or temperature of the direct sample introduction probe.

The electron energy regulator controls the voltage that accelerates the ionizing electron beam. This voltage is applied between the filament and ion source body. It is adjustable from 5 to 100 volts and usually is operated around 70 volts. The electron current (emission) regulator controls the filament temperature to regulate the electron beam current that may be set

118
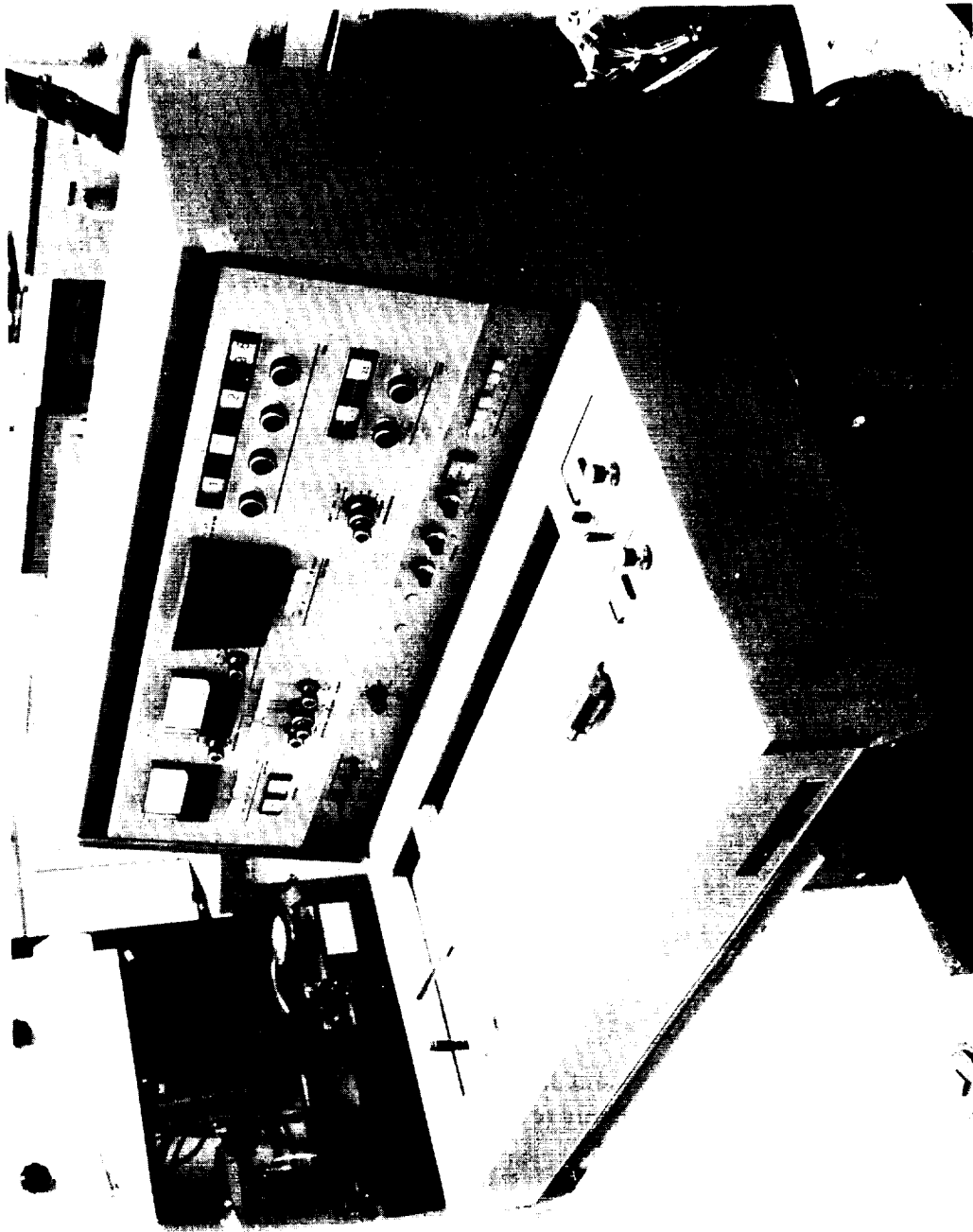
Figure 96. Solid sample introduction probe with XY recorder.
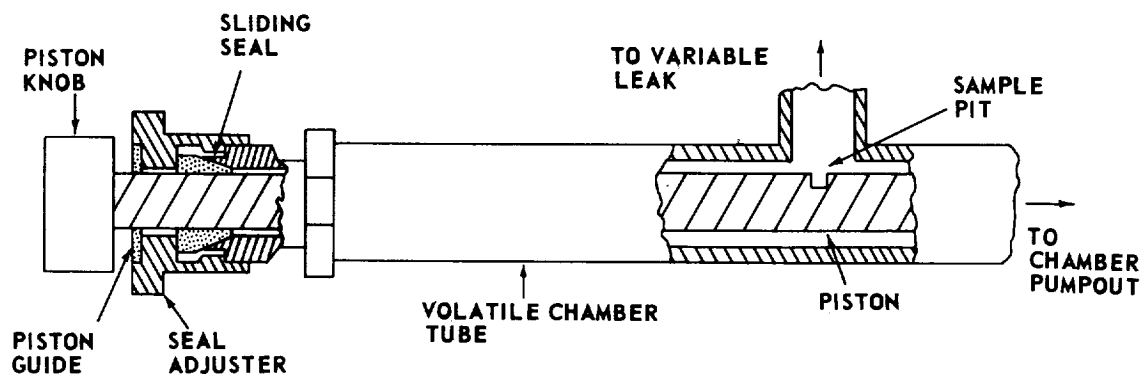
Figure 97. Volatile chamber with piston.
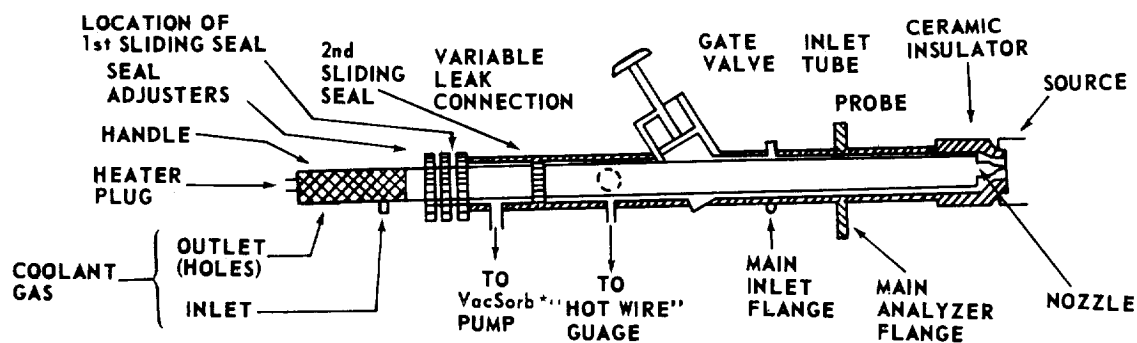
* TRADEMARK

Figure 98. Sketch of probe in inlet.

between 2 and 100 ma. The filament is protected with a filament current control that regulates the upper limit of the filament current.

The ion energy is the energy the ions gain between their formation in the electron beam and the source exit slit. Ions are directed toward the analyzer by a potential drop between the front and back of the source. The source body voltage (50 to 100 volts) is always one-half the repeller voltage with the voltage at the source slit remaining at zero.

The temperature controller regulates the source temperature, which is a function of the analyzer and filament temperatures. Operating temperatures range from approximately 100° C above analyzer ambient to 400° C.

120

The total ion current monitor shows the rate of ion flow from the source into the analyzer. This current indicates that the source is creating ions.

The mass spectrometer is calibrated using Bromoform $CHBr_3$. The volatile sample chamber is pre-evacuated by opening the chamber pumpout valve with the piston in the inlet and the variable leak valve closed. Then the chamber pumpout valve is closed and the variable leak valve is open to check for contaminants (the gate valve is open at this time and remains open). By observing the oscilloscope or by running a quick spectrum, one can determine whether the inlet is clean.

With the system clean, the variable leak and chamber pumpout valves are closed; the system is ready for sample introduction. The piston is pulled back far enough for a sample of Bromoform to be placed in the pit and then pushed back into the chamber. Once the sample is in the chamber, it will remain there until some valve is opened. When necessary, the temperature is adjusted to help volatilize the sample. To move the sample into the source, the variable leak valve is opened. With the gate valve open, the variable leak valve can be adjusted to allow the proper flow of sample into the source and to maintain the desired pressure difference between the source and sample chamber. The pressure gage will increase for the analyzer, and the total ion current monitor will register an increase. Once the signal is seen on the oscilloscope, the sample level can be monitored. The spectrum amplitude is set for the desired height as monitored on the oscilloscope. The electron energy is set at 70 eV, and the mass dial is set for the Bromoform peak at 172.84 amu. Mass calibration is then performed. In addition, the ion energy and resolution controls are adjusted for the most narrow and most symmetrical peaks with maximum intensity. The Bromoform sample is then evacuated, after a spectrum has been run, by closing the variable leak valve and opening the chamber pumpout valve. Any sample remaining in the tube between the variable leak valve and source will be pumped out via the source providing the gate valve is left open.

Backround scans of analyzer were performed with the control settings of the mass spectrometer set at the following values:

Inlet System Temperature	50° C
Analyzer Temperature	150° C
Electron Energy	70 eV
Electron Current	40 μa

These control settings remained at their designated values for the entire test.

The mass spectrometer was calibrated using Bromoform $CHBr_3$. After calibration was completed, two backround scans of the analyzer were made — one with the gate valve closed (mass spectrum No. 1) and one with the gate valve open (mass spectrum No. 2). For the gate valve closed scan, the starting mass was 10 amu and the width scanned was 250 amu. The scan rate was 2.5 minutes. The spectrum amplitude was set at 0.5×10^{-12} amperes. The pressure in the analyzer was 8.4×10^{-8} torr. The starting mass for the gate valve open scan was 10 amu. The width scanned was 500 amu. The scan rate was 5 minutes, and the spectrum amplitude was set at 1.0×10^{-12} amperes. The pressure in the chamber was 8.6×10^{-8} torr.

The solid sample introduction probe was used in the inlet system for the mass spectrum scans. The solid sample probe, without any sample, was first inserted into the analyzer of the mass spectrometer. The nozzle, containing no sample, was secured to the probe. The probe was then inserted into the tube of the inlet system until it had passed the first sliding seal. At this time the manifold pumpout valve was open to evacuate the probe vacuum lock and the volume between the second sliding seal and the gate valve. When this volume was evacuated to less than 10^{-3} torr, the probe was pushed through the second sliding seal. With the probe past both seals, the gate valve was open to allow passage of the probe. The probe was then pushed through the open gate valve, placing the tip next to the source of the analyzer. Mass spectrum was then taken of the probe from ambient to 250°C at 25°C intervals. The operating conditions and analyzer pressures are listed in Table 15.

The clean probe was then removed. A mass spectrum of the backround of the analyzer was then taken with the gate valve closed. Since only the inlet system for the solid probe was being used, it was not necessary to leave the gate valve open. The high pressure side of the gate valve was exposed to the atmosphere. The combination of the solid probe, the sliding vacuum seals, and the inlet pumping system provided the vacuum tight seal needed to open the gate valve to the analyzer section. The remaining part of the inlet system was isolated (valves closed) from the analyzer. The operating conditions for the mass spectrum scan of the backround were as follows:

Mass Spectrum No. 8

Starting mass . . . . 10 amu		Electron energy. . . . 70 eV
Scan width . . . . 500 amu		Electron current . . . 40 μa
Scan rate . . . . 2.5 min		Analyzer pressure . . 1.5×10^{-7} torr
Spectrum amplitude . . . 2.5×10^{-12} a		

122

TABLE 15. CLEAN PROBE OPERATING CONDITIONS

Operating conditions that remained unchanged:

Starting mass . . . . 10 amu

Scan width . . . . 500 amu

Scan rate . . . . 5 min.

Electron energy . . . . 70 ev

Electron current . . . . 40 μa

Inlet temperature . . . . 50°C

Analyzer temperature . . . . 150°C

Mass Spectrum No.	Probe Temp, °C	Spectrum Amplitude, Amp	Analyzer Pressure, Torr
3*	25	2.5×10^{-12}	8.9×10^{-8}
3	50	2.5×10^{-12}	9.0×10^{-8}
4	75	2.5×10^{-12}	9.1×10^{-8}
4	100	2.5×10^{-12}	9.3×10^{-8}
5	125	2.5×10^{-12}	9.6×10^{-8}
5	150	2.5×10^{-12}	9.8×10^{-8}
6	175	2.5×10^{-12}	1.1×10^{-7}
6	200	2.5×10^{-12}	1.0×10^{-7}
7	225	2.5×10^{-12}	1.2×10^{-7}
7*	250	2.5×10^{-12}	1.4×10^{-7}

* Normalized mass spectrum included in report.

An uncontaminated piece of aluminum foil, the same type used on the test bed in chamber A, was inserted into the tip of the solid probe and then secured by the nozzle. The probe was inserted into the analyzer using the same technique as for the clean solid probe. Mass spectrum of the standard aluminum foil was made from ambient to 300°C at intervals of 25°C. The operating conditions and analyzer pressures are listed in Table 16.

The solid probe with the standard aluminum foil sample was removed from the analyzer. A backround mass spectrum was then made of the analyzer with the gate valve closed. The operating conditions for the mass spectrum scan were as follows:

Mass Spectrum No. 16

Starting mass . . . . 10 amu

Scan width . . . . 500 amu

Scan rate . . . . 5 min.

Spectrum amplitude . . . . 2.5 × 10^{-12} a

Electron energy. . . . . 70 eV

Electron current . . . . 40 μa

Analyzer pressure . . . . 2 × 10^{-7} torr

The contaminated aluminum foil, sample 7B2, was removed from test bed No. 7 and placed in the nozzle of the solid probe. The nozzle was secured to the tip of the probe. The solid probe was then inserted into the analyzer section of the mass spectrometer. The same procedure for insertion was used as for the clean solid probe. The operating conditions and analyzer pressures are listed in Table 17.

The mass spectrum scans for the contaminated 7B2 sample were made at a faster scan rate. This was a result of the fact that the vapors that had deposited on the aluminum foil might re-evolve before a mass scan could be run. It would be much better to scan at a slower speed so that the recorder remains over the peaks for a longer time thereby giving a more distinct spectrum. This was accomplished for the higher temperature mass spectrum scans, sacrificing the loss of some of the sample.

124

TABLE 16. STANDARD ALUMINUM FOIL OPERATING CONDITIONS

Operating conditions that remained unchanged:

Starting mass . . . . 10 amu

Scan width . . . . 500 amu

Scan rate . . . . 5 min.

Electron energy . . . . 70 ev

Electron current . . . . 40 μa

Inlet temperature . . . . 50°C

Analyzer temperature . . . . 150°C

Mass Spectrum No.	Probe Temp, °C	Spectrum Amplitude, Amp	Analyzer Pressure, Torr
9	25	2.5×10^{-12}	1×10^{-6}
9*	50	2.5×10^{-12}	6×10^{-7}
10	75	2.5×10^{-12}	4.8×10^{-7}
10	100	2.5×10^{-12}	3.8×10^{-7}
11	125	2.5×10^{-12}	3.6×10^{-7}
11	150	2.5×10^{-12}	2.8×10^{-7}
12	175	2.5×10^{-12}	2.5×10^{-7}
12	200	2.5×10^{-12}	2.3×10^{-7}
13	225	2.5×10^{-12}	2.2×10^{-7}
13	250	2.5×10^{-12}	2.0×10^{-7}
14	275	2.5×10^{-12}	2.3×10^{-7}
14	300	2.5×10^{-12}	2.6×10^{-7}
15*	300	0.5×10^{-12}	2.0×10^{-7}

* Normalized mass spectrum included in report.

TABLE 17. CONTAMINATED ALUMINUM FOIL, SAMPLE 7B2, OPERATING CONDITIONS

Operating conditions that remained unchanged:

Electron energy .... 70 ev
Electron current .... 40 μa
Inlet temperature .... 50°C
Analyzer temperature .... 150°C

Mass Spectrum No.	Probe Temp, °C	Starting Mass, amu	Scan Width, amu	Scan Rate, Min.	Spectrum Amplitude, Amp	Analyzer Pressure, Torr
1A	25	10	100	0.5	2.5×10^{-12}	9.1×10^{-7}
2A	50	10	100	1.0	2.5×10^{-12}	9.2×10^{-7}
3A*	50	10	100	1.0	2.5×10^{-12}	9.4×10^{-7}
4A	50	10	250	2.5	2.5×10^{-12}	7.4×10^{-7}
5A*	75	10	100	2.5	2.5×10^{-12}	1.2×10^{-6}
6A	100	10	500	5.0	2.5×10^{-12}	2.2×10^{-6}
7A	100	190	100	10.0	0.25×10^{-12}	8.4×10^{-7}
8A	300	200	25	10.0	0.25×10^{-12}	9.2×10^{-7}

* Normalized mass spectrum included in report.

The most intense peak in the spectrum is called the base peak and is assigned the value of 100 percent. The intensities of the other peaks are recorded as percentages of the base peak. Percent relative abundance is used in the following tables to express the peak height as a percentage of the largest peak (base peak) in the mass spectrum.

Mass Spectrum No. 1 (Fig. 99) — Analyzer Backround, Gate Valve Closed. This spectrum was not normalized since the only peak that was detected was at mass 18. This is the H_2O peak.

Mass Spectrum No. 2 (Fig. 100) — Analyzer Backround, Gate Valve Open (Normalized, Table 18). Peaks were detected at masses 32, 28, 18, and 17. These peaks indicate the presence of O_2, N_2, H_2O, and OH, respectively. CO could also contribute to the 28 peak. Note that there is no peak at mass 44 which would indicate CO_2. The most abundant peak was at mass 28. All these peaks correspond to the main gaseous components of air.

Mass Spectrum No. 3 (Fig. 101) — Clean Probe at a Temperature of 25°C (Normalized, Table 18). Peaks were detected at masses 17, 18, and 28. These peaks indicate the presence of OH, H_2O, CO, and N_2. Note that the CO_2 at mass 44 was not detected. If CO_2 was detected, it would probably contribute substantially to the 28 peak because of the fragmentation of the CO_2 peak into CO. The most abundant peak was at mass 18.

Mass Spectrum No. 7 (Fig. 102) — Clean Probe at a Temperature of 250°C (Normalized, Table 18). Peaks were detected at masses 17, 18, and 28. The OH peak at mass 17 increased in relation to that of mass spectrum No. 3, while the N_2 and CO peak at mass 28 decreased. The most abundant peak was the H_2O peak at mass 18.

Mass Spectrum No. 8 (Fig. 103) — Backround of Analyzer, Clean Probe Removed, Gate Valve Closed (Normalized, Table 18). Peaks were detected at masses 28 and 32. The N_2 and CO peak at mass 28 was the most abundant. The O_2 peak is at mass 32. Note the absence of the OH and H_2O peaks at masses 17 and 18 respectively.

Mass Spectrum No. 9 (Fig. 104) — Standard Aluminum Foil in Probe, Probe Temperature 50°C (Normalized, Table 18). Peaks were detected at masses 17, 18, 28, 32, and 44. These peaks indicate the presence of OH, H_2O, CO, N_2, O_2, and CO_2, respectively. Note that CO_2 at mass 44 was detected for the standard aluminum foil. The peak at mass 28 indicates the presence of CO and N_2. The most abundant peak was H_2O at mass 18.

Figure 99. Backround, gate valve closed, mass spectra.

Figure 100.   Backround, gate valve open.

129
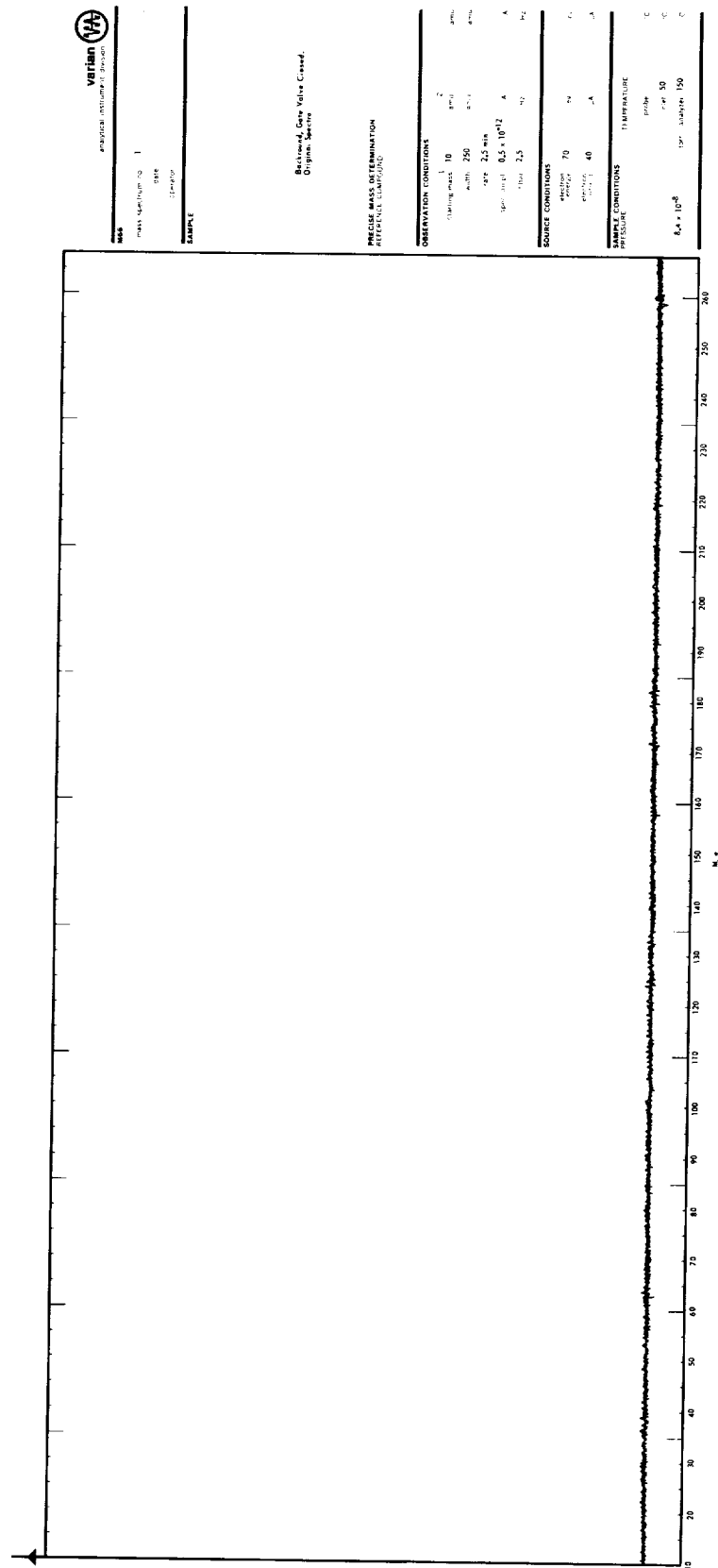
TABLE 18. RELATIVE ABUNDANCES

Mass Spectrum	m/e	% Relative Abundances
Mass Spectrum No. 2		
Backround gate valve open	17	16.0
	18	33.0
	28	100.0
	32	33.0
Mass Spectrum No. 3		
Clean probe	17	25.0
Probe temperature 25°C	18	100.0
	28	75.0
Mass Spectrum No. 7		
Clean probe	17	43.0
Probe temperature 250°C	18	100.0
	28	52.0
Mass Spectrum No. 8		
Probe removed — backround	28	100.0
Gate valve closed	32	15.3
Mass Spectrum No. 9		
Standard aluminum foil in probe	17	86.0
Probe temperature 50°C	18	100.0
	28	32.5
	32	16.2
	44	4.6
Mass Spectrum No. 15		
Standard aluminum foil in probe	17	36.0
Probe temperature 300°C	18	92.0
	28	40.0
	44	100.0
Mass Spectrum No. 16		
Backround of analyzer with gate	17	5.0
valve closed — after probe with	18	10.0
aluminum foil standard removed	28	100.0
	32	23.0

130

Figure 101. Clean probe, A.

131

Figure 102. Clean probe, B.

Figure 103. Probe removed, backround, gate valve closed.

133

Figure 104. Standard aluminum foil in probe, A.

Mass Spectrum No. 15 (Fig. 105) — Standard Aluminum Foil in Probe, Probe Temperature 300° C (Normalized, Table 18). Peaks were detected at masses 17, 18, 28, and 44. These peaks indicate the presence of OH, H_2O, CO, N_2, and CO_2, respectively. Note the absence of the O_2 peak at mass 32. The most abundant peak is the CO_2 peak at mass 44. The most abundant peak in mass spectrum No. 9 was the H_2O peak for a probe temperature of 50° C.
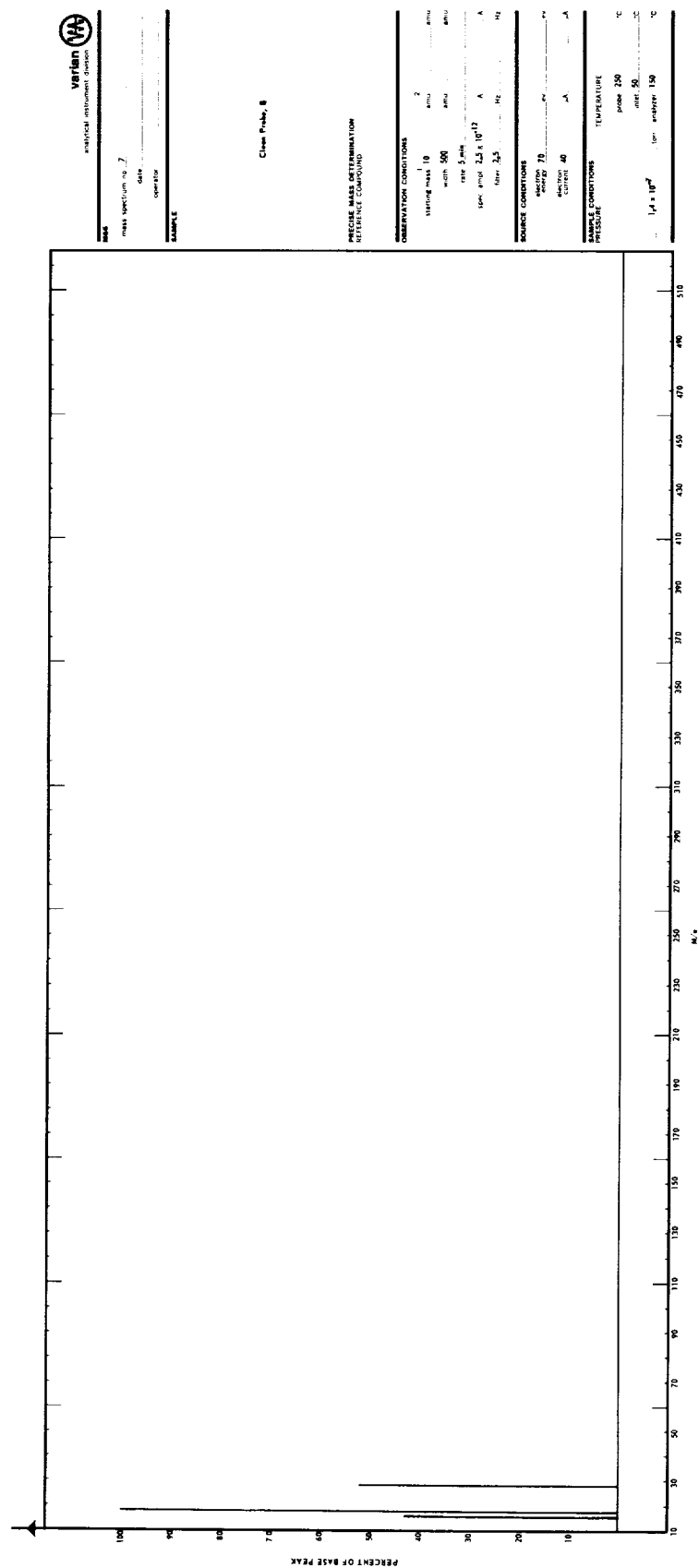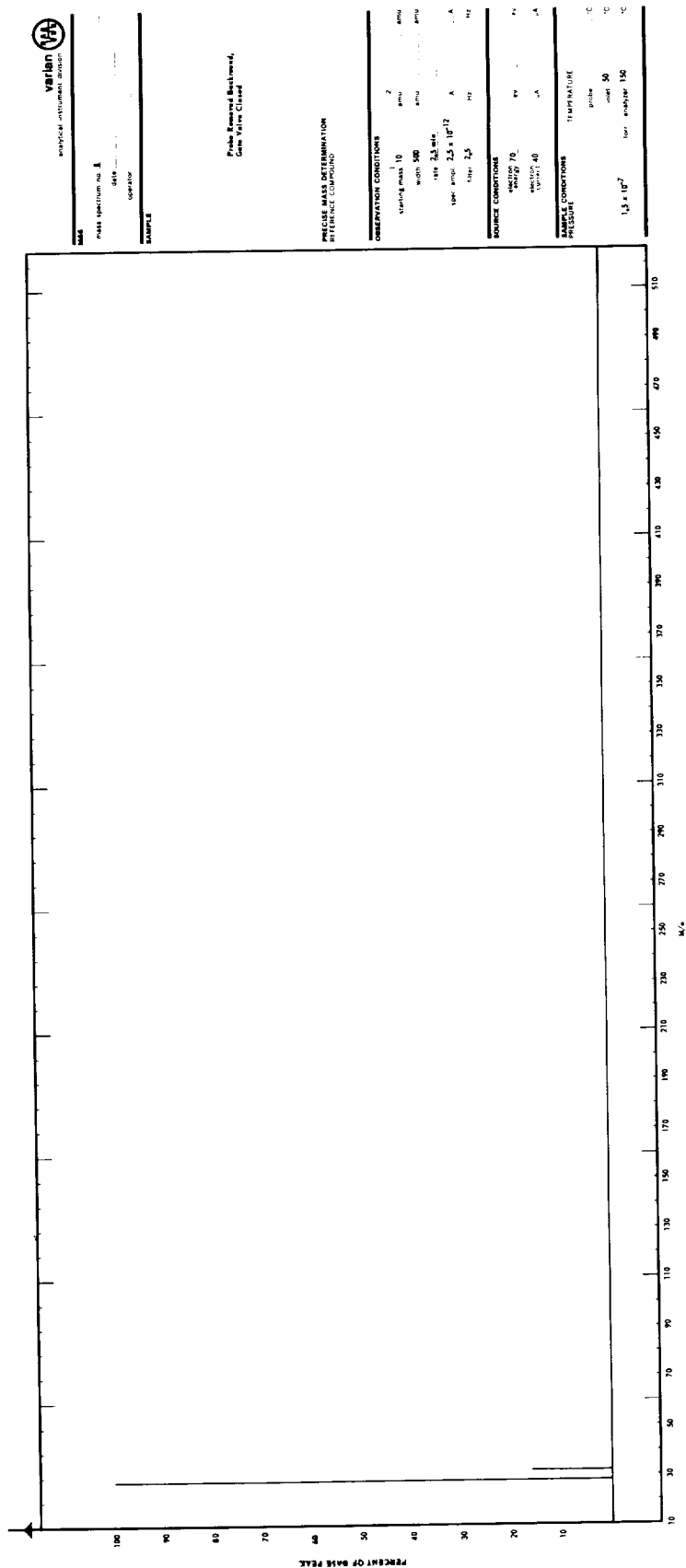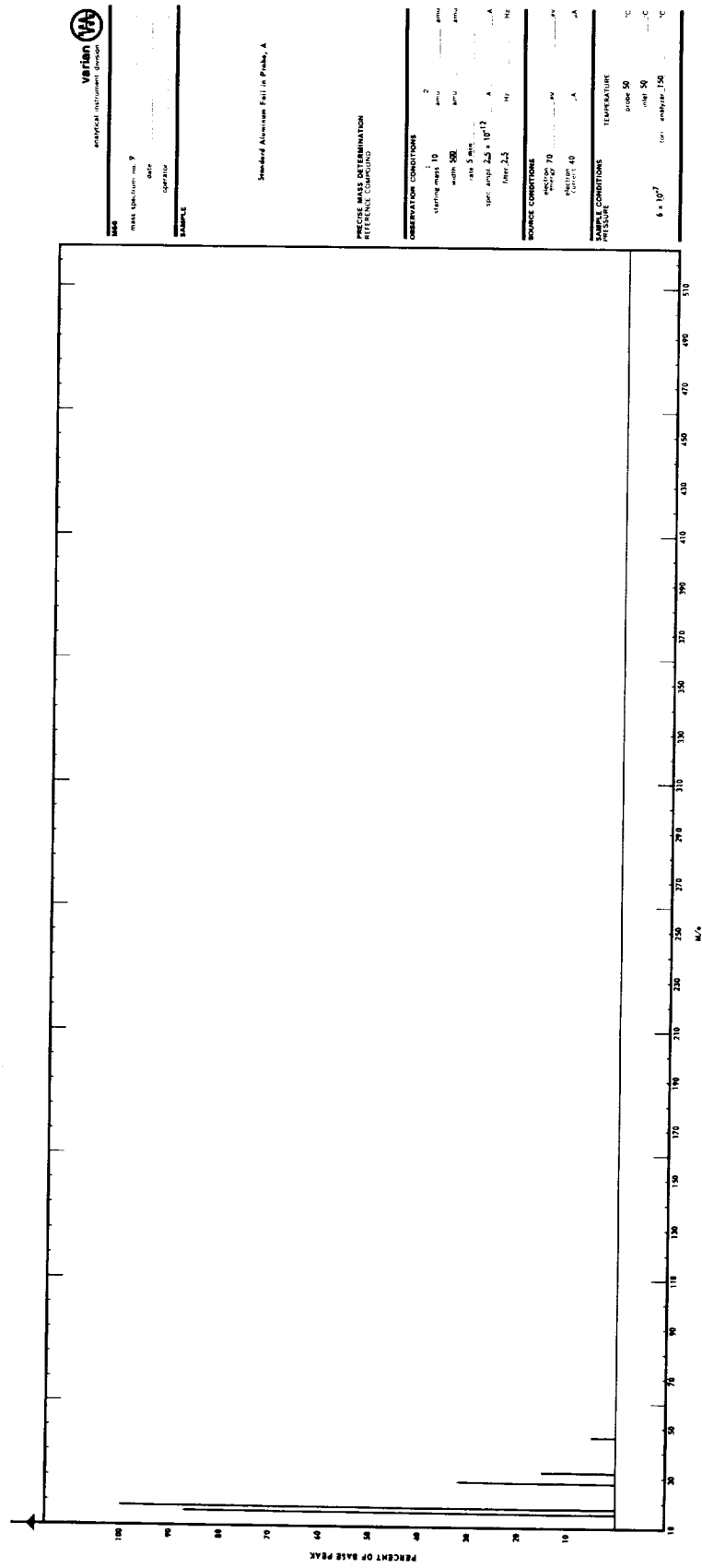
Mass Spectrum No. 16 (Fig. 106) — Backround of Analyzer with Gate Valve Closed, Standard Aluminum Foil and Probe Removed (Normalized, Table 18). Peaks were detected at masses 17, 18, 28, and 32. These peaks indicate the presence of OH, H_2O, N_2, CO, and O_2. The CO_2 peak at mass 44 was not detected. The CO and N_2 peak at mass 28 was the most abundant peak.

Note that in the mass spectrums (1 through 16) there are no peaks at masses 13, 14, and 15 which would indicate the CH_n groups in the spectra of CH_4 and CH_3OH. There is also the absence of a peak at mass 40 which would indicate $argon^+$. Double ionization is also possible in the ion source. That is, two electrons are dislodged from the neutral molecule to produce an ion with two positive charges. An example would be $argon^{++}$ which would have a peak at mass 20. Doubling of the charge produces a low amplitude mass peak at half of the true atomic mass of the element.

Water and the atmospheric gases are a limiting factor for the total pressure in the analyzer of the mass spectrometer. This is because they are carried into the analyzer by the insertion of the solid probe and the standard aluminum foil. Since the solid probe temperature was increased up to 300° C, CO_2 was among the gases evolved.

The next set of mass spectrums are that of the contaminated 7B2 sample. The average amount of H_2O, N_2, CO, O_2, and CO_2 backround contributing to the 7B2 peak heights from the previous presented mass spectrum (1 through 16) are:

	m/e	Average % Contribution
Backround of Analyzer	18	0.8
	28	12.4
	32	5.8
Clean Probe	18	1.5
	28	1.4

Figure 105. Standard aluminum foil in probe, B.
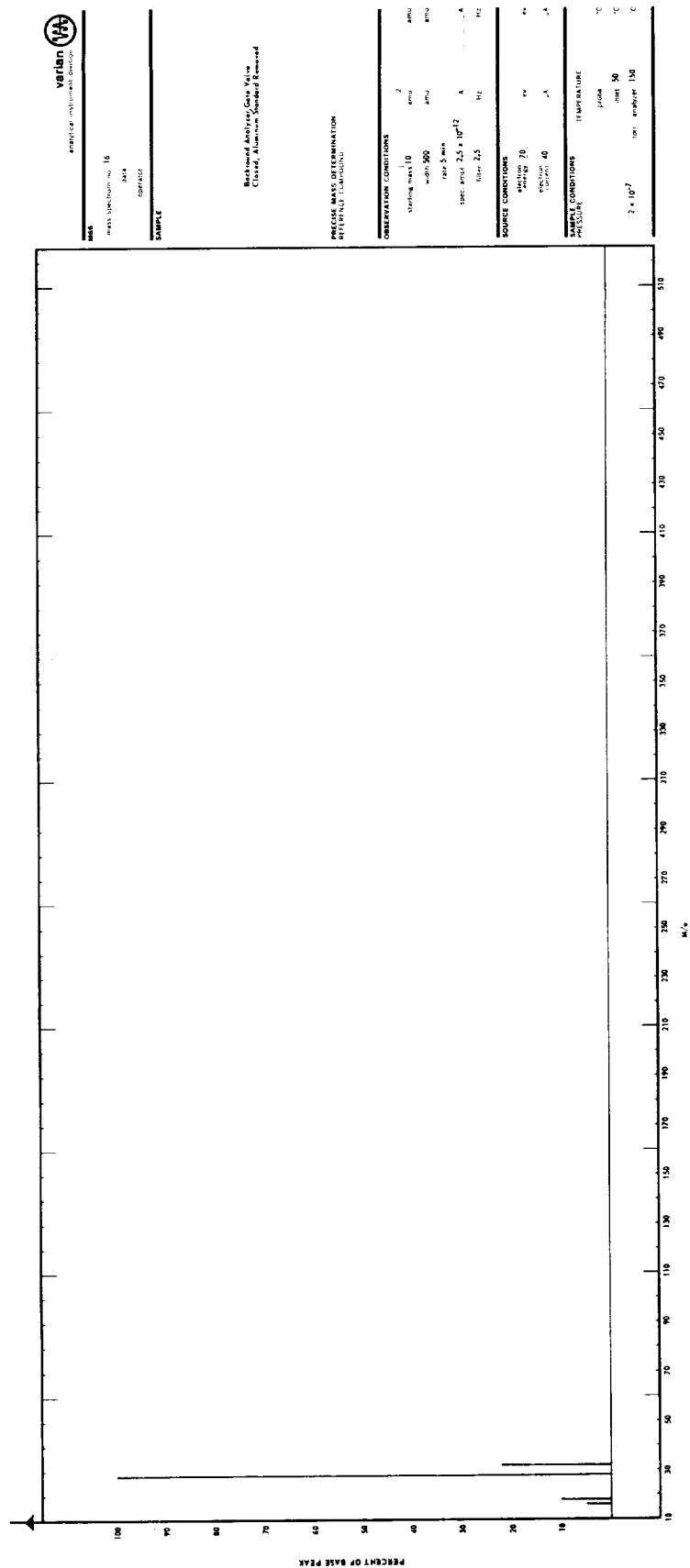
Figure 106. Backround analyzer, gate valve closed, aluminum standard removed.

137

	m/e	Average % Contribution
Standard Aluminum Foil in Probe	18	14.6
	28	8.0
	32	4.7
	44	8.4

Mass Spectrum No. 3A (Fig. 107) — Contaminated Aluminum Foil, Sample 7B2, Probe Temperature 50°C (Normalized Spectrum, Table 19). The peak at mass 45 indicates the presence of $(CH_3)_2 NH$. The fragmentation pattern of the $(CH_3)_2 NH$ molecule from the mass spectrum is:

m/e	Fragment Ion
45	$(CH_3)_2 NH$
44	$(CH_3)_2 N$
43	C_2H_5N
42	C_2H_4N
41	C_2H_2NH
40	$CH_2 CN$
31	$CH_3 NH$
30	$CH_2 NH_2$
28	$CH_2 N$
15	NH and CH_3
14	N and CH_2
12	C

The peak at mass 32 indicates the presence of N_2H_4. The fragmentation pattern of the N_2H_4 molecule from the mass spectrum is:

m/e	Fragment Ion
32	N_2H_4
31	N_2H_3
30	N_2H_2

138
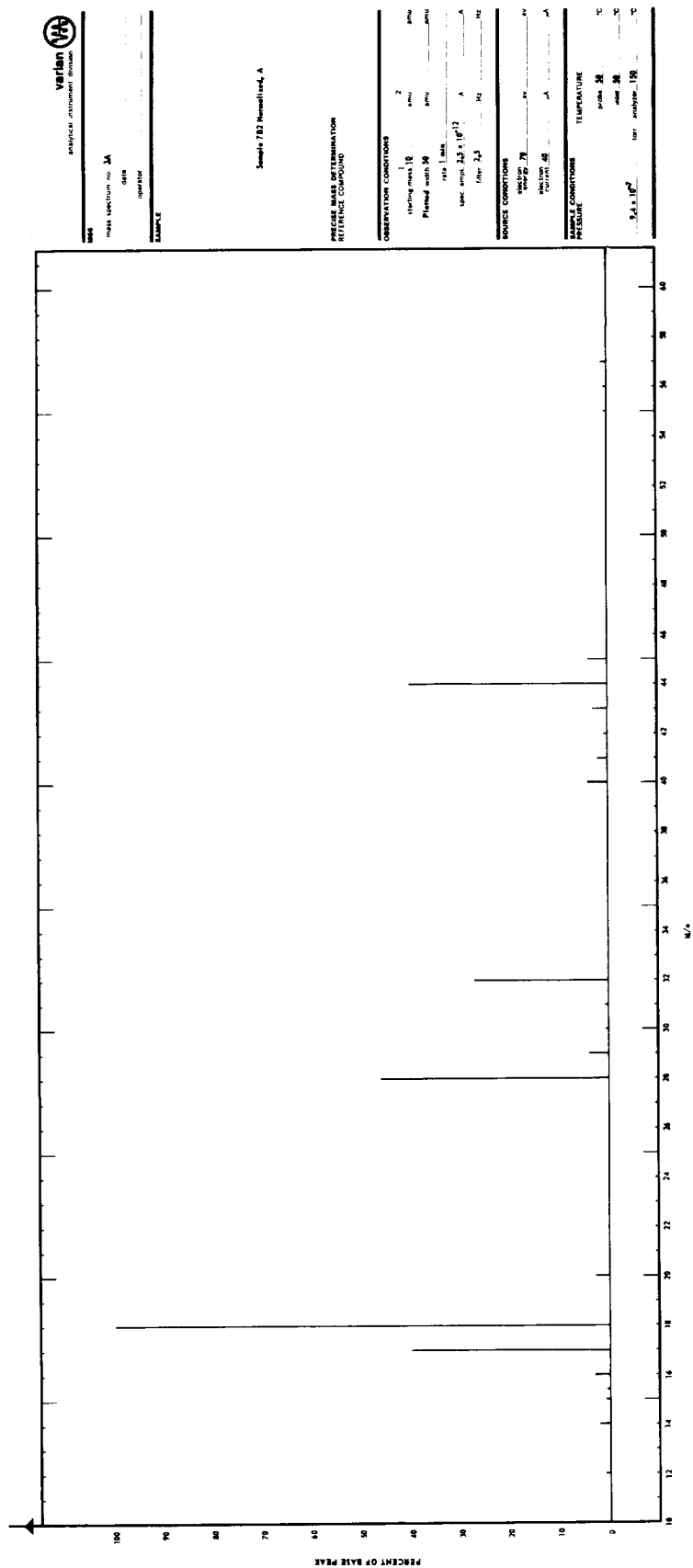
Figure 107.   Sample 7B2 normalized, A.

139

TABLE 19. RELATIVE ABUNDANCE FOR SPECTRUM 3A

Mass Spectrum	m/e	% Relative Abundance
Mass Spectrum No. 3A Contaminated sample 7B2 Probe temperature 50°C	12.	0.9
	14	1.8
	15	0.4
	15.5	0.3
	16	5.9
	17	40.0
	18	100.0
	20	3.1
	28	46.3
	29	4.5
	30	0.9
	31	0.9
	32	27.2
	40	4.0
	41	1.3
	42	0.9
	43	2.7
	44	40.0
	45	4.0
	55	0.9
	56	0.4
	57.	1.8

140

m/e	Fragment Ion
29	N_2H
28	N_2
18	NH_4
17	NH_3
16	NH_2
15	NH
14	N

The following masses are indications of the additional molecules present:

m/e	Fragment Ion
44	CO_2 and NH_2 CO
42	C_3H_6
41	C_3H_5
40	Ar
32	O_2
31	CH_2 OH
30	NO
29	C_2H_5
28	CO
20	Doubly charged mass at 40
18	H_2O
17	OH
16	CH_4

Mass Spectrum No. 5A (Fig. 108) — Contaminated Aluminum Foil, Sample 7B2, Probe Temperature 75° C (Normalized Spectrum, Table 20). The following table indicates the presence of additional molecules not found in mass spectrum No. 3A.
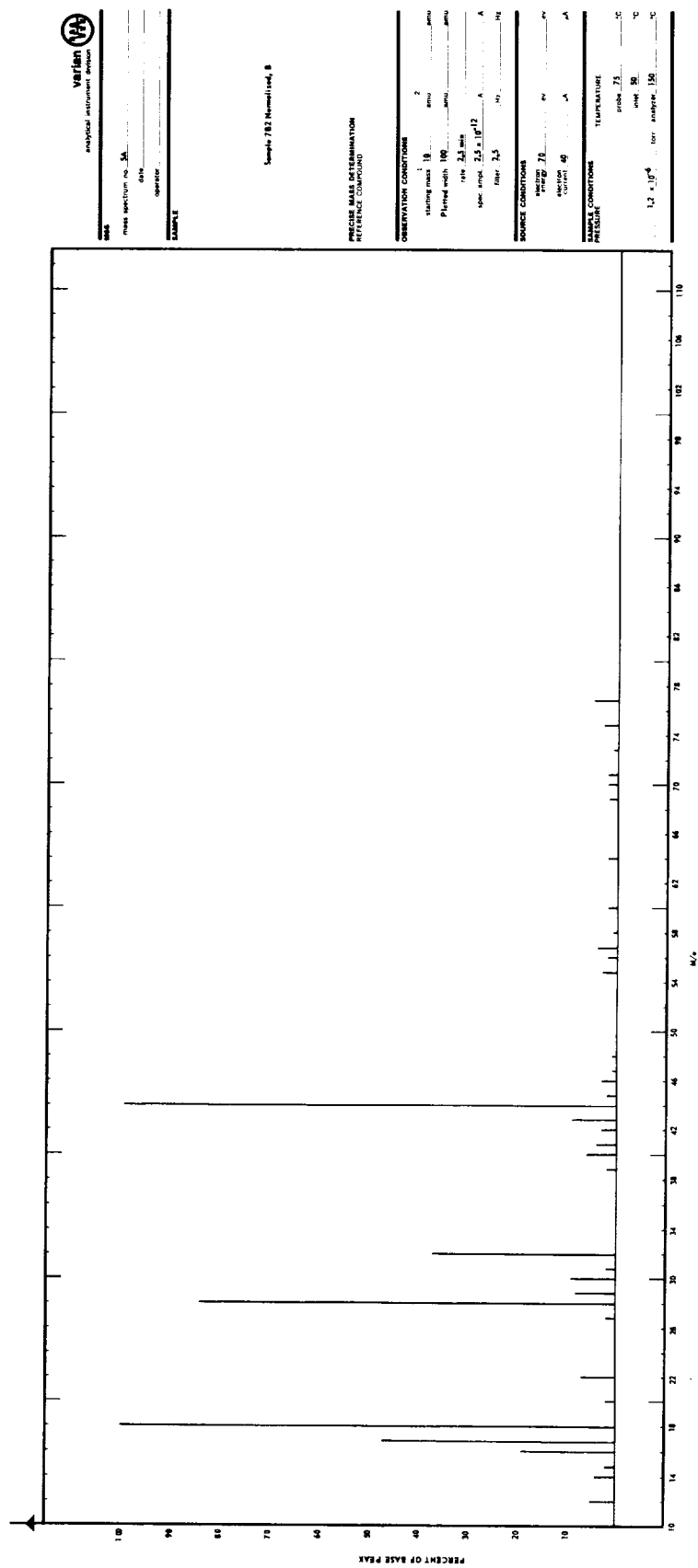
Figure 108. Sample 7B2 normalized, B.

142

TABLE 20. RELATIVE ABUNDANCE FOR SPECTRUM 5A

Mass Spectrum	m/e	% Relative Abundance
Mass Spectrum No. 5A		
Contaminated sample 7B2	12	5.6
Probe temperature 75°C	14	3.4
	15	1.3
	16	18.9
	17	47.4
	18	100.0
	20	1.7
	22	6.8
	27	2.1
	28	84.4
	29	7.3
	30	8.6
	31	1.7
	32	37.2
	39	1.7
	40	6.4
	41	3.6
	42	2.5
	43	8.5
	44	99.1
	45	1.3
	46	3.4
	47	0.9
	48	0.8
	55	3.4
	56	2.1
	57	4.3
	58	1.4
	60	2.1
	64	2.4
	69	2.5
	70	2.1
	71	2.2
	73	1.7
	75	3.4
	77	5.3

m/e	Fragment Ion
77	C_6H_5
60	$(CH_3)_2\,NNH_2$
47	NHO_2
46	NO_2

The combustion products of N_2O_4 and aerozine 50 (50 percent unsymmetrical dimethylhydrazine + 50 percent hydrazine) are listed below:

Combustion Products

CO_2

N_2

CO

H_2O

H_2

NO

OH

O_2

H

O

In addition, all 50 percent hydrazine and 50 percent UDMH systems are flushed with methyl alcohol (methanol CH_3 OH) and then purged with hot gaseous nitrogen. This liquid is an excellent drying agent because of its ability to absorb moisture. All nitrogen tetroxide systems are flushed with freon fluorinated hydrocarbon solvents, CCl_3F.

Rocket exhaust gases released into the upper atmosphere will absorb solar radiation. As an example, NO is a good absorber in the region below Lyman α. The exhaust products are considered in Tables 21 and 22 along with other types of molecules. These tables give the bond dissociation energy values and the ionization potential values of the molecules.

144

TABLE 21. BOND DISSOCIATION ENERGY VALUES [12]

Name	Energy, ev	Reaction
Ammonia	4.42	$NH_3 \rightleftarrows NH_2 + H$
Carbon diatomic	6.5	$C_2 \rightleftarrows C + C$
Carbon monoxide	11.11 ± 0.01	$CO \rightleftarrows C + O$
Carbon dioxide	5.45	$CO_2 \rightleftarrows CO + O$
Hydrazine	2.6 ± 0.2	$N_2H_4 \rightleftarrows NH_2 + NH_2$
	3.30 ± 0.20	$N_2H_4 \rightleftarrows N_2H_3 + H$
Hydrogen	4.476	$H_2 \rightleftarrows H + H$
	2.648	$H_2^+ \rightleftarrows H + H^+$
Hydrogen cyanide	4.94	$HCN \rightleftarrows H + CN$
Hydrogen peroxide	2.07 ± 0.10	$H_2O_2 \rightleftarrows OH + OH$
Hydroxyl	4.40	$OH \rightleftarrows O + H$
	4.4	$OH^+ \rightleftarrows O + H^+$
Imidogen	3.78	$NH \rightleftarrows N + H$
Molybdenum oxide	5.0 ± 0.7	$M_0O \rightleftarrows M_0 + O$
Amidogen	3.9 ± 0.2	$NH_2 \rightleftarrows NH + H$
Nitric oxide	6.49 ± 0.05	$NO \rightleftarrows N + O$
	10.6	$NO^+ \rightleftarrows N + O^+$
Nitrogen	9.762	$N_2 \rightleftarrows N + N$
Nitrogen dioxide	3.13	$NO_2 \rightleftarrows NO + O$
Nitrogen trioxide	0.43	$N_2O_3 \rightleftarrows NO_2 + NO$
Nitrogen tetraoxide	0.56	$N_2O_4 \rightleftarrows NO_2 + NO_2$
Nitrous oxide	4.50	$N_2O \rightleftarrows N + NO$
	1.34	$N_2O \rightleftarrows N_2 + O$
Oxygen	5.115	$O_2 \rightleftarrows O + O$
	6.48 ± 0.1	$O_2^+ \rightleftarrows O + O^+$
Silicon monohydride	3.2	$SiH \rightleftarrows Si + H$
Silicon mononitride	4.5 ± 0.4	$SiN \rightleftarrows Si + N$
Silicon monoxide	7.33 ± 0.15	$SiO \rightleftarrows Si + O$
Silicon dioxide	12.96 ± 0.43	$SiO_2 \rightleftarrows Si + 2O$
Water	5.01	$H_2O \rightleftarrows H_2 + O$
	5.12	$H_2O \rightleftarrows H + OH$
Acetyl	0.7	$CH_3CO \rightleftarrows CH_3 + O$
Benzene	4.42	$C_6H_6 \rightleftarrows C_6H_5 + H$
Formaldehyde	3.3	$HCHO \rightleftarrows CHO + H$
Methyl alcohol	4.34	$CH_3OH \rightleftarrows CH_3O + H$
	3.95	$CH_3OH \rightleftarrows CH_3 + OH$
Methyl cyanide	4147	$CH_3CN \rightleftarrows CH_3 + CN$
Monomethyl hydrazine	2.9	$CH_3N_2H_3 \rightleftarrows CH_3NH + NH_2$
Vinyl	1.8 ± 0.1	$C_2H_3 \rightleftarrows C_2H_2 + H$

TABLE 22. IONIZATION POTENTIAL VALUES [12]

b	Electron Impact Technique
c	Photoionization Technique

Name	Energy, ev	Formula
Amidogen	11.3 b	NH_2
Ammonia	10.52 b	NH_3
	10.15 ± 0.01 c	
Carbon, diatomic	11.5 ± 0.1 b	C_2
Carbon, triatomic	12.6 ± 0.6 b	C_3
Carbon, tetratomic	12.6 b	C_4
Carbon, pentatomic	12.5 ± 1.0 b	C_5
Carbon monoxide	14.01 ± 0.01 c	CO
Carbon dioxide	13.85 b	CO_2
	13.79 ± 0.01 c	
Cyano	14.5 ± 0.5 b	CN
Cyanoacetylene	11.6 ± 0.2 b	HC_3N
Cyanogen	13.6 ± 0.2 b	C_2N_2
Dicyanoacetylene	11.4 ± 0.2 b	C_4N_2
Dicyanodiacetylene	11.4 ± 0.2 b	C_6N_2
Diimide	9.85 ± 0.1 b	N_2H_2
Disilicon dioxide	10.0 ± 1.0	Si_2O_2
Hydrazine	9.00 ± 0.1	N_2H_4
Hydrazyl	7.88 ± 0.2 b	N_2H_3
Hydrogen	15.44 b	H_2
	15.4 c	
Hydrogen cyanide	13.86 b	HCN
Hydrogen peroxide	11.26 ± 0.05 b	H_2O_2
Hydroxyl	13.49 ± 0.08 b	OH
Imidogen	16.4 b	NH
Nitric oxide	9.25 ± 0.02 c	NO
	9.4 ± 0.2 b	
Nitrogen	15.60 ± 0.01	N_2
Nitrogen dioxide	9.78 ± 0.05 c	NO_2
Nitrous oxide	12.90 ± 0.01 c	N_2O
	12.9 ± 0.5 b	
Oxygen	12.075 ± 0.01 c	O_2
	12.1 ± 0.2 b	

146

TABLE 22. (Concluded)

b Electron Impact Technique		
c Photoionization Technique		
Name	Energy, ev	Formula
Silicon tetrahydride	12.2 ± 0.3 b	SiH_4
Silicon monoxide	10.8 ± 0.5 b	SiO
Silicon dioxide	11.7 ± 0.5	SiO_2
Triazene	9.6 ± 0.1 b	N_3H_3
Water	12.69 ± 0.08 b	H_2O
	12.59 ± 0.01 c	
Acetone	9.69 ± 0.01 c	$(CH_3)_2CO$
Acetyl	7.92 b	CH_3CO
Benzene	9.245 ± 0.01 c	C_6H_6
Cyanomethyl	9.87 b	CH_2CN
Diethyl amine	8.01 c	$(C_2H_5)_2NH$
Ethyl	8.72 b	C_2H_5
	8.4 c	
Ethyl alcohol	10.48 ± 0.05 c	C_2H_5OH
Ethyl amine	8.86 c	$C_2H_5NH_2$
	9.32 b	
Formaldehyde	10.87 ± 0.01 c	$HCHO$
Formic acid	11.05 ± 0.01	H_2CO_2
Methane	12.98 ± 0.01 c	CH_4
	13.12 b	
Methyl	9.82 ± 0.04 c	CH_3
Methyl alcohol	10.85 ± 0.02 c	CH_3OH
Methyl amine	8.97 c	CH_3NH_2
Methyl cyanide	12.23 ± 0.01 c ⋅	CH_3CN
Nitromethane	12.46 b	CH_3NO_2
	11.08 ± 0.03 c	
Phenol	8.50 ± 0.01 c	C_6H_6OH
Phenyl	9.89 b	C_6H_6
Propylene	9.73 ± 0.01 c	C_3H_6
Triethyl amine	7.50 c	$(C_2H_5)_3N$
Vinyl	9.45 ± 0.05 b	C_2H_3

The 7B2 sample was exposed to the RCS engine and a variety of different environments including the vacuum chamber with its sources of contamination, and the exposure to the atmosphere. The combination of these factors did degrade the 7B2 sample. As examples, aerozine 50 will deteriorate rapidly when exposed to air; hydrazine is a powerful reducing agent, particularly with acids, oxidizers and organic substances; and carbon dioxide reacts with UDMH to form a carbonic acid salt. UDMH is also miscible in all proportions with most common liquids including water, ethanol, gasoline, and other petroleum products, whereas nitrogen tetroxide is a powerful oxidizing agent. Contact with water in any form, such as moisture in the air produces nitrous or nitric acid that is extremely corrosive.

Placing the contaminated aluminum foil into the direct sample introduction probe was required to record mass spectra of the 7B2 sample. When the probe was inserted into the first sliding seal, there was the possibility that some of the sample would evolve before reaching the analyzer section. In addition, since there was only a minute amount of sample, the sensitivity of the instrument had to be increased. This resulted in sacrificing the instrument's resolution.

The mass spectra recorded for the 7B2 sample indicated the presence of H_2O, NH_3, CH_3, C_6H_5, N_2H_4, and $(CH_3)_2 NNH_2$, and their fragments. The most abundant peaks were at masses 17, 18, 28, 32, and 44. These masses indicate the presence of the reaction products of nitrogen tetroxide and aerozine 50. A low amplitude peak at mass 30 was detected indicating the presence of nitric oxide (NO). Nitrous acid (HNO_2) was detected at mass 47 along with nitrogen dioxide (NO_2) at mass 46. The backround spectra of the analyzer consisted of the atmospheric gases. This backround contributed a negligible amount to the 7B2 spectra.

It was noticed that the 7B2, in being exposed to the atmosphere, was losing some of the contaminants because of evaporation. In addition, a peak of very low amplitude was detected at mass 203 for a probe temperature of 300°C. This peak was detected for a very high amplitude setting and was almost impossible to distinguish from the noise backround of the instrument. The peak had a triplet structure, indicating the presence of a silicon molecule or a high molecular weight hydrocarbon.

The data presented for the 7B2 sample are only the initial findings. A careful study of this spectra along with data being gathered from the other contaminated samples will be presented at a later date.

148

A residual gas analysis was made of sample discs 6C1 and 5C1. Both discs were electropolished 304 stainless steel to insure a true analysis of the redeposited contaminant. The quadrupole residual gas analyzer had a capability of detecting mass fragments to 750 amu.

A sample disc facing the RCS engine, 6C1, was placed in a vacuum chamber and evacuated to 2×10^{-7} torr. At ambient temperature, 25°C, the major system peaks were m/e 18 and m/e 60. High molecular weight fragments were present to 350 amu. Major spectra constituents above 44 amu were m/e 58, 60, 69, 71, 74, 84, 88, 92, 94, 110, 120, 136, 140, 141, 156, 220, 240, 242, 295, 325, and 350. Identifiable species from the exhaust products are m/e 60 (unoxidized UDMH), m/e 92 (N_2O_4 oxidizer), and m/e 18 (water). Fragments greater than 92 amu could occur through recombination reactions of the exhaust gases with the oblative silicone coating on the interior of the RCS engine.

At 50°C, the pressure rose to 4×10^{-7} torr with peaks at 18, 60, and 110 amu. When the disc was heated to 75°C, the gas load induced by the sample caused an automatic shutdown of the getter ion pump.

Sample disc 5C1 at 25°C, 1×10^{-7} torr, was examined for outgassing products. The residual gas analysis revealed contaminant peaks at 60, 85, 92, and 110 amu. These peaks increased in intensity when the sample was heated to 50°C. Pump shutdown again occurred with the disc at 75°C. Molecular weight fragments above 110 amu were not detected in this disc facing the liner as they were in sample disc 6C1 facing the engine.

CONCLUSIONS

The two principal objectives as stated in the introduction were (1) to evaluate the existing capabilities of the MSFC contamination evaluation team and (2) to study the type and severity of damage from an RCS engine on optical surfaces. In respect to the first objective, the following conclusions were reached as have applications in improving contamination analysis and procedures.

It became quite evident that with time, portions of the contaminant, through some mechanism, evolve from the surface causing a dynamic optical property situation. This concretely establishes the importance of a time-line contamination monitor for both ground-based testing and in-flight monitoring of flight payloads containing critical optical elements. After-the-fact evaluation of optical surfaces is both desirable and necessary to determine the source and gross effects of contamination, but it cannot reveal quantitatively total contamination available on representative payloads. It is unrealistic to attempt to eliminate all sources of contamination; therefore the flight and ground-based programs are attempting to identify the most damaging contaminants as a function of wavelength, in order to formulate meaningful materials criteria for payload engineers.

Conclusions which can be drawn that relate to the second objective are as follows. Unburned fuel, both UDMH and hydrazine including the oxidizer N_2O_4, was identified as a contaminant along with the many yet unidentifiable constituents. Thicknesses were shown to be on the order of 600 Å, consisting of an inhomogeneous surface composed of microscopic droplets. Optical degradation consisted of scatter in the visible and infrared with absorption in the ultraviolet. It was interesting to note that scatter was a transient phenomenon that practically disappeared with time. In general, it can be said that any optical surface exposed to the plume of an LM RCS type engine will undergo severe optical degradation, especially if the surface can react with the fuel. It was shown that the surface need not be directly within the plume but only unprotected (uncovered). In this respect it is interesting to loosely correlate the results obtained from this study with the results from the Apollo 9 thermal control coating degradation experiment.[1] In this experiment the primary coatings of interest were a zinc oxide pigmented potassium silicate (Z-93 Apollo radiator coating) and titanium dioxide pigmented silicone. These coatings are white reflective coatings. One set of samples was located in proximity to the RCS engine of the "Service Module" and another was located circumferentially from the direction of the engine. In both cases extreme degradation was suffered by the coatings and the damage ranged up to a 67 percent increase in absorption (in the wavelength region of $0.25\ \mu$ to $2.5\ \mu$) in the case of the samples located in the path of the nozzle gases. As mentioned earlier, some of the contamination appears to evolve from the surface with time, but as our studies show, this is minimized if ultraviolet and/or proton irradiation is impinging upon the surface. Irradiation of this type will tend

---

1. Private communication with James A. Smith, NASA/MSC.

to permanetize the damage especially in the near ultraviolet, with less effect in the visible and near infrared region. Results such as this might imply that the damage could have been more severe than measured on the Apollo 9 experiment, in the visible and near infrared region, since the samples were returned to ground based laboratories before measurements could be made. Also, the gross type of damage experienced on the Apollo 9 samples was somewhat similar, both qualitatively and quantitatively, to the results of this study, therefore indicating that the results obtained herein are not extremely more severe than might be encountered by some optical elements aboard a manned spacecraft.

Future ground-based studies will include investigating synergistic environmental effects on contaminants (i.e., ultraviolet and particulate irradiation in vacuum with in situ optical measurements). Also of interest are the interactions of ionized gases with contaminants, as exist at various orbital altitudes. Extension of the optical reflection measurements into the X-ray region (1 to 100 Å) and the far ultraviolet region (200 - 1000 Å) are being pursued. Improvements in compositional evaluation including application of new techniques are anticipated, such as utilizing X-ray fluorescence, infrared ATR, auger spectrometry, or electron emission techniques. Techniques are being investigated and applied in the realm of time-line monitors using such devices as quartz crystal microbalance and in situ reflection measurements.

All the above experimental data are of little help in understanding the physics of what is occurring without a good supporting program in basic mechanisms. Therefore, such a group has been formed within MSFC and is presently digesting the experimental results in hopes of determining the true surface interaction and degrading mechanisms involved. With a better understanding of the physical mechanisms, a great step forward will have been made in solving the optical contamination problems, both ground-based and in-flight.

APPENDIX

RCS FIRING TEST — SAMPLE CONTAMINATION
SAMPLE ARRAY CONFIGURATION

Notes

On the succeeding pages, the following individuals are mentioned by surname only:

Zwiener, J. M. — S& E-SSL-TR

Moore, W. W. — S& E-SSL-PO

Tashbar, P. W. — S& E-SSL-PO

Williams, J. R. — S& E-SSL-PO

Fields, S. A. — S& E-SSL-TE

Miller, E. R. — S& E-SSL-TE

Horton, J. C. — S& E-ASTN-MEV

Upon return from MSC test, samples 1C2, 1C3, 2C2, 2C3, 3C2, 3C3, 4C2, 4C3, 5C3, 6C3, 7C3, and 8C3 will be stored in the S& E-SSL-TR clean room until a new X ray unit is available for measurements.

Symbol B/A under Applied Tests means measurements will be made before and after Houston test. If B/A is not listed, measurements will be made only after Houston test.

Sample Directory

N = Test Bed Designation
(N = 1 to 8)

SAMPLE CODE	DESCRIPTION
NA1	Aluminum on quartz
NA2	Aluminum on quartz
NA3	Gold on quartz
NA4	Gold on quartz
NB1	Aluminum foil over quartz
NB2	Aluminum foil over aluminum
NB3	Quartz
NB4	Aluminum foil over quartz
NC1	Stainless steel
NC2	Nickel on quartz
NC3	Nickel on quartz
NC4	Cesium bromide

Test Bed No. 1

CONTROL, INERT GAS ENVIRONMENT, S&E-SSL-PO

MODULE A	MODULE B	MODULE C

1A1	1A2	1B1	1B2	1C1	1C2
1A3	1A4	1B3	1B4	1C3	1C4
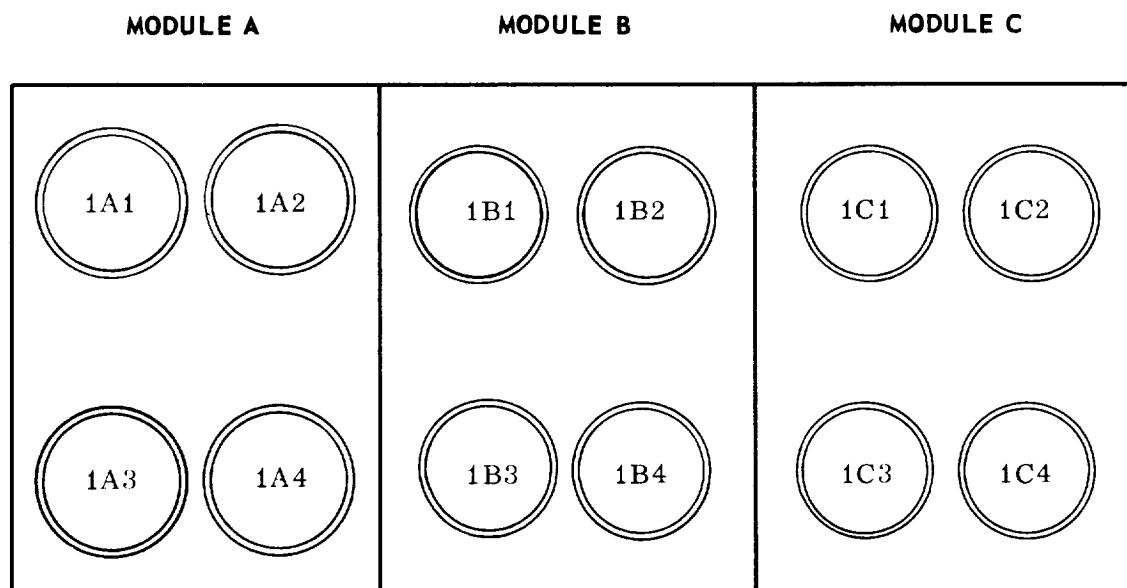
Sample	Description	Source	Applied Tests
1A1	Vacuum-deposited aluminum on quartz	S&E-SSL-TR (Zwiener)	Prime: Zwiener Reflectance, B/A 189 to 2500 nm, Beckman DK-2A, Control — 2A1, Ref. — 2A2 Secondary: Zwiener Scattering, DK-2A, Control — MgC, Ref. — 2A2
1A2	Vacuum-deposited aluminum on quartz	S&E-SSL-TR	Prime: none Secondary: Zwiener Reserved as control for possible use in DK-2A reflectance measurements

154

1A3	Vacuum-deposited gold on quartz		Prime: Zwiener Reflectance, vacuum UV, B/A, McPherson 225; ref. sample 2A4 lower limit (140 nm) Secondary: Zwiener Reflectance, 189 to 2500 nm, DK-2A
1A4	Vacuum-deposited gold on quartz		Prime: None Secondary: Zwiener Reserved for possible use with McPherson Dual Beam Reflectometer Unit
1B1	Foil over 1/3 of quartz disk	Quartz (Williams) Foil (Tashbar)	Prime: (a) Foil (Tashbar) mass spectrometer, upper limit 2000 amu (b) Quartz (Williams) No measurements prior MSC after MSC tests (1) Relfection photographs (2) Microphotography 10 x mag (3) Dark field photography — HeNe laser source (4) Fourier subtraction — hologram, Ar laser (5) Interferometry — 4 holograms, HeNe laser (c) Transmission (Moore), visible, Perkin-Elmer spectrophotometer, B/A
		Referenced hereafter as (1), (2), (3), (4), (5).	

1B1 (cont'd)			Secondary: Tashbar Composition analysis of quartz disk
1B2	Foil over 1/3 of aluminum mirror disk	Mirror (Williams) Foil (Tashbar)	Prime: (a) Foil (Tashbar) Same as Sample 1B1

For 1B2:

Prime:

(a) Foil (Tashbar) Same as Sample 1B1

(b) Mirror (Moore, Williams). Thickness of contaminant:

(1) Angstrometer (Moore)
(2) Interferometer (Williams)

Secondary: Zwiener Reflectance, DK-2A

1B3   Quartz disk   Williams

Prime:
(a) Transmission (Moore) B/A near UV-visible-near IR Perkin-Elmer M-13u

(b) Microphotography (Williams). No data before MSC test, after MSC test (See Sample 1B1), (1), (2), (3), (5)

Secondary: Zwiener Visible transmission DK-2A

1B4   Foil over entire quartz disk   Quartz (Williams) Foil (Tashbar)

Prime:
(a) Foil (Tashbar) same as Sample 1B1
(b) Quartz (Moore) B/A, Transmission, same as Sample 1B1

Secondary: Tashbar Composition analysis of quartz disk

| 1C1 | Electropolished 304 stainless steel disk | Horton, ASTN | No test prior to MSC RCS test. Reserved for possible use in RGA test or IR emission spectroscopy |

1C2 ⎫
1C3 ⎭ Vacuum-deposited nickel on quartz — Fields, Reynolds — No tests prior to MSC test. X ray reflectance to be done when new X ray unit is received

1C4 — Cesium bromide — Miller — Prime: Miller B/A Transmission, IR Upper limit 40 microns; IR 12. Secondary: Miller Visible transmission, DK-2
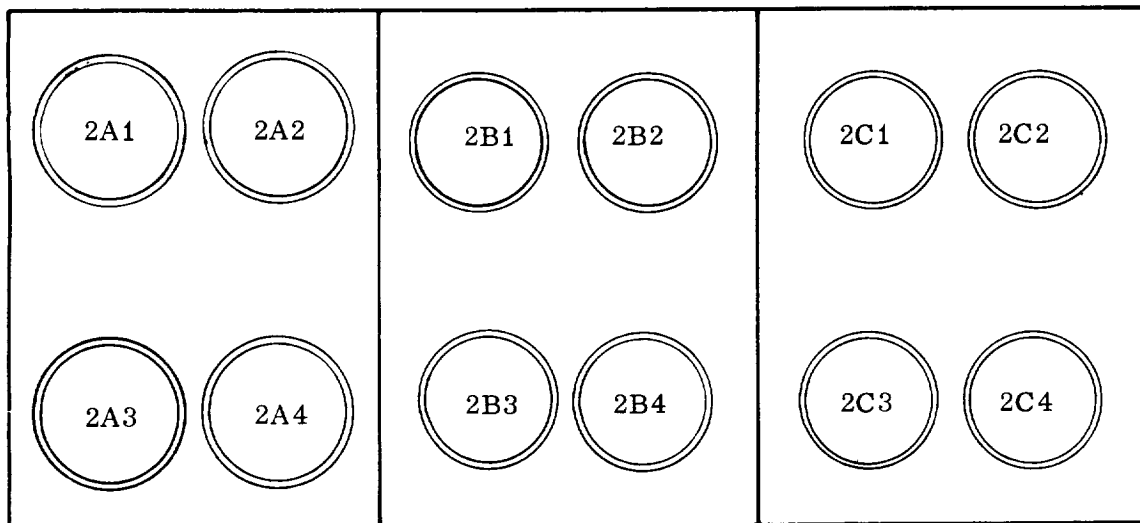
Test Bed No. 2

STORAGE CONTROL, CLEAN ROOM, S& E-SSL-TR
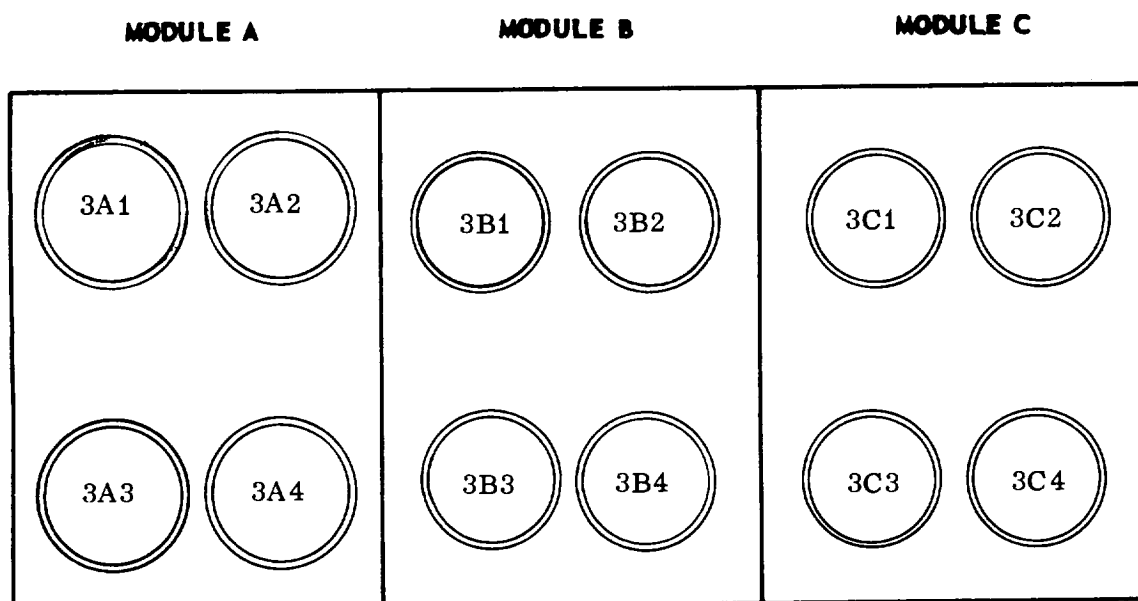
MODULE A **MODULE B** **MODULE C**

| 2A1 | 2A2 | 2B1 | 2B2 | 2C1 | 2C2 |
| 2A3 | 2A4 | 2B3 | 2B4 | 2C3 | 2C4 |

Sample	Description	Source	Applied Tests
2A1	Vacuum-deposited aluminum on quartz	Zwiener	Prime: Zwiener Reflectance: 189 to 2500 nm. Used as prime control sample for DK-2A reflectance data. Secondary: Control for DK-2A scattering data
2A2	Vacuum-deposited aluminum on quartz	Zwiener	Prime: Zwiener DK-2A reflectance data, as before, used as prime reference for all such measurements. Secondary: DK-2A scattering used as prime reference for all such measurements
2A3	Vacuum-deposited gold on quartz	Same as Sample 2A2	Prime: Zwiener Reserved for use as control for vacuum UV reflectance measurements
2A4	Vacuum-deposited gold on quartz	Same as Sample 2A3	Prime: Zwiener Vacuum UV reflectance. Prime reference, B/A. Secondary: Zwiener Control for DK-2A reflectance
2B1	Foil over 1/3 of quartz disk	Quartz (Williams) Foil (Tashbar)	Same as Sample 1B1
2B2	Foil over 1/3 aluminum mirror	Mirror (Williams) Foil (Tashbar)	Same as Sample 1B2
2B3	Quartz disk	Williams	Same as Sample 1B3

158

2B4	Foil over entire quartz disk	Quartz (Williams) Foil (Tashbar)	Same as Sample 1B4 except that no transmission measurements planned
2C1	Electropolished 304 stainless steel disk	Horton, ASTN	No tests prior; reserved for possible use in RGA test or IR emission spectroscopy
2C2 2C3	Vacuum-deposited nickel on quartz	Reynolds, Fields	No tests prior; Same as Sample 1C2
2C4	Cesium bromide	Miller	Same as Sample 1C4

Test Bed No. 3

LABORATORY STORAGE CONTROL, S& E-SSL-TR

MODULE A   MODULE B   MODULE C

Sample	Description	Source	Applied Tests
3A1	Vacuum-deposited aluminum on quartz		Same as Sample 1A1
3A2	Vacuum-deposited aluminum on quartz		Same as Sample 1A2
3A3	Vacuum-deposited gold on quartz		Same as Sample 1A3
3A4	Vacuum-deposited gold on quartz		Same as Sample 1A4
3B1	Foil over 1/3 of quartz disk	Quartz (Williams) Foil (Tashbar)	Prime: (a) Foil (Tashbar) Mass spectrometer, to 2000 amu (b) Quartz (Williams) Before: (1), (2), (3), (4). After: (1), (2), (3), (4), (5). (c) Quartz (Moore) B/A, Transmission, visible, Perkin-Elmer M-13u Secondary: Tashbar Composition analysis of heated quartz disk.
3B2	Foil over 1/3 of aluminum mirror	Mirror (Williams) Foil (Tashbar)	Same as Sample 1B2
3B3	Quartz disk	Williams	Prime: (a) Transmission (Moore) B/A near-UV, visible near-IR, Perkin-Elmer M-13u (b) Microphotography (Williams) Before: (1), (2), (3), (5) After: (1), (2), (3), (5)

3B3 (cont'd)			Secondary: Zwiener (a) Visible transmission, DK-2A (b) Composition analysis (Moore), emission spectroscopy
3B4	Foil over entire quartz disk	Quartz (Williams) Foil (Tashbar)	Prime: (a) Foil (Tashbar) Same as Sample 1B1 (b) Transmission (Moore). No tests planned before or after. Secondary: Tashbar Quartz composition analysis, emission spectroscopy
3C1	Electropolished 304 stainless steel disk	Horton, ASTN	Same as Sample 1C1
3C2 3C3	Vacuum-deposited nickel on quartz	Fields, Reynolds	Same as Sample 1C2
3C4	Cesium bromide	Miller	Same as Sample 1C4

Test Bed No. 4

HANDLING CONTROL, TO MSC AND RETURN

MODULE A **MODULE B** **MODULE C**
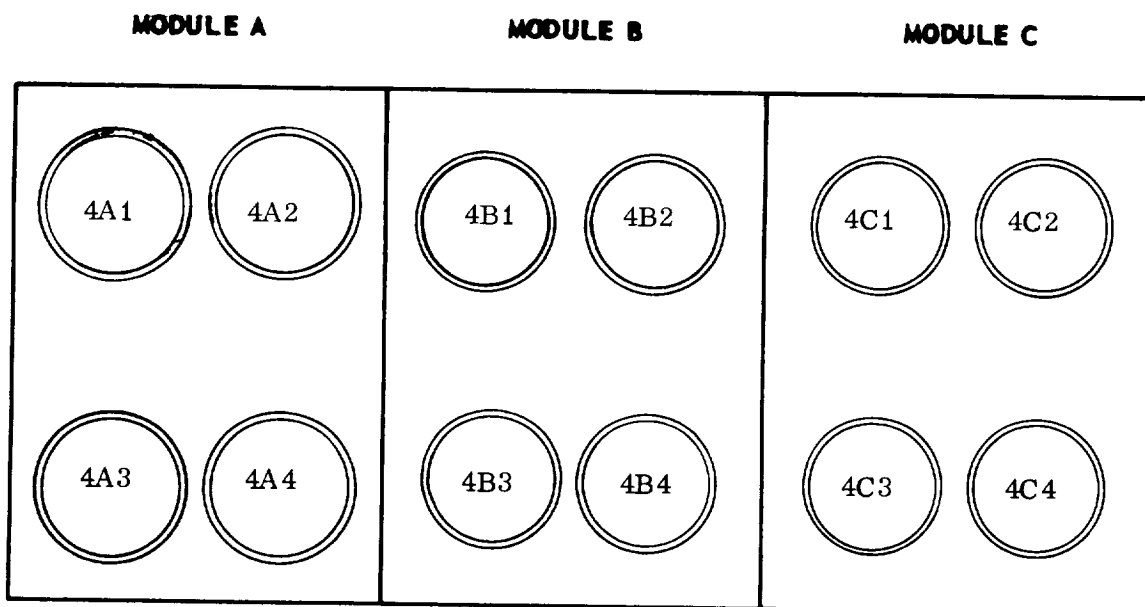
Sample	Description	Source	Applied Tests
4A1	Vacuum-deposited aluminum on quartz	Zwiener	Same as Sample 1A1
4A2	Vacuum-deposited aluminum on quartz	Zwiener	Same as Sample 1A2
4A3	Vacuum-deposited gold on quartz	Zwiener	Same as Sample 1A3
4A4	Vacuum-deposited gold on quartz	Zwiener	Same as Sample 1A4
4B1	Foil on 1/3 of quartz disk	Quartz (Williams) Foil (Tashbar	Same as Sample 3B1

| 4B2 | Foil over 1/3 of aluminum mirror | Mirror (Williams) Foil (Tashbar) | Same as Sample 3B2 |
4B3	Quartz disk	Williams	Same as Sample 3B3
4B4	Foil over entire quartz disk	Quartz (Williams) Foil (Tashbar)	Same as Sample 3B4
4C1	Electropolished 304 stainless steel disk	Horton, ASTN	Same as Sample 1C1
4C2 4C3	Vacuum-deposited nickel on quartz	Fields, Reynolds	Same as Sample 1C2
4C4	Cesium bromide	Miller	Same as Sample 1C4

Test Bed No. 5

TEST — INSIDE MSC CHAMBER "A"

MODULE A **MODULE B** **MODULE C**

Sample	Description	Source	Applied Tests
5A1	Vacuum-deposited aluminum on quartz	Zwiener	Same as Sample 1A1
5A2	Vacuum-deposited aluminum on quartz	Zwiener	Same as Sample 1A2
5A3	Vacuum-deposited gold on quartz	Zwiener	Same as Sample 1A3
5A4	Vacuum-deposited gold on quartz	Zwiener	Same as Sample 1A4
5B1	Foil over 1/3 of quartz disk	Quartz (Williams) Foil (Tashbar)	Same as Sample 3B1
5B2	Foil over 1/3 of aluminum mirror	Mirror (Williams) Foil (Tashbar)	Same as Sample 3B2
5B3	Quartz disk	Williams	Same as Sample 3B3
5B4	Foil over entire quartz disk	Quartz (Williams) Foil (Tashbar)	Same as Sample 1B4
5C1	Electropolished stainless steel disk	Horton, ASTN	Prime: Horton (a) RGA mass analysis (Granville-Phillips) to 600 amu (b) Emission spectroscopy, Perkin-Elmer 521, 2 to 40 microns. No prior tests. Secondary: (a) (Horton) Weight loss in vacuo-quartz X-tal microbalance (b) (Zwiener) DK-2a reflectance

164

| 5C2	Vacuum-deposited nickel on quartz	Fields, Reynolds	Prime: Fields, Reynolds Reflectance, X ray, B/A $\lambda = 1.54$; more extensive X ray reflectance data to be obtained when advanced X ray equipment is available.
5C3	Vacuum-deposited nickel on quartz	Fields, Reynolds	Same as Sample 1C2
5C4	Cesium bromide	Miller	Same as Sample 1C4

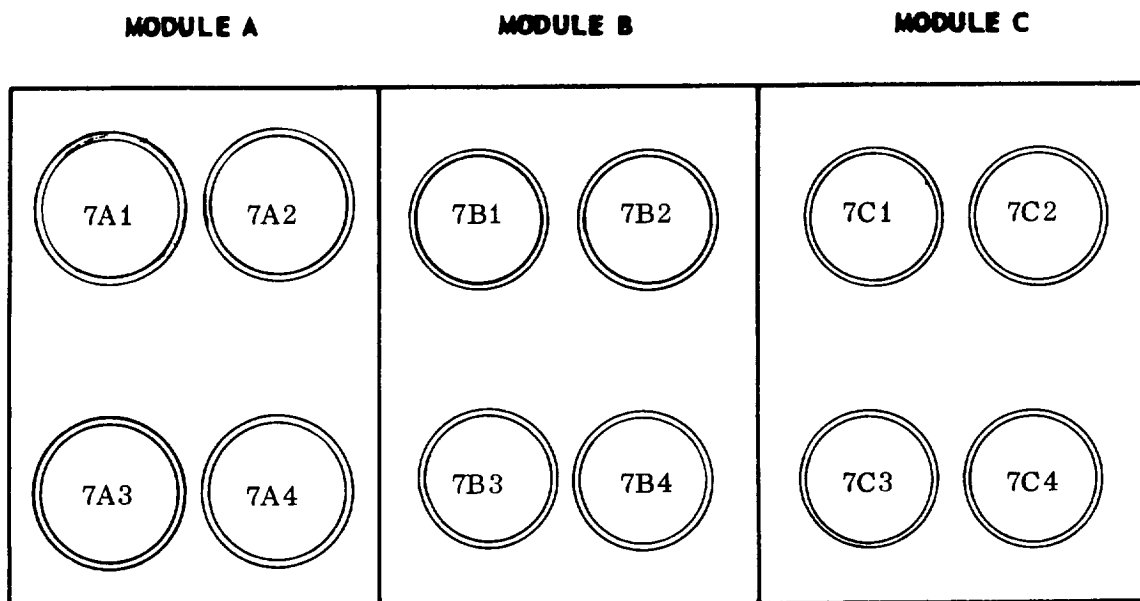# Test Bed No. 6

TEST — INSIDE MSC CHAMBER "A"

MODULE A **MODULE B** **MODULE C**
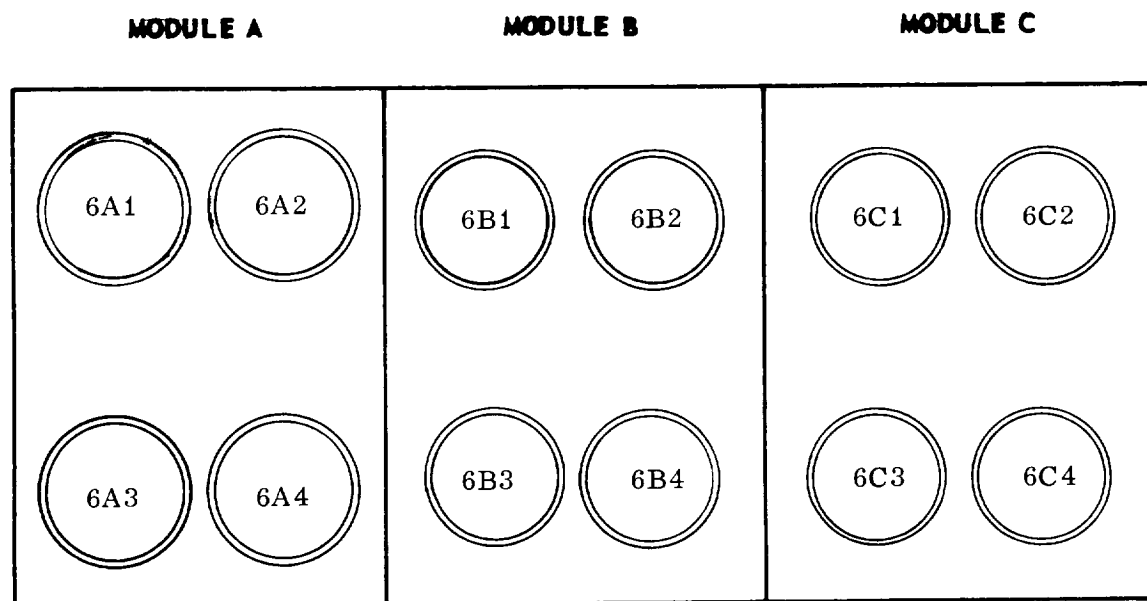
Sample	Description	Source	Applied Tests
6A1	Vacuum-deposited aluminum on quartz	Zwiener	Same as Sample 1A1

6A2	Vacuum-deposited aluminum on quartz	Zwiener	Same as Sample 1A2
6A3	Vacuum-deposited gold on quartz	Zwiener	Same as Sample 1A3
6A4	Vacuum-deposited gold on quartz	Zwiener	Same as Sample 1A4
6B1	Foil over 1/3 quartz disk	Quartz (Williams) Foil (Tashbar)	Same as Sample 3B1
6B2	Foil over 1/3 of aluminum mirror	Mirror (Williams) Foil (Tashbar)	Same as Sample 3B2
6B3	Quartz disk	Williams	Same as Sample 3B3
6B4	Foil over entire quartz disk	Quartz (Williams) Foil (Tashbar)	Same as Sample 3B4
6C1	Electropolished 304 stainless steel disk	Horton, ASTN	Same as Sample 5C1
6C2	Vacuum-deposited nickel on quartz	Fields, Reynolds	Same as Sample 5C2
6C3	Vacuum-deposited nickel on quartz	Fields, Reynolds	Same as Sample 1C2
6C4	Cesium bromide	Miller	Same as Sample 1C4

166

Test Bed No. 7

MODULE A　　　　　**MODULE B**　　　　　**MODULE C**

| 7A1 | 7A2 | 7B1 | 7B2 | 7C1 | 7C2 |
| 7A3 | 7A4 | 7B3 | 7B4 | 7C3 | 7C4 |

Sample	Description	Source	Applied Tests
7A1	Vacuum-deposited aluminum on quartz	Zwiener	Same as Sample 1A1
7A2	Vacuum-deposited aluminum on quartz	Zwiener	Same as Sample 1A2
7A3	Vacuum-deposited gold on quartz	Zwiener	Same as Sample 1A3
7A4	Vacuum-deposited gold on quartz	Zwiener	Same as Sample 1A4
7B1	Foil over 1/3 of quartz disk	Quartz (Williams) Foil (Tashbar)	Same as Sample 3B1

|			
7B2	Foil over 1/3 of aluminum mirror	Mirror (Williams) Foil (Tashbar)	Same as Sample 3B2
7B3	Quartz disk	Williams	Same as Sample 3B3
7B4	Foil over entire quartz disk	Quartz (Williams) Foil (Tashbar)	Same as Sample 3B4
7C1	Electropolished 304 stainless steel disk	Horton, ASTN	Same as Sample 5C1
7C2	Vacuum-deposited nickel on quartz	Fields, Reynolds	Same as Sample 5C2
7C3	Vacuum-deposited nickel on quartz	Fields, Reynolds	Same as Sample 1C2
7C4	Cesium bromide	Miller	Same as Sample 1C4

Test Bed No. 8

TEST — INSIDE MSC CHAMBER "A"

MODULE A	MODULE B	MODULE C

168
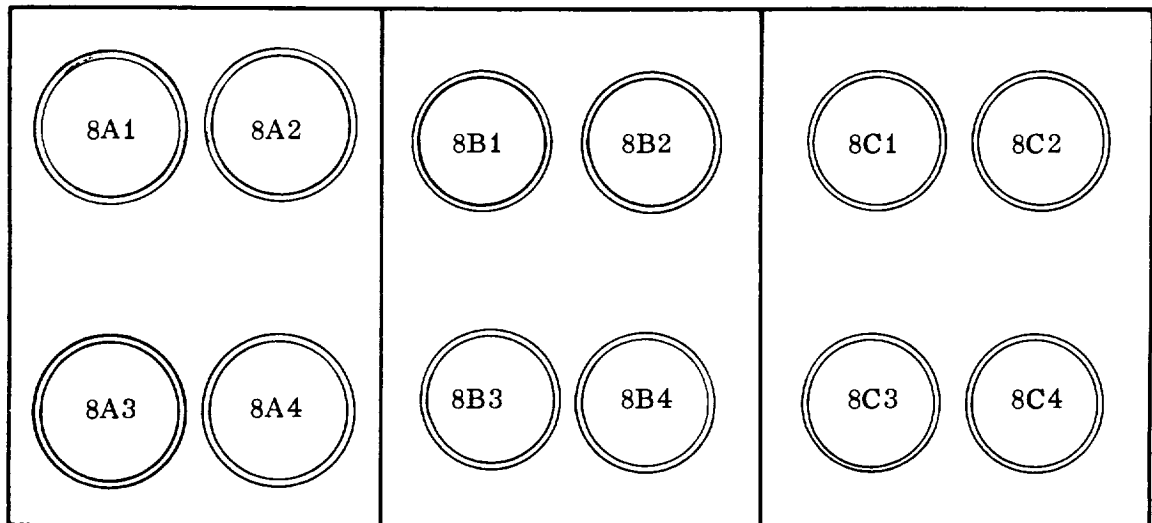
Sample	Description	Source	Applied Tests
8A1	Vacuum-deposited aluminum on quartz	Zwiener	Same as Sample 1A1
8A2	Vacuum-deposited aluminum on quartz	Zwiener	Same as Sample 1A2
8A3	Vacuum-deposited gold on quartz	Zwiener	Same as Sample 1A3
8A4	Vacuum-deposited gold on quartz	Zwiener	Same as Sample 1A4
8B1	Foil over 1/3 of quartz disk	Quartz (Williams) Foil (Tashbar)	Same as Sample 3B1
8B2	Foil over 1/3 of aluminum mirror	Mirror (Williams) Foil (Tashbar)	Same as Sample 3B2
8B3	Quartz disk	Williams	Same as Sample 3B3
8B4	Foil over entire quartz disk	Quartz (Williams) Foil (Tashbar)	Same as Sample 3B4
8C1	Electropolished 304 stainless steel disk	Horton, ASTN	Same as Sample 5C1
8C2	Vacuum-deposited nickel on quartz	Fields, Reynolds	Same as Sample 5C2
8C3	Vacuum-deposited nickel on quartz	Fields, Reynolds	Same as Sample 1C2
8C4	Cesium bromide	Miller	Same as Sample 1C4

REFERENCES

1. Work Control Document in Support of LM-RCS Engine Exhaust Impingement Evaluation Test. Space Environment Test Division, Space Environment Simulation Branch, MSC.

2. Borson, E. N. and Landsbaum, E. M.: A Review of Available Rocket Contamination Results. Air Force Report No. SAMSO-TR-69-82, December 15, 1968.

3. Propulsion Subsystem Student Study Guide Unit 1. Course Number C3-A412, February 25, 1966.

4. LEM Propulsion and RCS Study Guide. Course No. 30215, March 7, 1966.

5. C-1 Engine Program Phase II — Development-Design Report. Thiokol Chemical Corporation, RMD 6203-DR2, Contract NAS* -15486.

6. Kit, Boris and Evered, Douglas S.: Rocket Propellant Handbook. The Macmillan Co., New York, N. Y., 1960.

7. Nitrogen Tetroxide. Product Bulletin, Allied Chemical.

8. A-Scope Interferometer. Instruction Manual, Varian Vacuum Division, Document No. 87-400 142, April 1966.

9. Holland, L.: The Properties of Glass Surfaces. First Edition, 1964.

10. Trujillo, E. F.: Model DK-A Ratio Recording Spectrophotometers. Beckman Instrumentation Manual, Third Edition, January 1967.

11. M-66 Mass Spectrometer Technical Notes and Operational Manuals.

12. Schexnayder, Charles J., Jr.: Tabulated Values of Bond Dissociation Energies, Ionization Potentials, and Electron Affinities for Some Molecules Found in High-Temperature Chemical Reactions. Technical Note D-1701, NASA, May 1963.
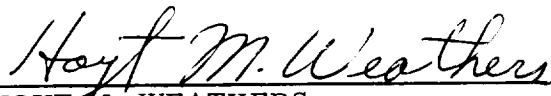
APPROVAL

TM X-53859

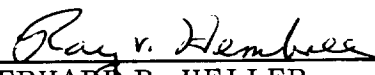# LUNAR EXCURSION MODULE RCS ENGINE VACUUM CHAMBER CONTAMINATION STUDY

By Gary M. Arnett
Technical Coordinator

The information in this report has been reviewed for security classification. Review of any information concerning Department of Defense or Atomic Energy Commission programs has been made by the MSFC Security Classification Officer. This-report, in its entirety, has been determined to be unclassified.

This document has also been reviewed and approved for technical accuracy.

WILLIAM C. SNODDY
Chief, Space Thermal Physics Division
Space Sciences Laboratory

HOYT M. WEATHERS
Contamination Program Manager
Space Sciences Laboratory

for GERHARD B. HELLER
Director, Space Sciences Laboratory

INTERNAL

DIR
  Dr. Wernher von Braun
  Mr. James T. Shepherd

DEP-T
  Dr. Eberhard M. Rees

AD-S
  Dr. Ernst Stuhlinger
  Dr. George Bucher

PA
  Mr. Bart J. Slattery

S& E-DIR
  Mr. Hermann K. Weidner
  Mr. L. G. Richard
  Mr. R. W. Cook

S& E-R
  Dr. W. G. Johnson
  Mr. R. E. Lake
  Miss M. J. Smith

S& E-P
  Mr. H. Kroeger
  Mr. F. Napper

S& E-CSE-DIR
  Dr. W. Haeussermann

S& E-CSE-P
  Mr. Rex Morton

S& E-CSE-A
  Dr. G. McDonough
  Mr. C. M. Davis

INTERNAL (Continued)

S& E-AERO-DIR
  Dr. E. Geissler

S& E-AERO-P
  Mr. J. Watkins

S& E-ASTR-DIR
  Mr. Brooks Moore
  Mr. W. P. Horton

S& E-ASTR-X
  Mr. E. Cagle
  Mr. A. White
  Mr. E. R. Cantrell

S& E-ASTR-S
  Mr. N. Gilino
  Mr. E. Noel

S& E-ASTR-I
  Mr. J. Powell

S& E-ASTR-IM
  Mr. T. Paludan
  Mr. T. Ponder
  Mr. J. Power
  Mr. A. Davis
  Mr. P. Hassler
  Mr. H. Burke

S& E-ASTR-R
  Mr. J. Taylor
  Mr. J. Franks
  Mr. R. Harwell

S& E-ASTN-DIR
  Mr. K. Heimburg

INTERNAL (Continued)

S& E-ASTN-XAJ
Mr. W. Richardson

S& E-ASTN-M
Mr. R. Schwinghamer
Mr. J. Horton
Mr. C. Smith
Mrs. C. Griner (25)

S& E-ASTN-E
Mr. W. Brooksbank

S& E-ME-A
Mr. R. Butler

S& E-QUAL-J
Mr. E. Buhmann

S& E-QUAL-PE
Mr. Max Rosenthal

S& E-QUAL-QC
Mr. E. Davis

S& E-SSL-DIR
Mr. G. B. Heller
Mr. R. Hembree

S& E-SSL-X
Dr. J. Dozier
Mr. H. Weathers
Dr. A. Weber

S& E-SSL-N
Mr. H. Stern
Dr. T. Parnell
Dr. A. DeLoach
Mr. M. Burrell

S& E-SSL-P
Mr. R. Naumann
Mr. R. L. Holland
Mr. E. Klingman
Mr. J. McGuire
Dr. S. Frary
Mr. P. Tashbar (25)
Mr. W. Moore (25)
Mr. J. Williams (25)
Mr. R. Jenkins

S& E-SSL-S
Dr. W. H. Sieber
Mr. L. Yarbrough
Mr. G. Loughead
Mr. B. Duncan

S& E-SSL-T
Mr. W. Snoddy
Mr. E. Miller (25)
Mr. G. Arnett (25)
Mr. B. Jones
Mr. S. Fields (25)
Mr. J. Reynolds
Mr. R. Linton
Mr. J. Zwiener (25)

S& E-SSL-C
Mr. J. Mathis
Reserve (200)

PD-DIR
Dr. W. Lucas

PD-MP
Mr. J. Downey
Mr. H. Gierow
Mr. H. Dudley
Mr. R. Potter

INTERNAL (Concluded)

PM-DIR
  Dr. W. A. Mrazek

PM-MO-MGR
  Dr. F. A. Speer

PM-MO-R
  Mr. H. Golden

PM-AA-MGR
  Mr. L. Belew

PM-AA
  Mr. R. Ise
  Mr. W. Keathley
  Mr. J. Igou
  Mr. D. E. Snoddy
  Mr. J. Waite

PM-PR-M

A&TS-PAT
  Mr. L. D. Wofford, Jr.

A&TS-MS-H
A&TS-MS-IP (2)
A&TS-MS-IL (8)
A&TS-TU (6)
A&TS-CC-P
I-RM-M

EXTERNAL

NASA Headquarters
Washington, D. C. 20546
Attn: Dr. G. E. Mueller — M
       Mr. William Schneider — ML
       Mr. P. E. Culbertson — MLA
       Dr. D. L. Forsythe — MLA
       Mr. J. E. Weldon — MLA
       Dr. L. N. Werner — MLA
       Mr. N. P. Frandsen — MLT
       Dr. John E. Naugle — S
       Mr. Jesse L. Mitchell — SG
       Mr. Maurice Dubin — SG
       Mr. R. E. Halpern — SG
       Dr. Henry J. Smith — SG
       Dr. H. Glaser — SG
       Dr. G. Oertel — SG
       Dr. Nancy G. Roman — SG
       Mr. R. Chase — SG
       Mr. B. T. Lundin — R
       Mr. R. D. Ginter — RF
       Dr. H. H. Kurzweg — RRP
       Mr. D. Novik — RFF
       Mr. M. B. Ames, Jr. — RV
       Mr. W. Keller — RV/1
       Mr. A. Reetz — RV/1
       Mr. C. Mook — RV/1
       Mr. H. L. Anderson — RET
       Dr. R. Nash — RRS
       Mr. J. Maltz — RRM

Manned Spacecraft Center
Houston, Texas 77058
Attn: Dr. O. G. Smith — KW
       Mr. J. A. Smith, Jr. — ES16
       Mr. J. T. Taylor — ES16
       Mr. A. McIntyre — ES7

EXTERNAL (Continued)

Manned Spacecraft Center (Concluded)
Attn: Mr. F. U. Williams — ES6
       Mr. W. K. Roberts — ES6
       Mr. J. Visentine — ES6
       Dr. E. G. Gibson — CB
       Mr. G. P. Bonner — TG-4
       Mr. B. R. Warden — AAP-KS

Kennedy Space Center
Kennedy Space Center, Florida 32899
Attn: Mr. R. A. Bland — AA-SVO-3

Langley Research Center
Langley Station
Hampton, Virginia 23365
Attn: Mr. J. P. Mugler, Jr. — MS-231
       Mr. E. L. Hoffman — 188B

Ames Research Center
Moffett Field, California 94035
Attn: Mr. E. R. Streed
       Vehicle Systems Design Branch

Goddard Space Flight Center
Greenbelt, Maryland 20771
Attn: Mr. James Milligan — 613
       Mr. J. H. Underwood — 614
       Mr. H. Shapiro — 322
       Dr. F. Paul — 327

Lewis Research Center
21000 Brookpark Road
Cleveland, Ohio 44135
Attn: Mr. J. G. Cassidy — 301-1

EXTERNAL (Continued)

Jet Propulsion Laboratory
4800 Oak Grove Drive
Pasadena, California 91103
Attn: Mr. W. F. Carroll - 158-235
      Mr. J. D. Acord - 198-326
      Mr. W. Goss - 198-112B

Naval Research Laboratory
Washington, D. C. 20390
Attn: Dr. Richard Tousey - 7140-137
      Dr. G. Carruthers - 7126-10
      Dr. T. C. Winter, Jr. - 7140W
      Mr. W. R. Hunter - 7143

High Altitude Observatory
P. O. Box 1558
Boulder, Colorado 80202
Attn: Dr. Gordon Newkirk, Jr.

Harvard College Observatory
Cambridge, Massachusetts 02138
Attn: Dr. Leo Goldberg
      Dr. E. Reeves
      Mr. H. L. Hazen
      Mr. W. Harby

American Science & Engineering
11 Carleton Street
Cambridge, Massachusetts 02142
Attn: Dr. Riccardo Giacconi
      Mr. L. P. Van Speybroeck
      Mr. A. G. Ead

EXTERNAL (Concluded)

Ball Brothers Research Corporation
P. O. Box 1062
Boulder, Colorado 80302
Attn: Mr. H. C. Poehlmann
      Mr. D. A. Toalstad
      Mr. J. Austin
      Dr. R. Herring

Martin-Marietta
Denver, Colorado 80201
Attn: Mr. R. Sawyer
      Dr. Muscari
      Mr. J. Wade
      Dr. Mangold
      Mr. Anthony

The Boeing Company
Seattle, Washington 98110
Attn: Dr. W. A. Eul
      Mr. Roger Gillette

General Electric Company
Valley Forge Technology Center
P. O. Box 8555
Philadelphia, Pa. 19101
Attn: Dr. D. Griffin

Scientific and Technical Information
   Facility (25)
P. O. Box 33
College Park, Maryland 20740
Attn: NASA Representative (S-AK/RKT)